Environmental variability in the Gulf of Guinea Large Marine Ecosystem

Physical features, forcing and fisheries

Nicholas John Hardman-Mountford, M.Sc., B.Sc. (Hons.)

A thesis submitted in fulfillment of the requirements for the degree of

Doctor of Philosophy

University of Warwick

Department of Biological Sciences

Ecology and Epidemiology Group

June 2000

Table of Contents

List of Tables and Figures

Tables

Figures

Acknowledgements

I am deeply grateful for all the help and support I have received from numerous people in a variety of institutions during the course of this research. Firstly, I would like to thank my supervisors: Jacquie McGlade and Charles Sheppard. Both of them have supported me throughout and provided me with numerous experiences and opportunities to broaden my horizons. They have also continually shown immense optimism and unswerving faith in my abilities.

I could not have carried out this work without the adminstrative and technical support of Susan Taylor, Jo Sheehan, Catherine Wattebot and Santokh Chahal at the University of Warwick and Lady Glenys Hicks and DTG, especially Sandra Chenery for UNIX support and Pete Mehigan for continually allowing me too much space on the N-drive, at CCMS in Plymouth. Above all in this regard, I would like to thank John Marshall for his profound knowledge and willingness to share it. I have learned, amongst other things, details of network maintenance, the finer points of technical design and page setting and a little bit about organ music! – all for the cost of a few cups of coffee.

I would like to thank my fellow PhD students, especially James Cole, Joost Maus and Rebecca Klaus for help with getting started using ERDAS *Imagine*, handling remote sensing data and getting to grips with PCA. Andrew Yool for UNIX instruction. Kwame Koranteng for organising things in the region, especially the Ghana trip. Paddy McCormack for enthusing me about Africa, and getting me started with power spectra. Alan Lovell for being another Gulf of Guinea student and sharing such burdens as being a rapporteur with me. Also, in Plymouth, Anthony King, Delphine Malleret-King, Kaija Metuzals, Nicky Beaumont and Georgina Spyres - thanks for all the encouragement and support.

From Plymouth, I would like to thank Arnold Taylor for introducing me to climate indices and providing me with data, Michael Jordan for providing me with atmospheric COADS data and Bob Clarke for helping me with statistics. Bablu Sinha for reading draft chapters and Robin Pingree for arguing the finer details of Canary Current circulation with me. In IRD, I would like to thank Gil Mahé for providing me with reams of data, Hervé Demarcq for help with remote sensing and an enjoyable visit to Montpellier and Claude Roy for providing me with the COADS CD-ROMs and CODE program and for reading through drafts of papers. At the JRC, I am grateful to Leo Nykjaer and Carlos Villacastin for providing me with the CORSA data and at JISAO, University of Washington in Seattle I would like to thank Todd Mitchell, not only for providing me with rainfall indices and individual station data, but also for remembering to send me the updates.

Finally, but most important of all has been the love and support of my wife, Mary-Ann and both sets of parents. Above all, I thank God for his strength, without which I can do nothing (Col. 3.17).

Declaration

I hereby declare that the work described in this thesis was conducted by myself, under the supervision of Prof. J.M. McGlade and Dr. C.R.C. Sheppard, with the exception of those instances where the contribution of others has been specifically acknowledged.

The research is based upon data sets not collected by the candidate. Consequently, this data has previously been used in publications and theses. However, the processing, application and interpretation of the data within this thesis is completely the work of the candidate and is, to the best of the candidate's knowledge, entirely original.

Chapter two comprises part of a review paper of which the candidate is first named author (Hardman-Mountford *et al*. 2000). Throughout this thesis, all sources of information have been specifically ackowledged by means of reference.

Abstract

This thesis examines the forcing and behaviour of oceanographic physical features, relevant to recruitment in fish populations, in the Gulf of Guinea Large Marine Ecosystem, on seasonal and interannual time scales. Remotely sensed sea-surface temperature (SST) data covering the period 1981 – 1991 was used to identify and describe a number of oceanographic features, including the Senegalese Upwelling influence, the Ghana and Côte d'Ivoire coastal upwelling, river run-off, fronts and the previously unrecorded observation of shelf-break cooling along the coast of Liberia and Sierra Leone during the boreal winter. Interannual variability in SST was observed on an approximate three year scale and an extended warm phase was noted between 1987 and 1991. Principal components analysis (PCA) was used to further investigate the variance structure of these SST data and this technique was shown to be able to accurately define boundaries of the Gulf of Guinea system and its constituent subsystems. River discharge data from throughout the Gulf of Guinea was also investigated using PCA, confirming the hydroclimatic regions identified by Mahé and Olivry (1999). The boundaries between these regions correspond closely to those identified between subsystems in the SST data, suggesting a degree of coupling between oceanographic and meteorological variability in the Gulf of Guinea. To further investigate this coupling, local climate data and global/basin scale indices were compared qualitatively and statistically with remotely sensed and *in situ* SST data and indices of interannual variability in oceanographic features. A new basin scale index was proposed as a measure of zonal atmospheric variability in the subtropical North Atlantic (SNAZI) and this was shown to be the dominant mode of climate variability forcing SST in the Gulf of Guinea. The implications of these results for fisheries recruitment dynamics are discussed.

List of Acronyms

AAIW	Antarctic Intermediate Water
AATSR	Advanced ATSR
AMT	Atlantic Meridional Transect
ATSR	Along Track Scanning Radiometer
AVHRR	Advanced Very High Resolution Radiometer
CCMS	Centre for Coastal and Marine Sciences (UK)
CDOM	Coloured Dissolved Organic Matter
CNES	Centre National d'Etudes Spatiales (CNES)
COADS	Combined Ocean Atmosphere Data Set
CORSA	Cloud and Ocean Remote Sensing around Africa
CPUE	Catch Per Unit Effort
CUI	Combined Upwelling Index
CWAU	Central West African Upwelling
CZCS	Coastal Zone Color Scanner
DLR	German Aerospace Research Establishment
EGOG	Eastern Gulf of Guinea
ENSO	El Niño-Southern Oscillation
EOF	Empirical Orthogonal Function
ERS	Earth Resources Satellite
ERTS	Earth Resources Technology Satellite
ESA	European Space Agency
FAO	Food and Agriculture Organisation of the United Nations
GAC	Global Area Coverage
GCM	General Circulation Model
GGRI	Gulf of Guinea Rainfall Index
GLI	Global Imager
GOCE	Gravity field and steady-state Ocean Circulation Experiment
GOSTA	Global Ocean Surface Temperature Atlas
GRACE	Gravity Recovery And Climate Experiment
I/G wave	Inertia/Gravity wave
ICES	International Council for the Exploration of the Seas
IPCC	Intergovernrnental Panel on Climate Change
IRD	Institut de Recherche pour le Developpement (France)
ISRO	Indian Space Applications Centre
ITCZ	Inter-Tropical Convergence Zone
JEBAR	Joint Effect of Baroclinicity and Relief
JISAO	Joint Institute for the Study of the Atmosphere and Oceans (USA)
JRC	Joint Research Centre
KARI	Korean Aerospace Research Institute
KOMPSAT	Korea Multi-Purpose Satellite
LAC	Local Area Coverage
LME	Large Marine Ecosystem
MCSST	Multi-Channel SST
MERIS	Medium Resolution Imaging Spectrometer
MODIS	Moderate resolution Imaging Spectrometer
MOS	Modular Optoelectronic Scanner
MSMR	Multifrequency Scanning Microwave Radiometer
NAO	North Atlantic Oscillation
NASA	National Aeronautics and Space Administration
NASDA	National Space Development Agency (Japan)
NCAR	National Centre for Atmospheric Research (USA)
NDVI	Normalised Difference Vegetation Index
NECC	North Equatorial Counter Current
NOAA	National Ocean Atmosphere Administration (USA)
OCI	Ocean Colour Imager
OCM	Ocean Colour Monitor

OCTS	Ocean Colour Temperature Sensor
OEW	Optimal Environmental Window
ORSTOM	Institut francais de recherche scientific pour le developpement en cooperation
OSC	Orbital Sciences Corporation
OSMI	Ocean Scanning Multispectral Imager
PC	Principal Component
PCA	Principal Components Analysis
PDO	Pacific Decadal Oscillation
PML	Plymouth Marine Laboratory (UK)
POES	Polar Orbiting Environmental Satellite
QBO	Quasi-Biennial Oscillation
RFRI	Roberts Field Rainfall Index
SACW	South Atlantic Central Water
SAI	Space Applications Institute
SAR	Synthetic Aperture Radar
SeaWiFS	Sea viewing Wide Field-of-view Sensor
S-GLI	Super GLI
SLFMR	Scanning Low Frequency Microwave Radiometer
SLGP	Sierra Leone and Guinea Plateau
SLP	Sea Level Pressure
SNAZI	Subtropical North Atlantic Zonal Index
SOI	Southern Oscillation Index
SST	Sea Surface Temperature
SUI	Senegalese Upwelling Influence
TBRI	Togo-Benin Rainfall Index
T-S diagrams	Temperature-Salinity diagrams
TSW	Tropical Surface Waters

"'Wouldst thou' - so the helmsman answered –
'learn the secret of the sea?
Only those who brave its dangers
Comprehend its mystery!'"

From *The Secret of the Sea* by Henry Wadsworth Longfellow.

"Small erections may be finished by their first architects; grand ones, true ones, ever leave the copstone to posterity. God keep me from ever completing anything. This whole book is but a draft – nay, but the draft of a draft. O, Time, Strength, Cash and Patience."

From *Moby Dick* by Herman Melville

1 Research Aims, Rationale and Global Background

1.1 Global Context

1.1.1 Focus

A fundamental problem in oceanography is how environmental variability over a range of different time and space scales relates to biological processes and ecosystem functioning. Certainly, there has been a realisation that coupling between atmospheric and oceanographic processes may be responsible for large fluctuations in the fundamental properties of marine ecosystems. Salinity, temperature and flow fields can all change on a variety of space and time scales from metres and minutes (turbulence), through 10s-100s of kilometres and months, to ocean basins and decades (Stommel 1963). Biological populations appear for a while then disappear on the same range of scales, e.g. plankton patches, tuna migrations, ecosystem collapse and recovery. Interaction also occurs between these scales, for example changes in the intensity of the North Atlantic Oscillation (NAO) index have been shown to influence wave heights in the North Atlantic (Kushnir *et al.* 1997), and hence storm surges and increased turbulence.

This thesis considers oceanographic and meteorological variability in the Gulf of Guinea, West Africa, over seasonal and interannual time scales. It particularly focuses on those oceanographic features which are thought to be important for successful recruitment in fish populations and attempts to relate them to large scale climate forcing.

To better understand the impact of human pressures on marine ecosystems, there needs to be a good understanding of the extent and effect of natural variability over the whole range of spatio-temporal scales. The focus of this thesis is on those temporal scales which have, until recently, been more difficult to address, i.e. those ranging from the seasonal to the decadal. Such a study requires multi-year time series of data. Thus, although measurements with

resolution as fine as a week have been used in this study, the focus remains on lower frequency features with seasonal importance or interannual importance, as these are the most difficult to observe experimentally.

Spatially, this study has focused on and around the Large Marine Ecosystem (LME) scale, however, both mesoscale features and basin scale events are of relevance to ecosystem dynamics and are, therefore, considered here. As with temporal variation, such a scale requires large amounts of data to be synthesised and viewed synoptically (e.g. the analysis of Longhurst 1998) – something which is difficult to achieve through individual *in situ* experiments.

1.1.2 Relevance of this study to fisheries

This study is concerned with investigating physical environmental variability of relevance to fisheries. Fisheries dynamics have been chosen as the focus for the ecological basis of this thesis for two reasons:

Firstly, to measure changes across the whole of a marine ecosystem would require huge amounts of effort and is not feasible for the majority of the world's oceans. Certainly no previous time series of data are available at this scale. Fish are found at various trophic levels in marine ecosystems (see section 1.6.2). They also have a wide spatial distribution, both horizontally and vertically (see section 2.5.3) and are subject to environmental changes in the system throughout time (see section 1.6.1). Thus, the intimate way in which fish are intertwined within the trophodynamic, temporal and spatial structure of the system means that changes at the ecosystem level are reflected in fish populations. The harvesting of fish populations means that, at least at a crude level, some measure of the variability of fish populations over time exists. Thus, changes in fish populations are a suitable proxy for changes in the dynamics of the whole ecosystem.

Secondly, the excessive harvesting of the oceans in many parts of the world has led many fish populations to near or actual collapse. Yet, these resources form a major source of protein for much of the world's population, especially in poorer countries (Scowcroft 1995, Hardman-Mountford *et al.* 2000). Techniques used for fisheries management are based on biological parameters, such as spawning stock biomass, and pay little or no attention to the role of parameters such as environmental variability, despite much evidence that the latter play an important role (see section 1.6.3). This is, to some extent, due to the lack of predictability of environmental fluctuations. Thus, a better understanding of the dynamics governing how physical environmental variability relates to productivity in fish populations will aid forecasting and allow for better management of fisheries, ultimately providing more food security for many of those dependent on fish as a primary source of protein.

1.1.3 Study region

The Gulf of Guinea, situated along the west coast of Africa in the equatorial region, was chosen as the study site for this thesis. Other regions, such as the North Atlantic shelf ecosystems, have been investigated much more intensely and would have provided a greater amount of background data for this study. However, human exploitation of biological resources in these areas has intensified to such a degree that to separate natural environmental fluctuations from anthropogenically induced ones may well be nearly impossible without a solid understanding of the underlying dynamics. In the Gulf of Guinea, on the other hand, biological resources have been subject to relatively light fishing pressure, at least up until the end of the 1980s (Shatz 1998). Thus, any relationships between natural environmental variability and fluctuations in fish populations should be more apparent.

Additionally, the Gulf of Guinea region has shown a high degree of both physical and biological environmental variability over time. Many of these changes, especially during the 1970s and 80s, have been adequately documented. But while a number of researchers have investigated the changes in this area, often such studies have been based on data from just a

few point sources collected over only one or two years. The complex nature of the dynamics of the region have meant that few conclusions have been reached regarding the causes of these changes.

The Gulf of Guinea is situated in a critical position for Atlantic equatorial dynamics. It is at the equivalent latitude to Ecuador and Peru in the Pacific. The importance of equatorial dynamics in the Pacific has been studied intensively over recent years resulting in the realisation of how interannual variability in this band can have global scale consequences.

Finally, the Gulf of Guinea is a very important area for fisheries. Artisanal fisheries have traditionally dominated the area and this is still the case, with over 70% of the catch coming from the artisanal sector (Tilot and King 1993), however, the impact of industrial fleets in the area is increasing (Koranteng 1998). A number of foreign fleets have been present in these waters on a large scale since the 1960s, most notably from the European Union, Korean Republic, Japan, Russia and ex-eastern bloc countries. European countries represent the largest fleet in the region and have fishing agreements with many of the nations (Tilot and King 1993). Understanding the natural dynamics of this region is, therefore, of vital importance if the fisheries resources of this productive area are to be sustainably managed and not exhausted as with so many other fish populations throughout the world.

1.1.4 Aims

The two fundamental aims of this thesis can be identified as:

1. to identify and describe the relevant spatio-temporal scales over which environmental forcing can be detected;

2. to investigate the relationship between environmental forcing factors and interannual variability in ecosystem behaviour.

To fulfil these aims the following steps were undertaken.

1. Description of physical environmental variability within the study region on both a seasonal and interannual basis, including identification of physical environmental features of potential relevance to ecosystem functioning.
2. Investigation of the coherence between natural length scales within the study region, leading to definition of the natural boundaries of the physical system and any subsystems.
3. Investigation of the relationships between local environmental parameters and basin/global scale climate patterns to determine ecosystem forcing factors.
4. Generation of testable hypotheses regarding mechanisms by which the ecosystem may be forced on seasonal and interannual time scales.

1.2 Thesis structure

The first three chapters of this thesis introduce the scientific concepts and background information relevant to this thesis. Chapter 1 lays out the objectives and rationale for the work and then reviews background information from the range of disciplines contributing to the study. The section on *Oceanographic Remote Sensing* gives a brief history of the use of satellites for marine studies before describing the range of oceanographic data now available from space-borne platforms. The *Oceanographic Principles* section then provides the theoretical background for previous hypotheses regarding physical dynamics in the Gulf of Guinea and for oceanographic features observed in this study. The section on *Basin-Wide Dynamics and Ocean-Atmosphere Coupling* provides a brief overview of recent work relating to global and basin scale climate variability, ocean-atmosphere interactions and the relative importance of natural versus anthropogenic climate change. The *Ecological Principles* section describes ecological concepts, later applied to the Gulf of Guinea LME. Chapter 2 moves away from global principles to focus on the Gulf of Guinea LME itself, providing an overview of its bio-physical structure. Chapter 3 then ‘zooms in’ to consider in detail

observations and theories pertaining to the most frequently studied oceanographic feature of the Gulf of Guinea: the coastal upwelling of Ghana and Côte d'Ivoire.

Chapters 4 to 8 describe the analyses carried out for this thesis. In chapter 4, oceanographic features are identified from remotely sensed sea surface temperature (SST) data and their seasonal and interannual variability is described. Chapter 5 then uses Principal Components Analysis (PCA) to investigate the variance structure of the same data set. Chapter 6 introduces local scale climate data, again using PCA to investigate its variance structure. Chapters 7 and 8 then attempt to relate SST variability to local and large (basin/global) scale climate variability, respectively.

Finally, chapter 9 reviews the conclusions made in each chapter and relates them to the overall aims of the thesis as well as to previous studies. Possible areas for future work are also discussed.

1.3 Oceanographic Remote Sensing from Satellites

Over the last few years, remote sensing has become a useful tool for a whole spectrum of disciplines, from meteorology (e.g. Stoffelen and Anderson 1995) to epidemiology (Linthicum *et al.* 1999). Various reviews of the history of remote sensing and basic principles exist (e.g. Lillesand and Kiefer 1987). In the oceanographic sciences, satellite based remote sensing has been available for nearly four decades (Sherman 1985). The most commonly used parameters are SST from infra-red radiometry (AVHRR, ATSR IRR), ocean colour and sea ice from visible radiometry (CZCS, SeaWiFS) and, more recently, dynamic heights from radar altimetry (GEOSAT, ERS-1 RA, TOPEX/Poseidon). Also available are brightness emissivity derived sea ice and global SST from passive microwave sensors (SMMR, SSM/I, ATSR MWS), sea surface roughness and winds from synthetic aperture radar (SAR, e.g. ERS-1 SAR, SeaSAT SAR) and sea state from scatterometers (ERS-1 SCATT).

Additionally, developments with high resolution SAR and Scatterometer data allow for the detection of internal waves and ocean swell.

1.3.1 Infra-red radiometry

The Advanced Very High Resolution Radiometer (AVHRR) sensors, on board the NOAA Polar Orbiting Environmental Satellites (POES) have been in use since 1978 when the first one was included in the payload of the TIROS-N satellite. They are used to measure SST and have an accuracy of 0.1K. The data have a spatial resolution of 1.1 km, known as local area coverage (LAC). On-board averaging also takes place to produce a lower resolution product with 4 km resolution, known as global area coverage (GAC). Additionally, 'Pathfinder' data, averaged to 9 km resolution, are available.

These data have been supplemented since 1981 by the European Space Agency's (ESA) Along Track Scanning Radiometer (ATSR) (ATSR 2000). ATSR-1 was launched in 1991 on board the ERS-1 satellite and ATSR-2 has been operational since 1995 on board the ERS-2 satellite. ATSR has a spatial resolution of 1 km, an accuracy of +/- 0.3K and is self-calibrating. It also has a dual view design which makes it possible to estimate and correct for atmospheric effects (ATSR 2000). This feature is of particular value in the tropics where atmospheric water vapour can cause serious contamination of images.

A drawback in using infra-red to measure SST is that it only measures the temperature of the upper few millimetres of the ocean. This can give rise to 'skin effects', such as diurnal heating patterns.

1.3.2 Ocean colour

Ocean colour is the radiation measured from the oceans in the visible light spectrum. It is contributed to by chlorophyll, unpigmented suspended sediments and gelbstoff (literally yellow substance) from decaying organic matter. Measurements are not restricted to surface

waters, but are possible to a depth of 2 attenuation lengths (Platt and Herman 1983), i.e. deeper for clearer waters.

Monitoring of ocean colour in the coastal zone from space was first made possible by the Earth Resources Technology Satellite (ERTS), later renamed Landsat. Landsat, however, is not optimised for oceanographic applications and is only activated for land observations. Therefore, only estuaries and nearshore waters associated with land scenes are available (Lavender, in prep.). The first dedicated marine sensor for ocean colour mapping was the Coastal Zone Color Scanner (CZCS) launched in 1978 on board the Nimbus-7 satellite. However, CZCS was operated on an intermittent schedule due to power demands and its sensors were known to be degrading from 1981 onwards (Lavender, *ibid.*). It remained in operation until 1986 (NASA 2000). There was then a gap of 10 years before the next ocean colour sensor was launched.

In 1996, two more ocean colour sensors were launched. The Modular Optoelectronic Scanner (MOS) has 3 modules: MOS-A is for measuring atmospheric parameters, MOS-B is for ocean colour sensing and MOS-C produces thermal imagery. It was built by the German Aerospace Research Establishment (DLR) and launched on-board the Indian IRS-P3 spacecraft (Zimmerman and Neumann 1997). A major drawback of MOS is that the IRS-P3 mission is pre-operational, serving for technology evaluation and scientific methodology studies only. There is no on-board data storage which means that data transmission to the three ground stations (Neustrelitz in Germany, Mospalomas in the Canary Islands and Hyderabad in India) can be done in real-time mode only. Additionally, as MOS shares the platform with a radioastronomy payload, the satellite is rotated for stellar observations for quarter of the year, resulting in no MOS data for that period (Lavender *ibid.*). Another MOS sensor was launched in 1996, within the PRIRODA module that was to be operated from the MIR space station, but this was never operational (Zimmerman 1997).

The Ocean Colour Temperature Sensor (OCTS) was an optical radiometer devoted to the frequent global measurement of ocean colour and SST, to be used for studying primary production and the carbon cycle in relation to fisheries and environmental monitoring. It was launched on-board ADEOS in 1996 but was lost when ADEOS failed during the following year (Gregg 1999).

In Autumn 1997, the Sea-viewing Wide Field-of-view Sensor (SeaWiFS), part of NASA's Mission to Planet Earth, was launched on-board the ORBVIEW-2 satellite owned by Orbital Sciences Corporation (OSC) (McClain *et al.* 1998, NASA 2000). It can store on-board a limited amount of 1 km resolution LAC data and a complete orbit of 4 km resolution GAC data. Derived products include chlorophyll-a concentration, CZCS-type pigment concentration, diffuse attenuation coefficient at 490 nm wavelength and several atmospheric parameters determined during the atmospheric correction procedure (Lavender, *ibid.*).

Separation of ocean colour constituents (chlorophyll-a, suspended sediments, gelbstoff) becomes increasingly difficult for more turbid waters. SeaWiFS standard products can only separate them for clear, oligotrophic (Case I) waters, although a routine developed by Gerald Moore and others at CCMS - Plymouth Marine Laboratory (PML), UK has had some success with defining individual constituents for turbid (Case II) waters (S. Lavender, CCMS-PML, Plymouth, UK, pers. comm.). The European Space Agency's (ESA) Medium Resolution Imaging Spectrometer (MERIS), due for launch on board their Envisat satellite in 2001, has been developed to separate these three constituents in Case II waters (Rast *et al.* 1999, Moore *et al.* 1999, Schiller and Doerffer 1999). This will allow more accurate estimates of primary production in turbid coastal areas as well as giving information on coastal erosion rates and sediment transport and deposition. Additionally, the separation of gelbstoff will enable levels of coloured dissolved organic matter (CDOM) to be estimated.

1.3.3 Radar altimetry

Radar altimeters measure the height of the sea surface. They have been used in spaceborne remote sensing since 1973 when the Skylab satellite was launched. This early system was only able to measure coarse features of the marine geoid, such as deep ocean trenches. Skylab was followed by GEOS-3 in 1974, SeaSat-1 in 1978 and Geosat in 1984, each contributing to the development of the technique. After GeoSat, two different approaches were taken in the improvement of performances, giving rise to two different families of satellite altimeters. The first family, developed by the USA (NASA) and France (CNES), was designed to optimise performance over the oceans and comprises the TOPEX/Poseidon sensors. The second family, developed by ESA, was optimised for use over all kinds of surfaces and includes ERS-1 RA and ERS-2 RA (ESA 1997).

Radar altimeter data from over the oceans have been used to estimate the steady state height of the sea surface from which bathymetry and marine geoid characteristics have been measured (ESA 1997). When these are removed, surface variability of the worlds oceans is visible. Such information is very useful for detecting variable features, such as eddies. It also has hydrodynamic uses since changes in the sea surface reflect dynamical behaviour of the interior ocean e.g. movement of internal waves within the thermocline. ESA is planning to launch a new radar altimeter (RA-2) on board its Envisat satellite. This will also be able to map and monitor sea ice, polar ice sheets, and most land surfaces (ESA 1997).

A current problem with altimeters is that changes in sea surface height (SSH) have no reference depth. Rather, deviations from the mean are calculated. This mean includes permanent features of the surface circulation, such as major currents, which cannot then be determined as separate from bathymetry. To overcome this problem two missions are being planned for satellite based gravity sensors: GRACE and GOCE. GOCE is ESA's Gravity Field and Steady-State Ocean Circulation Explorer mission and GRACE is NASA's Gravity Recovery and Climate Experiment. The primary objective of GOCE is a high-resolution

determination of the constant part of the gravity field of the earth. The GRACE mission is also focusing on monitoring changes in the earth's gravity field (Visser 1999). These missions will allow for features of the steady-state ocean circulation to be separated from the topography of the seafloor, giving improved estimates of ocean dynamic topography and thereby improved information on ocean surface velocities (Legrand and Minster 1999).

1.3.4 Future satellites and applications

A number of new satellites have been launched recently, or are due to be launched in the near future. The Taiwanese Ocean Colour Imager (OCI) was launched in January 1999 on board the ROCSAT-1 satellite. It has been specifically designed for the study of equatorial waters (Lavender, *ibid.*). The IRS-P4 satellite was launched in May 1999 by the Indian Space Applications Center (ISRO). This carries the Ocean Colour Monitor (OCM) and Multifrequency Scanning Microwave Radiometer (MSMR) instruments (Lavender, *ibid.*). The Moderate Resolution Imaging Spectrometer (MODIS) was launched on the EOS-AM satellite in December 1999 and will also be on the EOS-PM satellite to be launched in 2000. Like SeaWiFS, it too is part of NASA's Mission to Planet Earth. Its aim is to measure the water leaving radiance in the visible, near infra-red and thermal infra-red wavebands for atmosphere, land and ocean products. It will have improved signal-to-noise ratio compared to SeaWiFS and additional ocean colour wavebands, e.g. chlorophyll fluorescence. It will also be able to measure SST (Lavender, *ibid.*). Also in December 1999, the Korean Aerospace Research Institute (KARI) launched the Ocean Scanning Multispectral Imager (OSMI) aboard the Korea Multi-Purpose Satellite (KOMPSAT). The National Space Development Agency (NASDA) of Japan is developing the Global Imager (GLI) for launch on-board the ADEOS-2 satellite in late 2000. It will have 36 sensors for use in land, atmosphere, ocean colour and ice measurements. NASDA is also in the planning stages for the ADEOS-3 satellite which will carry the Super-GLI (S-GLI). ESA is planning to launch a dedicated environmental satellite, Envisat, in 2001. It will carry a total of 9 instruments, including the Advanced ATSR

(AATSR) for measuring SST and MERIS (discussed above) for observations of ocean colour (Lavender, *ibid.*; ESA 1997).

Another possibility for the future of marine remote sensing is that of resolving salinity from satellites. Such a system is still in development, however, there has been some success using a light aircraft platform over the Chesapeake and Delaware bays in the USA, as well as in Sweden and Finland. The system is called the Scanning Low-Frequency Microwave Radiometer (SLFMR) and combines microwave and infra-red sensors. It can resolve salinity to 1‰ and has a spatial resolution of 100 m (Goodberlet *et al.* 1997). The implementation of such a system on a satellite platform would have huge implications for marine sciences, especially in the classification of the marine environment into oceanic provinces (see Longhurst 1998) as salinity indicates features in marine surface waters that are not always obvious using SST, such as river and estuarine plumes.

1.4 Oceanographic Principles

The details of oceanographic circulation and structure in the Gulf of Guinea are dealt with in the next chapter. This section is a summary of some of the relevant oceanographic principles.

1.4.1 Shelf-slope dynamics

Processes occurring along eastern ocean boundaries at the continental shelf edge and slope have recently become the focus of a number of studies, notably the Ocean-Margin Exchange (OMEX) programmes, investigating the western European shelf-slope region.

Oceanic transport along eastern ocean boundaries is generally equatorward and wind-driven. However, in a number of areas, poleward currents exist, often in subsurface layers and concentrated over the continental slope region. These flows tend to be driven by the meridional gradient in thermal structure, with temperatures decreasing in a poleward direction (Decleuse and Philander 1983). The density changes associated with this thermal gradient

result in a pressure gradient force causing onshore geostrophic flow in sub-surface layers. When this flow reaches the slope it becomes trapped at the boundary. Because the slope intersects contours of dynamic height, which also decrease poleward because of the increasing sea water density, the onshore flow becomes diverted in a poleward direction along the slope (Pingree *et al.* 1999). This property is due mainly to conservation of potential vorticity, which is approximately equal to f/h, where f is the Coriolis parameter and h is the depth. Rapid depth change in the continental slope region means that, for a particular area, changes in h are great compared to f, thus geostrophic flow on the slope has to follow depth contours, giving rise to a slope current. This process was termed 'the joint effect of baroclinicity and bottom relief (JEBAR)' by Huthnance (1984). Thus the continental slope acts as a conductor or chute channelling alongslope flow poleward (Pingree *et al.* 1999).

Continental shelf waters are relatively shallow, so flows on the shelf are generally wind driven (Pingree and Griffiths 1980) and strong tidal currents are also often present (Pingree *et al.* 1999). These processes tend to result in shelf waters being well mixed. Thus, temperatures on the shelf are more homogenous than in the open ocean. This homogeneity means temperatures on the shelf will exhibit less of a poleward decrease in temperature than oceanic waters, leading to a latitudinally increasing temperature gradient across the continental slope, which in turn acts to strengthen the slope current.

Because net flow in the upper slope region is relatively fast compared to water movement on the continental shelf, the slope current acts as an insulator, preventing exchange between oceanic and shelf waters. This insulating effect is very strong, however, it can be weakened by processes which reduce slope current flow. The two main types of process which allow for weakening of this insulating effect are inertial and frictional processes.

Inertial processes are important in areas of abrupt topography, such as canyons or spurs (Pingree *et al.* 1999). The inertia of the slope current in spur areas can cause it to overshoot the change in topography and be dissipated to the open-ocean. Pingree *et al.* (1999) showed

such losses to be occurring at Goban Spur, in the Celtic Sea area of the European shelf-edge. Similarly, canyons can divert slope current water on to the shelf. Formation of Swoddies (Slope Water Oceanic Eddies) is effectively an inertial loss of slope water to the ocean (Pingree and Le Cann 1992), thus in the Goban Spur example, above, Pingree *et al.* (1999) predict an increase in eddy activity to the north of the spur in the Porcupine Seabight. Additionally, many mesoscale eddies impinge on the slope or are even trapped by slope topography (e.g. in Torrelavega and Santander Canyons, Lisbon and Setubal Canyons, see Pingree 1995) and these eddies will affect the local slope currents even inducing eddies on the shelf (Pingree *et al.* 1999).

The other major cause for weakening of slope flow, and thereby insulation, is frictional processes. Bottom friction reduces the speed of currents and causes offshore transport. Pingree *et al.* (1999) undertook a mathematical treatment of a slope flow which is entirely frictionally and rotationally controlled, neglecting nonlinearities (inertial effects) altogether. The results of this study implied downslope transport for poleward flow and upslope transport for equatorward flow or flow reversals. They showed that generally, a less steep, broader slope can sustain a greater along-slope transport than a steeper, narrower slope, whereas, the steeper, narrower slope will have greater across-slope transport leading to greater offshore losses of slope water. However, the steeper, narrower slope is also a better insulator of shelf water, because depth changes across the slope are more rapid, leading to greater potential vorticity constraints between shelf and ocean water. Thus, insulation between the shelf and slope will be reduced where the gradient of the continental slope weakens markedly (Pingree *et al.* 1999) despite the increases in slope flow, and vice versa.

Because the shelf slope is a topographic barrier, it can be a strong generator of internal tides and waves, leading to mixing throughout the water column in these areas. In some areas this mixing has been observed as cooling at the shelf-break, coupled with large increases in biological activity. Pingree (1984) used infra-red satellite imagery to identify shelf-break cooling from May to September of about $1^{o}C$ in the Celtic Sea region of the European shelf

edge. He also noted from *in situ* measurements that marked increases in primary productivity were associated with this cooling. Coombs *et al.* (1983) noted local maxima of mackerel eggs in this region of the shelf-slope during May and June, coinciding with the observed cooling and phytoplankton blooms.

1.4.2 Fronts

Oceanic surface fronts are the sea surface manifestations of sharp boundaries between adjacent water masses of different properties. Important physical driving forces for these features are those associated with air-sea transfers, including global and local wind stress and seasonal and planetary vertical transports of heat (heating and cooling of the sea surface) and water (precipitation and evaporation). Other processes to be counted include riverine inputs of fresh water, confluences and shears of tidal and surface geostrophic flows, turbulent stirring due to the topography and roughness of the sea bottom, stirring due to internal wave and internal tide shear and nonlinear instabilities, and centrifugal effects due to curvature in the flow. The dynamics of larger fronts are significantly influenced by the rotation of the earth, whereas small scale fronts are likely to be dominated more by nonlinear inertial and frictional effects (Bowman 1978).

Continental shelves are mosaics of water masses with different properties (Mann and Lazier 1996). Oceanic fronts are important in ocean dynamics. Large scale fronts have important effects on the weather and climate so an understanding of their causes and effects is necessary in forecasting the ocean climate. Fronts in the marine environment also have significant biological consequences. They are areas of high productivity for the whole food chain from phytoplankton through fish to marine mammals. This has made them areas of intense fishery exploitation. Therefore, an understanding of the role of fronts is needed in the construction of biological models of ocean productivity and fisheries management strategies (Bowman and Esaias 1978).

Fronts are found at all depths in the ocean. Bowman and Esaias (1978) conveniently classify them into six categories:

1) Fronts of planetary scale. These are ususally associated with the convergence of surface Ekman transports and found away from major oceanic boundaries (e.g. within the Sargasso Sea, Southern Ocean).
2) Fronts representing the edge of major western boundary currents. These fronts are associated with the intrusion of warm, salty water of tropical origin into higher latitudes (e.g. Gulf Stream, Kuroshio Current).
3) Shelf break fronts formed at the boundary of shelf and slope waters, such as are found in the middle Atlantic Bight. Circulation along the front may or may not be baroclinic depending on whether the temperature and salinity fronts coincide, and whether their contributions to the density field are compensating or reinforcing.
4) Upwelling fronts, essentially the surface manifestation of an inclined pycnocline, commonly formed during a coastal upwelling, i.e. as a result of an offshore surface Ekman transport associated with alongshore wind stresses (e.g. along the west coast of the USA, Peru, northwest and southwest Africa).
5) Plume fronts at the boundaries of riverine plumes discharging into coastal waters (e.g. Amazon, Columbia, Hudson, Connecticut, etc.)
6) Shallow sea fronts, formed in continental seas and estuaries and around islands, banks, capes and shoals. These are commonly located in boundary regions between shallow, wind and tidally mixed nearshore waters and stratified, deeper offshore waters (e.g. Celtic and Irish Seas, approaches to English Channel, Long Island Sound).

All these frontal systems share common properties of persistence, ranging from hours to months. These occur in spite of diffusion properties across strong horizontal gradients and surface convergence, with associated strong vertical convection, usually being at least an order of magnitude greater than in the open ocean (Bowman and Esaias 1978). This thesis is generally concerned with continental shelf dynamics in the eastern equatorial Atlantic.

Therefore, only the last four frontal categories, defined above, are of relevance to this thesis. Shelf break fronts and upwelling fronts are described by Mooers *et al.* (1978). These authors prefer the terminology retrograde and prograde fronts as the former terminology implies mutually exclusive dynamics. A review of shallow sea fronts is given by Pingree (1978), estuarine and plume fronts are described by Bowman and Iverson (1978) and a brief review of headland fronts is given by Pingree *et al.* (1978). A fuller review of the physical nature and structure of oceanic fronts is given by Fedorov (1986).

1.4.3 Upwelling dynamics

Upwelling is the process by which subsurface water ascends to the surface. It is of both biological and climatological significance. When the sub-surface waters come from below the thermocline, they are cooler and generally richer in nutrients than the surface waters. In such cases, the increased nutrient input can fuel biological productivity in the nutrient depleted but well-lit surface waters and, therefore, has important consequences for the local ecology. Additionally, the cooler surface waters help stabilise the atmosphere resulting in reduced precipitation. These features are typical of the major coastal upwelling regions across the globe: along the eastern boundaries of the Pacific and Atlantic Oceans. The high fisheries yields from the Peruvian, California current, Canary current and Benguela regions are well known and all four areas are backed, to some extent, by coastal deserts (see Mann and Lazier 1996 for reviews of each of these areas).

Some of the physical processes typically involved in upwelling are described here. Upwelling occurs at divergence zones, where surface water is removed from an area and cannot be replaced in the horizontal so instead is pumped from depth. In eastern boundary regions, coastal upwelling is generally driven by equatorward winds which prevail along their coasts inducing alongshore surface flow. Coriolis force then turns this water away from the coast, to the right of the wind stress in the northern hemisphere and to the left in the southern hemisphere, leading to removal of surface water from the coastal boundary. The wind driven

transport of the surface boundary layer, termed Ekman transport, has a mass transport magnitude equal to the wind-stress divided by the Coriolis parameter, provided that the water is significantly deeper than the surface boundary layer (Smith 1995). The 'gap' left at the coastal boundary is subsequently filled with sub-surface water and mass-balance then requires an onshore flow of water at depth. The upward movement of water causes isopycnals to shoal towards the region of divergence. After the pycncoline reaches the sea surface the front starts to move offshore, with the width of the region where the interface rises to the surface being determined by the Rossby internal deformation scale (Mann and Lazier 1996). The boundary between the upwelled water and the adjacent oceanic surface water is often a front with an associated equatorwards jet and polewards undercurrents are also an ubiquitous feature of many upwelling regions (Smith 1995). An in depth review of the physical processes involved in coastal upwelling systems is given by Smith (1995).

Not all upwelling, however, is driven by local winds, neither does it have to occur at the coastal boundary. Large upwelling areas are found along the equator in the eastern Atlantic and Pacific and these are thought to be driven, to some degree, by remote wind forcing transmitted by internal waves from the western equatorial ocean. A similar mechanism has been proposed for the coastal upwelling regions of the Gulf of Guinea and is discussed in depth in Chapter 3. Upwelling has also been observed to take place at the shelf break, in some areas, perhaps caused by the interaction of topography with Ekman transport (Summerhayes *et al.* 1995). Additionally, topographic features such as headlands and canyons can influence upwelling (Mann and Lazier 1996).

Despite the large spatial extent of the major eastern ocean upwelling regimes, mesoscale features appear to dominate many upwelling systems. The quasi-geostationary front between coastal upwelled water and oceanic waters is distorted, not only by eddies, but also by plumes and filaments extending out to hundreds of kilometers from the adjacent coast (Summerhayes *et al.* 1995). Examples of these are provided by Lutjeharms and Stockton (1987), Stockton and Lutjeharms (1988), Shannon *et al.* (1985), Brink and Cowles (1991) and Smith (1995).

Recent studies off northern California show that the filaments are the offshore directed legs of meanders in the jet that separates the coastal and open ocean systems (Brink and Cowles 1991). Modelling suggests that the filaments may arise where interaction between the current system and the protruding capes causes offshore deflection, steepening frontal meanders (Haidvogel *et al.* 1991).

The biological significance of upwelling systems, mentioned above, is not reviewed further here. Man and Lazier (1996) and Summerhayes *et al.* (1995) both provide further details of biological production associated with upwelling systems.

1.4.4 Internal waves

Waves generated within the ocean's internal density structure are called internal waves. Additionally, interface waves, which constitute a special type of internal wave, flow along more pronounced internal surfaces such as thermoclines (Mann and Lazier 1996). The passage of some waves affects the vertical density distribution, so that isopycnals are caused to intersect isobars, hence these are termed baroclinic waves and, similarly, waves that do not affect the vertical density distribution are termed barotropic waves. Interface waves are, therefore, baroclinic and baroclinic waves generally have larger amplitudes than barotropic waves (Open University 1989).

Waves propagate with a *phase speed* (c) which is determined by the wavelength (L) over the wave period (T). Groups of waves of a particular type are termed *beams*. *Group speed* is the speed at which energy associated with the disturbance is propagated and for gravity waves in deep water this is less than the phase speed. To describe waves mathematically, modellers use a variety of mathematical functions or *modes*. Waves can have both horizontal and vertical modes. The zero-order vertical mode is the homogenous constant density solution at the equator, hence such a mode is barotropic. The first-order vertical mode is the solution needed to be added to the constant density solution in order to produce the two layer solution.

Higher order modes provide greater detail (Dyke 1996). First and higher order vertical modes are baroclinic and, therefore, apply to internal waves. For internal waves phase speed can also be given as:

$$c = (g'H)^{1/2}$$

Where H is the depth of the mixed layer and g' is the reduced gravity = $(\rho_2-\rho_1/\rho_1)g$, i.e. (density change over the pycnocline/density of the upper layer) × gravity.

EQUATORIAL WAVES

Knowledge of the time-dependent dynamics of the ocean at low latitudes in response to large-scale winds is based on the theory developed by Moore (1968) and Lighthill (1969). Reviews, given by Moore and Philander (1977), Gill (1982), McCreary (1981, 1984) and Philander (1990), provide the background for studies of the dynamics of equatorial waves (Verstraete 1992).

Coriolis force becomes zero at the equator and the associated rotation reverses across it. This mathematical solution forms a physical boundary at the equator causing waves to become trapped along it, as at a coastal boundary. This is due to the strong constraints placed on water particles by laws governing the conservation of angular momentum, i.e. a particle would have to undergo a 180^o change in angular momentum to cross the equator.

There are four classes of waves that have equatorially trapped modes: Kelvin waves, high-frequency Inertia-Gravity (I/G) waves, low-frequency Rossby waves and mixed Rossby-gravity (or Yanaï) waves (Verstraete 1992). High frequency waves, such as the I/G and Rossby-gravity waves are relatively unimportant in this context (Philander 1981, 1990).

Theoretically, a Kelvin wave is a wave with a perfect exponential profile offshore and a perfect sinusoidal nature which travels along a boundary of infinite length adjacent to an infinitely wide ocean. In the real ocean these conditions are not met, however, waves approximating these characteristics are found (Dyke 1996). Kelvin waves are similar to

surface wind waves in that the principal maintaining force is gravity, but particle movement within the wave is such that the amplitude of the vertical displacement is greatest at the boundary and decreases exponentially away from it, so that at any point and time the Coriolis force balances the pressure gradient due to the slope of the sea-surface or thermocline (Open University 1989). For an equatorial Kelvin wave, the sea surface displacement is maximum at the equator and falls off symmetrically to the north and south with a Gaussian shape (Verstraete 1992). The distance associated with this decay is the Rossby radius of deformation. Equatorial Kelvin waves have no meridional velocity component (Weisberg *et al.* 1979). Coriolis force requires that phase always propagates with the boundary to the right (left) of the Kelvin wave in the northern (southern) hemisphere. This means that phase will propagate eastward at the equator for Kelvin waves. Energy also propagates eastward for Kelvin waves (Verstraete 1992).

Long Rossby waves, otherwise known as planetary waves, occur in the oceans and in the atmosphere and can oscillate in both the vertical and horizontal planes. Rossby waves have minimum amplitude at the equator due to the Coriolis parameter being zero. Phase propagates westwards for Rossby waves and energy propagates in either sense. Long Rossby waves are nearly non-dispersive in nature which means that their group speed is almost equivalent to their phase speed (Verstraete 1992).

Because equatorial waves travel with high phase speed, they are of paramount importance in the oceanic adjustment to a change in the winds. The fastest waves are the Kelvin waves which carry the energy eastwards. The long Rossby waves propagate the energy westwards at a slower rate. The adjustment time of the equatorial ocean is the sum of the time a Kelvin wave takes to propagate eastwards, plus the time a long Rossby wave takes to propagate back westwards across the basin. This is estimated to be 150 days in the Atlantic and 450 days in the Pacific (Cane 1979, Philander 1981).

Equatorial trapping of waves is a special case of waves being trapped along a boundary. Coastal boundaries, can therefore, act in the same way. Because Kelvin waves phase always propagates with the boundary to the right (left) in the northern (southern) hemisphere, it will propagate poleward along the eastern ocean boundaries (Verstraete 1992). Coastally trapped barotropic Rossby waves also propagate with the boundary to the right (left) in the northern (southern) hemisphere (Clarke 1977). Coastal barotropic Rossby (shelf) waves are found in situations with homogenous water and shelf topography with no longshore variation; internal (baroclinic) Kelvin waves are found in situations with no bottom topography and stratified water (Clarke 1977). In a situation of stratification and no longshore variation in topography, Clarke (1977) presented evidence for internal waves that are a hybrid of the two.

When equatorial waves impinge on a continent the energy propagates poleward away from the equator along the coast as trapped waves (Verstraete 1992). Because the offshore scale of the waves is larger than the scale of coastal topography, they generally behave like internal Kelvin waves trapped by a vertical wall (Allen and Romea 1980).

1.5 Basin Wide Dynamics and Ocean-Atmosphere Coupling

Investigation of coupling between large scale features of oceanic and atmospheric systems is at the forefront of natural environment research. The large El Niño–Southern Oscillation (ENSO) events of 1982/3 and 1997 have been the focus of much investigation, both on a local scale in the equatorial Pacific and in terms of their global teleconnections (a recent review of El Niño is given by Webster and Palmer 1997). Less well understood, although also the subject of a wide range of studies, is the North Atlantic Oscillation (NAO) and its links to oceanic phenomena such as Gulf Stream position (Taylor and Stephens 1998), arctic sea ice (Kwok and Rothrock 1999) and wave height (Kushnir *et al.* 1997) throughout the North Atlantic basin (for recent reviews of the NAO see Uppenbrink 1999 and Morton 1998).

Rodwell *et al.* (1999) used an atmospheric general circulation model (GCM) to investigate the ocean's role in forcing North Atlantic and European climate. There is an observed decline of the NAO from the late 1940s to the late 1960s and a subsequent rise to the early 1990s. Their simulations indicate that much of the multiannual to multidecadal variability of the winter NAO over the past half century can be reconstructed from a knowledge of North Atlantic SST. They argue that SST characteristics are communicated to the atmosphere through the positive feedback processes of evaporation, precipitation and atmospheric heating. Other authors, however, find little evidence of positive feedbacks (e.g. Frankignoul and Hasselmann 1977, Frankignoul 1985). Other analyses indicate significant decadal predictability of North Atlantic SST, arising from the advective propagation of SST anomalies and the existence of a regular period of 12-14 years in the propagating signals. The same time scale can be identified in the NAO. This may be part of a coupled ocean-atmosphere mode of variability (Sutton and Allan 1997).

Ideas concerning the time scales over which these ocean-atmosphere interactions operate are also being re-evaluated. ENSO phenomena are thought to occur every 3-5 years, however, lower frequency variations are becoming apparent. Over the last two decades, the two largest El Niño events of the century have occurred, separated by a period of 15 years (Kerr 1999). Interactions between cycles of different frequencies have been observed in Pacific SST. An interdecadal (10-20 year) scale ENSO type cycle has been noted in the eastern tropical Pacific. This cycle began to warm in the early 1970s, reaching a peak in the early 1980s. Furthermore, another decadal scale cycle, which operates in a large westward pointing wedge of the central tropical Pacific, also warmed sharply in the late 1970s. Thus it appears that the interaction between ENSO and these decadal/interdecadal cycles caused the strong El Niño event of 1982-83 and also contributed to the record El Niño of 1997 (Kerr 1999).

El Niño events have also been linked to decadal scale changes occurring over the North Pacific, where two distinct climate oscillations have been noted in the SST record. These raise temperatures in the central basin while lowering them over the rest of the ocean and *vice*

versa (Kerr 1999). The more rapid of these two has been termed the Pacific Decadal Oscillation (PDO) and this also showed tropical warming in the late 1970s. Interactions between the PDO and El Niño are apparent with the El Niño pattern being stronger and more consistent when the PDO is in its cold phase, and vice versa (EOS 1999). Gershunov and Barnett (1998) suggest that during the winter of 1997/1998, the powerful El Niño was felt even more keenly in North America because the PDO was in its cold phase. They also found that the PDO interacts more strongly with La Niña. A cold North Pacific disrupts the La Niña pattern of a dry Southwest and wet northern states, and a warm North Pacific strengthens it (Kerr 1999).

What causes these oscillations in the Pacific is not certain, however, it may be a feedback loop between winds, currents and temperature. Occasionally such loops could produce simultaneous warming in several cycles (Kerr 1999, Meehl *et al.* 1998). The NAO has also been seen to operate on both high (interannual) and low (decadal) frequency scales, so perhaps interactions between these cycles also occur in the Atlantic.

Another question currently being addressed is what level of interaction occurs between ocean-atmosphere feedbacks from different ocean basins? Although studies have shown the Southern Oscillation index (SOI) to be uncorrelated with the NAO index (Rogers 1984), there is evidence of ENSO and the NAO both influencing the same features and areas in the western Atlantic. Over the past three decades, the annual mean latitude of the Gulf Stream off the coast of the US has been forecastable from the intensity of the NAO (Taylor and Stephens 1998), the predictions accounting for more than half the variance. Much of the unexplained variance, however, can be accounted for by the Southern Oscillation in the Pacific, the Gulf Stream being displaced northwards following ENSO events (Taylor *et al.* 1998). Additionally, in Puerto Rico, ENSO control of annual mean air temperatures has been observed since 1914, with El Niño years being associated with warm air temperatures and La Niña years being cooler. On the other hand, since 1911, fluctuations in annual rainfall amounts have been synchronous with variations in the winter NAO and are not controlled by

ENSO. During years of a high NAO index, when the axis of moisture transport in the North Atlantic changes to a more southwesterly-northeasterly orientation, annual precipitation in Puerto Rico is lower than average (Malmgren *et al.* 1998). Meehl *et al.* (1998) noted from observations and results of a global coupled climate model that coherent decadal climate variability extends over the entire Pacific basin, is associated with processes in the Atlantic and Indian Oceans and appears to be connected to the oceanic gyral circulation of each of these basins.

Finally, of current research interest is the extent to which recent climate change is attributable to anthropogenic forcing compared to natural modes of climate variability. Certainly it is likely that natural variability occurs at frequencies too low to be detectable in modern time series measurements (Kerr 1999). A recent study by Corti *et al.* (1999), using atmospheric circulation data from the Northern Hemisphere, has shown that recent climate change can be interpreted in terms of changes in the frequency of occurrence of natural atmospheric circulation regimes and concludes that recent northern hemisphere warming may be more directly related to the thermal structure of these circulation regimes than to any anthropogenic forcing pattern itself. However, the authors also acknowledge that this cannot be used as evidence of no anthropogenic effect on climate. They suggest that, although it is commonly thought that anthropogenic forcing should be distinct from patterns of natural variability, non-linear chaotic models with preferred states or regimes show that spatial patterns of anthropogenic forcing responses may in fact project principally onto modes of natural climate variability (Corti *et al.* 1999). Certainly, the IPCC report of 1995 concluded that 'the balance of evidence suggests a discernible human influence on global climate' (Houghton *et al.* 1996).

1.6 Ecological Principles

In this section, approaches and considerations for ecosystem and fisheries recruitment analysis are presented. The ecology of the Gulf of Guinea is considered in the next chapter.

1.6.1 Comparative analysis of ecosystems

According to Mayr (1982), the experimental method and the comparative method are the "two great methods of science". The comparative method is the method of choice in situations not amenable to controlled experiments (Bakun 1993). Mayr (1982) identified it as the basis for "nearly all of the revolutionary advances in evolutionary biology" (Bakun 1993). Because marine ecosystems are hardly amenable to experimental controls, the comparative method presents an available alternative for assembling the multiple realisations of a process needed to draw scientific inference (Baird *et al.* 1991, Bakun 1996).

Thus, comparisons of different ecosystems can lend support to areas of investigation where local data are scarce, for instance, a decade of annual fish catch data gives only 10 data points making a robust analysis of major changes impossible. If, however, similar changes have occurred elsewhere, more robust conclusions can be formed. An example of such a situation is the apparent synchrony in changes in sardine populations (*Sardinops sagax*) from around the Pacific basin (Kawasaki 1983, Lluch-Belda *et al.* 1992, Bakun 1996) and, perhaps, further afield (Schwartzlose *et al.* 1999).

The previous example leads to another major area for comparison between different species and locations: the issue of how climate change relates to marine ecosystems on a global scale. The simultaneous changes observed in Pacific sardine populations have also been noticed to occur with the opposite phase in the sardine fisheries (*Sardinops ocellatus*) of the Benguela system (Lluch-Belda *et al.* 1992). Bakun (1996) argues that to explain such coincident changes it is logical to look to global-scale climate linkages. Several other examples exist of fish populations changing in relation to known large-scale climatic phenomena, e.g., both landings of several Pacific salmon species (Salmonidae) and Japanese sardine (*S. sagax*) catches have been related to interdecadal climate variations in the North Pacific (Mantua *et al.* 1997, Yasudo *et al.* 1999). In the Atlantic Ocean, stocks of cod *Gadus morhua* have declined drastically in recent years. The North Sea population has been in decline since the late 1980s

(O'Brien *et al.* 2000) and the Grand Banks fishery collapsed in the early 1990s (Longhurst 1998). Overfishing has undoubtedly played an important part in the deterioration of these populations, but environmental variability may also be of key importance. So far no climatic changes have been successfully correlated with these events, however, changes in oceanic conditions have been noted over the same period. In the North Sea, mean SST during the first half of the year has been higher since 1988 than during the previous three decades. Increasing temperatures are known to be detrimental for cod stocks at the southern extent of their limit in the Northern Hemisphere, such as the North Sea population (O'Brien *et al.* 2000). Additionally, the decline of North Sea cod is coincident with the disappearance of triggerfish *Balistes capriscus (=carolinensis)* from the Gulf of Guinea (Bakun 1996), followed by the rise of the globefish *Lagocephalus laevigatus* and cuttlefish *Sepia officinalis* in the same region (Koranteng 1998).

1.6.2 Fish populations for ecosystem analysis

All of the examples given above are from fish populations and in section 1.1.2 the usefulness of fisheries for investigating changes across the whole of the ecosystem was briefly covered. The reasons for this are further described in this section.

Marine ecosystems typically have more trophic levels lying between primary producers and top predators than terrestrial ecosystems (Bakun 1996). The number of species at lower (planktonic) trophic levels is typically very large and includes the egg and larval phases of many fish species which exist at higher trophic levels in adulthood. Additionally, a substantial number of species exist at the apex or near-apex levels (e.g. predatory fish, large coelenterates, seabirds, marine mammals). In many of the more richly productive ecosystems of the world, however, there is an intermediate trophic level generally dominated by only one or two species of small, planktivorous fishes, forming a narrow 'wasp-waist' between the larger numbers of species at the higher and lower trophic levels (Bakun 1996). These wasp-waist level species typically have a very high biomass and tend to be dominated by one

species of sardine (*Sardinops* spp., *Sardina* spp.), anchovy (*Engraulis* spp.) or menhaden (e.g. *Brevoortia tyrannus*) in temperate coastal upwelling ecosystems (e.g. Canary current, California current and Benguela current) and western boundary current ecosystems (e.g. Kuroshio current, Falklands/Malvinas current, Gulf Stream). Analogous species are found in tropical ecosystems, such as *Sardinella* spp and thread herring *Opisthonema oglinum*. Other examples are the herring *Clupea harengus* or sand eels (Ammodytidae) of boreal shelf ecosystems, such as the North Sea or Bering Sea, and the capelin *Mallotus villosus* of the subarctic Atlantic (Bakun 1996).

Despite the typically large biomass of these populations, they are prone to very large, rapid fluctuations. The Peruvian anchovy (*Engraulis ringens*) population had the largest biomass ever recorded, with landings around 12 million tons, just prior to its complete crash in 1972 (Bakun 1996, Mann and Lazier 1996). According to Bakun (1996), this variability of wasp-waist populations has important consequences for the lower trophic levels upon which the wasp-waist populations feed and also for the levels higher up the food chain which depend on these wasp-waist populations as a major food source. Thereby, the major control in marine ecosystems is neither top-down or bottom-up, but from the middle outwards. This theory is justified because, although larval fish feed at a low trophic level leading to the supposition that variations in primary production should be a major factor underlying fluctuations in reproductive success, validation of this hypothesis based on real data in natural oceanic conditions has been surprisingly difficult to find (Bakun 1996). Therefore, Bakun (1996) suggests that the existence of weak links in the life-cycle of these intermediate-level fish populations may overwhelm effects that might propagate up the food web from variability occurring at the lowest trophic level. The weak links in the life-cycle occur prior to recruitment and are covered further in section 1.6.3.

Thus, it appears that variability at the ecosystem level is not just reflected in these wasp-waist populations, it is to some degree governed by them. Data on the quantity of fish caught in different areas has been collected for many years, both by national agencies and international

organisations such as the FAO and ICES, and is available for most of the major fisheries throughout the world's oceans, at least at a crude level. For many areas, data on fishing effort are also available. Because these intermediate levels tend to have very high population biomasses, they are often the target of major fisheries exploitation. In this way we have a time series record of changes in these fish populations, and hence ecosystems.

As well as showing natural environmental variability, fish catch data can also be used to show anthropogenic impacts on ecosystems. Pauly *et al.* (1998) took FAO landings statistics by area for the years 1950 to 1994 and combined them with trophic levels, obtained from Ecopath models (see Christensen and Pauly 1993, Pauly and Christensen 1995), for 220 different species or groups of fish and invertebrates. They showed that the mean trophic level of the species groups caught had declined over this period, reflecting a gradual transition from long-lived, high trophic level, piscivorous bottom fish toward short-lived, low-trophic level invertebrates and planktivorous pelagic fish. This 'fishing down the food web' can lead to complete ecosystem collapse, as in the case of the Black Sea, where first the apex predators were removed, leaving an ecosystem dominated by anchovy. Further heavy fishing and other problems, including eutrophication, then appear to have left the ecosystem in such a weakened state that jelly-predators (jellyfish and ctenophores), introduced in ballast water from ships, were able to overtake the ecosystem. This resulted in an almost total collapse of the remaining fisheries (Bakun 1996). The area is now considered a major international ecological disaster (Mee 1992). Similarly, Robertson *et al.* (1996) have shown that excessive fishing of sandeels in the North Sea has the potential to reduce the availability of higher predators in this ecosystem.

1.6.3 Recruitment variability

Probably, the most fundamental question for fisheries science is: what controls adult population size in the absence of overfishing? To reach adulthood, fish have to grow through a great range of sizes. These growth stages form a continuous chain of life-cycle events,

extending from the formation of reproductive products within the adult fish, through various egg, larval and juvenile phases, until finally they join the adult population. This process is termed recruitment and reflects not a single event but a large number of interacting processes by which huge numbers of tiny eggs and larvae undergo drastic reduction to a very much smaller number of surviving recruits. This sequence of events is further complicated because the great differences in size and consequent life-styles characterising the various stages means an identical process may affect survival in different ways at different stages of development (Bakun 1996). Exactly what is the most critical stage of larval development, the 'weak link' in terms of final recruitment success, remains a matter of speculation, although for marine fisheries in general there is increasing evidence it is the later larval stages and not the first feeding stages (Cushing 1996).

A number of mechanisms have been proposed as to what is the major cause of recruitment variability and these have been reviewed by Cole and McGlade (1998). To summarise, mechanistic theories revolve around starvation, advection and predation. Starvation theories are based on the premise that if larvae do not encounter sufficient quantities of food after yolk-sac absorption they will die (Blaxter and Hunter 1982). This has led to a number of theories, including Hjort's (1914) critical period, Cushing's (1975) match-mismatch theory, Lasker's (1975) vertical stability hypothesis and Rothschild *et al.*'s (1989) turbulence hypothesis. Advection theories are concerned with the transport of eggs and larvae towards or away from suitable nursery areas (e.g. Iles and Sinclair 1982, Parrish *et al.* 1983). Predation, including cannibalism, theories generally look to density-dependent dynamics (e.g. Valdés *et al.* 1987, Valdés *et al.* 1992), although temperature may also play a role by affecting growth rates (Laurence 1992).

Another approach is to consider that the interaction of different processes most likely controls recruitment success. A number of synthesis theories have thus been developed in an attempt to combine the various mechanisms by which pre-recruitment mortality can take place. Bakun (1996) generalises three broad categories of oceanographic process thought to be

important in influencing recruitment success; namely nutrient *enrichment* of the environment to support appropriate levels of primary production, *concentration* of food particles into denser aggregations to facilitate foraging and *retention/transport* of eggs and larvae within/to suitable nursery areas. Bakun refers to these three factors as a fundamental triad and gives examples of enrichment (upwelling, river run-off, micro-scale turbulence), concentration (fronts, river plumes, thermocline) and transport/retention mechanisms (fronts, coastal boundaries, thermocline, currents, local gyral circulation patterns).

The Optimal Environmental Window (OEW) theory of Cury and Roy (1989) shows that rather than any particular environmental parameters being 'good' for recruitment *per se*, a balance between relevant parameters is required to provide optimal conditions for recruitment. For example, in a wind driven upwelling region, increase in wind stress will increase the offshore Ekman transport and hence the influx of nutrients to the euphotic layer to stimulate primary production. However, it will also lead to increase in the level of wind mixing, disrupting vertical stratification and the formation of chlorophyll maximum layers, and offshore advection of eggs and larvae. Therefore, the optimal conditions for recruitment occur at intermediate levels of wind stress, where there is a balance between the upwelling of nutrient rich water and calm conditions required for successful first feeding and retaining eggs and larvae in the nursery area.

1.6.4 Ecosystem definition

According to McGlade (1999), system description is still one of the least resolved aspects of ecology. Indeed, one of the challenges faced by pelagic marine ecology is how to define individual marine ecosystems (as opposed to the concept). Terrestrial and benthic ecology has, for many years, been able to define biomes based on knowledge of a few simple factors (latitude, altitude, temperature, rainfall, slope, substrate and underlying rock type) for anywhere on the continents (Longhurst 1998). For the less intuitive pelagic environment, however, such a set of parameters has not been defined, although several attempts have been

made to this end. Criteria such as surface water mass characteristics (e.g. Emery and Meincke 1986), nutrient distributions (Fanning 1991), features of the surface circulation (Ware and McFarlane 1989) and depth of the mixed layer (Longhurst and Harrison 1989) have been proposed as suitable parameters for such a classification. Cushing (1989) suggested that division should take place simply on the basis of strong or weak stratification. Banse and English (1993) proffered that three domains based on relative seasonal variation of chlorophyll and relative nutrient depletion should be recognised: (i) low-latitude oligotrophic gyres with little seasonality in phytoplankton production, (ii) regions where phytoplankton growth does not exhaust available nitrate at any season and (iii) regions where a spring bloom is followed by summer oligotrophy. In the same vein, Barber (1988) identified six characteristic ecosystems (coastal upwelling, low-latitude gyre, equatorial upwelling, subarctic gyre, southern ocean and eastern boundary current), although he did not suggest that the whole surface of the ocean could be allocated to one of them (Longhurst 1998). Longhurst (1998) has suggested a list of information required to predict the course of the ocean calendar for any surface ocean region (latitude, depth of water, proximity of coastline, seasonal irradiance cycle, local wind regime, local precipitation regime, distant forcing of pycnocline depth, nutrients in the intermediate water mass and external sources of iron).

Another problem is how to define the spatial extent of particular marine ecosystems. Generally, arbitrary definitions are used which depend on the scale and perspective of individual studies. For example, coral reef 'ecosystems', mangrove 'ecosystems' and seagrass bed 'ecosystems' all interact to form a tropical coastal 'ecosystem'. Keeling *et al.* (1997) proposed a theoretical approach to defining natural length scales in ecological systems, based on correlations between windows of different sizes.

Thus, it appears that a frame of reference is needed by which different areas of the world's oceans can be compared objectively and within context. Longhurst (1998) has attempted to define a biogeography of the surface oceans, mainly using remotely sensed CZCS ocean colour data. He divides the oceans up into 5 biome types: polar biome, westerlies biome,

trades biome, coastal boundary zone biome and exceptional regions (e.g. boundary layers and high-nutrient, low-chlorophyll areas). These biomes are then associated with each of the Atlantic, Pacific, Indian and Southern oceans and subdivided into 51 oceanic provinces. The boundaries, or ecotones, between each of the provinces are generally defined by natural environmental features, such as fronts. The main focus of this classification was to provide a framework for calculating the global primary production (Longhurst 1995).

Sherman, Alexander and Gold proposed an alternative approach based on classifying the coastal marine environment, termed the Large Marine Ecosystem (LME) concept (Sherman *et al.* 1992). LMEs are relatively large regions of ocean space, of the order of 200,000 km^2 or greater, characterised by distinct bathymetry, hydrography, productivity and trophically dependent populations. They extend from the nearshore areas, including river basins and estuaries, out to the seaward boundary of the continental shelf or the seaward margin of coastal current systems (Sherman *et al.* 1998). The LME concept was designed as a basis for management of the marine environment and natural resources (GOG-LME 1996). Fifty large marine ecosystems have been defined around the world. It is recognised that the boundaries between LMEs are not fixed, rather they tend to be defined by natural environmental features, such as fronts, which can change position through time. However, to be useful for management, LME boundaries need to be delineated with some precision. Many of the current LME boundaries are arbitrary and may well be redefined with further investigation. A number of LME projects are underway in various parts of the globe. The large areas of LMEs means that they, like natural resources and pollution, do not acknowledge political boundaries. This has meant implementation of these projects has required a regional approach and cooperation between neighbouring countries. The fact that this regional cooperation has been obtained in some areas is, in itself, a justification of the concept.

Both the LME concept and the oceanic province approach are useful ways of partitioning the marine environment into manageable units for investigation and analysis. Each has its merits and disadvantages for scientific research, depending upon the focus of the study. One of the

major differences is that Longhurst's provinces are defined solely by the physical environment and primary production, making them essentially equivalent to terrestrial biomes based mainly on vegetation types, whereas LMEs take biological interactions between different trophic structures into account, thereby showing the dynamics of the system much more. This also makes them harder to define precisely. For this study, the LME concept has been used as a starting point because it defines the Gulf of Guinea LME better than Longhurst's province approach.

2 Overview of Conditions in the Gulf of Guinea LME

2.1 Systems and Subsystems

The coastal marine environment of West Africa has been classified into three Large Marine Ecosystems (LMEs): the Canary Current LME (NW Africa), the Gulf of Guinea LME (Central West Africa) and the Benguela Current LME (SW Africa) (Binet and Marchal 1993).

The Gulf of Guinea LME, as defined by Tilot and King (1993) or Binet and Marchal (1993) lies between the Bijagos Islands (Guinea-Bissau, ~ 11º N) and Cape Lopez (Gabon, ~ 1º S). This area includes the maritime waters of 12 coastal states (Guinea-Bissau, Guinea, Sierra-Leone, Liberia, Côte d'Ivoire, Ghana, Togo, Benin, Nigeria, Cameroon, Equatorial Guinea and Gabon) as well as the island states of Equatorial Guinea (Bioko, formerly Fernando Po) and São Tomé and Principe (see fig. 2.1). The system is generally defined by the flow of the Guinea current so is sometimes referred to as the Guinea Current LME. It is bounded to the north by the Canary Current and to the south by the South Equatorial Current (Binet and Marchal 1993).

Because of its heterogenous nature, Tilot and King (1993) divide the Gulf of Guinea LME into three subsystems. Each is defined by particular characteristics, which nevertheless contribute to the functioning of the ecosystem as a whole and interact with each other. These subsystems are:

1. Sierra Leone and Guinea Plateau (SLGP): from the Bijagos Islands (Guinea-Bissau) to Cape Palmas (Liberia/Côte d'Ivoire). This area is characterised by the largest continental shelf in West Africa and has large riverine inputs, giving thermal stability. It is also in the seasonal passage of the Inter-Tropical Convergence Zone (ITCZ).

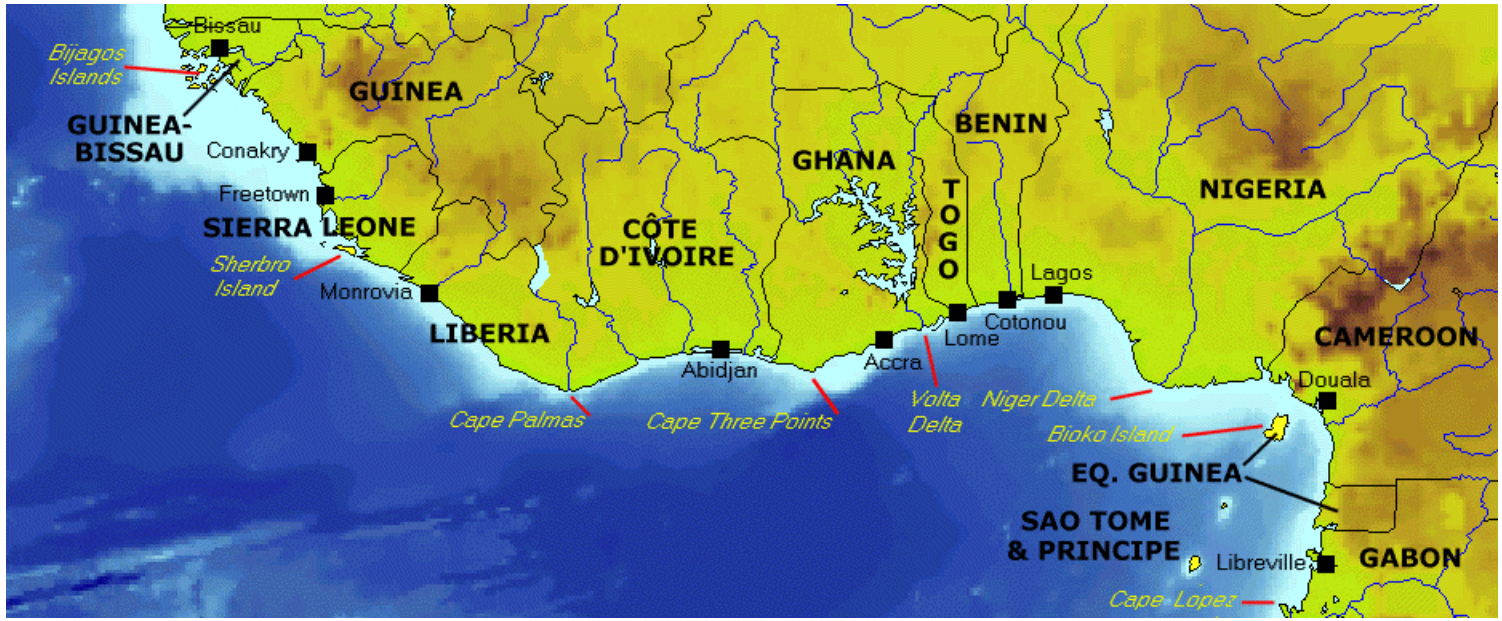

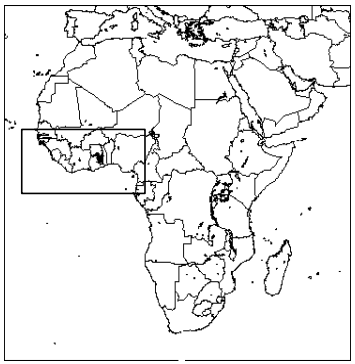

Figure 2.1. Map showing the Gulf of Guinea Large Marine Ecosystem, as defined by Binet and Marchal (1993), including bathymetry, topography, major rivers, country names and boundaries, some major coastal cities and prominent geophysical features.

2. Central West African Upwelling (CWAU): from Cape Palmas to Cotonou (Benin). This thermally unstable subsystem is characterised by seasonal upwelling of cold, nutrient rich, subthermocline water, which dominates its annual cycle and drives the biology of the subsystem. Variability in upwelling strength leads to variability in productivity.
3. Eastern Gulf of Guinea (EGOG): from Cotonou to Cape Lopez (Gabon), including the offshore islands of Bioko and São Tomé and Principe. This area is characterised by thermal stability and a strong pycnocline. Its productivity depends on nutrient input from land drainage, river flood and turbulent diffusion through a stable pycnocline. Variability of river input depends on climatic fluctuations of the monsoon.

2.2 Bathymetry

The continental shelf of the Sierra Leone-Guinea Plateau is the largest in West Africa, especially off Guinea-Bissau, covering approximately 53,000 km^2 and up to 150 km wide (Tilot 1993, Longhurst 1998). In the central and eastern Gulf of Guinea, the continental shelf is narrow. Shelf widths are 20-25km along the coast from Côte d'Ivoire to Cameroon, except between Cape Three Points and the Volta Delta, where it reaches 80km wide in parts, and around the Niger Delta, where it has a width of 50-65km (Allersma and Tilmans 1993). A number of submarine canyons are known or appear to exist on charts. These are Trou sans Fond off the Canal de Vridi, Côte d'Ivoire; Avons Deep off West Nigeria; the Mahin Canyon off the western coast of the Niger Delta; the Gabon Canyon north of the island of Principe and similar structures off the Volta Delta and the Calabar Estuary (Allersma and Tilmans 1993, BODC 1997). Two large river fans modify the continental shelf structure in the region: the Niger Fan off the Niger Delta and the Guinea Fan, formerly known as the Guinea Plateau, off the coasts of Guinea and Guinea-Bissau (BODC 1997).

2.3 Climatology

2.3.1 Climate and seasons

The Gulf of Guinea is in an equatorial humid zone: a humid tropical climate with almost constant monthly temperatures and a relatively large amount of precipitation. Precipitation is generally much more important than evaporation (Tilot 1993, Allersma and Tilmans 1993).

The annual climatic cycle is dominated by the Saharan atmospheric depression that begins around April and is caused by increased solar insolation warming the continental landmass (1993). The low-pressure zone increases rapidly and migrates past 20°N in July. This depression plays a fundamental role in both climatology and oceanography, generating the monsoon, which is responsible for most of the region's rainfall (1993).

Four maritime seasons are seen in the Gulf of Guinea region: a short cold season from December to January (~26.5^{o}C), a long warm season from February to June (27-29 ^{o}C), from July to September is a long cold season (22-25 ^{o}C) and finally in October and November there is a short warm spell (27-29 ^{o}C) (Longhurst 1962, Koranteng 1995, 1998).

2.3.2 Winds

In the central and eastern Gulf, the wind is a persistent south-westerly monsoon, modified by land and sea breezes in the coastal area. Speeds vary between 0.5m/s (night) and 1.5-2m/s (day) along the coast of Côte d'Ivoire and increase to between 0.5-2.5m/s (night) and 2-6m/s (day) in Nigeria. Storms are very rare; weaker line squalls with heavy rain and strong winds of short duration occur occasionally (Allersma and Tilmans 1993). The Sierra Leone-Guinea Plateau area also has monsoon winds blowing from April to October. During the rest of the year winds in this region are north-easterly maritime tradewinds.

A major feature of the climate system in the tropical Atlantic Ocean is the Inter-Tropical Convergence Zone (ITCZ), a region of atmospheric instability at the convergence of the

northern and southern tradewinds. This frontal zone separates the northern dry, heavy, continental air masses from the southern humid, lighter, marine air masses. Latitudinal migration of the ITCZ generates seasons over the tropical Atlantic Ocean and African landmass (Binet and Marchal 1993).

During the boreal winter, there are some occurrences of the hot, dry, north-easterly harmattan wind when the ITCZ deviates from its normal southerly position at 5-7°N (Allersma and Tilmans 1993).

2.3.3 Rainfall

Although rainfall is generally high throughout the Gulf, there are considerable differences in the amount and seasonal distribution of precipitation. Rainfall greater than 1,500 mm per year feeds tropical rainforests in Côte d'Ivoire and western Ghana and east from Cotonou. There are two maxima: May-June and October-November. In the eastern Gulf of Guinea, however, the monsoon climate leads to one long rainy period (Allersma and Tilmans 1993). Cameroon has the highest rainfall with Mount Cameroon receiving 11,000 mm per year. This is mainly due to orographic effects of the imposing volcano and the perpendicular orientation of the coast to the main oceanic flows.

The central coast from Takoradi to Cotonou is known as the Accra dry belt, with only 2-3 months receiving more than 100 mm of rain (Allersma and Tilmans 1993). It is thought that this low rainfall is due to stabilisation of the atmosphere by cold, upwelled surface waters.

2.4 Oceanography

2.4.1 Sea water structure and temperature

The high precipitation and numerous rivers in the eastern Gulf of Guinea result in large masses of warm, low salinity water, called Guinean waters, mixing with the Tropical Surface

Waters (TSW) and circulating throughout the Gulf of Guinea. These are invariably shallow and rest on colder water, their extent varying greatly throughout the year. Guinean waters are permanent in the Bight of Biafra (UNEP/IUCN 1988). In the central and eastern areas of the Gulf, sea surface temperature (SST) varies between 27 and 29°C outside of the upwelling seasons (Allersma and Tilmans 1993) but can drop to below 22°C at the coast during the major upwelling (Longhurst 1962).

The TSW overlie colder South Atlantic Central Water (SACW) (Longhurst 1962, Verstraete 1992). Stratification becomes enhanced during the warm seasons, especially the long warm season. The depth of the tropical thermocline can vary seasonally from approximately 10-60 m in the Gulf of Guinea (Longhurst 1962, Koranteng 1998). SACW lies below the tropical thermocline to depths of around 500 m. Beneath this, down to approximately 800 to 1500 m, is found Antarctic Intermediate Water (AAIW). North Atlantic Deep Water then underlies the AAIW (Longhurst 1962, Verstraete 1992).

2.4.2 Ocean circulation

The Guinea current dominates the oceanography of the Gulf of Guinea Large Marine Ecosystem. This current is an eastward, superficial flow, fed by the North Equatorial Counter Current (NECC) off the Liberian coast. The Guinea current is quite shallow, having an average depth of 15m near the coast and 25m offshore (Binet and Marchal 1993). Generally it flows barely near the coast except near promontories (Allersma and Tilmans 1993). Although the location of the NECC changes seasonally according to the position of the ITCZ, the position of the Guinea current remains fairly constant (Binet and Marchal 1993), however, it is reinforced by the monsoon and can be modified by the harmattan wind. Underneath the Guinea current flows the westward Guinea undercurrent (Lemasson and Rébert 1973a,1973b). This appears to originate in the Bight of Biafra as a return branch of the Equatorial undercurrent. The Guinea undercurrent can be observed at the surface in the Bight

of Biafra (Longhurst 1964) before it sinks under the Guinea current as it flows westward (Binet and Marchal 1993).

The analysis of the thermocline water masses suggest that the EUC supplies the coastal upwellings because the Guinea and Gabon-Congo undercurrents carry a well defined SACW type, nearly identical to the SACW carried by the EUC. This implies a northward and southward extension of the EUC. The observed splitting of the EUC core in 1982-1984 at São Tomé island, lying at 0^o to $0^o30'$N, is consistent with the geostrophic westward flows observed in the thermostad to the north and south of the EUC. These observed westward compensation flows, flanking the EUC at 2^o to 3^o north and south, coincide with the observed maximum thickness of the thermostad at these latitudes (Verstraete 1992).

2.4.3 Upwelling

The central West African upwelling region of the Gulf of Guinea, situated between Cape Palmas (Côte d'Ivoire) and Cotonou (Benin), is characterised by seasonal upwellings of cold, nutrient rich, sub-thermocline water, which dominates its annual cycle and drives the biology of the subsystem. The upwellings tend to occur on the concave coasts to the east of Cape Palmas and Cape Three Points (Ghana). There are two periods of upwelling each year. The major upwelling occurs throughout the long cold season (June to October), whereas the minor upwelling normally only lasts for about 3 weeks and generally coincides with the short cold season (January to February), although it has been known to occur anytime between December and March (Roy 1995, Koranteng 1998). During these periods SST falls, surface salinity and nutrient levels increase and dissolved oxygen levels generally fall (Houghton and Mensah 1978, Mensah and Koranteng 1988).

According to Bakun (1978), the region is similar to other eastern ocean boundary upwelling areas in the appearance of cool sea temperatures near the coast, productive coastal fisheries and a zone of low rainfall on the adjacent coast. Also the eastward Guinea current flow and

westward Guinea undercurrent give the system a structure of surface and subsurface circulation similar to other eastern ocean boundary upwelling areas (Roy 1995). There are, however, several important differences between the Guinea current region and other eastern boundary systems. These include the zonal rather than meridional trend of the coast, the influence of a rather narrow, intense, coastal current, a rather unusual lack of correspondence on a seasonal time scale between sea-temperature features attributable to the major upwelling and features in the overlying wind stress field (Bakun 1978) and the westward propagation of the upwelling against the flow of the Guinea current (Picaut 1983). These differences have made understanding the system extremely complex.

A mechanism for driving the major upwelling has not yet been agreed upon, although a number of hypotheses have been postulated. These include wind driven Ekman upwelling (Verstraete 1970), intensification of the Guinea current (Ingham 1970), dynamic interaction of the Guinea current with Cape Palmas and Cape Three Points (Marchal and Picaut 1977) and remote forcing from the western Atlantic (Moore *et al.* 1978, Servain *et al.* 1982). However, none of these mechanisms appear to fully explain the upwelling and many contradictory factors exist. The mechanism is probably, in reality, a combination of these factors (Roy 1995).

The winter upwelling has received less attention than the summer upwelling. Intensification of the Guinea current in January and February may contribute to the upward movement of the thermocline associated with this upwelling (Morlière 1970). Local winds may also be an important contributor to the winter upwelling (Roy 1995) as may remote forcing. According to Arfi *et al.* (1991), the intensity of this secondary upwelling is maximal in the surrounding of Cape Palmas and sharply decreases toward the east to become almost unnoticeable on the SST time series of Ghana's coastal stations.

Possible causal mechanisms for the upwellings are further discussed in Chapter 3.

2.5 Biology

2.5.1 Phytoplankton

Plankton communities in the Gulf of Guinea have not been extensively studied. Investigations, conducted mainly off Ghana and Côte d'Ivoire, have shown that phytoplankton cell counts, chlorophyll *a* concentrations and primary productivity rates are high during the major upwelling period (>1,000 mg C m^{-2} day^{-1}) and low during the non-upwelling period (<700 mg C m^{-2} day^{-1}) (Anang 1979). These have been confirmed from CZCS imagery (Longhurst 1998). Dinoflagellates form the main components of the phytoplankton population during the non-upwelling period and diatoms dominate at other times. The dinoflagellates consist of such genera as *Peridinium*, *Ceratium*, *Prorocentrum* and *Dinophysis* and the diatom flora include *Skeletonema*, *Nitzschia* and *Thalassiosira* (Anang 1979). In some of the larger embayments, such as the wide Sierra Leone estuary where tidal currents are strong, production is probably limited by light rather than nutrients. Thus, the seasonal cycle is the reverse of that of the open sea, with phytoplankton growth being maximal in the boreal winter dry season (~850 mg C m^{-2} day^{-1}), when estuarine water is relatively clear. Productivity is greatly reduced in the boreal summer wet season (<75 mg C m^{-2} day^{-1}) when inshore water carries a heavy silt load (Longhurst 1998). Investigations from Sierra Leone have shown that diatoms are more abundant in inshore waters, while dinoflagellates are more frequent offshore (Aleem 1979).

2.5.2 Zooplankton

The following zooplankton groups have been identified in samples collected from the region: Copepoda, Ostracoda, Cladocera, Decapoda, Larvacea, Thaliacea, Chaetognatha and larvae of bottom invertebrates. Copepods outnumber any other taxonomic group of zooplankton. During the upwelling season, up to 88 % of the zooplankton organisms in the coastal area are copepods. In the open sea, the percentage is generally much smaller (20-40 %). *Calanoides*

carinatus is the most abundant copepod (Mensah 1995, Greze *et al.* 1969), rising to surface waters over the shelf during the major upwelling season and remaining beyond the shelf at depths below 500 m outside this period (Longhurst 1998). Swarms of salps and pyrosomids (Thaliacea) are often observed in the deep-sea parts of the Gulf of Guinea (Le Borgne 1983).

Seasonal patterns of variability in zooplankton biomass appear similar from year to year, though absolute values vary monthly and annually. Underlying the fluctuations is a general declining trend in abundance of zooplankton (Mensah 1995). It is unclear whether the decline is associated with variation in species composition of the plankton. This observation has serious implications for pelagic fisheries, especially the West African sardine *Sardinella aurita*, which feeds directly on calanoid copepods (Longhurst 1998).

2.5.3 Fish populations and Assemblages

The distribution and abundance of pelagic fish in the Gulf of Guinea depends mainly on environmental parameters (Bard and Koranteng 1995), while depth and type of substrate are important factors that influence fish community structure (Koranteng 1998). Demersal fish and crustacean populations in the region are known to be uniform and stable.

From the results of the Guinean Trawling Survey (Williams 1968), the fish communities identified in the region are summarised as follows (from Longhurst 1969):

A. Sciaenid community
B. Eurybathic or thermocline species
C. Lutjanid community
D. Sparid community (shallow element and deep element)
E. Deep shelf community
F. Continental slope community

Recent investigations (Koranteng 1998) have confirmed these species groupings and also shown that a number of species remain faithful to their assemblages over time. It appears that

there are clear faunal discontinuities around 30 m, 100 m and 200 m deep with the first ecotone closely related to depth and thermocline, the second to drastic shelf drop, and the third to division between shelf and slope fish assemblages. It also seems that the dynamics of the assemblages are influenced by physico-chemical parameters of the water masses, mainly temperature, salinity and dissolved oxygen (Koranteng 1998).

Fishery resources in the Gulf of Guinea are usually classified into small pelagic species, large pelagic species, coastal demersal species and deep-water demersal species (Koranteng *et al.* 1996). Some of the most important fish species exploited in the Gulf of Guinea are listed in Table 2.1.

Three commercially important penaeid shrimps occur in the Bight of Biafra. These are *Penaeus notialis* (pink shrimp), *Parapenaeopsis atlantica* (Guinea shrimp) and *Palaemon hastatus* (estuarine white shrimp). The shrimps use the sea as well as the bays, estuaries and mangrove swamps during their life cycle (Ssentongo *et al.* 1986, Ajayi and Anyanwu 1997). Cephalopods are also important commercially. Species include cuttlefish *Sepia officianalis*, squid *Loligo* sp., and to some extent octopus *Octopus vulgaris* (Tilot 1993).

Significant changes have occurred in Gulf of Guinea fish stocks, most notably the collapse of the *Sardinella aurita* fishery in the central upwelling region in 1973, coinciding with the proliferation of triggerfish *Balistes capriscus*. There was then a rapid decline in abundance of triggerfish in the late 1980s, coinciding with a rise in abundance of cuttlefish *Sepia officinalis* and globefish *Lagocephalus laevigatus* (Koranteng 1998). It is not known to what extent these species shifts were due to fishing pressure or environmental forcing.

Table 2.1. Commercial fish species in the Gulf of Guinea (Source: Koranteng *et al.* 1996).

Resource	Families	Species
Small (coastal) Pelagic	Clupeidae (small pelagics: sardines, bonga shad etc.)	*Sardinella aurita* *Sardinella maderensis* *Ethmalosa fimbriata*
	Scombridae (mackerel)	*Scomber japonicus*
	Engraulidae (anchovies)	*Engraulis encrasicolus*
	Carangidae (scads)	*Decapterus rhonchus*
Large Pelagic	Scombridae (tuna)	*Thunnus albacares* *Thunnus obesus* *Katsuwonus pelamis* *Euthynus alletteratus* *Istiophorus albicans* *Xiphias gladius* *Makaira nigricans* *Tetrapturus albidus*
Coastal Demersal	Sparidae (porgies, seabreams)	*Pagellus bellottii* *Sparus caeruleostictus* *Dentex canariensis*
	Haemulidae (grunts)	*Pomadasys incisus* *Pomadasys jubelini* *Brachydeuterus auritus*
	Sciaenidae (croakers, drums)	*Pseudotolithus* spp. *Umbrina* spp.
	Lutjanidae (snappers)	*Lutjanus fulgens,* *Lutjanus agennes*
	Mullidae (mullet)	*Pseudupeneus prayensis*
	Serranidae (groupers)	*Epinephelus* spp.
	Polynemidae (threadfins)	*Galeoides decadactylus*
	Penaeidae (shrimp)	*Parapenaeopsis atlantica* *Penaeus notialis*
Deep water Demersal	Sciaenidae (croakers, drums)	*Penteroscion mbizi*
	Ariommatidae	*Ariomma bondi*
	Geryonidae (deep sea crabs)	*Geryon maritae*
	Penaeidae (shrimp)	*Parapenaeus longirostris*

Variability of river inputs, depending upon climatic fluctuations of the monsoon, generally determines the distribution, life cycle and sizes of fish species in the thermally stable subsystems of the Gulf of Guinea. Since 1970, river inputs have decreased, as has the seasonal equatorial upwelling (Mahé 1991). It has been observed that generally abundant and comparatively large migrating pelagic fishes are displaying sedentarism and dwarfism (Marchal 1991) and adapting to scarcer nutrient inputs by living in deeper, colder waters and consuming less oxygen (Longhurst and Pauly 1987). This is presumed to be an adaptive response to environmental conditions and has been seen in other species from other areas (Tilot 1993).

3 Upwelling Dynamics in the Gulf of Guinea

The physical dynamics of the upwellings observed at the equator and along the coasts of Ghana and Côte d'Ivoire dominates previous oceanographic research in the Gulf of Guinea and eastern equatorial Atlantic. The coastal upwelling area has significant biological importance because it is an area of high fisheries productivity, particularly for the pelagic *Sardinella aurita* population. The various causal mechanisms that have been proposed for the coastal upwelling are reviewed here. The equatorial upwelling is not the subject of this investigation, however, its dynamics appear to be integral to those of the coastal upwelling so it is featured to some extent in this review. Interannual variability in the upwellings is also considered. A list of proposed mechanisms for the upwellings, and references supporting and opposing each theory, are given in table 3.1.

3.1 Wind driven Ekman divergence

Cold waters appear along the central Gulf of Guinea coast from 2^{o}E to 8^{o}W, where the winds blow nearly parallel to the coast (Picaut 1983). The coldest water is always found east of Cape Palmas and Cape Three Points. Because here the coastline is nearly parallel to the prevailing southwest wind, it suggests a typical coastal upwelling situation with a wind-driven offshore divergence of the surface water (Houghton 1976). Other early studies of this region (Longhurst 1964, Morlière and Rébert 1972, Verstraete 1970) also made this assumption, however, Longhurst's own work and that of FRU (1970) and Bakun *et al.* (1973) showed increasing evidence that such a simple mechanism doesn't suffice (Houghton 1976).

Certainly, local winds blow parallel to the shore all year round and cause offshore Ekman drift (Philander 1979, Bakun 1978). The wind speed in the region rarely exceeds 5 m s^{-1} (Roy 1995) which is weak compared to other upwelling regions. Nevertheless, the low latitude of the region means that the Coriolis parameter is large enough to generate offshore Ekman transport of sufficient strength to cause some upwelling of sub-surface, if not sub-thermocline, water (Ingham 1970).

Table 3.1. List of mechanisms proposed to explain the Ghana/Côte d'Ivoire coastal upwelling and references supporting or opposing each theory.

Physical forcing function	*References supporting*	*References opposing*
Local wind driven Ekman divergence	Longhurst 1964 Verstraete 1970 Morlière and Rébert 1972 Philander 1979	Houghton 1976 Bakun 1978 Picaut 1983
Heat gain through atmosphere	Pople and Mensah 1971	Houghton 1973 Verstraete 1985
Geostrophically induced upwelling	Ingham 1970 Philander 1979	Clarke 1979 Cane 1979
Advection by Currents		Bakun 1978
Current-Cape Interaction	Marchal and Picaut 1977	
Locally forced trapped waves	Clarke 1979	Picaut 1983 Verstraete 1992
Remotely forced trapped waves	Moore *et al*. 1978 Adamec and O'Brien 1978 O'Brien *et al*. 1978 Philander and Pacanowski 1980 Servain *et al*. 1982 Busalacchi and Picaut 1983 Houghton 1983 Picaut 1983 McCreary *et al*. 1984 Houghton and Colin 1986 Philander and Pacanowski 1986a Verstraete 1987 Verstraete 1992	Clarke 1979 Philander 1979

Seasonal intensification of winds occurs each year (Picaut 1983), however, this is weak both at the coast and offshore (Verstraete *et al.* 1980). This annual intensification of the southerly winds in the Gulf of Guinea is also called the African monsoon (Verstraete 1992). At 2^{o}-6^{o}N and east of 5^{o}W, the local alongshore winds are weakest in May and strongest in August. They increase by less than 0.25 dyne cm^{-2} (Verstraete 1992), yet somehow the seasonal upwelling which occurs along these coasts between June and September is strong enough to cool SST by about 5^{o}C (Verstraete 1992).

Verstraete (1970) found that the weak mean winds along the coast of Côte d'Ivoire should give a maximum vertical upward movement of 0.7 m day^{-1} (8.1×10^{-6} m s^{-1}). This is much smaller than vertical velocities inferred from observations of vertical displacement of isotherms in the thermocline. Houghton (1976) observed vertical flow on the continental shelf off Tema, Ghana of 8×10^{-5} m s^{-1} or 6.9 m day^{-1}. Picaut (1983) computed an upward phase

propagation of the upwelling event of 7 m day^{-1} from 350 m to 50 m from the isotherm vertical displacements at a station situated 40 km off Abidjan, Côte d'Ivoire.

Additionally, a study of the Sverdrup balance in the Gulf of Guinea in 1982–1984 showed that the frictional influence of the average local meridional wind stress component was unable to penetrate through the strong tropical thermocline lying at 50 m (Verstraete and Vassie 1990).

Another problem with the theory of Ekman transport driven by local alongshore winds being responsible for the observed cold water upwellings in the Gulf of Guinea is that Bakun (1978) found the alongshore winds produced an offshore seasonal Ekman transport maximum off the Togo and Benin coasts (0^o-4^o E) and further east in the Bay of Biafra. This area lies to the east of the observed SST minimum and upwelling of cold water is very poor or non-existent here (Picaut 1983).

Thus, all attempts to correlate the intensity and duration of the upwelling with local coastal winds have failed. Particularly, the studies of Houghton (1976), Bakun (1978) and Picaut (1983) all failed to find a correlation between the near shore SST variations and local winds (Verstraete 1992).

Some studies had proposed that meridional, cross equatorial winds in the eastern tropical Atlantic could account for both the equatorial and coastal upwellings. Cromwell (1953) first suggested how a southerly wind may influence equatorial upwelling (McCreary *et al.* 1984), supported by data for the Pacific Ocean. The models of Philander (1979) and Cane (1979) demonstrated how southerly winds could drive an eastward surface current around 3-4^oN (discussed later), however, they did not produce Ekman divergence along the eastern boundary north of the equator. The 3D model of Philander and Pacanowski (1981a) showed upwelling at and south of the equator and the eastward jet around 3^oN, but as with the earlier models, no upwelling was produced along the eastern boundary north of the equator. However, these models also showed that southerly winds at the equator produce the

characteristic asymmetry observed in equatorial circulation patterns (Houghton and Colin 1986). Verstraete (1992) observed that in 1984 the minimum in sea level at the equator, associated with upwelling, occurred prior to the intensification of southerly winds, so they could not have caused the upwelling.

Thus, observations as well as numerical experiments show that neither Ekman divergence at the equator nor at the coast can explain a significant part of the annual upwellings in the Gulf of Guinea (Verstraete 1992).

3.2 Heat gain from atmosphere and coastal thermohaline convection

During mid-July in 1970, it was noted that SSTs fell 6^{o}C over a 3 day period during which there were no local winds (Pople and Mensah 1971). To account for this change, Pople and Mensah (1971) examined measurements of temperature and salinity profiles and concluded that the upwelling was the result of evaporation, which increases the surface salinity, initiating a thermohaline convective cell of sinking water being compensated by upwelling in adjacent areas, vertically mixing the water column down to the seabed (Houghton 1973).

This hypothesis was questioned by Houghton (1973) for several reasons. Primarily, he found it impossible to balance the local heat budget; in order to drive the large evaporation rates deduced from the observed salinity changes, more heat would be required than is ever available from solar radiation or thermal conduction. Houghton also found no significant difference between the evaporation measured before and during upwelling and no significant deviation from bulk predictions.

Verstraete (1985) also showed that surface coolings are not the result of the seasonal variations in heat gain from the atmosphere through the surface and are not confined to the upper mixed layer. Additionally, estimates of the seasonal variation of heat content in various parts of the equatorial Atlantic Ocean were found to be about 10 times larger than the seasonal variations of the heat gain from the atmosphere through the surface (Merle *et al.*

1980). The annual cycle of heat content actually appears to be mainly due to vertical movements of the thermocline by dynamical processes (1980), especially the upward movement of cold, subthermocline SACW (Verstraete 1985).

3.3 Mechanisms involving currents

3.3.1 Geostrophically induced upwelling

Ingham (1970) was the first to present the idea of "current-induced" upwelling along the central coast of the Gulf of Guinea. Along the Ghanaian and Ivorian coast, the thermocline shoals towards the coast and the Guinea current is in geostrophic balance associated with this slope. Additionally, the thermocline rises seasonally from ~60m to ~10m depth (Roy 1995). It had been suggested that an acceleration of this eastward current, as observed by Ingham (1970) during the northern summer, could increase the slope and thus give favourable conditions for coastal upwelling (Picaut 1983). Ingham (1970) actually concluded that current induced upwelling was present throughout the year and was supplemented by wind-driven upwelling during the boreal summer to produce the observed SST decrease.

The idea was developed by Philander (1979) in a non-linear two-dimensional numerical model driven by meridional, cross equatorial winds. This study showed that intensification of winds at and south of the equator during the northern summer can strengthen the Guinea current causing a shoaling of the thermocline near the Ghana and Côte d'Ivoire coast. This leads to favourable conditions for upwelling along the coast where local winds drive an offshore Ekman drift. On the other hand, this model results in insignificant coastal upwelling and the thermocline remains undisplaced at the coast (Clarke 1979). Therefore, coastal SST decreases only by vertical mixing in the Guinea current (Picaut 1983). The three dimensional equatorial ocean model of Cane (1979) showed analogous phenomena to Philander's model as a nonlinear response to southerly wind forcing, however, the eastward jet in this model produced downwelling rather than upwelling. Thus, although meridional winds do contribute

to the intensification of the Guinea current during the northern summer, the upwelling they generate along the northern coast is either insignificant or non-existent and cannot, on its own, explain the observed cooling along the central Gulf of Guinea coast.

3.3.2 Advection by currents

Another problem with the theory of currents contributing to coastal upwelling is that the region of maximum upwelling is situated to the west of the region of maximum alongshore wind stress and Ekman drift (Bakun 1978). As the Guinea current flows eastwards, it could not have advected the cold SST associated with the upwelling from the area of maximum Ekman drift to the area of maximum observed upwelling intensity because this is in the opposite direction. In the subsurface layer flows the westward Guinea undercurrent (LeMasson and Rébert 1973a,1973b). This does flow in the right direction for advection to take place, however, it is too small to account for the observed difference in position (Picaut 1983).

3.3.3 Current-cape interaction

Another mechanism by which currents could force upwelling was proposed by Marchal and Picaut (1977). They noticed the presence of a shallow thermocline and cold water patches downstream of Cape Palmas and Cape Three Points and a deep thermocline and accumulation of warm water upstream of these capes (Picaut 1983). This led them to suggest that dynamic interaction between the two capes and the flow of the Guinea current could lead to a shallowing of the thermocline downstream of the capes and an accumulation of water upstream. This would be enhanced on the wide and shallow shelf east of Cape Three Points (Picaut 1983), although Morlière and Rébert (1972) showed that the cold water patch near Cape Palmas extends further downstream (Picaut 1983). The ‘cape effect’ also appears to increase from July to September (Picaut 1983), coinciding with intensification of the Guinea

current. However, this interaction probably plays a secondary role in the mechanism of the coastal upwelling (Picaut 1983).

3.4 Locally forced trapped wave theory

The failure of these mechanisms led Clarke (1979) to use coastal trapped wave dynamics, described by Gill and Clarke (1974) and Clarke (1977), to attempt an explanation of the coastal upwelling (Picaut 1983). Bakun (1978), as previously mentioned, noted that maximum values of offshore transport occur to the east of the location of the most intense upwelling, and that there was nothing in the local Ekman transport distribution to account for the continuity of the temperature minimum to the west. Clarke (1979) proposed that the sudden increase in local winds might force a westward propagating, first order, baroclinic wave, resembling a coastally trapped internal Kelvin wave. Allowing for dissipation of the wave over approximately 450-1500 km, a hindcast of the upwelling using coastally trapped forced wave theory gave qualitatively reasonable results. In particular, the coastal wind appeared to produce upwelling several hundred kilometres to the west of the region of forcing. Unfortunately, his model produced a sea level response that was too small by a factor of 3-5, the length of the forcing area being too small (Picaut 1983) and the coupling coefficient used (which measures how efficiently wind stress couples to the ocean) was much too big to be realistic (Verstraete 1992).

3.5 Remote forcing

3.5.1 Mechanism

The lack of support for a local forcing mechanism for both the coastal and equatorial upwellings led to remote forcing being proposed as a driving mechanism for the processes (Picaut 1983). The term generally refers to remote forcing west of the Gulf of Guinea (Picaut 1983).

Based on the theoretical works of Moore (1968) and Lighthill (1969), Moore *et al.* (1978) were the first to suggest that, both at the equator and along the coasts of the Gulf of Guinea, a significant fraction of the annual upwelling is forced remotely by a sudden increase of the easterly wind in the central-western equatorial Atlantic (Picaut 1983, Verstraete 1992). This impulse generates equatorially trapped Kelvin waves which travel eastwards across the Atlantic until they reach the west coast of Africa. There they diverge north and south, becoming trapped by the coast. The coastally trapped waves propagate westward along the zonally oriented Ghana and Côte d'Ivoire coastline, observed through a phase lag (Picaut 1983). The theory was later modified to include the reflection of Rossby Waves back across the Atlantic in a westward direction travelling both north and south of the equator (O'Brien *et al.* 1978, Adamec and O'Brien 1978).

3.5.2 Modelling studies

The theoretical idea has been illustrated in the numerical one-and-a-half layer model studies of O'Brien *et al.* (1978), Adamec and O'Brien (1978) and Bah (1981). In these models, the winds were switched on impulsively (Picaut 1983). The numerical studies of O'Brien *et al.* (1978) and Adamec and O'Brien (1978) gave an extremely simple linear model of the equatorial Atlantic which showed the physical mechanism in a theoretical context. The trapping scales used were 225 km at the equator (corresponding to the second baroclinic mode) and 100 km along the northern coast. In both studies, a westward impulse of 0.25 dyne cm^{-2} was applied in the western equatorial Atlantic. At days 55 to 70, the progression of the upwelling Kelvin wave along the equator and along the coasts raised the thermocline by 45 m and lowered sea levels by nearly 10 cm, values consistent with observations (Verstraete 1992). By including the effects of nonlinearities, such as Doppler shift due to current advection along the equator in an opposite sense to wave propagation and an amplified stress term due to the inclusion of local depth, Adamec and O'Brien (1978) were able to amplify and prolong the upwelling to more closely resemble the observed event.

The authors recognised that their model and its forcing were undoubtedly too simple (Verstraete 1992). The model was analogous to the explanation for the El Niño event in the eastern Pacific proposed by McCreary (1976) and Hulburt *et al.* (1976). However, these early theoretical and numerical works were very important in demonstrating the power of the 'remote forcing' concept in explaining the seasonal upwelling in the eastern Atlantic as well as the El Niño in the eastern Pacific.

Philander and Pacanowski (1980) used impulsive forcings of zonal winds in a multi-layer ocean model. Their simulations showed that zonal winds excited wave fronts at the coast which then propagated across the ocean setting up zonal pressure gradients. The wave modes within and above the strong shallow tropical thermocline are responsible for the adjustment of the upper ocean at low latitudes. These thermocline trapped modes were able to extend to depths greater than those of the wind-driven surface currents, giving rise to the Equatorial undercurrent in the thermocline.

A linear reduced gravity model of the tropical Atlantic was developed by Busalacchi and Picaut (1983) incorporating realistic coastline geometry and a single baroclinic mode. It was periodically forced using realistic winds from the whole of the tropical Atlantic. They found that the annual sea level response, relating to the major upwelling season along the coast of the Gulf of Guinea, is most strongly influenced by zonal winds west of 10^{o}W. Zonal winds east of 10^{o}W were observed to have a secondary influence along the zonally oriented coast of the Gulf of Guinea, but were cancelled out by meridional wind stress variations at the eastern boundary. The semi-annual sea level response, relating to the minor upwelling season along the Gulf of Guinea coast, was shown to be forced to approximately the same extent by local and remote winds.

Problems with reduced-gravity models, such as these, are their inability to generate vertical phase propagation, observed both in the eastern equatorial Pacific (Lukas 1981) and in the Gulf of Guinea (Picaut 1983, Verstraete 1985) and only continuously stratified models can

simulate this feature (McCreary 1981, 1984). This may explain why the model of Busalacchi and Picaut (1983) showed poleward propagation of the upwelling signal as far north as Senegal, much further north than observations suggest. Additionally, Cane and Sarachik (1979) questioned the significance of forcing based on a single baroclinic mode.

McCreary *et al.* (1984) used a linear, viscid and continuously stratified 3D model to investigate remote forcing in the eastern tropical Atlantic. The ocean basin is an idealised version of that of the tropical Atlantic and the wind stress used to force the model was an idealised representation of the annual variation of the equatorial trades in the western Atlantic. The model contained no wind forcing in the eastern Atlantic. A single baroclinic mode did not dominate the response of this model. Instead, waves associated with several modes superimposed to form beams that propagate energy vertically as well as horizontally (McCreary 1984). The response along the equator was predominantly a combination of a beam of equatorial Kelvin waves and a lowest order Rossby beam. Along the coast of Africa around 5^{o}N, it was approximately a beam of coastal Kelvin waves. The phase speeds produced by the model of horizontal and vertical propagation of the upwelling along the coast are consistent with observations.

One characteristic of equatorially trapped Kelvin waves, and hence remote forcing, is that their meridional structure should be distributed symmetrically about the equator, however, this is not generally observed in the eastern equatorial Atlantic. Instead, the meridional structure in and above the thermocline is asymmetrically distributed (Houghton and Colin 1986). As previously mentioned, models such as Philander (1979) have shown this to be a property of meridional wind forcing.

Nonetheless, numerical experiments by Philander and Pacanowski (1986) confirm that remote forcing by changes in zonal wind stress in the western central equatorial Atlantic is the main process in seasonal changes in the thermocline depth in the eastern equatorial Atlantic, and a secondary process along the coasts (Verstraete 1992).

3.5.3 Observational evidence

The suggested mechanism for remote forcing involves an abrupt intensification of winds in the western Atlantic and propagation in the horizontal plane, eastward along the equatorial wave guide and westward along the coast, and also in the vertical plane. Thus, the proposed mechanism suggests a probable connection between the equatorial and coastal upwellings in the Gulf of Guinea (Verstraete 1992). The poleward propagation of upwelling internal Kelvin waves means upwelling should also be observed along the tropical west African coast south of the equator. A number of observations support the idea of remote forcing (Picaut 1983) by providing evidence for the various processes involved. Others, however, appear to contradict it.

WIND FORCING

The rapid seasonal increase of westward wind stress in the western Atlantic can be considered as an initial forcing factor (Verstraete 1992). Continuous observations (1979-1988) of wind stress at St Peter and St Paul rocks, in the western Atlantic (1^{o}N, 29^{o}W), indicate that the trade winds relax and strengthen through a series of strong bursts superimposed on the seasonal cycle, and that an impulse forcing is appropriate from intraseasonal to seasonal time scales (Verstraete 1992). West of 0^{o}-5^{o}W, the easterly trade winds prevail. In general, intensification of the westward wind stress first begins in April, between 0^{o} and 10^{o}W, and then moves westward. Between 0^{o} and 30^{o}W, the zonal component of the wind stress presents a biannual signal, with two maxima and two minima. At 30^{o}-40^{o}W, winds are weakest in April and strongest in September, increasing by about 0.5 dyne cm^{-2} (Verstraete 1992). Additionally, the most pronounced seasonal variation of the wind stress is to be found in the western part of the equatorial Atlantic (Picaut 1983).

Servain *et al.* (1982), on a non-seasonal time scale, correlated SST variability in the Gulf of Guinea with wind stress variability from various regions of the tropical Atlantic. They showed the highest correlation between the two for the zonal component of the wind stress off

the northern coast of Brazil with a one month lag. This is the time required for an equatorial Kelvin wave, with phase speed of approximately 1 m s^{-1} to travel from the forcing area to the Gulf of Guinea. It is slower than a first baroclinic mode and is more in line with a second mode or a combination of several lower order modes.

Houghton and Colin (1986) noticed that the sudden intensification of the zonal wind stress recorded at 29°W was approximately 6 weeks earlier in 1983 than in 1984 and this time shift was repeated in the SST record, with cooling at the equator occurring approximately 6 weeks earlier in 1983. They, therefore, concluded that the equatorial upwelling is forced primarily by the zonal wind stress distributed to the west of 4°W. On the other hand, the relationship between westward wind forcing and coastal upwelling is less distinct occurring only 2 weeks earlier in 1983 (Houghton and Colin 1986).

The existence of a semi-annual signal in the zonal wind stress over the western Atlantic matches the distinct semi-annual cycle observed in the thermal and salinity structures in the Gulf of Guinea (Verstraete 1992).

HORIZONTAL PROPAGATION

As previously discussed, the large seasonal variations in the rate of change of heat content observed in the Gulf of Guinea cannot be explained by the seasonal variations of the heat gain from the atmosphere through the surface. However, Verstraete (1987) managed to balance this heat budget by showing that SACW is present in the cold surface waters during upwelling. SACW is advected into the Gulf of Guinea from the west by equatorial counter-currents, especially the Equatorial undercurrent, and poleward along the shelf edge by the coastal Guinea undercurrent (Verstraete 1987, 1992). These movements were demonstrated in Philander and Pacanowski (1986) using a GCM of the tropical Atlantic. There is also a return westward flow in the thermostad regions flanking the Equatorial undercurrent at 2°-3°N and 2°-3°S (Verstraete 1992).

The Equatorial undercurrent is theoretically driven by the zonal pressure gradient across the Atlantic (Katz *et al.* 1977, Philander and Pacanowski 1981b). Additionally it appears that zonal wind forcing is responsible for the sloping thermocline and hence zonal pressure gradient, in the equatorial Atlantic. Katz *et al.* (1977) showed strong correlation between the seasonal cycle of the zonal pressure gradient in the central equatorial Atlantic and zonal wind stress in the western equatorial Atlantic. This work is supported by the observations of Katz and Garzoli (1982). More recently, Verstraete and Vassie (1990) have shown the vertically integrated zonal pressure gradient to 130 m is in equilibrium with the zonal wind stress in the western Atlantic.

Although these zonal pressure gradient studies do not directly support the remote forcing mechanism of Moore *et al.* (1978), they do demonstrate the effect of wind forcing on the vertical thermal structure of the equatorial Atlantic and the movement of subthermocline water from the western to eastern equatorial Atlantic along the path proposed by Moore *et al.* (1978). Using sea level data, Verstraete and Vassie (1990) found evidence of remotely forced second baroclinic mode Kelvin waves in the equatorial Atlantic between February 1983 and November 1984. Additionally, Houghton (1983) noticed that the rapid vertical displacement of the thermal structure between the warm (March-May) season and the cold (July-August) season was trapped at the equator with vertical and meridional scales appropriate to a second or third mode baroclinic Kelvin wave.

Detailed analysis of SST and subsurface thermal structure by Merle (1978) and Houghton (1983) reveal that the equatorial and coastal regions are separate and their trapping scales do not overlap. This is consistent with the proposed remote forcing theory because the trapped waves travel along boundaries with no requirement for their meridional scales to overlap.

One problem with the original theory of Moore *et al.* (1978) is that data they presented indicated that the internal Kelvin wave they refer to would have, at the most, 15 days to travel from 10^{o}W on the equator to Tema on the coast of Ghana, a distance of approximately 3700

km. Taking the realistic speeds of 100 km day^{-1} for the internal equatorial wave and 60 km day^{-1} for the coastal wave implies it would take the wave 45 days to travel the required distance, much longer than the observed time of 15 days (Clarke 1979). Further analysis of the paper by Moore *et al.*, however, reveals that they probably did not record the beginning of the equatorial upwelling signal. Servain *et al.* (1982) obtained a much more realistic phase lag of 1 month. Houghton (1983) also observed, in 1964, the time lag between the onset of upwelling at the equator and the coast as being of the order of one month.

Picaut (1983) directly observed poleward propagation of the major upwelling along the central coast of the Gulf of Guinea using historical SST data. The upwelling event propagated westward with a mean speed of 0.7 m s^{-1}. Houghton (1983), on the other hand, observed the vertical displacement of the thermal structure associated with the coastal upwelling to be tightly trapped at the coast from 2^{o}E to 10^{o}W in much the same way as the band of low SST. However, the trapping scales of this displacement implied a westward propagation speed for a coastal Kelvin wave nearly twice that observed by Picaut (1983). Houghton and Colin (1986) showed phase propagation at the equator to lead propagation at the coast during 1983 and 1984.

Although the upwelling has been observed along the Ghana and Côte d'Ivoire coasts and at the equator, no upwelling signal has been recorded further east along the coast, as would be expected for a coastal trapped Kelvin wave. If an upwelling signal did in fact propagate to the Ghana and Côte d'Ivoire coasts from the western equatorial Atlantic as suggested, one would expect to find upwelling all along the Gulf of Guinea coast but this is not reflected in the SST data (Clarke 1979). This may be due to the presence of a lens of warm, low salinity waters in the surface layer of this region, originating from the discharge of the Niger and Cameroonian rivers (Merle 1978, Mahé 1993).

Many of the features observed along the Ghana and Côte d'Ivoire coastlines have also been observed south of the equator. Picaut (1983) observed poleward propagation of upwelling

from 1°S to at least 13°S at the same phase speed as north of the equator. Furthermore, the northern and southern hemisphere coastal upwelling signals both appeared to start at the same time from the equator (Picaut 1983).

The upwelling event at Pointe-Noire (Angola) precedes that at Abidjan by about one month, both at the surface and at depth, with two warm seasons in February-March and October-November (high sea levels) and two cold seasons in December-January and June-July (low sea levels) (Verstraete 1992). This is consistent with Pointe Noire being situated closer along the coastal boundary to the equator than Abidjan but lying at approximately the same latitude.

VERTICAL PROPAGATION

Vertical propagation of upwelling has been shown both at the equator and at the coast. Houghton (1976) observed vertical flow on the Ghana coast of 6.9 m day^{-1}. Picaut (1983) showed upward phase propagation of the upwelling event at 7 m day^{-1} from 300 m to the surface. Houghton and Colin (1986) showed vertical displacement of isotherms associated with the seasonal upwellings throughout the upper 350 m at both the equator and the coast for 1983 and 1984. In all instances, the phase at depth led the surface. Verstraete (1992) analysed the upper water masses and thermostad regions of the eastern equatorial Atlantic. He noted the advection and vertical spreading of SACW between 500 m and 50 m from May to July off Abidjan.

As well as general uplifting of the vertical structure, Verstraete (1992) describes a deep eastward jet at the equator, isolated from the Equatorial undercurrent core, between 325 m and 250 m in July 1984. Its Rossby radius of deformation was consistent with the second baroclinic mode. This is in agreement with the theory of a remotely forced deep equatorial jet generated by equatorial Kelvin beams (McCreary 1984). Weisberg and Weingartner (1986) observed that the vertical structure of the baroclinic response to the winds and thermocline depth varied seasonally in the western Atlantic. When the winds were weak and the thermocline was shallow, the baroclinic response was primarily effected over the upper 50 m.

After the winds intensified and the thermocline deepened, the baroclinic response extended down to at least 150 m.

At depth, the coastal upwelling has an amplitude and duration that resemble more the upwelling at the equator than the thermocline above. Due to sparse and noisy data obtained in 1983, Houghton and Colin (1986) acknowledge that the data suggest, but do not unambiguously define a fixed phase lag between the equatorial and deep coastal upwelling that would be required if the coastal event were forced by a wave propagating from the equator. However, Houghton and Colin (1986) noted that at the coast there was such a qualitative difference between the shape of the curves in the isotherms at depth and from the thermocline upwards, that it is doubtful whether a single event was acting throughout the water column. The coastal upwelling is also found to be associated with a sloping thermocline that often extends nearly to the equator. The shoaling of the 20^{o}C isotherm, which is representative of the thermocline depth, is at first trapped close to the coast with a length scale of less than 100 km but later extends equatorward with scales of 200–300 km. This is in contrast to the upwelling at depth which remains trapped to within 100 km of the coast.

3.6 Interannual variability in upwelling

Seasonal variability in the equatorial Atlantic is generally greater than interannual variability (Servain *et al.* 1985). Nevertheless, marked interannual variability does occur in this region. Along the Ghana-Côte d'Ivoire coastal system a constant intensification of the wind stress appears to have taken place over the last 30 years (Roy 1995). An intensification of the coastal westward undercurrent is also thought to have occurred during the 1980s (Binet and Marchal 1993), however, this is based on current observations collected during FOCAL/SEQUAL in 1983 and 1984, a period of unusual conditions in the Atlantic due to one of the strongest El Niños this century occurring in the Pacific in 1983.

During the first half of 1984, the upper ocean was unusually warm in the eastern equatorial Atlantic and upwelling was inhibited along the southwestern coast of Africa (Philander 1986). Weisberg and Colin (1986) reported an absence of the zonal SST gradient along the equator during the season it would normally have been at a maximum. Additionally, the tropical thermocline deepened by about 50 m and sea levels rose in the eastern equatorial Atlantic (Verstraete 1992) and simultaneously the eastward zonal pressure gradient in the western-central Atlantic nearly disappeared (Katz *et al.* 1986, Verstraete and Vassie 1990). The event was linked to a huge reduction of the surface trade winds (Hisard *et al.* 1986, Katz *et al.* 1986, Horel *et al.* 1986). These regional changes in the atmospheric circulation over the equatorial Atlantic coincided with planetary-scale adjustments in the tropical atmosphere. The major equatorial upwelling season in 1984 did, however, take place, although SST at 6^{o}E and 4^{o}W on the equator was about 3^{o}C warmer in June-August 1984 than over the same time period in 1983 (Verstraete 1992). It appears that this warm event was phase-locked to the annual cycle, a characteristic of the ENSO events in the Pacific. This has led to the phenomenon being termed an Atlantic Niño.

Atlantic warm events (Niños), have been noted to occur periodically in the western Atlantic. These cause the incursion of warm water from the equatorial region into the Gulf of Guinea, which travels down the coast as far as the Benguela current in the south (Hisard 1988). The two previous Atlantic warm events with comparable amplitude occurred in 1934 and 1963 (Hisard 1988, Hisard *et al.* 1986). It has also been noted that Atlantic Niños tend to occur the following year to ENSO events, suggesting that the two phenomena are connected (Bakun 1996). This time lag between the basins was seen in 1973, 1984 and 1987, however, the warm event of 1962-63 in the Gulf of Guinea appears to have preceded the Pacific El Niño of 1963-64. According to Verstraete (1992), it is very likely that remotely-forced equatorial dynamics also govern this “quasi El Niño” in the eastern equatorial Atlantic Ocean.

An intensification of the minor upwelling season along the coast has been observed with a continuous decrease of SST starting in the mid 1970s. An increase in SST difference between

coastal and offshore areas has also been observed over the same period (Pezennec and Bard 1992). Decomposition of the SST signal into various components showed that the long term trend was one of SST increase, perhaps linked to global warming (Mendelssohn and Roy 1994, Koranteng 1998).

3.7 Discussion

Many mechanisms have been suggested to explain the seasonal upwellings observed in the eastern equatorial Atlantic, both at the coast and at the equator, however, none have been able to account for all the observed features of these phenomena. Theories are mainly for the major upwelling as this is the most studied, however, there is evidence, such as the semi-annual signal in wind stress in the western Atlantic, that they may also apply to the minor upwelling. The greatest amount of support is for the remote forcing mechanism. This is seen in the good correlation between intensification of wind stress in the western equatorial Atlantic and the observed upwelling events along the equator and the coast in the Gulf of Guinea, combined with evidence from observations and models for trapped internal waves leading to thermocline adjustment in these regions. The symmetrical upwellings seen either side of the equator at the eastern Atlantic boundary also support this theory. Thus, it appears that this is the dominant force driving these upwellings.

On the other hand, the lack of symmetry in the equatorial surface circulation and upwelling observed in the eastern equatorial Atlantic appear to support the role of local southerly wind forcing in equatorial dynamics. Further contradiction to the remote forcing theory is apparent in the observed insensitivity of the upwelling along the Ghana and Côte d'Ivoire coasts to shifts in the timing of the wind forcing west of the Gulf of Guinea and the large deformation scale of the upwelling in the surface layers along this coastline. This issue is partly resolved by the discovery of both deep and shallow upwelling signals at the equator and the coast. The deep signals appear consistent with the theory of remote forcing, however, the shallow signals are somewhat modified. At the equator, this can be explained by the influence of southerly

cross-equatorial winds. At the coast, however, the signal is so different that Houghton and Colin (1986) suggested a different event may be acting in these surface layers.

Even so, none of the other proposed mechanisms (local wind forcing, current induced upwelling, coastal trapped waves) are sufficient to generate the observed drop in SST. Additionally, the westward and vertical propagation of the upwelling at the coast and the abrupt thermocline shoaling provide enough evidence for the remote forcing hypothesis to not disregard it. Rather, it would appear that the remotely forced signal at the coast is modified by some other process in the surface layers within and above the thermocline. Although the effects of local wind forcing may contribute to this modification, they are probably too weak to directly modify the remote signal to the extent observed, however, the coastal trapped waves of Clarke (1979) could possibly enhance and modify the signal to more closely resemble the observed upwelling. So too could the intensified Guinea current, observed at this time of year, as suggested by Houghton and Colin (1986) and shown in the GCM of Philander and Pacanowski (1986).

Another potential consequence of the deep upwelling signal is the depth along the continental shelf slope at which the coastal signal is trapped. If the deep internal wave, seen trapped along the coastal boundary, were to split from the equatorial boundary at the island of São Tomé, in the same place the Equatorial undercurrent splits into the Guinea undercurrent and Gabon-Congo undercurrent, and then propagated along the shelf slope from there, it might avoid travelling through the Bight of Biafra altogether, further explaining the lack of an upwelling signal along this part of the coastline. This route would also reduce the distance the wave must travel to reach the coastal upwelling region.

Interannual variability in the coastal regime has also been noted. The conditions during 1984 were exceptional and it appears that similar warm events occur periodically in the equatorial Atlantic. The similarity between the conditions during this event and those during El Niño events in the Pacific has resulted in them being termed ‘Atlantic Niños’. Additionally, the

coincidence between several Atlantic Niño and Pacific El Niño events has led to suggestions that the two phenomena are linked. Interannual changes have also been observed as a long term trend with the minor upwelling season strengthening relative to the major upwelling season. It has been suggested this may be linked to global warming.

To recapitulate, the observed upwelling signal in the Gulf of Guinea is probably remotely forced by winds in the western equatorial Atlantic on a semi-annual basis and modified by a range of processes local to the Gulf of Guinea in the surface mixed layer. All the suggested mechanisms may play a part, with the exception of evaporation, but the lack of correlation with some mechanisms suggests they are not crucial to the upwelling. The extent of local forcing is probably greater for the minor upwelling season (January - February) than for the major upwelling season (July - September). Interannual variability also exists for this region, perhaps as a quasi-El Niño signal, and appears to be phase-locked to the dominant seasonal signal. Global warming may also be contributing to interannual changes in the upwellings.

4 Remote Sensing of SST

4.1 Introduction

4.1.1 Use of remote sensing

The two most important physical properties for tracing processes in the oceans are temperature and salinity. Because these properties are largely conserved, T-S diagrams have been used for many years to identify different water masses. Additionally, these can be used for showing mixing between water masses. As discussed in Chapter 1, SST is the only one of these two properties available from satellite-based remote sensors. Analysis of multi-year data sets of remotely sensed SST allows us to build up a picture of the time dependent ocean dynamics using relative differences in the radiative balance. This study used SST data derived from NOAA's AVHRR sensors. SST was used instead of ocean colour for two main reasons. Firstly, ocean colour, although resolving patterns in surface waters well, is not necessarily representative of the underlying physical dynamics, and secondly, due to problems throughout most of the 1980s with the CZCS sensors degrading, the quality of the data available over this period is poor. AVHRR SST data were used in preference to other SST products because they have the longest time series and are the best quality data available for the period. ATSR data have only been available since the early 1990s, so despite having a finer resolution and better atmospheric correction than AVHRR, ATSR had only been operational for five years at the start of this study and didn't cover the time frame of interest, the 1980s. The modern generation of Meteosat data (MOP generation) have only been available since 1989 and have poorer spatial resolution (5km) than AVHRR, although better temporal resolution (30 minutes). Meteosat was designed primarily for cloud detection and not SST measurement, so removal of atmospheric effects from SST is more difficult than with AVHRR.

In this study, remotely sensed SST has been used in preference to *in situ* data sets, such as COADS, because remote sensing provides much finer resolution in both space and time. Global SST monthly climatologies (e.g. Reynolds and Smith 1995), which blend *in situ* and remotely sensed data, were not considered suitable for this study because they do not give fine enough spatial resolution (1^{o}) and provide only long term averages, unsuitable for studies of interannual variability. The main drawback of using remotely sensed SST is measurements are restricted to the top few millimetres of the surface ocean, so provide no indication of subsurface thermal structure and are prone to 'skin effects' from diel variations in solar irradiance.

This study used the CORSA-AVHRR product (for details see below), instead of products available directly from NASA or produced by other organisations. This was for consistency with other studies that have been undertaken along the West African coast (see Cole 1997 and Maus 1997).

4.1.2 Remote sensing of the West African region

Remote sensing has been used extensively for monitoring the global oceans and a number of studies have used satellite derived SST data to study coastal regions along the coast of West Africa. These include studies on the north-west African region (Hernández-Guerra and Nykjaer 1997), the coastal area of Mauritania (Maus 1997), the Senegalese upwelling (Demarcq and Citeau 1995) and the Northern Benguela off Namibia (Cole 1997). CZCS data have been used to study the Benguela off Namibia and South Africa (Weeks and Shillington 1994). Additionally, compound remote sensing studies, combining SeaWiFS data with *in situ* measurements, have taken place on recent cruises along the north-west and south-west African coastlines as part of the Atlantic Meridional Transect (AMT) program (Robins and Aiken 1996, Aiken *et al.* 2000).

In the Gulf of Guinea, Aman and Fofana (1995, 1998) used Meteosat SST data to identify the location of upwelling and study seasonal variability along the coast of Côte d'Ivoire. They identified the major upwelling season and two periods of minor upwelling. The first of these minor events occurred in January during the harmattan period and the second event took place in March. The harmattan can cause deviations of the ITCZ, which may perhaps lead to upwelling (Allersma and Tilmans 1993). Demarcq and Aman (in press) have attempted to supplement Meteosat data with two *in situ* data sets: offshore COADS data (see below for details of COADS) and SST data from coastal stations in Ghana and Côte d'Ivoire. They report considerably improved spatial and seasonal precision with the blended product.

This chapter focuses on seasonal and interannual variability in SST. Special attention is paid to specific features related to the underlying physical dynamics of the system and of relevance to fisheries recruitment.

4.2 Data Acquisition and Pre-processing

The satellite data used is extracted from the Cloud and Ocean Remote Sensing around Africa (CORSA) AVHRR data set produced by the Space Applications Institute (SAI) at the Joint Research Centre (JRC) of the European Commission, located in Ispra, Italy. The data have been level 2 and level 3 pre-processed by the Marine Environment Unit of the SAI from level 1 GAC AVHRR data obtained under a scientific collaboration agreement with NASA. This processing includes masking out land and cloud pixels, validating the images against SST data from the Combined Ocean Atmosphere Data Set (COADS), NASA Multi-Channel SST (MCSST) and the Global Ocean Surface Temperature Atlas (GOSTA) and processing the daily images into 8-bit weekly composite images. Four weekly composites are produced for each month of the time series: the first three composites being seven-day averages and the final composite being an average of all the remaining days in the month (Cole 1997). The time series used extended from week 2 of July 1981 to week 4 of December 1991 with two missing weekly composites (week 1 of November 1989 and week 1 of January 1991), giving

a total of 501 weekly composite images. The CORSA-AVHRR images have a spatial resolution of 4km at the equator (GAC), which is sufficient for the investigation of shelf processes. The conversion of pixel digital number values (DNs) in the 8-bit images obtained from the JRC to SST values is

$$SST = \left(DN \big/ 10\right) + 8 \qquad 4.1$$

A comparative analysis between the CORSA-AVHRR product and NASA 'Pathfinder' 9km resolution AVHRR data showed the two data sets to agree within 1^{o}C in 96% of cases (C. Villacastin, JRC, Ispra, Italy, pers. comm.).

4.3 Cloud Contamination

The tropical location of the Gulf of Guinea means that the region has particularly high cloud cover and high levels of atmospheric water vapour content, which can influence the accuracy of satellite-borne radiometers. Therefore, to assess the usability of the data set, the degree of cloud contamination was derived. The term 'cloud contamination' is used to describe non-land pixels which had previously been recoded during the cloud-removal process of the JRC to have a value of zero. Firstly, a reclassification routine was applied to the images, which converts the original weekly composites into binary images. Non-cloud pixels were given a value of one and cloud pixels remained at zero. The percentage of cloud pixels for each weekly composite layer was then calculated by counting the proportion of pixels in each layer with a value of zero, excluding land areas. This calculation was performed for the whole Gulf of Guinea region and for each of the subsystem areas (shown in fig. 4.1a). The spatial distribution of cloud contamination was generated by summing the values for each pixel site from the binary layers. This procedure was carried out for the whole time series to show the overall spatial distribution of cloud contamination and on a month basis to show the seasonal pattern of cloud contamination.

The spatial distribution of cloud contamination throughout the entire data series clearly shows the area of highest cloud contamination to lie in a central band around 3°N (fig. 4.1a). This area of heavy cloud is associated with the mean position of the ITCZ. The monthly spatial distribution of cloud contamination shows the seasonal meridional migration of the ITCZ (fig. 4.1b). The frequency distribution of the degree of cloud contamination in 5% bands for the weekly composite layers is shown in figure 4.2a for the whole Gulf of Guinea region. Almost 80% of layers had less than 50% cloud contamination. Figure 4.2b shows the proportion of layers in each 25% band of cloud contamination for each of the subsystem areas. For the SLGP and CWAU subsystems, between 75% and 80% of the layers have less than 50% cloud contamination. This figure is lower for the EGOG subsystem (60.3%).

On average, for the whole Gulf of Guinea, cloud cover is highest from May to September, however, each subsystem shows a different seasonal cycle. The EGOG has the highest cloud cover in most months and peaks in August, as does the SLGP. Cloud cover in the CWAU peaks in June and then drops in July before increasing again slightly until September. Seasonal cycles of cloud cover are shown in figure 4.3.

4.4 Data Processing and Analysis Methods

4.4.1 Temporal statistics (spatial variability)

Descriptive statistical images (mean SST, standard deviation) were calculated across time from the weekly SST composite images to show the mean spatial pattern for the whole time series and areas of greatest variance, as well as the seasonal and interannual spatial variability. These images were examined to identify important oceanographic features, as well as large scale patterns of seasonal and interannual variability.

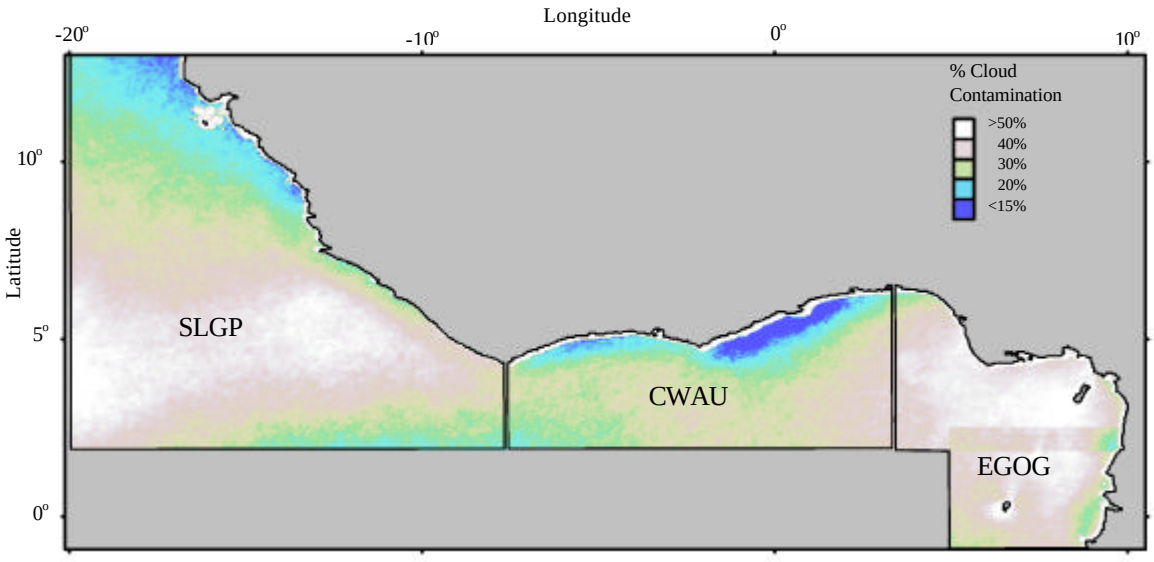

Figure 4.1a. Mean cloud contamination of images, averaged over the whole time series. Subsystem areas are shown. The term cloud contamination is used to describe cloud pixels which were recoded to a have a DN value of zero by the JRC during pre-processing.

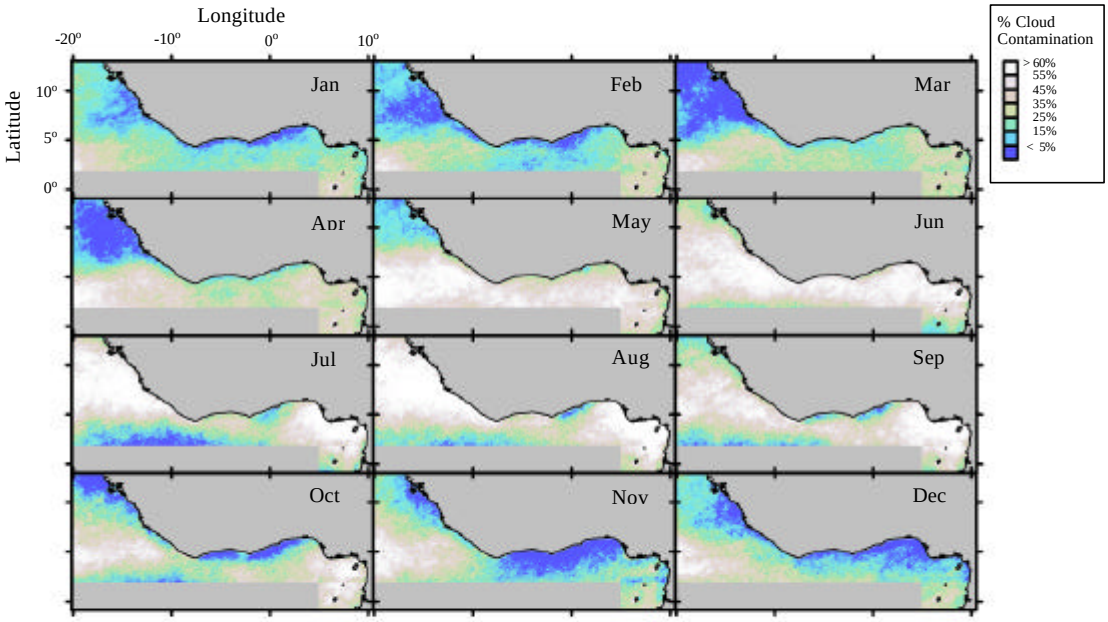

Figure 4.1b. Monthly mean cloud contamination from the CORSA-AVHRR data set, calculated from weekly composite images.

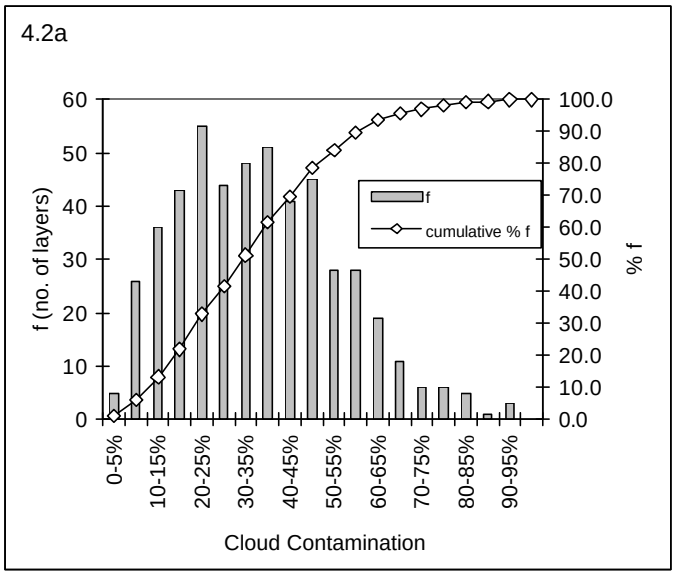

Figure 4.2a. Frequency of input images (layers) with different levels of cloud contamination (5% bands).

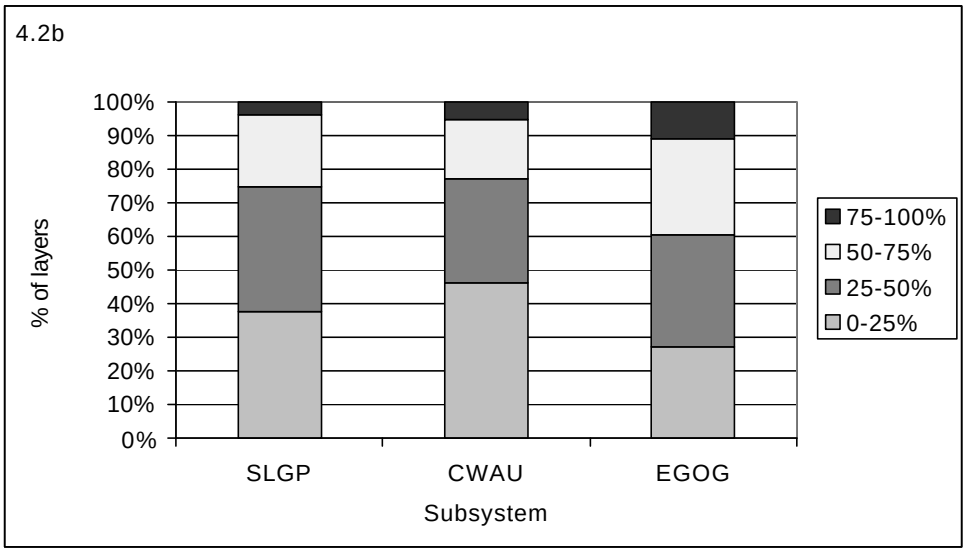

Figure 4. 2b. Proportion of input images (layers) showing different levels of cloud contamination (25% bands) in each subsystem.

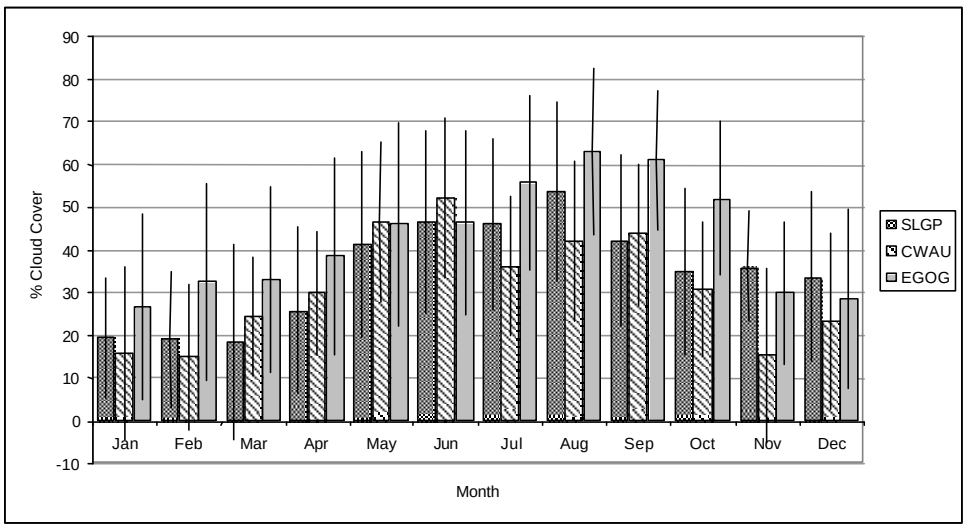

Figure 4.3. Mean seasonal cycle of cloud contamination in the Gulf of Guinea by subsystem. Error bars show one standard deviation.

4.4.2 Spatial statistics (temporal variability)

The weekly composite images were averaged spatially to show temporal trends in SST. Time series charts were constructed to show temporal variability in mean SST, both of a seasonal and interannual nature. The resulting mean SST time series was subjected to a 49 point moving average smoothing routine (modified from Chatfield 1989) to emphasise interannual variability.

Standardised SST anomalies were calculated to show unsmoothed seasonal and interannual variability on a weekly time scale. Interannual variability was shown by standardising data with respect to the week of the year (1-48), thereby eliminating seasonal variability (see equation 4.2a). Seasonal variability was shown by standardising with respect to the year (1981-1991), thereby eliminating interannual variability (see equation 4.2b).

$$\text{a) } X_{j_{week}} = \frac{r_j - \bar{r}_{week}}{s_{week}} \qquad \text{b) } X_{j_{year}} = \frac{r_j - \bar{r}_{year}}{s_{year}} \qquad 4.2$$

where $X_{j_{week}}$ and $X_{j_{year}}$ are the SST anomalies standardised with respect to the week and the year, respectively, r_j is the weekly mean SST value, $\bar{r}_{week}$ and $\bar{r}_{year}$ are the weekly and annual means, respectively and s_{week} and s_{year} are the weekly and annual standard deviations, respectively (modified from Koranteng 1998).

4.4.3 Spectral analysis

Spectral analysis is essentially a modification of Fourier analysis to make it suitable for stochastic rather than deterministic functions of time (Chatfield 1989). Power spectra (i.e. the absolute square of the complex Fourier transform) of the mean corrected time series, filtered with a Hanning window with 5 degrees of freedom, were generated, using a Fast Fourier Transform (FFT) routine, to show the period of any cycles present in the data. This was carried out using NAG routine G13CAF (Mark 18) in a FORTRAN program (NAG 1997).

SST signals relating to specific spectral peaks were extracted using a rectangular band pass filter in the SANTIS software package (Vandenhouten *et al.* 1996). This filters the signal in the frequency domain by cutting off specified low and high frequencies (Vandenhouten *et al.* 1996).

4.4.4 Indices of interannual variability in oceanographic features

SENEGALESE UPWELLING INFLUENCE

Interannual variability in the dominance of the Senegalese upwelling influence (henceforth known as the SUI) over the SLGP subsystem was measured as the anomaly from the latitude of the most southerly position reached by the feature. This occurred during either March or April for each year throughout the time series. The southern boundary is seen in the monthly composite images as a region of rapid temperature change (temperature gradient >1^{o}C per 100 km).

COASTAL UPWELLING

Interannual variability in upwelling along the coast of Ghana and Côte d'Ivoire was assessed quantitatively by calculating measures of both upwelling intensity and spatial extent for the major and minor upwelling seasons. These measures were calculated for a strip of 1^{o}x1^{o} boxes stretching along the coast from Cape Palmas to Cotonou (shown on fig. 4.4a). Upwelling intensity (I) was calculated for each box by subtracting the mean SST value for each box ($\overline{SST}$) from a SST of 25^{o}C, i.e. SSTs below 25^{o}C have positive values.

$$I = 25.0 - \overline{SST} \qquad 4.3$$

The value of 25^{o}C was chosen as this was the contour used to define the upwelling by Bakun (1978). The overall value for the season was then taken as the box with the maximum upwelling intensity value.

Spatial Extent (E) was calculated as the proportion of the total area (all boxes) having SST values less than a threshold level (T).

$$E = \frac{no.of\ pixels < T}{total no.of\ pixels} \qquad 4.4$$

For the major season the threshold level was SST below 23^{o}C and for the minor season it was SST less than 24.5^{o}C. These threshold limits were determined from examination of the SST contours associated with each of the upwelling seasons in the weekly SST composites.

The two indices were multiplied together to give a combined upwelling index (CUI).

4.5 Results

4.5.1 Overall

The overall mean SST image (fig. 4.4a), averaged through time for the whole time series, shows the southerly intrusion of water from the Senegalese upwelling region and the major upwelling areas along the coast of Ghana and Côte d'Ivoire to be the dominant cold water features of the system, superimposed on the warm waters of the tropical Atlantic. This image also shows a cold water influence, probably of equatorial upwelling origin, around the southern limit of the image. Additionally, there is a small, cool strip of water along the coast of Sierra Leone. Warm water, probably originating from river run-off, is visible around the mouths of major rivers. This is particularly noticeable around the Niger Delta and Cameroon coast, over the continental shelf of Guinea and Guinea-Bissau and around the Bijagos islands. A strong SST gradient, suggestive of a front, exists at the interface between the SUI and warmer, coastal waters around the Bijagos Islands.

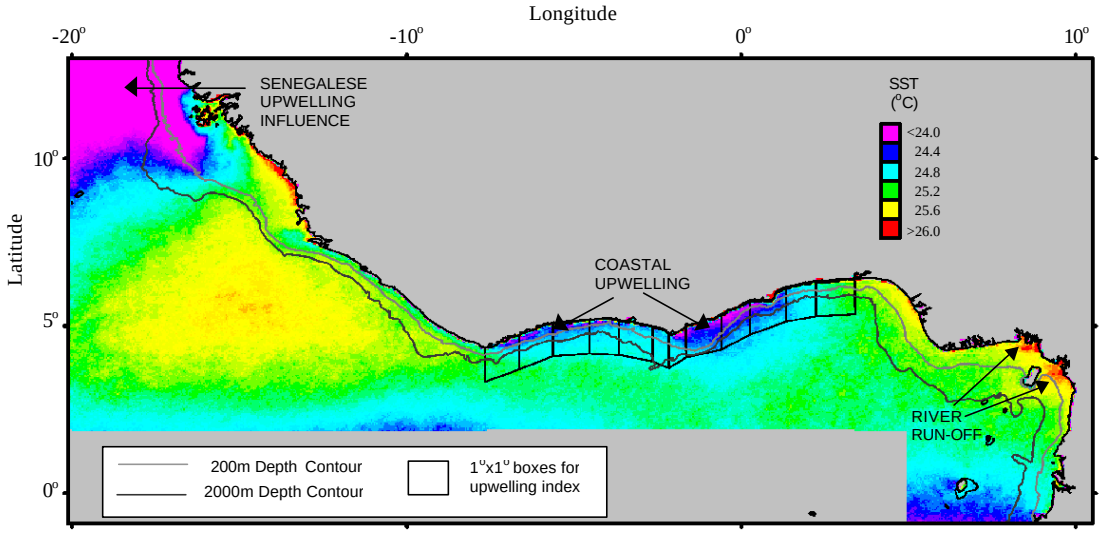

Figure 4.4a. Satellite derived SST for the Gulf of Guinea LME annotated to show major oceanographic features. This image is the mean SST derived from CORSA-AVHRR weekly SST composites for the period July 1981 to December 1991.

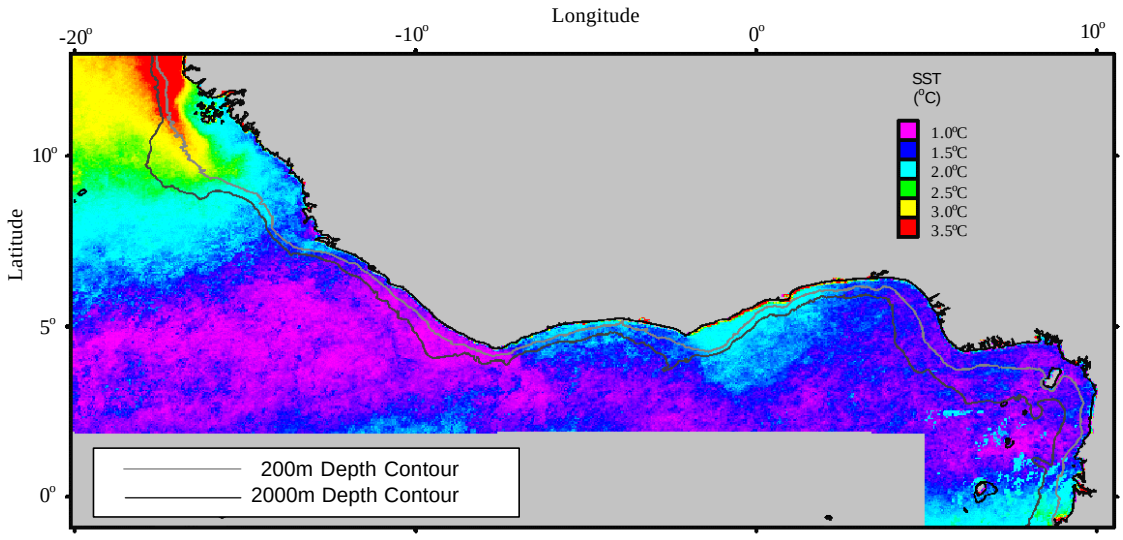

Figure 4.4b. Standard Deviation of SST in the Gulf of Guinea derived from weekly SST composites of CORSA-AVHRR data for the period July 1981 to December 1991.

Figure 4.1a shows the mean percentage cloud contamination of weekly SST composites for the region. The similarity in patterns between this image and the mean SST image reflects the high degree of coupling between atmospheric and oceanographic conditions in the region. The overall standard deviation image (fig. 4.4b) shows the greatest variance to be associated with the SUI. The coastal and equatorial upwelling areas also show a reasonably high degree of variability. This is expected given the seasonal nature of the upwellings.

4.5.2 Seasonal variability

Seasonal SST variability in the Gulf of Guinea is shown in figure 4.5.

SENEGALESE UPWELLING INFLUENCE

The SUI is composed of cold water (<19^{o}C at its core) originating from the Senegalese and Mauritanian coastal upwellings. It usually becomes visible in the Gulf of Guinea region during December and continues to move south until March or April. It then begins to recede. During this period, the coldest water extends in a narrow finger close to the coast of Senegal and Gambia, but then moves away from the coast of Guinea-Bissau, appearing to be trapped along the shelf break rather than the coast. The result is a cold tongue of SUI water encircling the Bijagos Islands. During May, the tongue of cold water is still present around the Bijagos Islands, but by June only a narrow cold water front remains. By July, the SUI is absent from the whole coast as far north as Cap Vert, Senegal and by August, the SUI is also absent from offshore waters.

TROPICAL SURFACE WATER

In the SLGP subsystem, warm Tropical Surface Waters (TSW) appear to be furthest south in March-April and then move north until November, when they begin to recede towards the south again. This coincides with the commencement of the southerly movement of the SUI. The movement of these warm tropical waters appears to be associated with the seasonal

migration of the ITCZ. The area of warm tropical waters appears to increase in size and temperature from January to May. Although they then appear to keep pushing north and growing in area, their temperature drops markedly from June to September. They have their greatest spatial extent, and are at their warmest (26^{o}-27^{o}C), during October and November.

In the CWAU subsystem, warming of the offshore area appears to start in February but is most noticeable from March to May. The warmer water tends to move in a north-easterly direction, associated with the seasonal movement of the ITCZ. The warm signal is damped from June to October by the summer upwelling along the Ghana-Côte d'Ivoire coastline to the north and by the equatorial upwelling to the south. This is especially visible during July to September when the warm signal is almost totally overridden. In November and December warmer waters appear over the whole area with the warmest waters in the north-easterly corner of the subsystem, towards the EGOG subsystem. These are related to the southerly movement of the ITCZ but could also be contributed to by river run-off from the EGOG subsystem.

In the EGOG subsystem, during February to March, warm water pushes in from the south. During April, the major warm water areas appear to be coming more from the east and north-east of the subsystem. In May, warm water areas are also present on the north coast. In June, the warm water extent diminishes and cold water appears in the south. The extent of warm water areas is minimal from July to September. Small warm water patches begin to occur along the Cameroon coast, in the north-east of the subsystem, in October, probably associated to some degree with river run-off. In November and December these areas spread and are also present along the northern coast. This southward expansion of warm water appears, again, to be associated with the seasonal movement of the ITCZ.

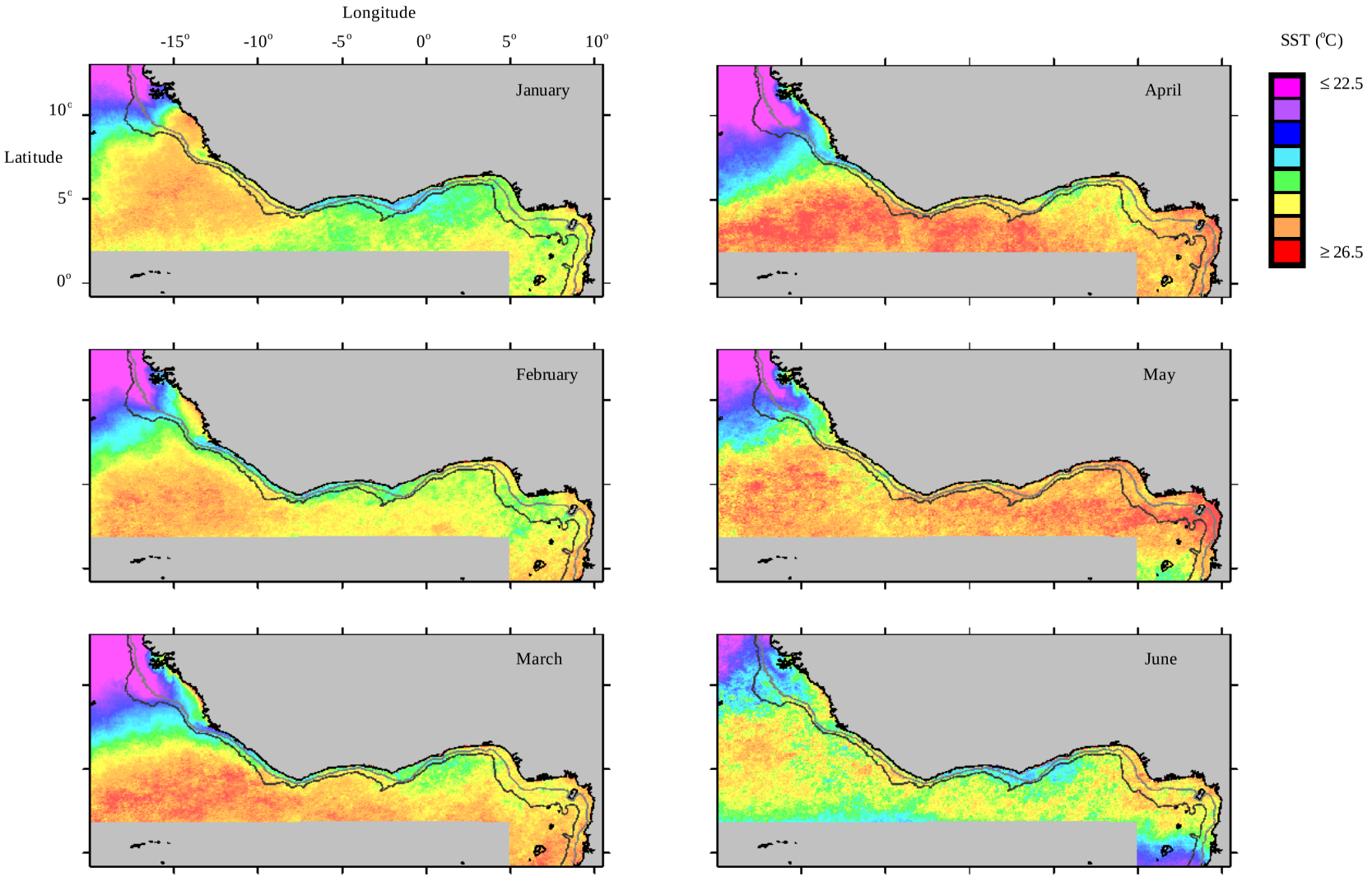

Figure 4.5. Monthly mean SST for the Gulf of Guinea from CORSA-AVHRR SST data. Each monthly mean is averaged from weekly SST composites for each month over the period July 1981 to December 1991.

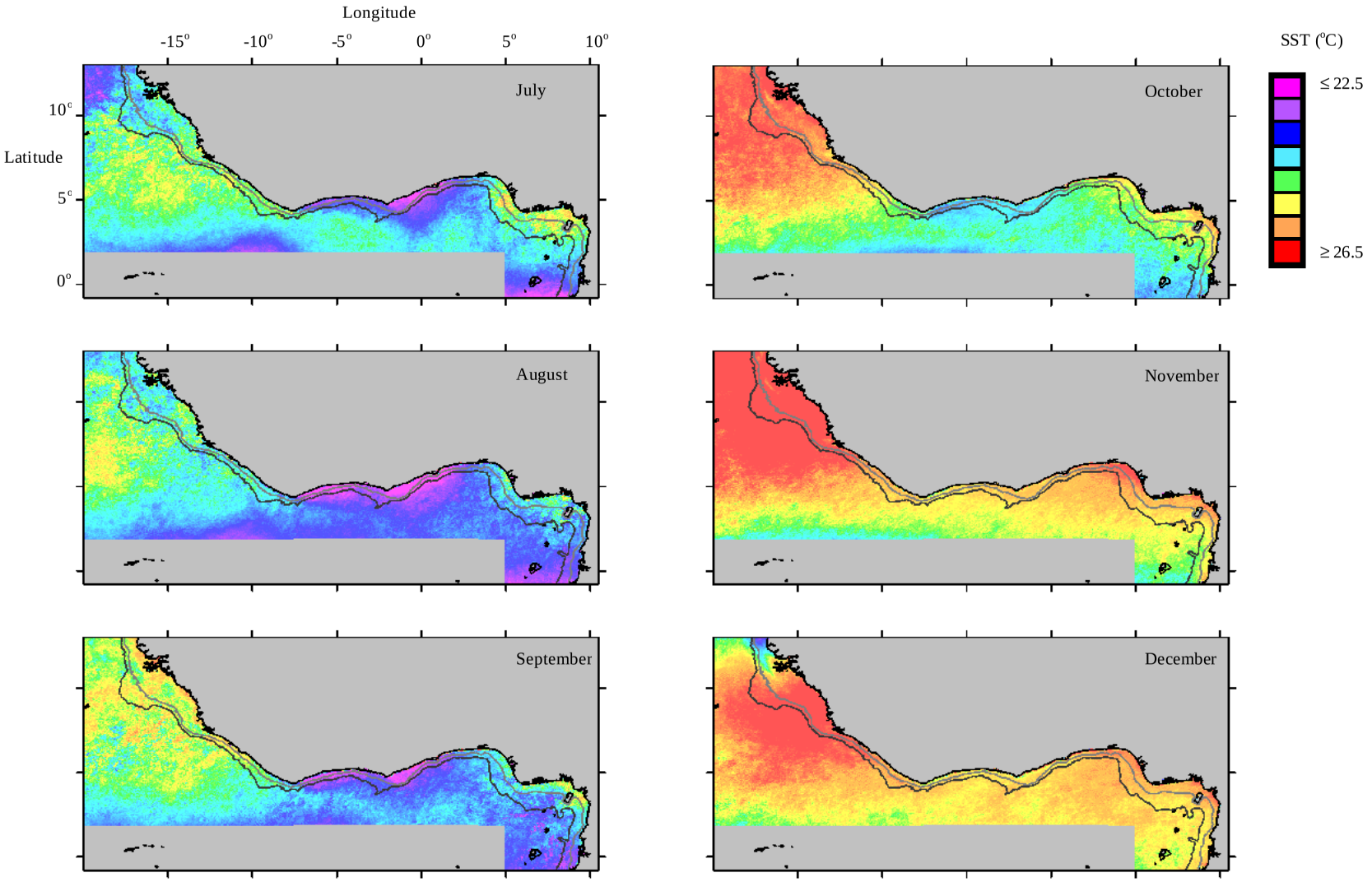

Figure 4.5 cont. Monthly mean SST for the Gulf of Guinea from CORSA-AVHRR SST data. Each monthly mean is averaged from weekly SST composites for each month over the period July 1981 to December 1991.

Minor coastal upwelling

The minor upwelling season along the Ghanaian and Ivorian coastlines appears to start in January, when upwelling appears over the continental shelf from Cape Palmas to the Volta delta, with the largest area over the wide shelf to the east of Cape Three Points. In February, upwelling appears to be absent from the area to the east of Cape Three Points, although upwelling is present around this headland. The spatial extent of upwelling along the concave coast to the east of Cape Palmas is approximately the same as in January, however, SST are slightly cooler. A cool water strip over the narrow continental shelf from Cape Palmas to Sierra Leone has also developed over this month. This appears coolest around the shelf break (50-200m). The cool strip turns offshore at Sherbro Island, following the continental shelf edge, and forms a 'pool' of cool water. It then appears to connect with the most southerly extent of the SUI. In March, it appears that cold waters are present along the entire coast from Togo to Sierra Leone. Along the Ghanaian coast, SST are warmer than in January and the spatial upwelling extent is reduced. Along the Ivorian coast, upwelling is reduced compared to February, with the main upwelling centre to the east of Cape Palmas. The cool strip is still present along the Liberia and Sierra Leone coasts, following the shelf edge at Sherbro Island to move offshore and meet up with the SUI. A cold water plume off Sherbro Island appears intense. In April, some upwelling is still observed off Ghana, along the coast to the east of Cape Three Points. A cool strip is also present along the coast west of Cape Three Points up to Sierra Leone.

Major coastal upwelling

The major upwelling season appears to start in June. Upwelling in this month is greatest to the east of Cape Three Points. In July, there is a large drop in SST and strong upwelling occurs along the entire coast from Cotonou, Benin to Cape Palmas. The upwelling is greatest to the east of Cape Three Points, where it has a considerable offshore extent, and there is strong putative frontal development between the upwelled water and offshore water. The most intense upwelling appears to occur in August along the entire coast from Cape Palmas to

Cotonou. The upwelled waters extend well beyond the continental shelf edge. SST are reduced from the coast to the equator throughout the whole of the CWAU subsystem. As such, frontal development between upwelled waters and offshore waters appears weakened. In September, upwelling is weaker than in August but still strong, extending to or beyond the shelf edge. In October, upwelling is greatly reduced in both spatial extent and intensity. The main upwelling area is seen on the Ivorian coast to the east of Cape Palmas, although some cold water is still visible around Cape Three Points. In November, warm water covers the whole coastal area. Cool waters are still observed in the equatorial area, but these are detached from coastal SST.

EQUATORIAL UPWELLING

The equatorial upwelling is not the focus of this study but is a dominant feature throughout the southern part of the area under consideration, therefore a description of its seasonal appearance is given here. Cold waters of equatorial origin appear in the southern part of the EGOG subsystem in May. They extend to around 1°N. In June, there is a large drop in SST in these waters, although their spatial extent is about the same. Cold waters are also present in the southern part of the CWAU subsystem, west of 8°W, with their greatest northern extent around 10°W (approximately to 2.5°N). During July, the upwelling appears intense to about 1°N in the EGOG subsystem, with cooler waters to about 2.5°N. In the southern part of the CWAU subsystem, equatorial upwelling appears present west of 7°W and extends meridionally to around 3°N at 10°W. Cooler waters associated with this upwelling extend to approximately 4°N at 10°W. In August, the equatorial upwelling extends further north. Cold waters are seen further north than 2°N as far west as 20°W (the limit of the scene). Warmer waters are seen only in the central SLGP subsystem and along the coast of Nigeria and Cameroon. Upwelling in September is less intense than in August, but cool SST are still present throughout the entire southern area of the scene. The cool waters recede much more during October until in November cool waters are only present in the southern part of the SLGP subsystem, west of 7°W, and from about 1°S to the equator in the EGOG subsystem.

River discharge

Warm waters are apparent in satellite images in the vicinity of river mouths for two main areas in the Gulf of Guinea: the continental shelf from Guinea-Bissau to northern Sierra Leone and the coastal area from Niger to Gabon (see figure 4.6). Putative runoff from the rivers of Guinea-Bissau and from the Kogon River of Guinea is visible as distinct plumes between March and May. In September, the major river flood is visible as a large plume around the Bijagos Islands. This putative run-off continues to be visible until November. Further to the south, warm putative run-off waters from the many rivers along the concave coast from Freetown (Sierra Leone) to the north of Guinea, are visible for most of the year. In the eastern Gulf of Guinea, warm waters are visible at part of the coast all year round. These appear to originate from the Niger delta and other rivers of Nigeria, Cameroon, Equatorial Guinea and Gabon. River discharge in the Gulf of Guinea is further investigated, using *in situ* data, in chapter 6 of this thesis.

Fronts

As the SUI annually migrates south, it is seen to encircle the Bijagos Islands of Guinea-Bissau for a few months every year. In the average monthly SST images, this first becomes apparent in December. By January, the cold waters of the SUI have encompassed the islands. During February, warmer waters of putative riverine origin begin to appear around the islands. As the extent of warm water around the islands increases throughout March, a very strong temperature gradient (~3.5^{o}C per 100 km), suggestive of strong frontal development, is apparent between the two water masses. In April, the SUI appears to encircle the islands even further. During May, the SUI begins to retreat but is still present in June as a thin plume around the islands, although the strength of the front is much reduced (~1.5^{o}C per 100 km).

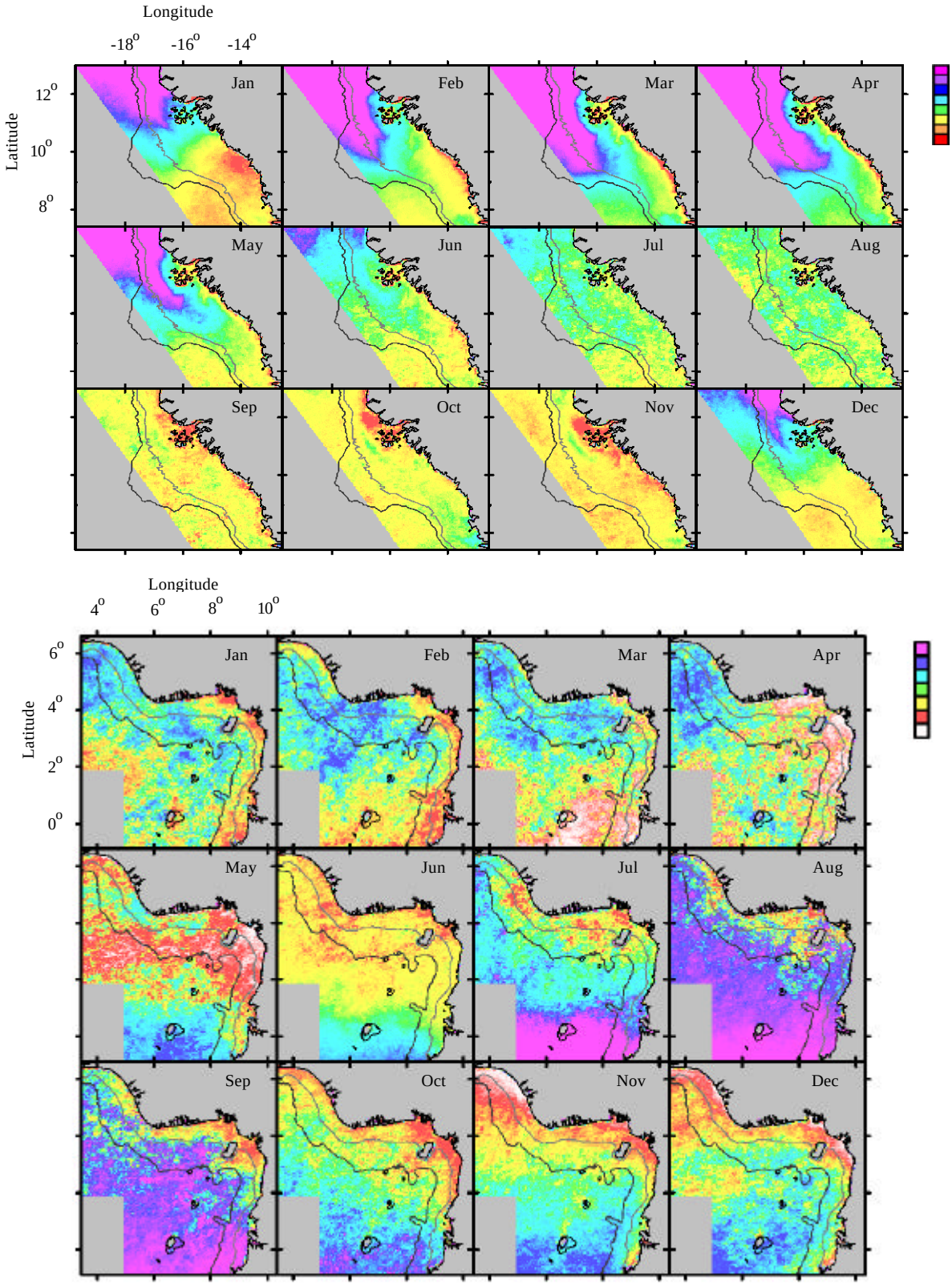

Figure 4.6. Putative river discharge visible in monthly mean SST images for a) Guinea-Bissau to Sierra Leone and b) the eastern Gulf of Guinea. The colour scales given are for arbitrary temperature ranges which vary between images as colours were chosen for each image to enhance putative run-off. For all images, magenta represents the coolest temperatures and red/white the warmest temperatures.

Additionally, from September to November, when the SUI is absent from the region, minor cooling is visible at the shelf break offshore of the Bijagos islands. This feature is strongest in October and November, giving an onshore-offshore temperature gradient of >1^{o}C per 100 km during these months. These structures are visible in figures 4.5 and 4.6.

The near connection of SUI waters with the Sherbro Island upwelling in February forms a strip of cool water that separates the warm shelf waters from the warm, offshore oceanic waters (fig 4.5). This putative front is also apparent in March and April, however, the extent of warm shelf waters is much reduced in these months. The temperature gradient between this cool strip and the warm waters to either side of it is approximately 1^{o}C per 100 km.

Figure 4.5 also shows the strongest frontal development associated with the major upwelling to be in July (~1^{o}C per 100 km). Strong temperature gradients are also well developed in June when the upwelling is not as intense and the upwelled water not as cool, but the putative front is closer to the shore. Additionally, strong temperature gradients exist in August but the fronts between water masses appear to break down due to cooling offshore. During the minor upwelling, the coolest temperatures and strongest putative frontal development (temperature gradient < 0.5^{o}C per 100 km) appear to occur in January.

SEASONAL SST ANOMALY

The spatially averaged seasonal SST anomalies were calculated for each of the subsystems of the Gulf of Guinea to provide a between-year comparison of variability in the seasonal cycle, with annual trends removed (fig. 4.7). For the SLGP subsystem, SST anomalies show the first part of the year (January to September) to be cooler and the second part of the year (October to December) to be warmer. The cooling from January to June is due to the southerly migration of the SUI, while the later warming is due to the absence of the SUI and the influx of warm tropical waters. The cool period from July to September is caused by general cooling seen in the SLGP subsystem at this time of year, as previously described.

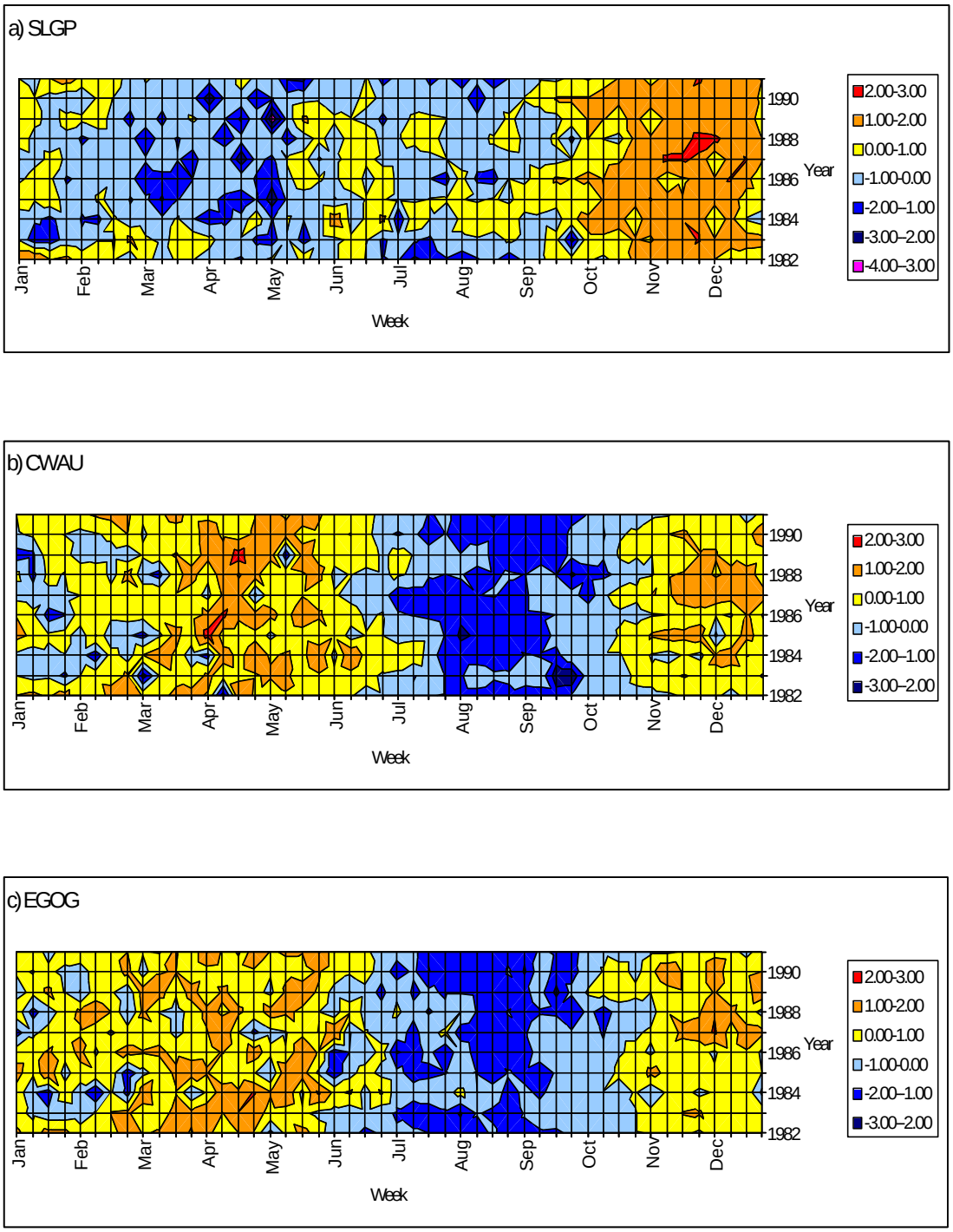

Figure 4.7. Charts showing the spatially averaged seasonal SST anomaly for each week of the CORSA-AVHRR time series for each subsystem: a) SLGP, b) CWAU and c) EGOG.

For the CWAU subsystem, the seasonal SST anomalies clearly show the upwelling seasons and the warm periods in-between. It can be seen that during the minor upwelling season, upwelling events can occur any time from January to March and sometimes more than one event can occur in a year. Single weeks with cool temperatures are observed from time to time during warm periods of the year. Some of these are due to atmospheric water vapour contamination. The seasonal SST anomalies for the EGOG subsystem show cold months from July to October, caused by equatorial upwelling, with the rest of the year being generally warm with some colder patches, especially from January to March. Outside of this period, other weeks also show cold temperatures, some of which are due to atmospheric water vapour contamination.

4.5.3 Interannual variability

GENERAL

Figure 4.8 shows the mean SST images for each year. In general, 1982-1986 was a cool period and 1987-1991 was warm. Also, 1984 appears to have been a warm year. The monthly composites of mean SST for each year show some change in the influence of the Senegalese upwelling throughout the time series, however, the warming visible in the central Atlantic and eastern Gulf of Guinea appears to dominate the interannual variability. The time series of spatial means shows SST to oscillate between warm and cool states from 1981 to 1986 then there is an extended warm period from 1987 to 1991 (fig. 4.9). This pattern is also clearly shown for each subsystem in the charts of interannual variability in global SST anomaly values for each week in the time series (fig. 4.10). Additionally, unusually warm conditions are visible in 1984, as is an anomalously cool period from mid-1982 to early 1983. The first half of 1985 also appears unusually cool.

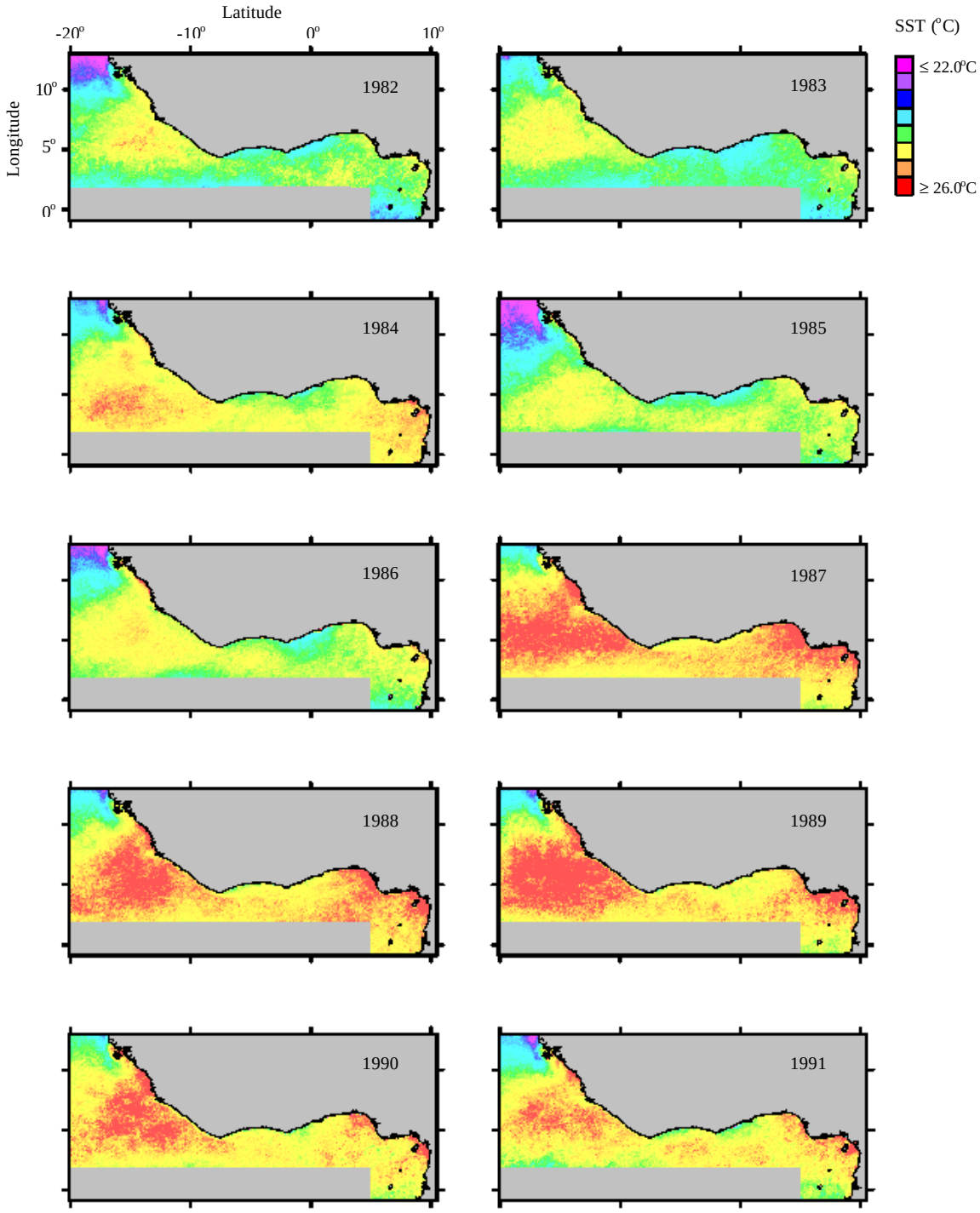

Figure 4.8. Annual mean SST calculated from CORSA-AVHRR SST data. Each annual mean is averaged from weekly SST composite images for each year of the time series July 1981 to December 1991.

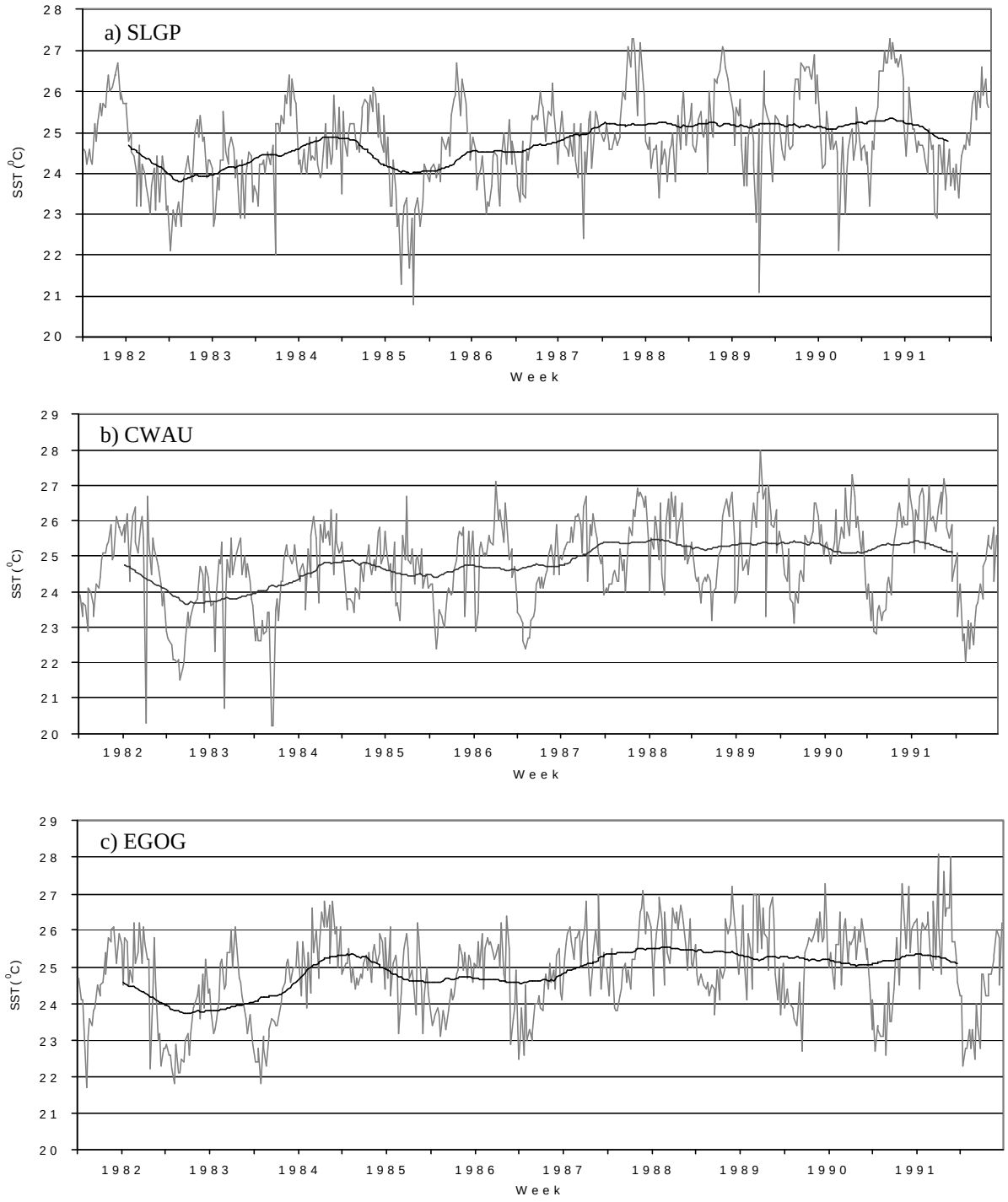

Figure 4.9. Time series plots showing the spatial mean SST (grey line) for each week of the CORSA-AVHRR series and the 49-point moving average (black line), showing interannual variability, for each subsystem of the Gulf of Guinea: a) SLGP, b) CWAU and c) EGOG.

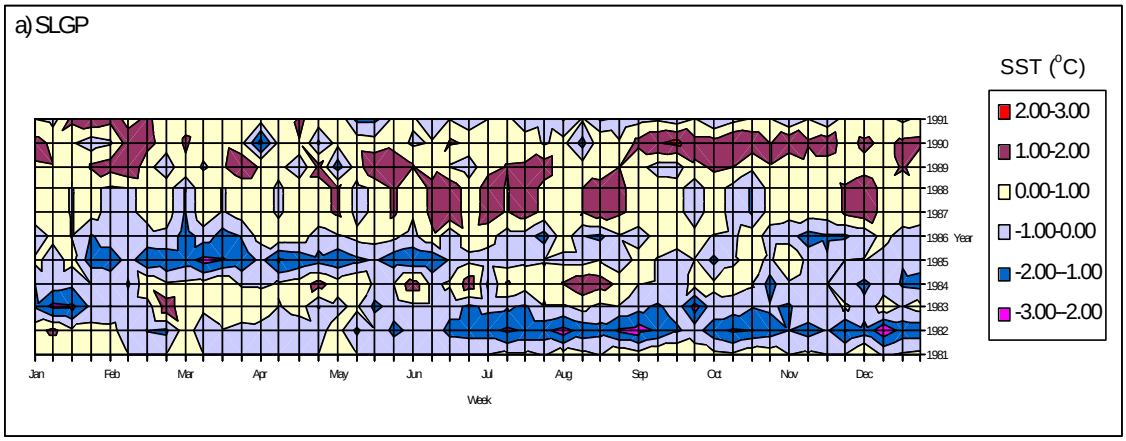

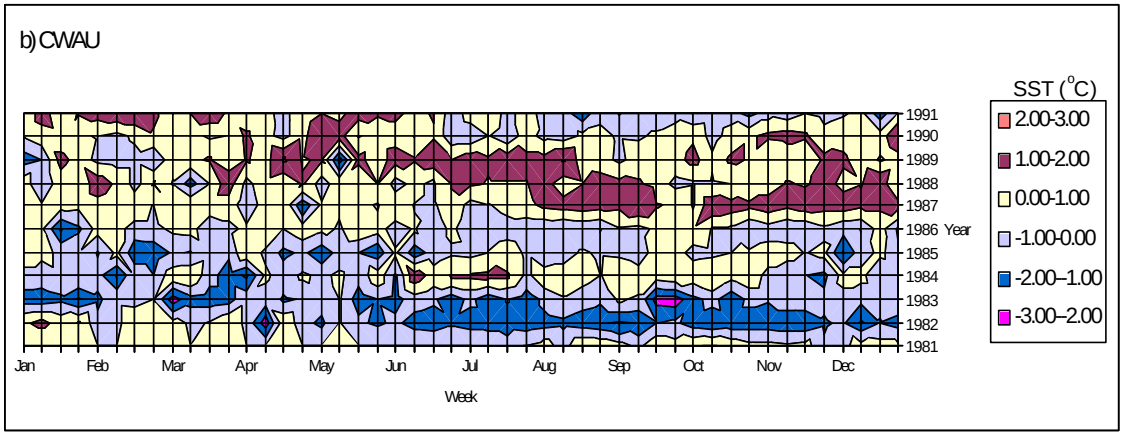

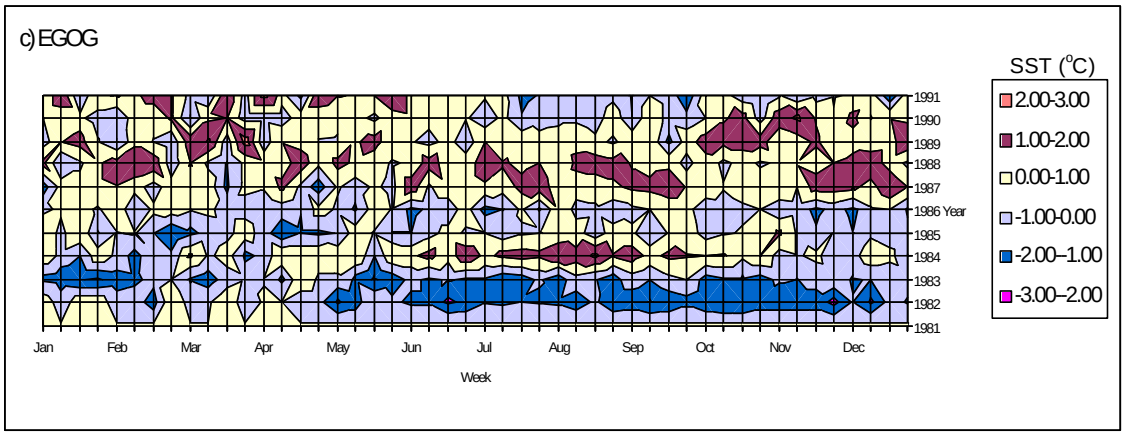

Figure 4.10. Charts showing the spatially averaged interannual SST anomaly for each week of the CORSA-AVHRR time series for each subsystem: a) SLGP, b) CWAU and c) EGOG.

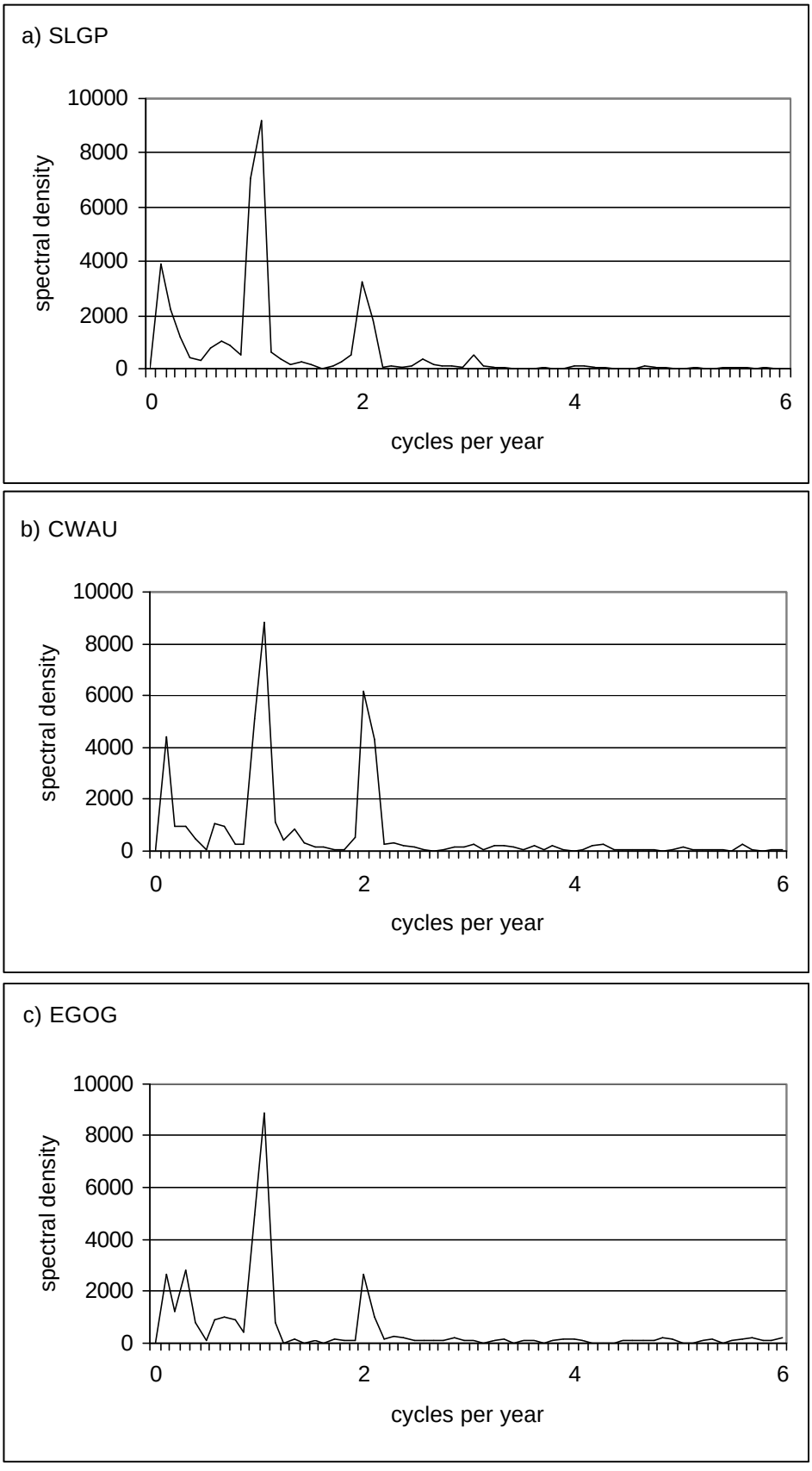

Figure 4.11. Power spectra of the time series of spatial mean SST for each subsystem: a) SLGP, b) CWAU and c) EGOG.

Power spectra generated for the spatial mean SST time series for each subsystem (fig. 4.11) show three peaks: two explaining the seasonal cycle (1 cycle per year and 2 cycles per year) and one explaining interannual variability (less than 1 cycle per year). The SST signal represented by the interannual peak shows the same trend as the smoothed time series for each subsystem but more clearly (fig. 4.12). The oscillations have a period of approximately 3 years. The amplitude of the oscillations varies between the subsystems with the CWAU and EGOG showing the greatest similarity. The SLGP shows the cooler trend from 1981 to 1987 most clearly, however, all three subsystems show a large peak around mid 1987 to 1988. In 1991, the SLGP appears to be entering a warm phase, whereas the CWAU and EGOG appear to be cooling.

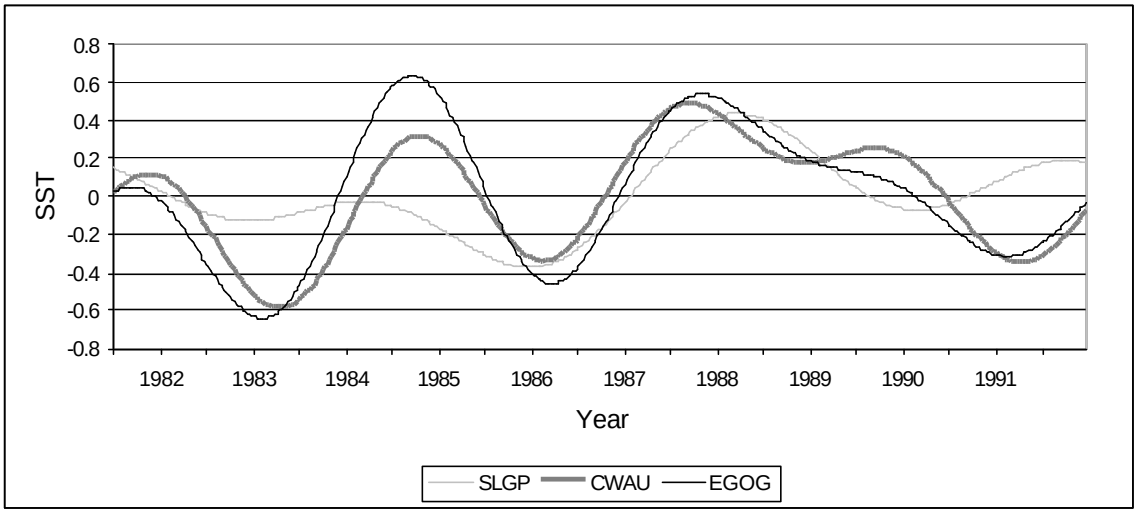

Figure 4.12. SST signal extracted from the time series of weekly spatial means using a rectangular bandpass filter, for frequencies corresponding to the interannual spectral peaks for each subsystem.

COASTAL UPWELLING

In the annual mean SST images, the spatial extent of coastal upwelling appears increased in 1983 and reduced in 1984 and from 1987 to 1990. Table 4.1 gives a qualitative measure of interannual variability in the strength of the upwelling along the coasts of Ghana and Côte d'Ivoire using the CUI, which takes both intensity and spatial extent into account.

Table 4.1. Combined Upwelling Index (CUI), combining spatial extent and intensity. * represents seasons severely contaminated by atmospheric water vapour.

Year	***Spatial extent***		***Intensity***		***Combined***	
	minor	major	minor	major	minor	major
1981	*No data*	*0.30*	*No data*	*53*	*No data*	*16.09*
1982	*0.06*	*0.82*	*20*	*52*	*1.11*	*42.88*
1983	*	*0.69*	*	*70*	*	*48.32*
1984	*0.40*	*0.13*	*25*	*41*	*9.98*	*5.51*
1985	*0.61*	*0.48*	*37*	*46*	*22.61*	*22.16*
1986	*0.51*	*0.61*	*37*	*52*	*19.00*	*31.65*
1987	*0.10*	*0.08*	*15*	*30*	*1.51*	*2.33*
1988	*0.11*	*0.11*	*36*	*39*	*3.92*	*4.24*
1989	*0.18*	*0.10*	*33*	*44*	*5.90*	*4.23*
1990	*0.14*	*0.28*	*19*	*39*	*2.69*	*10.79*
1991	*0.01*	*0.46*	*10*	*53*	*0.12*	*24.44*

This index, presented in figure 4.13a, shows the same pattern of variability as the SST images. The combined upwelling index for the major season shows strong upwelling in 1982 to 1983, weak upwelling in 1984 and an extended period of weak upwelling from 1987 to 1990. The minor upwelling shows a similar pattern from 1984 to 1989, but then diverges with a continued weakening of the upwelling from 1990 to 1991. It is mainly the spatial component of the upwelling index that follows this pattern. The upwelling intensity shows strong interannual variability with peaks in 1983 and 1986 and troughs in 1984 and 1987, however, this interannual scale variability also dominates from 1987 to 1991 rather than the longer-term pattern of an extended warm period seen in the spatial upwelling extent and other indices.

SENEGALESE UPWELLING INFLUENCE

In the mean annual SST images, the SUI appears to be reduced in 1983 and 1984 and from 1987 to 1991 and to increase slightly in 1985. Table 4.2 shows interannual variability in the most southerly extent (latitude) of the SUI from the monthly mean SST images for each year. The SUI was always seen to be furthest south during March or April.

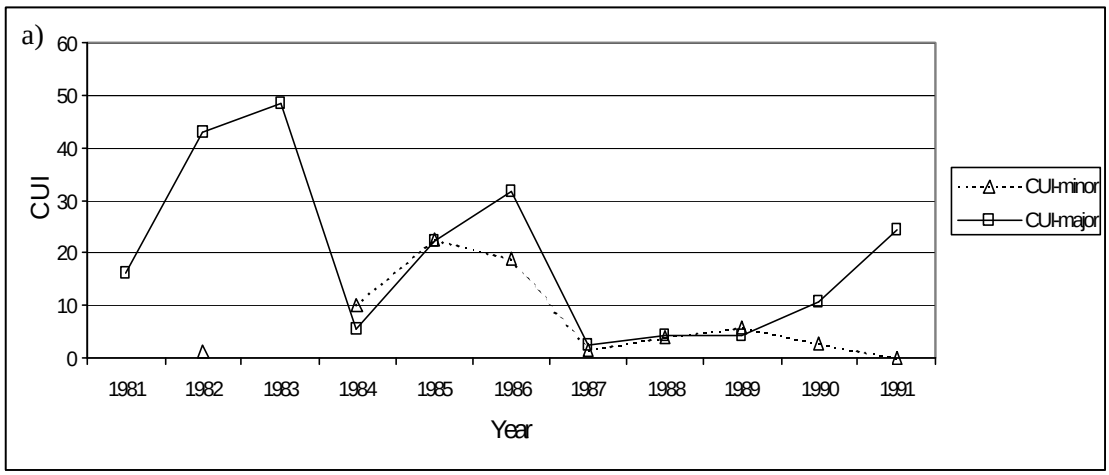

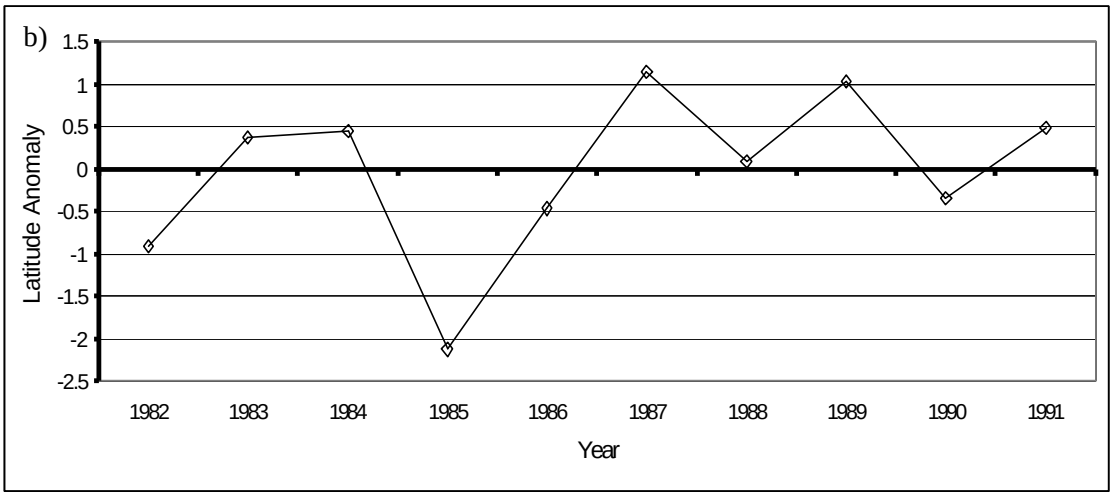

Figure 4.13. a) Combined upwelling index (CUI) values for the major (CUI-major) and minor (CUI-minor) upwelling seasons. b) Standardised anomaly from the mean most southerly position of the Senegalese upwelling influence (SUI) for each year.

The pattern of reduced and strong years for the SUI, observed qualitatively in the SST images, is also seen using this index, plotted in figure 4.13b as the interannual anomaly from the mean most southerly position, standardised with respect to the standard deviation.

Table 4.2. Most southerly latitude of SUI, standardised anomaly from the mean most southerly position and month of reaching this limit.

Year	***Latitude (°N)***	***Latitudinal Anomaly***	***Month***
1982	*5.719*	*-0.91*	*March*
1983	*7.071*	*0.37*	*April*
1984	*7.483*	*0.75*	*April*
1985	*4.425*	*-2.13*	*March*
1986	*6.189*	*-0.47*	*April*
1987	*7.894*	*1.14*	*April*
1988	*6.777*	*0.09*	*March*
1989	*7.777*	*1.03*	*April*
1990	*6.307*	*-0.35*	*April*
1991	*7.189*	*0.48*	*April*

OTHER FEATURES

It was not possible to obtain a reasonable estimate (qualitative or quantitative) of interannual variability in river discharge or in the strength and position of surface fronts from the CORSA-AVHRR images because of the effects of cloud cover and atmospheric water vapour contamination in individual weekly composites. An assessment of the interannual strength of equatorial upwelling was not made as part of this study because only a fraction of the full spatial extent of this phenomenon is visible in the Gulf of Guinea SST images.

4.6 Discussion

4.6.1 Seasonal pattern

The temporal mean SST images clearly show the SUI and the upwelling seasons, as does the seasonal SST anomaly. These dominant features of the subsystem are also the most variable, with most of the variance being explained by the seasonal cycle. The cold SUI is present in the Gulf of Guinea from December to May. The SUI almost encircles the Bijagos Islands

from February to May with a strong temperature gradient, suggesting strong frontal development, between the warm and cold water masses. Demarcq and Citeau (1995) also showed this pattern. The SUI then recedes to the north and is absent from the Gulf of Guinea from June to November.

The major upwelling season occurs during June to October but is dominant from July to August; the minor season appears strongest in January but is also visible during February and March, and cool temperatures have been observed in some areas both in December and as late as May. Both upwelling seasons appear to commence to the east of Cape Three Points. This also appears to be the area of greatest upwelling strength. The upwelling appears then to shift westwards towards Cape Palmas. The position of the major upwelling cells to the east of the capes, downstream in the Guinea current, provides support for the cape effect theory of Marchal and Picaut (1977). This effect is also seen to a lesser degree around the mouth of the Volta Delta. The observed westward shift in dominance from Cape Three Points to Cape Palmas is consistent with the results of Picaut (1983) who observed a westward propagation of the upwelling, counter to the dominant surface flow. Such observations support the theory of the upwelling propagating via a coastally trapped wave (Moore *et al.* 1978, Clarke 1979).

The timing of these seasons seen in the CORSA-AVHRR data is in agreement with other observations (Aman and Fofana 1995, 1998, Roy 1995), as is the position of the major upwelling. However, the position of the minor upwelling contradicts the results seen in the Côte d'Ivoire and Ghana coastal station SST time series, which recorded its presence only along the Ivorian coast (Arfi *et al.* 1991). The appearance of cool surface waters along the coast of Liberia and Sierra Leone in early February suggests that the minor upwelling may extend northward up the coast from Cape Palmas during February to April. The rapid appearance of this cooling is consistent with the speed of a coastally trapped Kelvin wave travelling at 0.7 ms^{-1} (Picaut 1983) to 1.7 ms^{-1} (Houghton 1983) along a coast of approximately 650 km in length (Cape Palmas to Sherbro Island) over a period of one to two weeks. The continental shelf is very narrow in this area and the shelf break is quite shallow.

Interaction between a trapped wave in the shoaling thermocline and the shelf break may also contribute to the observed cooling in this area. Alternatively, the position of the cooling along the shelf edge suggests it may be produced by mixing in a poleward, coastal slope current as is seen along the north-west European continental shelf edge. Further work will be required to determine the dynamics of this feature. This cooling also turns offshore at Sherbro Island, following the continental shelf edge and connecting with the SUI during February and March. Whether the cooling along this coast is strengthened by this connection, perhaps with cold SUI water pushing south along the coast, is not clear.

Bakun (1996) also describes a seasonal cooling observed off the coast of Sierra Leone in the 1970s, which he attributed to a coastally trapped wave. However, this feature was present in August and September, coincident with the major upwelling season. The atlas of Merle (1978) also shows this cooling during July to September, however, no cool feature is observable during these months in the seasonal SST images used for this study. Bakun's observation could be related to a general cooling in the central SLGP subsystem during July to September, however, this observed cooling coincides with the maximal level of cloud cover over this area associated with the overhead presence of the ITCZ. Thus, the cooling may be caused by contamination of the images by atmospheric water vapour or high cloud albedo leading to reduced insolation of surface waters. Whether the observed large scale cooling is a real oceanographic phenomenon or not, no upwelling signal is observed to propagate along the coast of Liberia and Sierra Leone at this time of year.

Both the major and minor upwelling seasons appear to commence with rapid drops in SST in January and July. These events, combined with the rapid propagation of the upwelling signal along the coast, suggest that the onset of upwelling is triggered by coastally trapped, upwelling Kelvin waves causing shoaling of the thermocline, as proposed by Moore *et al.* (1978) and Clarke (1979). However, this does not explain why weaker coastal cooling is seen in June. This response could be explained by seasonal changes in the local and cross-equatorial winds and the seasonal intensification of the Guinea current, as demonstrated in the

models of Philander (1979) and Philander and Pacanowski (1981a). Additionally, Ingham (1970) suggested that upwelling along the coasts of Ghana and Côte d'Ivoire occurred all year round but was not strong enough to penetrate the strong thermocline in the area. Instead, minor cooling took place through mixing in the Guinea current.

Fronts associated with the seasonal upwellings are visible in the SST record. Along the coasts of Ghana and Côte d'Ivoire during the major upwelling, the strongest frontal development tends to occur in July and occurs beyond the shelf edge. The offshore position of this front explains why no such structure was observed in the coastal studies of Houghton (1976). During the minor upwelling, the strongest frontal development is associated with the areas of lowest SST and appears to occur in the vicinity of the shelf edge along the coast of Ghana and Côte d'Ivoire in January and Côte d'Ivoire in February. The connection of the cool waters along the coasts of Liberia and Sierra Leone with the SUI in February and March forms a cold water front along the shelf edge between the warm shelf waters of the wide Guinea continental shelf and the warm, offshore oceanic water.

Warm coastal areas are visible in the images, particularly along the continental shelf of Guinea and Guinea-Bissau, including the area around the Bijagos Islands, and in the Bight of Biafra, particularly along the Niger delta and Cameroon coasts. The location of this water around the mouths of major rivers, sometimes in discernible plumes, strongly suggests that it originates from river run-off, however, larger areas of warm water, probably of oceanic origin (TSW), mask this coastal run-off during certain months. It is, therefore, not possible to extract a measure of river flow during all months from these SST data. Although river discharge was calculated for the Gulf of Guinea by Mahé and Olivry (1999) and Allersma and Tilmans (1993) have reviewed the sediment balance and littoral flows resulting from this discharge, no studies of the river plumes themselves have been identified.

As previously stated, the equatorial upwelling is not the focus of this study and only glimpses of it are visible in the SST images. However, some of the observations made appear of

interest, particularly that the images show a lag of approximately one month between the onset of upwelling at the equator and the start of the major upwelling season at the coast. This time scale is consistent with the observations of Servain *et al.* (1982) and Houghton (1983) and with the equatorial route proposed by Moore *et al.*'s (1978) remote forcing theory.

4.6.2 Interannual pattern

The mean SST images show a cool period from 1982 to 1986 and a warm period from 1987 to 1990. During the initial cool period, 1982 to 1983 was cooler than average and 1984 was exceptionally warm. This pattern is also observed in the spatial mean SST time series, the interannual spatial mean SST anomalies, and the SST signal represented by the interannual peak of the power spectra. The initial cycles have a period of around 3 years. Additionally, the combined upwelling index shows the same pattern, with strong upwelling in 1982 to 1983, weak upwelling in 1984 and an extended period of weak upwelling from 1987 to 1990. This is more obvious for the major upwelling season. The interannual behaviour of the seasons appears to diverge from 1990 to 1991 with the major upwelling beginning to strengthen but the minor upwelling continuing to weaken. It is mainly the spatial component of the upwelling index that follows this pattern. The upwelling intensity shows strong interannual variability with a period of approximately 3 years throughout the time series rather than giving way to the longer-term pattern of an extended warm period, observed in other indices. Underlying both components of the upwelling index is a long-term linear trend of weakening in the upwelling.

The three year period of cycles seen in these data makes it tempting to suggest that the action of an interannual mode of variability, such as El Niño, is responsible. Indeed, the unusually warm conditions in 1984 have been attributed to an Atlantic Niño event (Hisard 1988, Hisard *et al.* 1986, Philander 1986). Furthermore, the exceptionally cool years observed either side of this warm event suggest that the opposite ENSO phase, the La Niña phenomenon, may also have an Atlantic equivalent. However, the disappearance of this cycle in the latter half of the

SST time series makes these observations insufficient to assert such a conclusion. The persistence of this signal throughout the upwelling index does strengthen the position, yet the time series itself is too short to draw conclusive evidence. The extended warm period in the SST time series also raises questions about the role of lower frequency modes of climate variability in forcing SST, and hence ocean dynamics, in the Gulf of Guinea. These relationships are investigated further in chapter 8.

Binet and Marchal (1993) reported considerable changes in the spatial distribution of the major upwelling season seen in the coastal station SST record (Arfi *et al.* 1991). From 1969 to 1980 the observed spatial pattern agreed with the concept of two upwelling cores, seen on the eastern side of Cape Palmas and Cape Three Points. Temperature dropped abruptly on the downstream side of each cape, then increased progressively eastward as the waters were carried by the Guinea current (Morlière and Rébert 1972). However, in 1982 the observed decrease in temperature was almost the same along the entire coast. Furthermore, from 1983 to 1986 the pattern was reversed with the coldest waters found to the western side of Cape Three Points. This study finds no evidence for such a shift, rather the upwelling is seen most strongly to the east of Cape Palmas and Cape Three Points in all years. However, the observation by Herbland and Marchal (1991) of very weak upwelling at all stations in 1987 is supported by the SST images used in this study.

Another trend has also been observed in the strengths of the coastal upwellings. Pezennec and Bard (1992) noted an intensification of the minor upwelling season and reduction in strength of the major upwelling season over the period 1970 to 1990. This trend is not seen in the combined upwelling index values from this study, although the strength of the minor upwelling is seen to weaken at a lesser rate than that of the major upwelling. This pattern is mainly contributed to by the intensity component of the index. Allowing for the methods used by Pezennec and Bard (1992), which removed any long term trend from seasonal components of the signal, these two studies are in agreement, i.e. the intensity of the minor season has increased relative to that of the major season.

The between-year index of the most southerly position of the SUI also shows a high degree of interannual variability, however, the pattern of this is different to that observed in SST and upwelling indices, described above. Rather, peaks occur in 1984 and 1987 (further north) and there is a trough in 1985 (further south). On the other hand, there is an extended period of high index values from 1987 to 1991, resembling the pattern in SST and upwelling index values.

No objective, quantitative measure of the interannual variability in the strength of fronts and river discharge were obtained. Mahé and Olivry (1999) compiled extensive data on river discharge rates for the Gulf of Guinea region and these are considered in chapter 6. No time series of data on identification or strength of fronts in the Gulf of Guinea is known to exist.

4.6.3 Relevance of features observed to fisheries recruitment

Oceanographic features of relevance to fisheries recruitment, according to the triad hypothesis (Bakun 1993, 1996), must affect enrichment, concentration and retention/transport mechanisms. In the Gulf of Guinea, several features have been identified from the SST images that influence these parameters. The Ghana and Côte d'Ivoire coastal upwelling appears to be the largest putative enrichment mechanism in the images. Both within and outside of the upwelling areas, river run-off also provides nutrient enrichment. Both river plumes, observed in the eastern Gulf of Guinea and Bijagos Islands, and fronts, such as are seen at the edge of the upwelling area, may act by concentrating the nutrients supplied by these enrichment processes.

Fronts can also act as retention mechanisms. The strong frontal development between the cold SUI and the warm Guinea-Bissau shelf waters around the Bijagos Islands may be a powerful example of this. The front observed at the edges of the coastal upwelling area is also a potential retention mechanism.

If the cooling along the coast of Liberia and Sierra Leone is produced by an extension of the minor upwelling or a poleward slope current, it may provide a transport mechanism by which fish populations present in the cold upwelled waters along the Ghana and Côte d'Ivoire coasts could be transported north to the cold waters of the SUI. This could perhaps lead to mixing between different pelagic fish stocks, as well as allowing for an area of high recruitment success to replenish an area with poor recruitment success.

Coincidence between the different factors required for recruitment is seen around the Bijagos Islands. The retention mechanism provided by the SUI encircling the islands occurs between February and May, at the same time as river run-off which may provide nutrient enrichment. Additionally, the river discharge is in the form of a river plume which can concentrate the nutrients. From September to November, a weaker putative front is observed at the shelf break. This coincides with the large September peak in run-off observed around the Bijagos islands. Another place and time when such coincidence may occur is in the coastal upwelling area during June. Although frontal development is most obvious in July, it also occurs in June closer to the coast. This provides a retention mechanism close to the area of enrichment from run-off during the period of the first rains.

Interannual variability in recruitment success is a well-known phenomenon of upwelling systems and is thought to be related to the variability of the environment. The interannual oscillations identified show in which years upwelling is strong or not and the predominance of warm or cool temperatures in particular years. The interannual SST anomaly shows variability on a finer temporal scale, i.e. in which particular weeks were temperatures enhanced or suppressed. However, the role of mesoscale features (e.g. filaments) over short (daily) time scales is probably as or more important for recruitment success than these large scale trends. Nonetheless, the relationships identified between large scale climate variability and recruitment success in other parts of the world shows that interactions on such time scales are important. It also raises important questions regarding the interaction of features over long and short time scales.

4.6.4 Conclusions

The results of this study show the usefulness of remote sensing for investigating seasonal and interannual variability in SST in the Gulf of Guinea. Additionally, many of the features observed are interpretable in terms of physical processes known to exist in the region and analysis of these data can aid understanding of the underlying physical dynamics. Of particular interest are observations associated with the coastal upwellings. Some of these corroborate previous observations, such as the westward propagation of the upwelling (Picaut 1983), the 'cape effect' (Marchal and Picaut 1977), the relative intensification of the minor upwelling season (Pezennec and Bard 1992) and the one month lag between the equatorial and coastal upwellings (Servain *et al.* 1982, Houghton 1983). Additionally, the observed rapid onset of upwelling lends some support to the remote forcing theory of Moore *et al.* (1978) and the coastally trapped wave theory of Clarke (1979). Other observations contradict earlier studies, such as the observed presence of an offshore front during the major upwelling season (Houghton 1976) and the absence of a shift in position of the main upwelling cores (Binet and Marchal 1993). Furthermore, the previously unrecorded observation of coastal cooling off Liberia and Sierra Leone, coinciding with the minor upwelling season in Ghana and Côte d'Ivoire, raises more questions regarding the mechanisms forcing this upwelling season. Quasi-cyclic behaviour of SST on interannual scales has also been observed. The presence of an El Niño scale cycle in the SST time series and upwelling indices and the presence of warmer than average temperatures throughout the region in 1984, coinciding with an Atlantic Niño event, hints that global scale climate interactions may be forcing SST in the Gulf of Guinea to some extent. However, the length of the time series used is insufficient to assert this conclusion. Finally, this study has shown how satellite derived SST time series can be used to resolve oceanographic features of putative relevance to fisheries recruitment, and their seasonal and interannual variability.

5 Detection of Major Patterns in SST Using Principal Components Analysis

5.1 Introduction

5.1.1 Use of PCA in remote sensing studies

Principal Components Analysis (PCA) has become a commonly used technique for remote sensing image analysis. It is generally used as a technique for data compression between highly correlated spectral bands, i.e. images from various wavelength bands often appear similar and convey essentially the same information (Lillesand and Kiefer 1987). PCA reduces redundancy in the images, thereby reducing the time and cost of data processing (Fung and LeDrew 1987).

PCA has also been used for change detection studies. Fung and LeDrew (1987) used PCA for detecting land-cover change in Canada from Landsat MSS data and Eastman (1992) assessed the usefulness of the technique for studying changes in vegetation cover over Africa using Normalised Difference Vegetation Index (NDVI) images. Eastman (1992) concluded that the technique has excellent capabilities in the detection of change, regardless of whether it is cyclic, aperiodic repeating or isolated. In addition, it appears to be equally sensitive to changes that are additive or multiplicative in nature. Gallaudet and Simpson (1994) used the technique to investigate oceanographic processes off Baja California using SST from AVHRR data. More recently, Cole and McGlade (1998), Hernàndez-Guerra and Nykjaer (1997) and Maus (1997) used PCA to show spatial structure and temporal variability in upwelling along the West African coast from the CORSA-AVHRR SST product. Cole and McGlade (1998) investigated the Benguela region off Namibia while Hernàndez-Guerra and Nykjaer (1997) and Maus (1997) studied the north-west African upwellings. This study attempts to apply this technique to the Gulf of Guinea region.

5.1.2 Principles for interpretation of results

Although there are rigorous statistical methods to interpret the results of PCA, it is difficult to ensure that meaningful patterns are explained. This is made more complicated by the dependence of the results on the initial values of the input data. Therefore, any interpretation is, by definition, subjective. For this reason, it is essential that interpretation be based on detailed knowledge of the system in question. Eastman and Fulk (1993) highlight this by showing the effect of an artefact in remotely sensed data due to sensor drift, which was explained by one of the component images. Vital mistakes can be made when such results are interpreted as natural phenomena (Maus 1997).

Dimensionality of the data set is another important consideration in interpretation of the results. For oceanographic remote sensing purposes, Gallaudet and Simpson (1994) define two types of dimensionality in the input images. Geometric dimensionality describes the spatio-temporal structure of the data and geophysical dimensionality is concerned with the number of important physical processes represented. Data with a relatively high degree of geometric and geophysical dimensionality will require a higher number of components to describe the majority of their residual variance. Less complicated data may be described with fewer components. However, this does not necessarily mean that when most of the variability can be explained by the first few components, the data will not contain other processes. Additionally, to consider both the spatial and temporal structure of the processes, a joint comparison of both the spatial and temporal outputs of the analysis is required for interpretation. Furthermore, it must be remembered that principal components are orthogonal. Thus, later components should be free from influences explained by earlier components. However, this does not mean that different aspects of the same process cannot be represented by different components.

Statistical significance of principal components is difficult to assess. Significance tests are useful for hypothesis testing, however, PCA is generally an exploratory technique. A

standard method for PCA is to use Bartlett's test for sphericity (Bartlett 1950), however, this has methodological problems, namely multiple testing. Alternatively, various selection rules can be used, as in the study of Gallaudet and Simpson (1994) or comparisons can be made with randomly generated products. This can be done using Monte-Carlo methods if the data are normally distributed, however, if this is not the case, it is better to use a permutation method, such as that of Potter *et al.* (submitted) for correlation coefficients. When PCA is used to explore data for underlying processes, it is usually sufficient to accept the results as significant if their geophysical interpretation is clear, as in the studies of Maus (1997) and Cole (1997). The significance of different temporal regimes in the output principal components can be determined using spectral analysis.

5.1.3 Rationale for use of PCA in this study

Analysis of the current data set, described in chapter 4, showed a high degree of variability through time with a strong seasonal cycle and a large degree of interannual variability. Additionally, the images were seen to have a spatially heterogenous structure, with three main areas or subsystems. Furthermore, within the images, a number of oceanographic features were identified. Thus, the SST time series has a high degree of both geometric and geophysical dimensionality. Therefore, because PCA works on the variance structure of the data, it seemed an appropriate technique to investigate further the different modes of temporal and spatial variability in this highly variable data set.

5.2 Methods

5.2.1 Data scales and areas

Composite SST images from the CORSA-AVHRR time series, described in chapter 4, were used for this analysis. To ensure that the analysis covered the appropriate scales for relevant oceanographic features and natural variability, three different spatial scales were used. The

temporal scale used was that of monthly composites as this allowed for the temporal sequence of the data to be best maintained when eliminating time steps with excessive cloud cover.

Firstly, the CORSA-AVHRR data used in chapter 4 of this study were combined with data for the North-West African region, as used by Maus (1997), the Benguela region, as used by Cole and McGlade (1998) and previously unused data for the Angolan offshore area. Monthly composites for each area were joined together using the mosaic routine of the ERDAS *Imagine*® software. Data was only complete up until the end of 1990 for all these areas, so only a 9.5 year time series was used. This combination of areas gave spatial coverage of tropical and subtropical West Africa, looking for significant features at the basin scale.

The 10.5 year time series of CORSA-AVHRR data for the Gulf of Guinea region only were used in the second analysis. The third analysis was undertaken on three spatial subsets of the Gulf of Guinea region, based on the subsystems of Tilot and King (1993): Sierra-Leone and Guinea Plateau (SLGP), Central West African Upwelling (CWAU) and Eastern Gulf of Guinea (EGOG). This third analysis also used 10.5 years worth of data.

5.2.2 Selection of layers and interpolation

For PCA to be performed, pixels classified as cloud by the JRC must be removed from the input layers. These input layers are the monthly SST composite images, in temporal sequence. To achieve this eradication of cloud, the Gulf of Guinea area was first divided into its three subsystems. Each of these subsystems was then divided into smaller blocks and the percent cloud cover of each layer was calculated for each block. Any layers with greater than 50% cloud cover in a block or with excessively large areas of cloud were removed from the data set. The 50% threshold was chosen arbitrarily, based on visual examination of the monthly composites. A total of 10 layers were removed for the Gulf of Guinea analysis. For the subsystem analysis, 5 layers were removed from both the SLGP and EGOG subsystems. No layers were removed from the CWAU subsystem. Remaining patchy cloud cover was

then eliminated by interpolating SST values from surrounding pixels using the Focal Analysis routine of the ERDAS *Imagine*® software. A square 7x7-pixel kernel was used with all pixels weighted equally. This allowed the interpolation procedure to retain the structure of mesoscale features without being overly dependent on single neighbouring pixel values. The interpolation procedure was repeated until all cloud cover was removed from the data set. No layers were removed for the West African analysis. Instead, focal analysis was used to interpolate all missing pixels. This was acceptable because only coarse scale features were of relevance to this analysis.

5.2.3 Spatial standardisation

The next stage of data preparation involved spatially standardising the data set so that each layer had zero mean and unit standard deviation.

$$\frac{x_i - \bar{x}}{\sigma} \tag{5.1}$$

where x_i is the pixel value at pixel site i, $\bar{x}$ is the mean of all pixels in the layer and σ is the standard deviation of all pixels in the layer.

Although a correlation matrix was used for the PCA, spatial standardisation was still performed to facilitate interpretation of the output principal component images by presenting them as positive and negative deviations from the mean.

5.2.4 Principal Components Analysis

Standardised PCA was performed on the prepared data using a modification of the PCA routine in the ERDAS *Imagine*® software package. Modifications included replacing calculation of the variance-covariance matrix with calculation of the correlation matrix. The mathematical basis of the analysis was modified from Cole (1997) and Cole and McGlade (1998), and is described in Appendix 1.

The output from this analysis consisted of principal component (PC) images, eigenvalues and eigenvectors for each image. The PC image gives the spatial output from the analysis and the eigenvalues are a measure of the percent variance explained by each PC image. The eigenvector gives the temporal output of the analysis, corresponding to each PC image. These are also termed the loadings.

5.2.5 Interpretation of principal components

To be able to interpret the patterns observed in component images and loadings in terms of features of the system, it is first necessary to understand the way the data are presented. The patterns in the component images are represented in standardised units. For convenience, positive values are coloured red and negative values blue, however, the sign of these units is arbitrary and only important for the relative relationship of pixels in the image. Therefore, in some images blue pixels will represent relatively cool areas and red will represent relatively warm areas, whereas in others the opposite pattern will apply. The relative intensity of the colours indicates the strength to which a certain pattern applies in certain areas. Hence, strong red or blue colours show the pattern is strong in a particular area and white represents areas where the pattern is weakly represented. These are often, but not always, close to boundaries between opposite patterns. Black pixels indicate the boundaries between opposite patterns. The relative importance of a particular pattern to each individual time step is given by the loadings. As with the component images, the sign of the loadings is arbitrary. Therefore, large peaks or troughs represent time steps when a pattern in the corresponding component image is either strongly represented or its opposite pattern is strongly represented. Loading values around zero represent time steps when the patterns seen in the corresponding component image are not relevant.

5.2.6 Selection of Components

Tests for statistical significance are useful for assessing whether patterns observed in data sets are significantly different from randomly generated data. However, if patterns identified in this study from principal component images and their loadings are clearly interpretable in terms of physical processes known to be present, then it is clear that these patterns are non-random and, therefore, significant. Conversely, if the physical processes underlying the principal component patterns cannot be identified, then even if they are non-random, they cannot be interpreted. The concept of statistical significance, therefore, is inappropriate to this chapter and tests were not used for the output principal components.

5.2.7 Spectral analysis

Power spectra were calculated for the loadings, according to the methods described in chapter 4, to show the temporal modes associated with each of the principal components.

5.3 Results and Discussion

5.3.1 Interpretation of PCA for West Africa

Inspection of the eigenvalues for the West African PCA shows only the first two to have easily interpretable patterns, explaining 79.8% and 13.6% of the total variance, respectively (fig 5.1). These were retained for interpretation. The other components were discarded on the basis that individually they explain very little of the remaining variance. PC I (fig. 5.2a) shows SST values in the tropics to be warm relative to the subtropics.

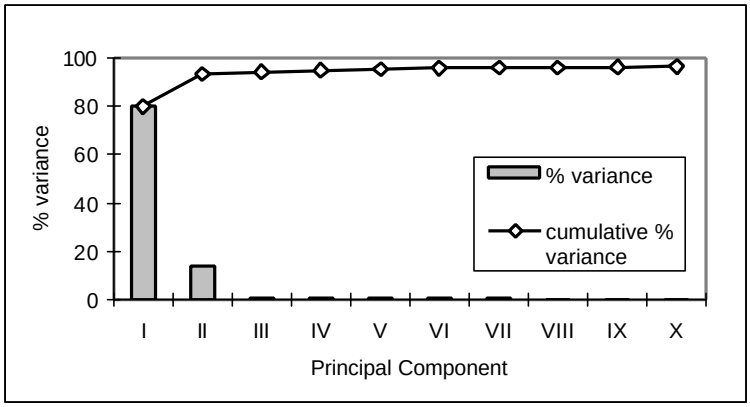

Figure 5.1. Percent variance (eigenvalues) explained by each of the first 10 principal components of the West African PCA.

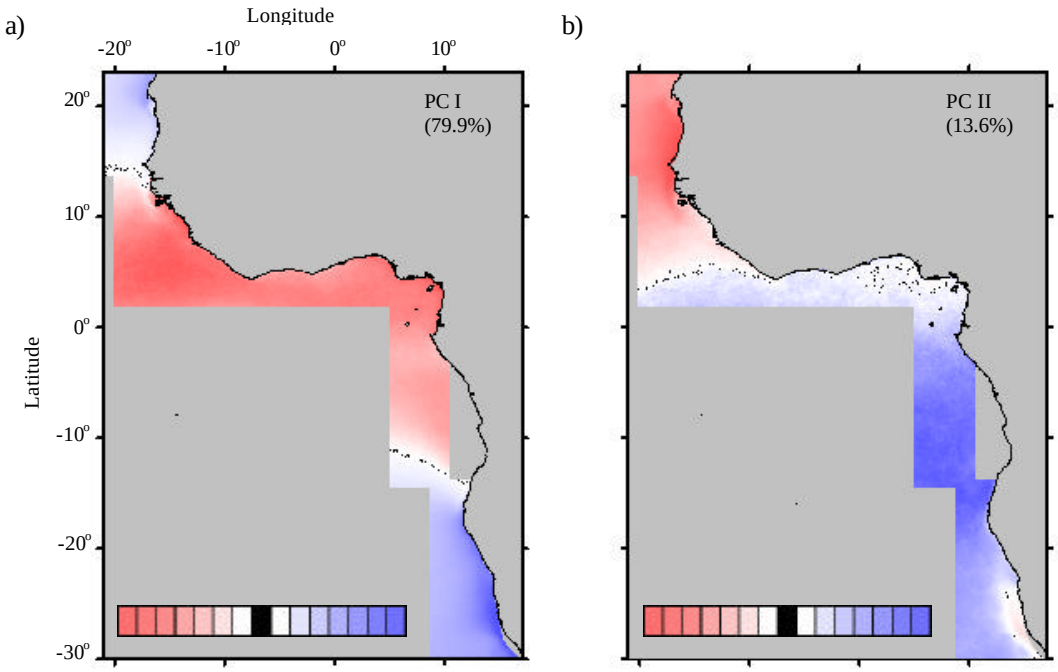

Figure 5.2. West Africa PC images. The colour scale is given in the bottom of each image. Blue represents strong negative correlation with the loadings, red represents strong positive correlation, white represents weak correlation and black represents the boundary between areas of positive and negative correlation (zero correlation).

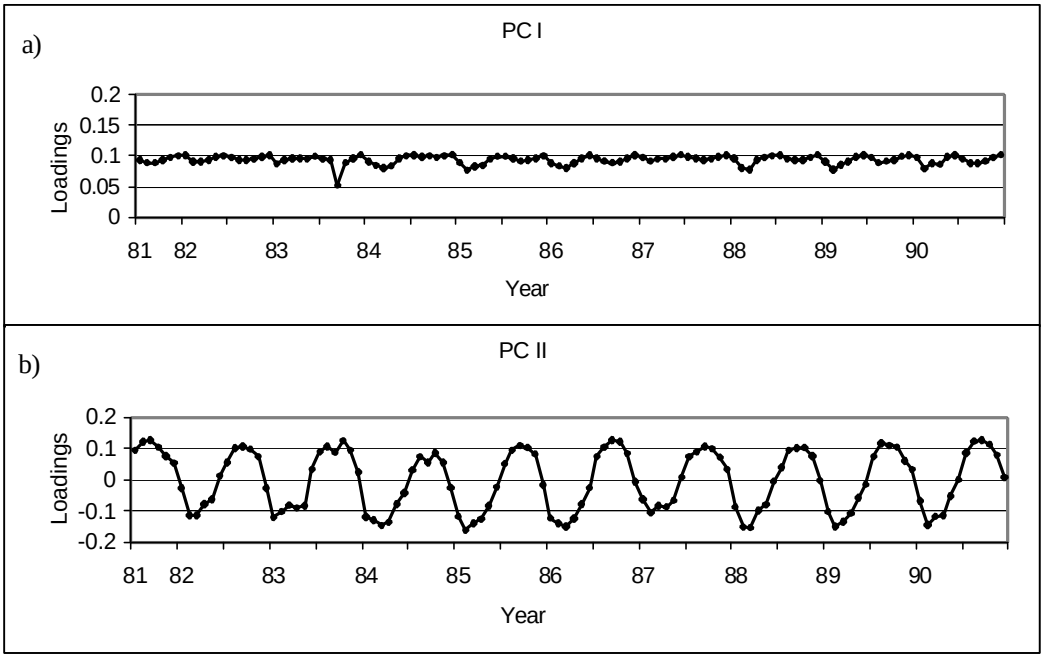

Figure 5.3. Loadings for PC I and PC II of the West Africa PCA.

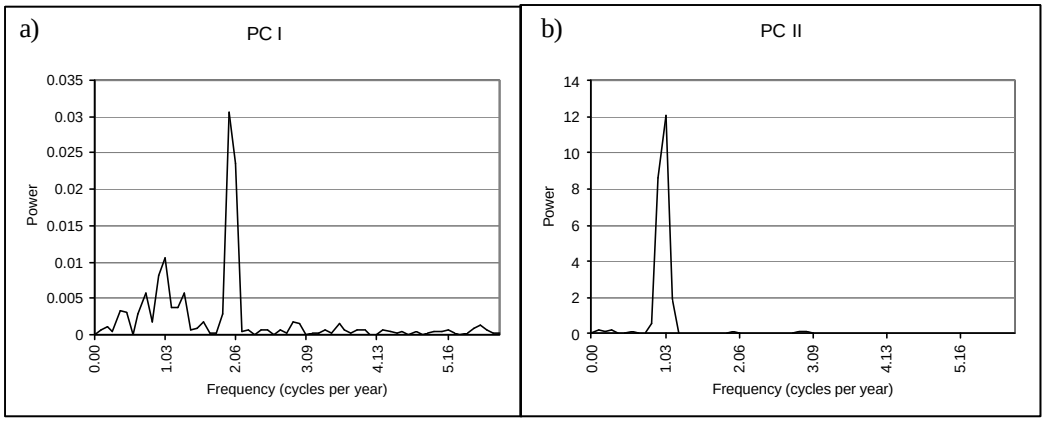

Figure 5.4. Power spectra for PC I and PC II of the West Africa PCA.

Its loadings (fig 5.3a) are always positive indicating that this dominant temperature structure is remarkably constant. Thus, it appears to relate to the global SST structure based on the area of greatest solar irradiance being the tropics. PC II (fig 5.2b) shows the North Atlantic to be warm with respect to the South Atlantic, but with the boundary between the two regions extending westward, perpendicular to the Liberian coast. The loadings (fig. 5.3b) and power spectra (fig. 5.4b) for this result show a strong annual cycle. Comparison of the loadings with the monthly SST composites (shown in appendix 2) showed that the peaks, representing the pattern seen in the component image, occur during September or October of each year. Similarly, troughs, representing the inverse of the pattern seen in the component image, generally occur during February or March, although occasionally they are seen in January.

Because the loadings have both positive and negative values, the relative SST pattern can be interpreted in two ways. When loadings are positive SST values are warmer north of the boundary than south of it. In the same way, when the loadings are negative, the SST pattern has the opposite structure. The north-south dipole in SST structure and strong seasonal cycle suggest that the observed pattern represents the reversed seasonal polarity of the different hemispheres. The position of the boundary, however, is situated around 5^{o}N rather than at the equator. This implies that the South rather than North Atlantic dominates the area from the equator to around 5^{o}N and, therefore, the observed pattern is related to oceanic circulation rather than solar irradiance. Additionally, the position of the boundary between the areas appears to correspond to the mean position of the ITCZ and migrates accordingly. This has two consequences: firstly, the boundary may change position seasonally like the ITCZ and secondly, the oceanic dominance of an area may be linked to climate circulation patterns.

5.3.2 Interpretation of PCA for the Gulf of Guinea

The first three Principal Components of the Gulf of Guinea analysis appeared to show meaningful patterns and were retained for interpretation. Between them, they account for approximately 62% of the total variance in the standardised input data set (fig. 5.5). As with

the previous analysis, the other components were discarded on the basis that individually they account for very little of the remaining variance. The first three components are discussed individually below.

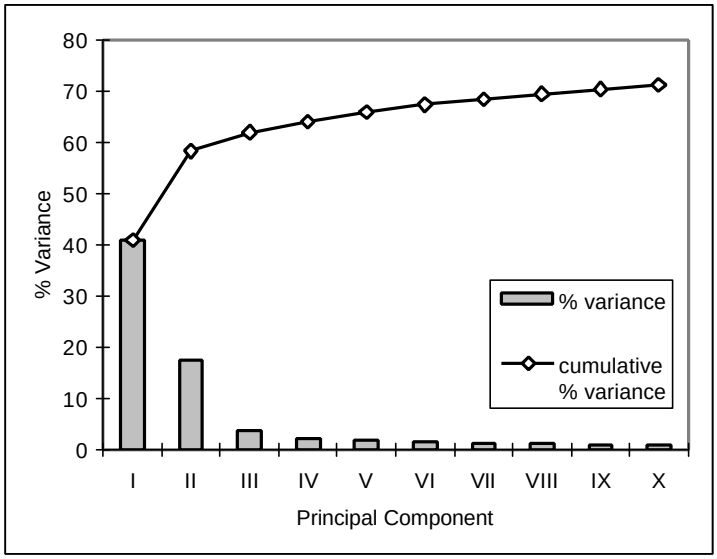

Figure 5.5. Percent variance (eigenvalues) explained by each of the first 10 principal components of the Gulf of Guinea PCA.

GULF OF GUINEA PC I

PC I (fig. 5.6a) accounts for 40.9% of the total variance. It represents the dominant pattern of variability in the data set and shows a meridional temperature gradient with the break between relative warm and cold temperatures extending westward from the Liberian coast. Its loadings show a strong seasonal cycle (fig. 5.7a). Power spectra of the loadings (fig. 5.8a) clearly show the annual peak and additional peaks with frequencies of 2 cycles per year and 4 cycles per year. The peak at 4 cycles per year and part of the peak at 2 cycles per year are probably harmonics of the annual peak, however, the biannual (2 cycles per year) peak is larger than the annual peak. This suggests that it is more than just a harmonic of the annual cycle and that if the harmonic effects were removed a real cycle of this frequency would remain with reduced amplitude. A discussion of harmonics in spectral analysis is given by Diggle (1990).

This component appears to have the same spatial and temporal structure as PC II for the West African PCA, however, a slight difference is seen in the position of the boundary between the relatively warm and cold areas. This could be an artefact of processing, based on the relative areas of the inputs for the two analyses. Comparison of the loadings with the monthly SST composites showed that the peaks, representing the pattern seen in the component image, occur each October or November. In these months, the central area of the SLGP subsystem is warm whereas the area to the south, is relatively cool. The SUI is not present in the Gulf of Guinea at this time. Troughs in the SST loadings generally occur during March to April, although have also been seen in January and February. They occur when the SUI is extended far to the south, making the northern area much cooler than the south. The explanation for this principal component is the same as for PC II of the West African PCA. The movement of the SUI and tropical surface water in the SLGP subsystem is consistent with the seasonal migration of the ITCZ.

GULF OF GUINEA PC II

PC II (fig. 5.6b) accounts for 17.4% of the total variance. It represents the main residual pattern of variability when the variability explained by PC I is removed. The pattern shows four areas of contrasting relative temperatures. Area 1 corresponds to the mean position of the Senegalese Upwelling influence in the Gulf of Guinea. Area 2 extends from the boundary with the SUI in the north to Cape Palmas in the south. Area 3 covers the equatorial Atlantic and Ghana/Côte d'Ivoire coastal upwelling area. Area 4 lies close to the coasts of Nigeria and Cameroon. The SST structure for Areas 1 and 3 varies in phase, as does the SST structure for Areas 2 and 4. Areas 1 and 3 have the opposite structure and phase to Areas 2 and 4.

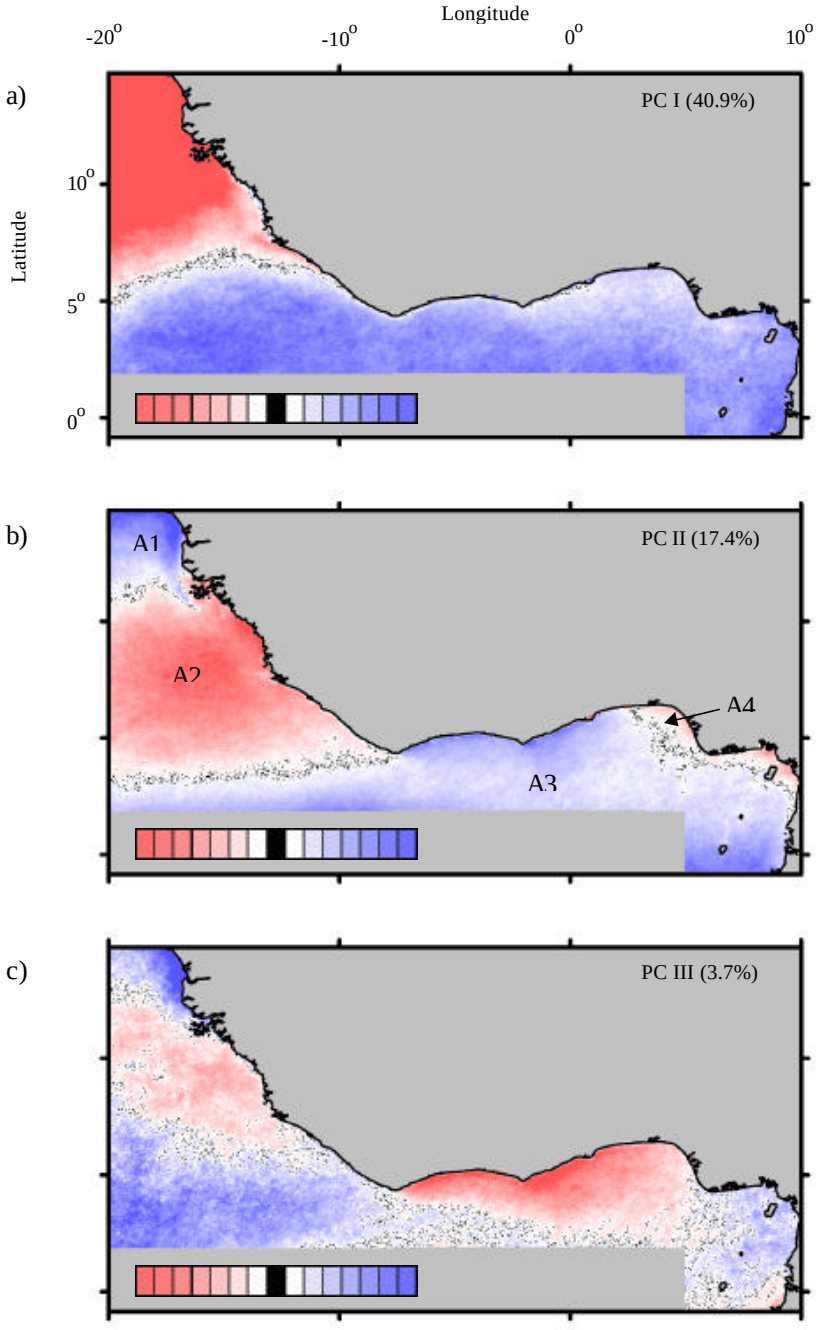

Figure 5.6. Gulf of Guinea PC images. The colour scale, given in the bottom left of each image, is the same as for figure 5.2. Areas labelled on PC II: A1 = Area 1, A2 = Area 2, A3 = Area 3 and A4 = Area 4.

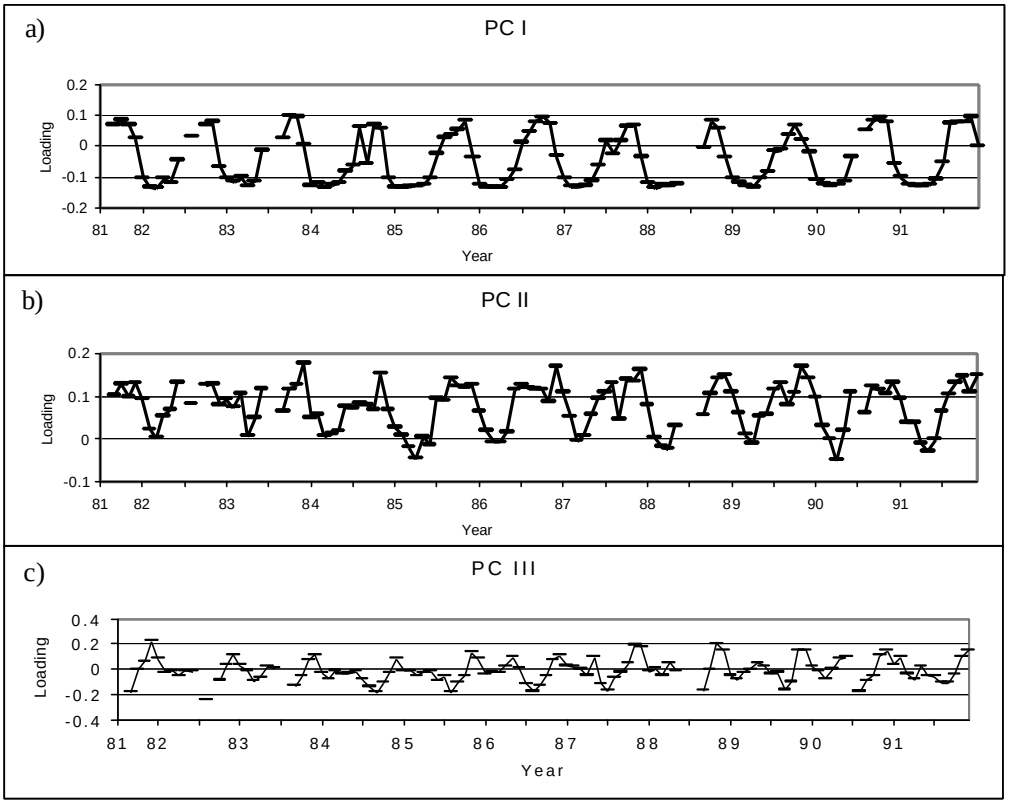

Figure 5.7. Loadings for PC I and PC II of the Gulf of Guinea PCA.

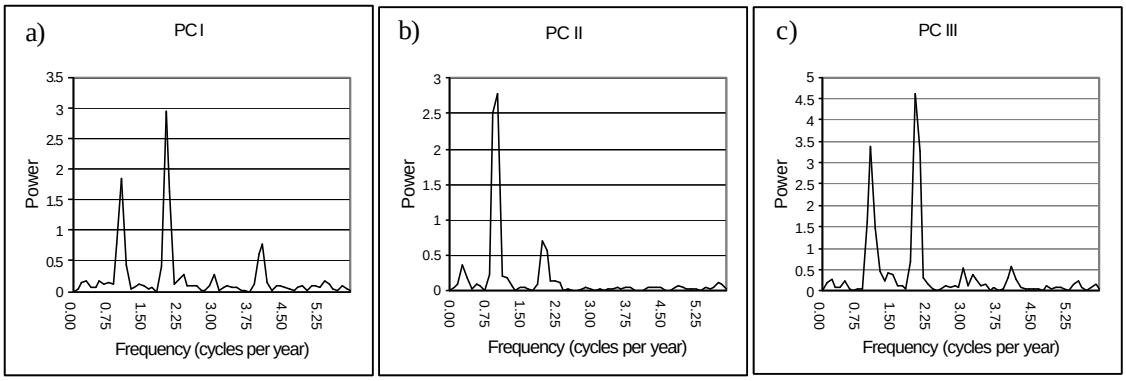

Figure 5.8. Power spectra for PC I and PC II of the Gulf of Guinea PCA.

The loadings for PCII (fig. 5.7b) appear to show two annual cycles as well as an interannual trend. This pattern is also seen in the power spectra of the loadings (fig5.8b), which show peaks at less than one (interannual), one (annual) and two (biannual) cycles per year. Despite their strong seasonality, the loadings are nearly always positive, suggesting this structure is present, either strongly or weakly, most of the time.

The characteristic shape and the position of Area 1 clearly identify it as the cold SUI, as already stated. As with PC I, the troughs in the loadings coincide with this feature being near the limit of its southerly extension, during March to April. When the loadings peak, the SUI is either in the far north or absent from the Gulf of Guinea. Area 2 corresponds to an area of ocean space not identified with any one particular process, but characterised by generally warm temperatures for most of the year. However, it can also be quite a variable area, under the seasonal influence of both the migration of cold SUI waters from the north and the influx of warm water from the tropical central Atlantic to the west. It is typically warm when the loadings are at a peak, between October and December, and cold when the loadings are at a trough and the SUI is extended. Area 3 represents the coastal upwelling areas along the coast, but offshore there is no boundary, instead the area extends both east and west and to the southern limit of the scene. This pattern is strongest in the coastal and equatorial upwelling areas, with a weaker band between them. Thus, Area 3 appears to couple the coastal and equatorial upwellings. The monthly SST composites show this pattern to be strongest after the end of the major upwelling, when the loadings are at a peak. This is because during this period Area 3 is relatively cool compared to Area 2. The position of Area 4, close to the coast of Nigeria and Cameroon, appears to identify it with the large areas of warm, low salinity water that exist in this location, originating from river discharge. Again, this pattern is observed when the loadings are at a peak.

The characteristics of these areas appear to be similar to those of Tilot and King's (1993) subsystems, with the exception of Area 1, which represents a boundary feature for the Gulf of Guinea LME, as previously discussed in chapter 4. Area 2 coincides with the major part of

the SLGP subsystem and Area 4 appears to be dominated by river run-off, a characteristic of the EGOG subsystem. The coastal section of Area 3 corresponds to the CWAU subsystem, however, PCA identifies this zone with equatorial dynamics offshore. This is consistent with studies of the equatorial Atlantic and the remote forcing theory of coastal upwelling, described in chapter 3. It appears, therefore, that the areas identified by this principal component can be used to redefine the subsystems of the Gulf of Guinea based on physical dynamics of the system rather than arbitrary boundaries.

GULF OF GUINEA PC III

PC III (fig. 5.6c) accounts for 3.7% of the total variance. It too shows an alternating pattern of areas that contrast in relative temperature. The dominant feature of this image is the area of relatively cold temperatures, which correspond to the maximum extent of the coastal upwelling area. In contrast to PC II, the upwelling area shown here is bounded offshore by a relatively warm area that extends from the western limit of the scene to the Cameroon coast in the east. North of this area is a relatively cool area, extending northwestward from the Sierra Leone and Guinea coasts. In the far north of the image is a relatively warm area. The loadings for PC III (fig. 5.7c) show two seasonal cycles which are identified in the power spectra (fig. 5.8c) as peaks with frequencies of one and two cycles per year. The monthly SST composites show these to correspond to the coastal upwelling seasons. Major troughs in the loadings coincide with the major upwelling season and minor troughs with the minor season. The weaker relatively cool area in the SLGP subsystem, which appears to vary in phase with the upwellings, may be due to the presence of the SUI in this region during the period of the minor upwelling season. The influence of processes apart from the upwelling seasons and the lack of any significant interannual cycles in this principal component mean it cannot be used as an index of interannual variability in the strengths of the upwellings, either absolutely or relative to each other.

5.3.3 Interpretation of PCA for Tilot and King's subsystems

The third PCA was carried out for subsystems of the Gulf of Guinea, according to arbitrary boundaries extended offshore from those proposed by Tilot and King (1993). The results are described for each subsystem.

SLGP

Only the first two principal components showed patterns that could readily be interpreted. These were kept for further inspection. The others were discarded. PC I (fig. 5.9a) shows a strong north-south dipole with a strong annual cycle, similar to PC II for West Africa and PC I for the whole Gulf of Guinea, only with the boundary further north. Additionally, the peaks and troughs of the loadings (fig. 5.10a) for this principal component occur at the same time as those for PC I of the whole Gulf of Guinea PCA. Therefore, the interpretation is the same for both of these principal components. The connection of the cold waters from the Sierra Leone coastal upwelling with the SUI is also represented as a very weak signal, due to the SUI waters being much colder than those off Sierra Leone. This connection is seen as a boundary that separates the warm waters on the continental shelf of Guinea and Sierra Leone from the warm, offshore oceanic waters.

PC II (fig. 5.9b) shows three areas of contrasting SST and has a strong seasonal cycle. The area in the far north appears to correspond to the SUI and south of this is an area which corresponds to relatively warm waters for most of the year. In the far south of the image is an area with an apparently cold temperature pattern. These areas appear to correspond most closely to those identified in PC II of the Gulf of Guinea PCA. The loadings for these two principal components also have the same pattern, although they are inverted for the loadings of this analysis (fig 5.10b). PC II for the whole Gulf of Guinea PCA was used to redefine the subsystems of the LME. It can be seen clearly from this analysis that the arbitrary boundaries used here to subdivide the Gulf of Guinea do not match those defined from PCA.

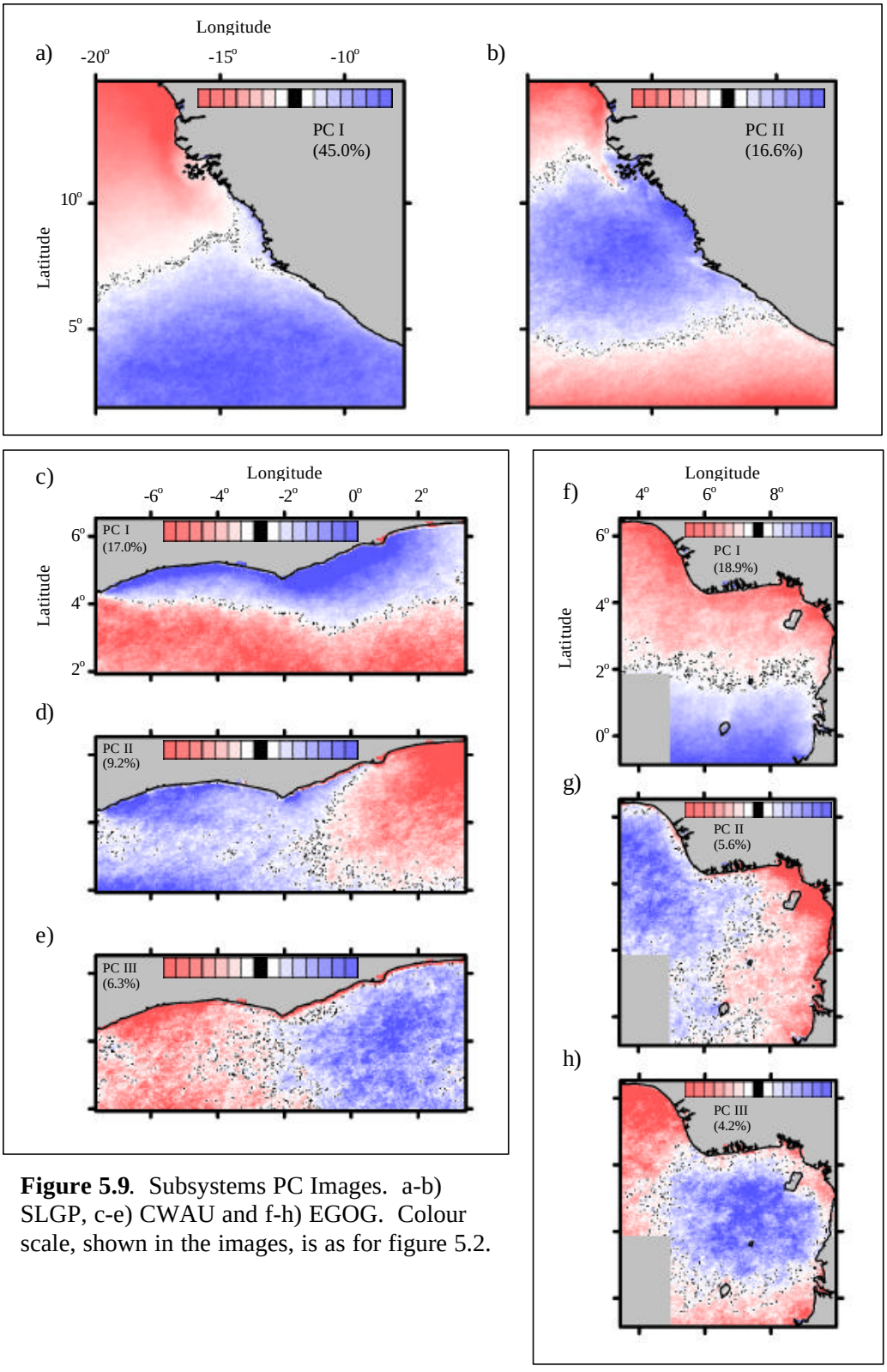

Figure 5.9. Subsystems PC Images. a-b) SLGP, c-e) CWAU and f-h) EGOG. Colour scale, shown in the images, is as for figure 5.2.

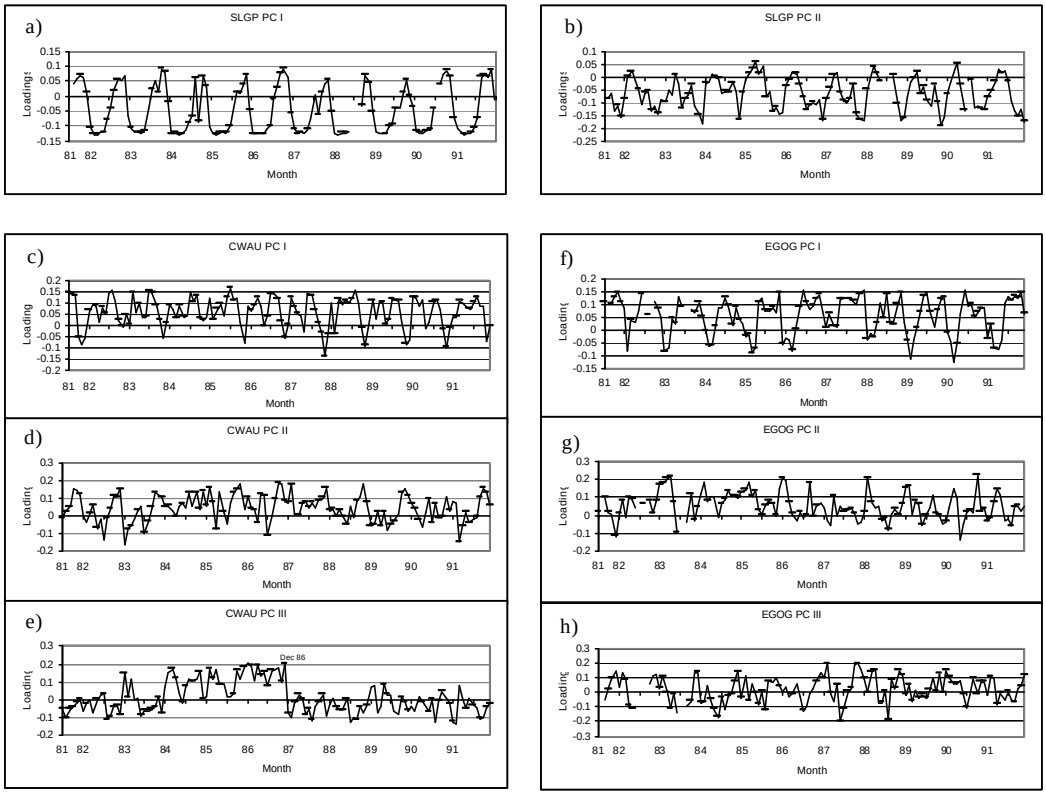

Figure 5.10. Subsystems loadings. a-b) SLGP, c-e) CWAU and f-h) EGOG.

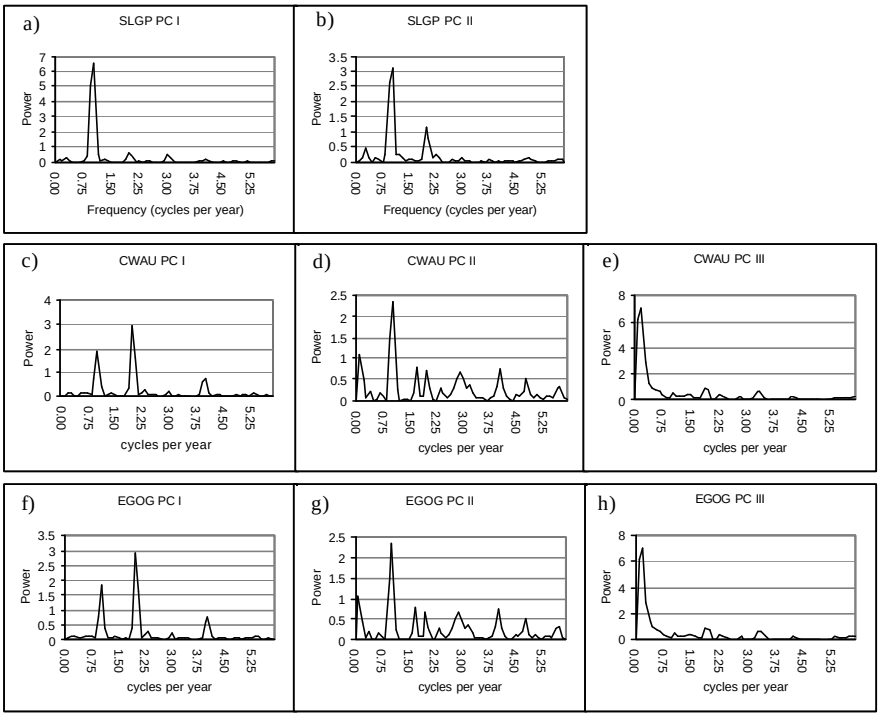

Figure 5.11. Subsystems power spectra. a-b) SLGP, c-e) CWAU and f-h) EGOG.

CWAU

The first three principal components of this analysis show interpretable patterns. PC I (fig. 5.9c) shows a strong meridional gradient in SST. The pattern has strong annual and biannual signals, seen in the loadings (fig. 5.10c) and their power spectra (fig. 5.11c). The pattern appears to correspond primarily to the biannual pattern of coastal upwelling seen in this subsystem. Certainly, the greatest peaks in the loadings correspond to the major upwelling seasons and the smaller peaks to the minor upwellings. However, the troughs in the loadings show that the pattern also represents the influx of warm waters along the coast, associated with the seasonal movement of the ITCZ. This gives a pattern of warmer waters at the coast than in the south of the scene, opposite to that of the upwelling seasons. The use of this principal component as an index of upwelling is not feasible. The strong gradient between warm and cold areas seen in the principal component image is not always reflected in the monthly SST composites which correspond to peaks in the loadings. Thus, it does not appear to give an accurate index of frontal strength, or retention. Similarly, the strength and timing of peaks in the loadings does not appear to always correspond to maximum upwelling strength. Rather, the peaks and troughs are representative of the situation throughout the whole area and can include the effects of more than one process.

PC II (fig. 5.9d) and PC III (fig. 5.9e) both appear to have the same structure but with opposite phase, i.e. a zonal gradient in SST. However, examination of the loadings (figs. 5.10d and e) and their power spectra (figs. 5.11d and e) show PC II to be dominated by an annual cycle, whereas PC III is dominated by interannual variability. Comparison with monthly SST composites shows peaks in the loadings of PC II to relate mainly to an influx of warm water from the east towards the end of the year, after the major upwelling season. However, the pattern is also found at times of unusually cold temperatures, related to upwelling, along the western coast, to the east of Cape Palmas. Similarly, troughs in the loadings tend to occur during periods of extremely low temperatures along the eastern coast relative to the west, again, usually associated with upwelling. The mixture of processes

contributing to this signal explains the noisiness of the signal, seen in the power spectra for the loadings. In PC III, this interannual scale variability is seen in the loadings as an increasing trend from low values in the early 1980s to a peak in 1986 and then a large, sudden drop between December 1986 and January 1987 to a period of very low values that continued throughout the rest of the time series. The peaks in the loadings correspond to cooler conditions in the east than the west and the troughs appear to coincide with influxes of warmer water from the east, on a non-seasonal basis. The dominant event in the loadings, corresponds to a large drop from an exceptionally cool situation in December 1986, to a large influx of warm water from the east in January 1987. By February, the whole area was covered by warm water.

EGOG

For the EGOG subsystem, the first three principal components show clear patterns, but only the first two are identifiable with known physical processes. PC I (fig. 5.9f) has a strong meridional gradient and seasonal cycle and the loadings for this principal component show two peaks per year (fig. 5.10f). These are attributable to the seasonal influx of cold water from equatorial upwelling in the south, usually during June or July and the influx of warm water in the north, associated with the seasonal migration of the ITCZ, usually during February or March. Run-off from rivers along the northern coast may also contribute to this.

PC II (fig. 5.9g) shows a strong zonal gradient. Power spectra of the loadings (fig. 5.11g) show them to be generally noisy with peaks either side of one cycle per year, but not exactly at this frequency. Inspection of the monthly SST composites shows peaks in the loadings (fig. 5.10g) to occur when warm waters dominate along the eastern coast. There are peaks in spring and autumn. The troughs appear to generally follow the peaks by between two and three months and represent cooler temperatures in the east than the west. The peaks may correspond to river run-off from the eastern coast, however, the only time when this is

vaguely visible is October 1990. No explanation in terms of physical processes can be provided from the SST structure observed during the troughs.

The circular pattern exhibited by PC III (fig. 5.9h) is extremely distinct, with SSTs in the central gyre having the opposite phase to those outside of it, and its loadings show a very strong annual cycle (fig. 5.10h). However, examination of the monthly SST composites could reveal no underlying physical process upon which to base this structure. Rather it appears to be caused by a coincidence of different processes bringing warm or cold waters into the area from all directions. Therefore, it appears that the underlying physical processes responsible for this pattern are the same ones discussed for the higher order SST structures shown by this analysis.

5.4 Redefining and Validating New Subsystems

The theoretical basis for this method to define ecological systems and subsystems was proposed by Keeling *et al.* (1997), as mentioned in chapter 1. PCA is a method of separating areas in which variance is positively correlated from those in which it is negatively correlated, thereby defining the natural length scale of the system or subsystem.

The PC II image for the whole Gulf of Guinea PCA appears to have structured the LME into its constituent subsystems according to patterns of SST variability. The location in coastal areas of the boundaries between these subsystems is remarkably close to those described by Tilot and King (1993), although the offshore extensions of these boundaries vary a great deal. This is not surprising as the offshore limits were defined arbitrarily for the purposes of this study. The loadings for this component show that although the pattern varies seasonally, it is nearly always present to some degree. The northern boundary of the LME is also delineated, in line with previous observations.

Additionally, PC I of the West African PCA shows a constant pattern of warm tropical waters contrasting with cooler subtropical waters. The northern boundary of the warm tropical

waters seen in this component corresponds closely to the northern limit of the Gulf of Guinea LME, as defined in this and the previous chapter. The southern boundary, however, is situated along the Angolan coast, far south of the predefined limit of the Gulf of Guinea LME at the equatorial upwelling. This raises important questions as to whether the Gulf of Guinea LME extends south of the equatorial upwelling, perhaps including the area around the Angola basin as another subsystem, or whether the tropical system to the south of the equatorial upwelling is a separate LME. Whatever the answers to these questions, they are outside the scope of this study. Nonetheless, the structure described in PC I of the West African PCA describes the Gulf of Guinea LME in its tropical context. Thus, these studies have described the structure of the Gulf of Guinea LME in nested spatial scales, from the global context, to the level of the LME and even into its constituent subsystems.

The conclusion that these structures identify different subsystems of the Gulf of Guinea LME is based on their interpretation in terms of geophysical features known to exist in the overall system. If these conclusions are correct, then the new subsystems should, according to Keeling *et al.*, appear both similar in nature to each other and different from surrounding systems. To investigate these relationships, time series of SST were calculated for the new areas by taking their spatial means for each week of the original data set. Area 1, because not part of the Gulf of Guinea LME under this description, was included as a control area. These time series were then used to explore the properties of the new subsystems.

5.4.1 Comparison of Areas

SST TIME SERIES

Visual comparison and statistical correlation between the SST time series for each of the new areas (fig. 5.12) showed Areas 2 to 4 to be closely related to each other but not to Area 1.

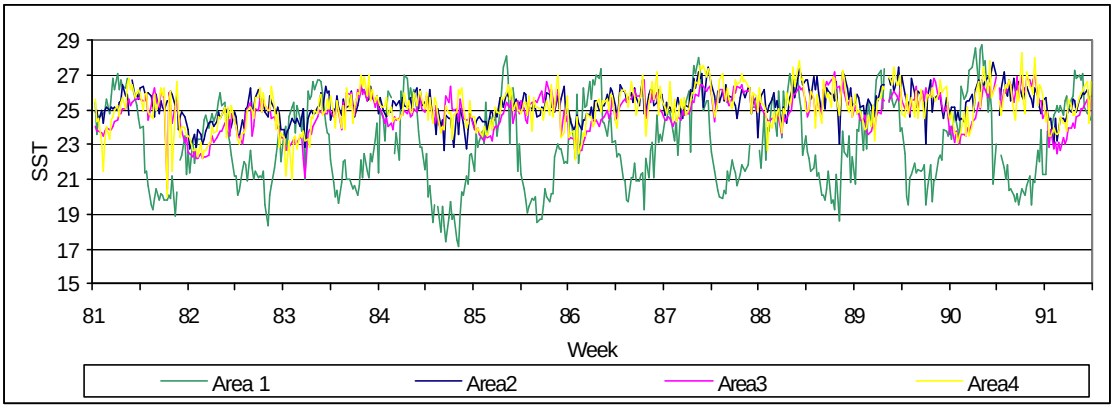

Figure 5.12. SST time series for each of the Areas identified in PC II of the Gulf of Guinea PCA.

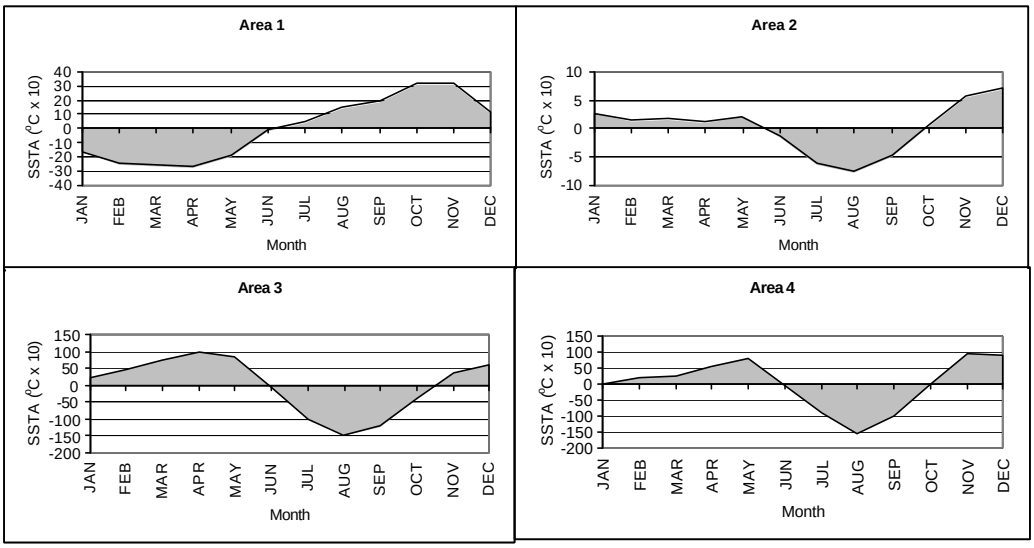

Figure 5.13. Seasonal mean SST anomaly for each of the Areas identified in PC II of the Gulf of Guinea PCA.

Areas 3 and 4 were the most closely correlated (r=0.812). Area 2 was almost equally related to Areas 3 and 4 (r=0.648 and r=0.632, respectively). No evidence of a relationship was found between Area 1 and Areas 2, 3 and 4 (r=0.100, r=0.300, r=0.032, respectively). All results are highly significant ($P<0.01$), except between Area 1 and Areas 2 and 4, which are still significant ($P<0.05$).

Visual comparison and correlation of two SST series from within each Area showed a stronger relationship than that between Areas, except for Area 4, which still showed a strong relationship. This relationship was strongest for Area 1 ($r=0.943$). Area 2 and Area 3 showed approximately the same level of coherence ($r=0.831$ and $r=0.825$, respectively). Area 4 was also significantly coherent ($r=0.721$). All results are highly significant ($P<0.01$).

Seasonal cycles

Charts of the seasonal cycles in each area (fig 5.13) show two to three seasons for Area 4 (6:4:2 months) and a similar pattern of two seasons for Areas 2 and 3 (8:4 months), however, although two seasons are also identified for Area 1, these have a very different structure to the other areas (6:6 months). Power spectra for each of the areas (fig 5.14) show peaks with frequencies at both one cycle per year and two cycles per year for Areas 2, 3 and 4, however, only an annual peak (one cycle per year) is seen for Area 1.

Comparison of the seasonal cycles for the two SST series from within each Area show the seasonal cycle of each Area to be consistent throughout that Area.

Interannual variability

Power spectra for each of the areas also showed interannual scale peaks on biennial (two year), intermediate (three to six year) and decadal scales for each area (fig. 5.14). To investigate interannual variability between the areas, these interannual peaks were used to extract the interannual SST pattern from the SST data (fig. 5.15). SST monthly anomalies were also calculated for the time series of monthly SST data and these were used for correlation between the areas.

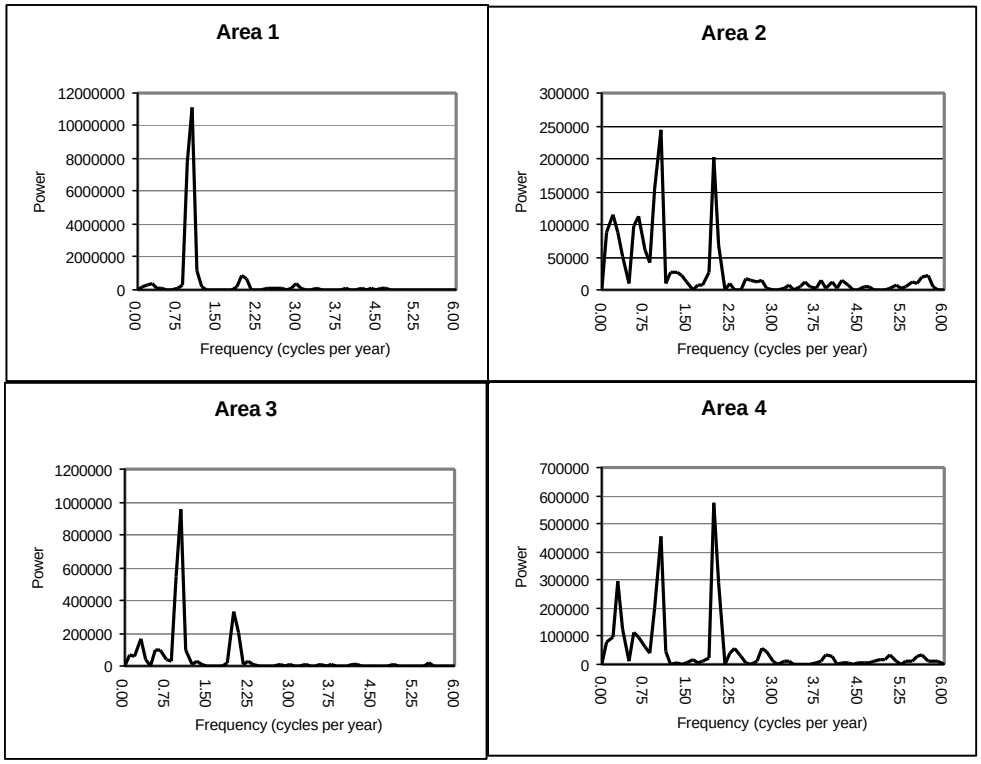

Figure 5.14. Power spectra of SST for each of the Areas identified in PC II of the Gulf of Guinea PCA.

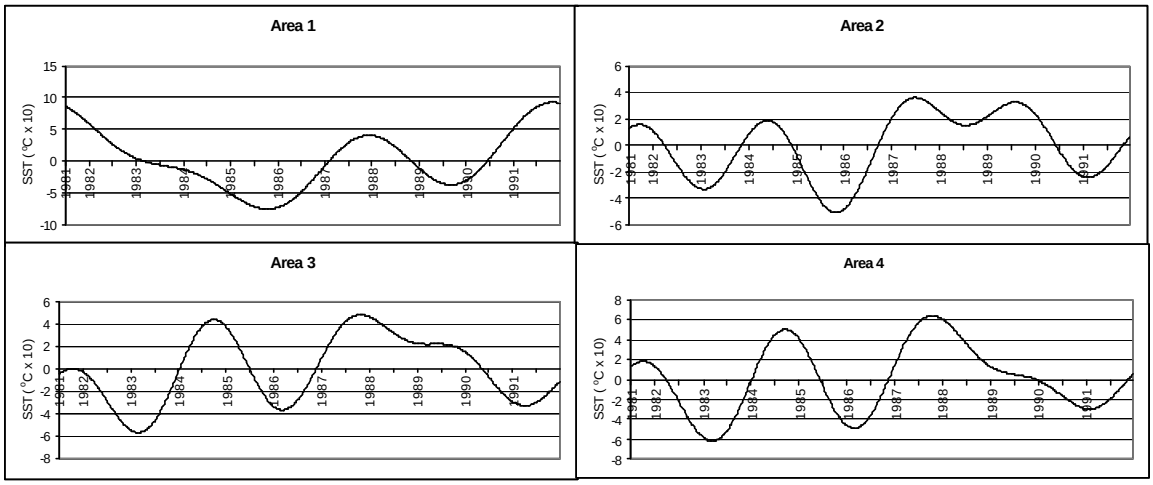

Figure 5.15. Interannual SST cycles from power spectra for each of the Areas identified in PC II of the Gulf of Guinea PCA.

The interannual pattern from power spectra for Areas 2, 3 and 4 showed an alternating cycle of warm and cool SSTs, with a period of about three years, with a superimposed prolonged warm period from 1987 to 1990. The prolonged warm period was seen most strongly for Area 2 and was least evident in Area 4. This pattern is very similar to that described for the CWAU and EGOG subsystems in chapter 4. The interannual pattern from power spectra for Area 1 was very different. SSTs appeared to be declining for the first half of the time series and increasing for the second half, with an additional increase in 1988. This pattern showed some similarity to that of the SLGP subsystem, described in chapter 4.

Correlation of the SST monthly anomalies showed stronger relationships than for the SST weekly values, however, the relationships were essentially the same in nature. Area 3 and Area 4 were most strongly correlated (r=0.866), Area 2 was more strongly correlated with Areas 3 and 4 (r=0.806, r=0.728, respectively) than Area 1 (r=0.469). Area 1 was least strongly correlated with Areas 3 and 4 (r=0.332, r=0.374, respectively). All results are highly significant ($P<0.01$).

Correlation of the SST monthly anomalies for the two SST series from within each Area also showed stronger relationships than for the SST weekly values for all Areas except Area 1. This Area showed strong coherence (r=0.877), but weaker than for regression of the weekly SST values. Area 3 showed the strongest coherence (r=0.894), closely followed by Area 2 (r=0.889). Area 4 again showed the weakest coherence (r=0.825). All results are highly significant ($P<0.01$).

5.4.2 Conclusion on new subsystems

The SST signals for Areas 2 to 4 confirm that they belong to the same system as each other and a different system from Area 1. This is apparent in the similarities between the signals on a seasonal and interannual basis. Areas 3 and 4 appear to be the most closely related. The fixed boundaries used for the subsystems in these validation studies mean that the seasonal

contraction and expansion of Areas 1 and 2 has not been taken into account. This means that Area 2 actually has a mixed nature, with cold SUI waters penetrating into the area on a seasonal basis. Nonetheless, the seasonal signal of Area 2 is still very distinct from Area 1. Perhaps, however, on an interannual basis, the closer relationship of Area 1 with Area 2 than with other Areas may be due to variability between years in the most southerly extent of the SUI.

The strong correlation seen for SST within each Area, compared with those between Areas, confirms that each Area is a coherent subsystem. The weak relationship within Area 4 compared to its relationship with Area 3 for weekly SST data may be due to high frequency, small scale variability in this Area caused by its dependence on meteorological conditions (rainfall and river run-off). The much stronger relationship seen in the monthly anomalies shows the Area is coherent on an interannual basis, although this is still weaker than the relationship between Area 3 and 4. Nonetheless, the fact that this Area can be interpreted in terms of physical processes known to occur justifies it being defined as a subsystem of the Gulf of Guinea.

5.5 General Conclusions

From the interpretations and discussion in the previous sections, the following conclusions can be drawn. Firstly, the Gulf of Guinea system can be seen to lie wholly within the warm waters of the tropical Atlantic and separate from the cooler waters of the subtropical gyral circulation. Its northern boundary is defined by the interface between the SUI and warmer tropical Atlantic waters to the south, with the SUI lying outside the Gulf of Guinea. The southern boundary of the system cannot be determined from this study.

Secondly, the Gulf of Guinea system can be divided into three subsystems, identified by Areas 2 to 4 of PC II for the whole Gulf of Guinea PCA. These areas correspond closely to the coastal subsystems defined by Tilot and King (1993) and are validated by investigation of

their SST signals, both seasonally and interannually. The importance of these boundaries is that they are delineated by the variance structure of physical data, rather than being arbitrarily determined, as has previously been the case.

Thirdly, the seasonal SST dipole picked out in both analyses shows the boundary between areas of North and South Atlantic influence to be situated around 5^{o}N and correspond to the mean position of the ITCZ. This implies that ocean-atmosphere interactions exist in determining seasonal circulation patterns and that, depending on the position of the ITCZ, areas of the Gulf of Guinea can be under the influence of either the North or South Atlantic at different times of the year.

Finally, PCA was able to identify, but not accurately define, physical processes and structures in this region on a finer scale than that of the whole system. This lack of accuracy may be due to PCA being too rigorous a procedure for the data used, which contain autocorrelation and non-linearities. The dominant processes in the system can be assumed to be close to linear in the short time frame looked at, however, this is not true for the noisier signals of weaker processes. Thus, in some principal components only part of a process is defined and in others multiple processes are shown. On the other hand, at the system level, all the processes present contribute to the variability of the system. Therefore, PCA can accurately interpret the variance structure of the data to define structures of relevance to the whole system, such as boundaries.

6 River Discharge and Coastal Run-off Data

6.1 Introduction

River discharge and coastal run-off data were obtained for the period 1951 to 1989 from Gil Mahé of IRD, in the form of annual means for each of 34 gauged rivers and 11 ungauged coastal areas. The 34 rivers used in this study are not all the same as the 33 rivers used in Mahé and Olivry (1999) . Rivers used here not used in Mahé and Olivry (1999) are Cacheu, Kogon, Little Scarcies, Farmington, Cavally, Benue and Rio Muni. Rivers used in Mahé and Olivry (1999) not used here are Senegal, Gambia, Casamance, Kienké, Kouilou and Congo. For 13 rivers monthly data were also available. The length of these monthly time series varied. Table 6.1 shows the rivers used in this study. Some of the data were reconstructed from rainfall-runoff relationships and the methods used are described by Mahé (1993).

The annual river data were grouped by Mahé and Olivry (1999) into eight regional hydroclimates, based on isohyetal lines, general climatic conditions and interannual variability in rainfall, as well as monthly regimes and interannual variability in river flow. These regional hydroclimates are Sénégal-Fouta, Guinée, Nordgolf, Niger, Adamaoua, Equateur, Congo and Angola (Mahé and Olivry 1999). This study was not concerned with Senegal, Congo or Angola (see fig. 6.1), therefore, only six of the eight hydroclimatic regions are used and Sénégal-Fouta is only called Fouta here. Apart from this change, the French names for each of the hydroclimatic regions was used in this study for ease of comparison with previous studies (e.g. Mahé 1993, Mahé and Olivry 1995, 1999). The names of countries within the coastal areas of these groupings may not correspond to the name of the hydroclimatic region. For example, the ungauged Guinée region contains the coastal areas of Sierra-Leone and Liberia while the coastal area of Guinea belongs to the ungauged Fouta region. Also, the coastal area of Nigeria fits into the ungauged Adamaoua region and the Niger region has no ungauged coastal zone.

Table 6.1. Rivers used grouped according to their regional hydroclimate. Rivers marked * were not used in Mahe and Olivry (1995). Monthly data were also available for rivers marked †. Data for hydoclimatic stations marked ‡ are mostly reconstructed. If no hydroclimatic station is given, all data are reconstructed.

Name	*Hydrometric Station*	*Country*	*Regional Hydroclimate*	*Surface area (km^2)*	*Observation period*
Cacheu*		Guinea Bissau	Fouta	28000	
Corubal	Saltinho Amont	Guinea Bissau	Fouta	23800	1977-1989
Kogon*	Le Pont‡	Guinea	Fouta	8000	
Fatala	Bindan	Guinea	Fouta	5100	1971-1986
Konkoure†	Amaria	Guinea	Fouta	16200	1951-1989
Kolente	Tassin	Guinea	Guinée	6600	1954-1980
Little Scarcies*		Sierra Leone	Guinée	21000	
Rokel	Bumbuna	Sierra Leone	Guinée	4000	1970-1978
Pampana	Matatota	Sierra Leone	Guinée	2400	1972-1977
Sewa	Jaïama	Sierra Leone	Guinée	6900	1972-1977
Mano	Mano Mines	Liberia	Guinée	5500	1951-1971
St Paul	Mount Coffe	Liberia	Guinée	21400	1958-1978
Farmington*		Liberia	Guinée	2750	
St John	St John Falls	Liberia	Guinée	11400	1958-1978
Cestos	Sawolo	Liberia	Guinée	4600	1960-1979
Cavally*	Tete‡	Côte d'Ivoire	Nordgolf	30000	
Sassandra†	Gaoulou	Côte d'Ivoire	Nordgolf	70600	1953-1986
Bandama	Daboitié	Côte d'Ivoire	Nordgolf	60000	1951-1985
Komoe†	Mbasso	Côte d'Ivoire	Nordgolf	70500	1951-1986
Bia	Ayamé	Côte d'Ivoire	Nordgolf	10000	1951-1989
Tano	Alenda	Ghana	Nordgolf	16000	1956-1978
Volta	Senchi Halcrow	Ghana	Nordgolf	394000	1951-1979
Mono†	Tététou	Togo	Nordgolf	20500	1952-1988
Ouémé†	Pont de Savé	Benin	Nordgolf	23600	1951-1984
Niger†	Onitsha	Nigeria	Niger	1100000	1951-1989
Benue	Makurdi	Nigeria	Niger	300000	
Wouri†	Yabassi	Cameroon	Adamaoua	8200	1951-1984
Mungo†	Mundame	Cameroon	Adamaoua	2400	1952-1984
Sanaga†	Édéa	Cameroon	Adamaoua	132000	1951-1980
Nyong†	Dehane	Cameroon	Equateur	26400	1951-1984
Ntem†	Nyabessan	Cameroon	Equateur	26300	1951-1984
Rio Muni*		Equatorial Guinea	Equateur	3200	
Ogooué†	Lambaréné	Gabon	Equateur	203000	1951-1989
Nyanga†	Tchibanga	Gabon	Equateur	12400	1954-1982

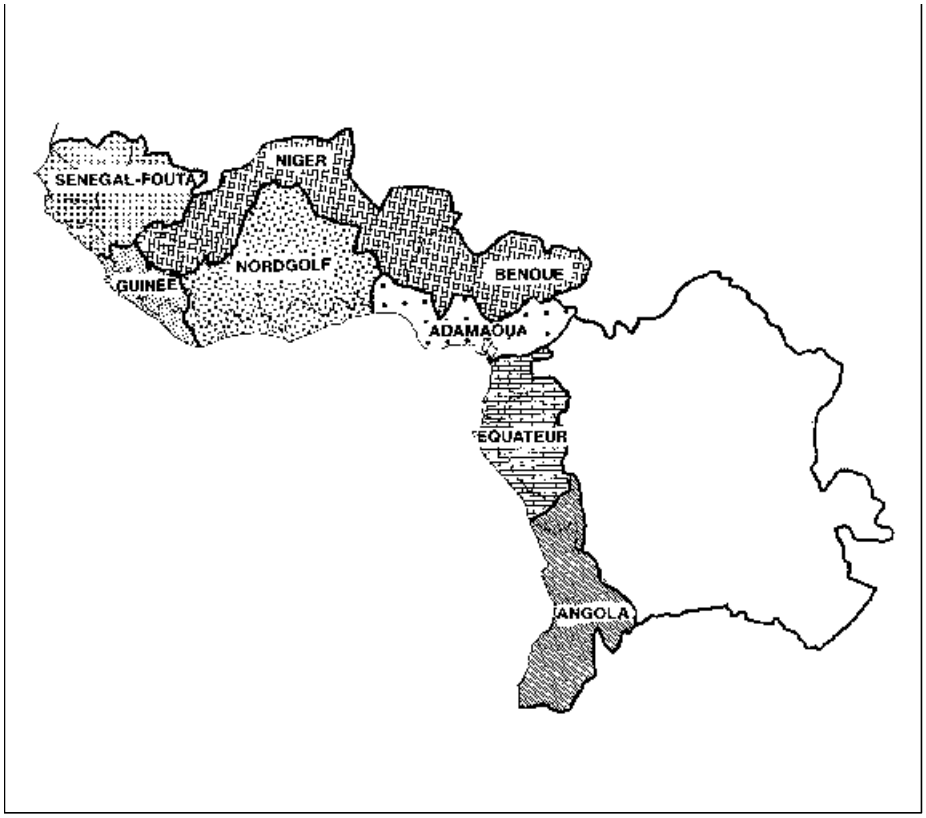

Figure 6.1. Regional hydroclimates used by Mahé and Olivry (1995, 1999). Figure taken from Mahé 1993.

Table 6.2. Ungauged run-off areas throughout the Gulf of Guinea. These include discharge from ungauged coastal rivers and streams.

Ungauged Area	*Countries*	*Regional Hydroclimate*	*Surface Area (km^2)*
North Nunez	Guinea Bissau	Fouta	7500
Nunez	Guinea	Fouta	11000
Conakry	Guinea	Guinée	10000
Freetown	Sierra Leone	Guinée	33000
Monrovia	Liberia	Guinée	25000
Coastal Nordgolf	Cote d'Ivoire to Benin	Nordgolf	180000
Adamaoua	Nigeria to Cameroon	Adamaoua	211000
Coastal Nigeria	Nigeria	Adamaoua	200000
North Equateur	Cameroon to north Gabon	Equateur	50000
Equateur	Cameroon to Gabon	Equateur	132000
South Equateur	South Gabon	Equateur	82000

Coastal areas were classified as ungauged zones in comparison to the larger drainage basins due to a lack of hydrometric stations in these areas. Runoff for these ungauged coastal areas was calculated using rainfall-runoff relationships established by Olivry (1986) for coastal streams in Cameroon. Run-off estimates are essential for these ungauged zones in order to

establish the quantity of freshwater entering the ocean from rivers and coastal streams. Some of the ungauged coastal areas correspond to regional hydroclimates, while others are named after local areas in the surroundings of certain cities or rivers. The coastal areas used are given in table 6.2.

6.2 Methods

Initially, monthly discharge data were examined for the 13 rivers for which they were available. Seasonal river discharge was plotted for each of the rivers. Annual discharge data were then plotted to show interannual variability throughout the time series.

To further examine the interannual variance structure of the data, PCA was used. The individual rivers' annual discharge data were temporally standardised and PCA was performed using the *SYSTAT*® 7.0 statistical software package with a variance-covariance matrix. The mathematical basis of this routine is essentially the same as that described for use with remotely sensed images, however, there are some differences (see Appendix 1). Essentially, because there is no spatial element to the input data, they have been temporally standardised and oriented for the input matrix. Consequently, the temporal output is given by the principal component matrix and the loadings of different rivers, relative to each other, are given by the eigenvectors.

PCA was performed on all rivers together and for rivers grouped according to their regional hydroclimate, identified by Mahé and Olivry (1999). The analysis was repeated using individual rivers' monthly discharge data and annual run-off estimates for coastal areas.

6.3 Results

6.3.1 Qualitative assessment

SEASONAL CYCLE

The mean monthly flow charts show meridional variations in seasonal river flow from Guinea to Gabon (fig. 6.2). The Konkoure river (Guinea) has peak flow in August. From Sierra Leone to Benin, this peak appears in September. From the Niger-Benue river system of Nigeria to the Sanaga River of northern Cameroon, peak flow is between September and October. It is in September for the smaller Mungo and Wouri rivers and in October for the larger Niger-Benue and Sanaga rivers. For the Nyong and Ntem rivers in southern Cameroon, there are two peaks in river flow. The major peak is around October to November and the minor peak is around May to June. For the Ogooue River in Gabon, there are also two peaks: the first in May and the other in November. However, a more noticeable pattern is that river flow is high for most of the year with a major drop in river flow between June and October. For the Nyanga River in Gabon, river flow is fairly constant from December to May, but also drops dramatically from June to October.

INTERANNUAL VARIABILITY

A reasonably high degree of interannual variability is seen in all the rivers and coastal areas studied (fig. 6.3). Much of this is consistent for rivers from the same country or area, however, there is also some river specific variability. Longer term trends are also observed in the data. The period from 1951 to the mid-1960s appears to vary around a moderately constant mean level, however, from the late 1960s onwards there has been a steadily decreasing trend. This is steepest in the rivers of Guinea-Bissau and Guinea, becoming less pronounced further south, until by Gabon it is almost negligible. In the Guinea-Bissau and Guinea data, this declining trend appears to commence with a large drop in 1968.

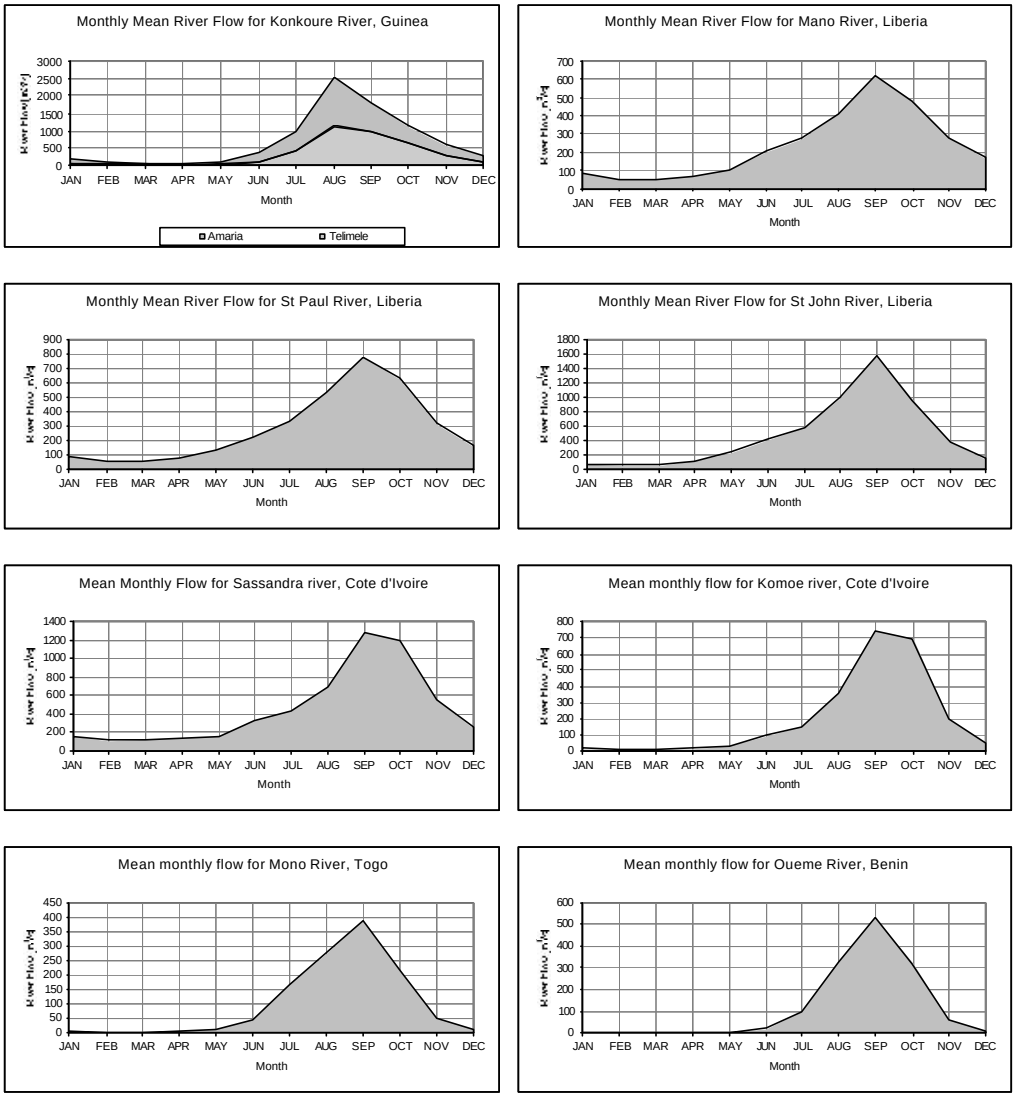

Figure 6.2. Seasonal river discharge throughout the Gulf of Guinea. For the Konkoure river of Guinea, river flow was measured at two stations: Amaria and Telimele. For all other rivers flow was measured at the stations given in table 6.1.

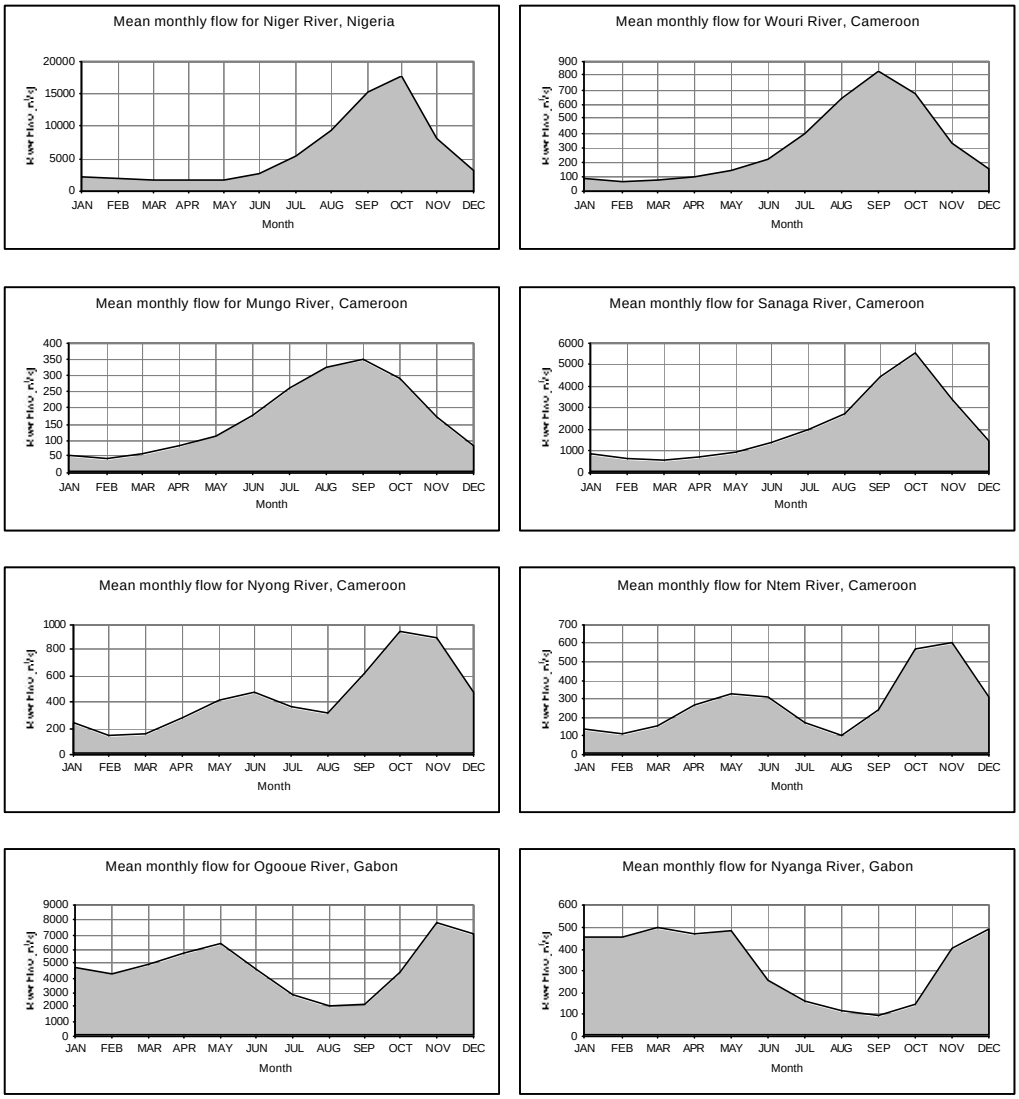

Figure 6.2 (cont.). Seasonal river discharge throughout the Gulf of Guinea. For the Konkoure river of Guinea, river flow was measured at two stations: Amaria and Telimele. For all other rivers flow was measured at the stations given in table 6.1.

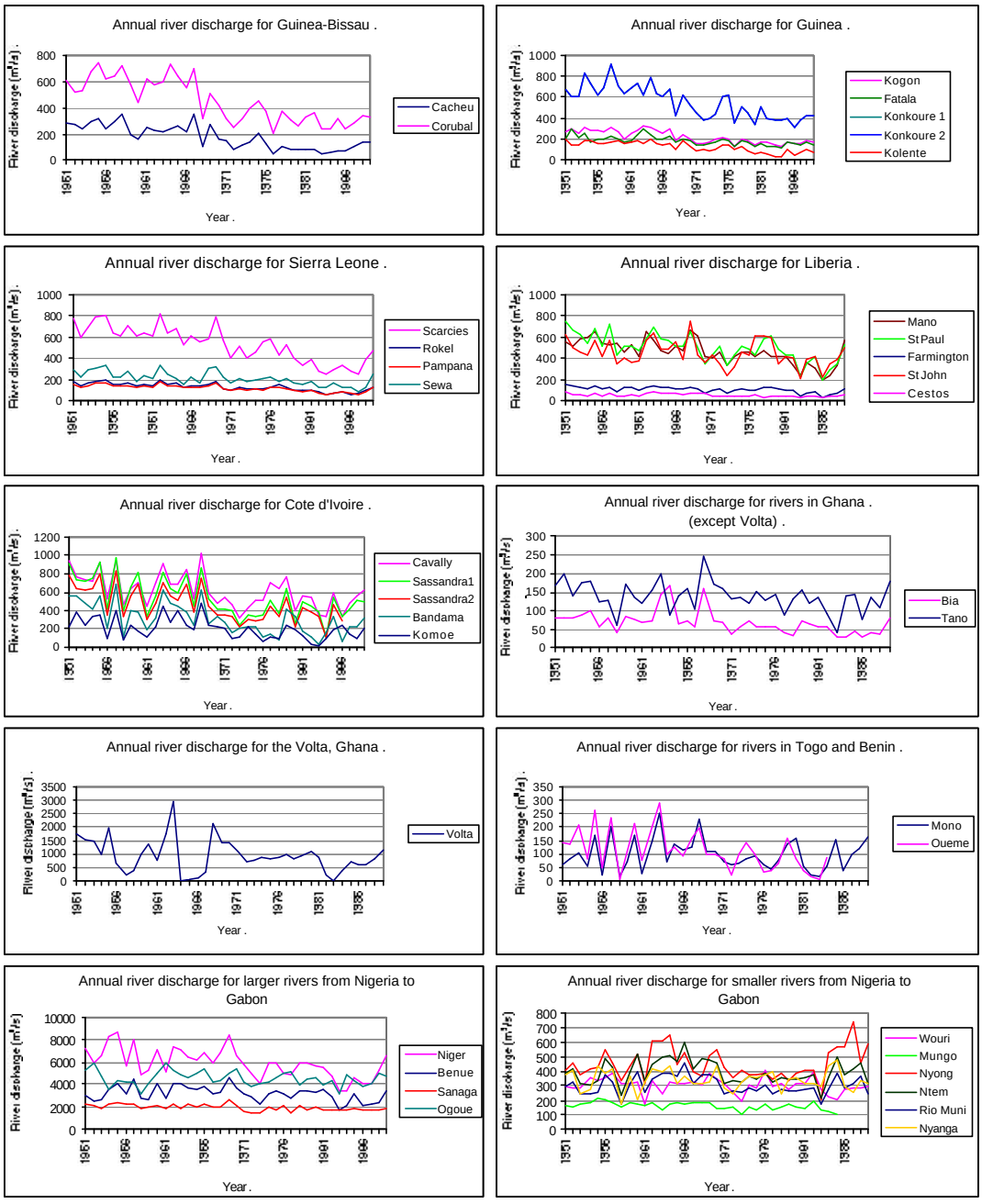

Figure 6.3. Annual river discharge (in m^3/s) from throughout the Gulf of Guinea region for the years 1951 to 1989.

There is then a partial recovery in 1969 before levels drop again to very low levels by 1972-73. In other areas, 1968 has very high levels of river discharge and coastal run-off, but by 1972-73, levels have also dropped severely. In most rivers and coastal areas, this declining trend continues, dropping suddenly again for 1983. There is another drop in 1986, before an upturn in the trend from 1986-89. The short period of this increasing trend means it is not possible to assess whether it signals an end to the decreasing trend or is just a short-term fluctuation.

6.3.2 Principal Components Analysis

WHOLE GULF OF GUINEA PCA USING ANNUAL RIVER DISCHARGE DATA

When PCA was performed on annual discharge data for all rivers together, 73% of the total variance of the data was explained by the first three principal components. These were retained for interpretation (fig. 6.4). The other components were discarded on the basis that individually they explain very little of the remaining variance. The loadings are shown in figure 6.5. PC I had high, positive loadings for all rivers and explained 52% of the total variance. PC II explained 13% of the total variance. It loaded negatively on all rivers from the Cacheu (Guinea Bissau) to the Moa (Sierra Leone); positively on all rivers from the Lofa (Liberia) to the Ouémé (Benin); negatively on the Niger; positively on the Benue (Nigeria); negatively for the Wouri and Sanaga rivers (Cameroon) and positively on the rivers from the Nyong (Cameroon) to the Nyanga (Gabon). PC III, explaining 7.9% of the total variance, loaded negatively on rivers from the Cacheu to the Kolente (Guinea); positively on rivers from the Little Scarcies (Sierra Leone) to the St John (Liberia); negatively for the Cestos (Liberia); positively for the rivers from the Cavally (Côte d'Ivoire) to the Niger and negatively from the Benue to the Nyanga.

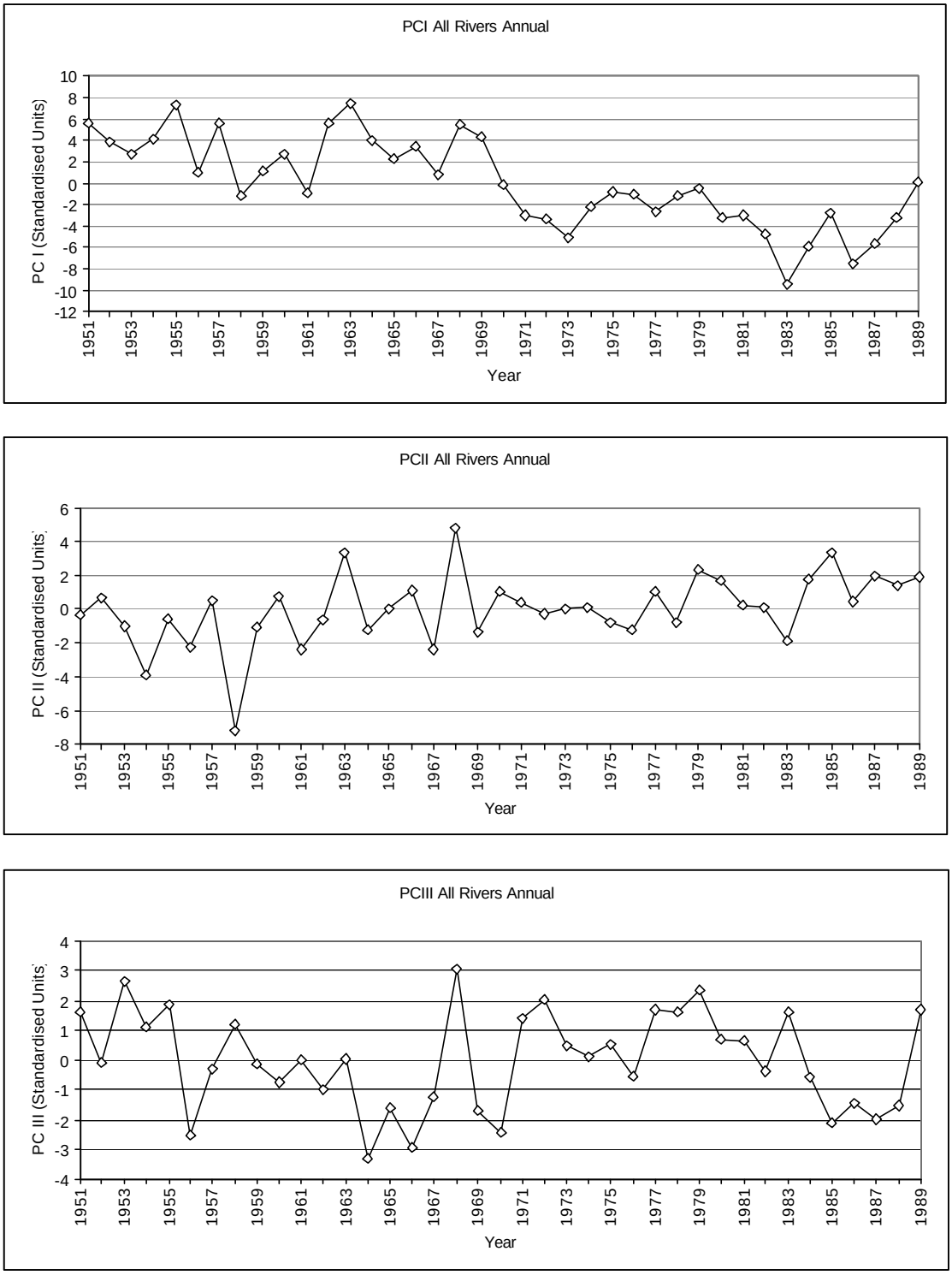

Figure 6.4. First three principal components of annual river discharge for all rivers.

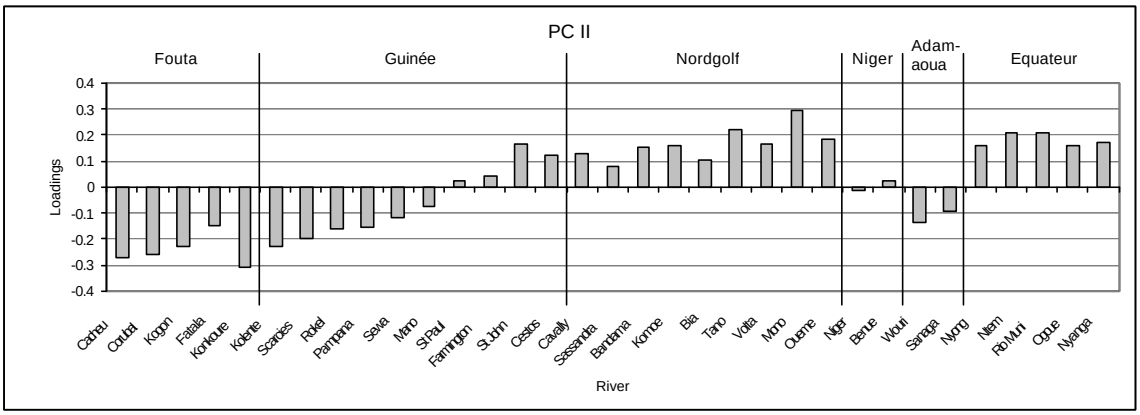

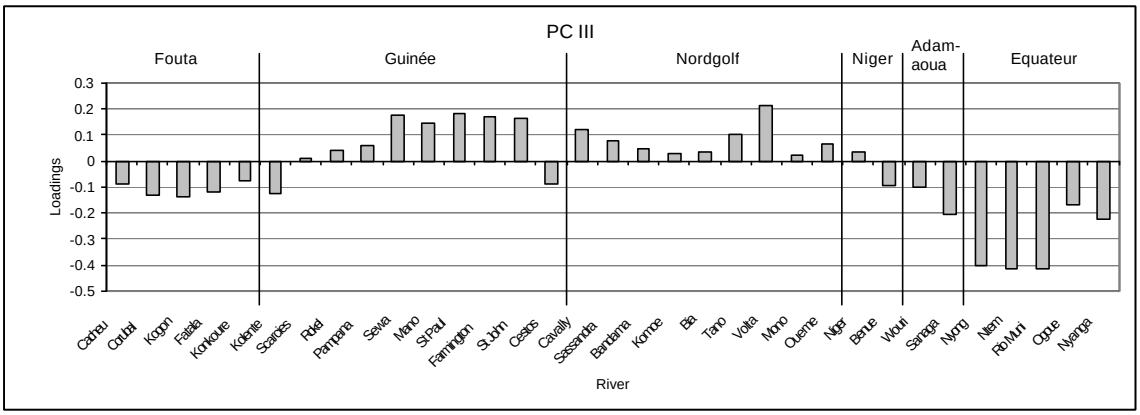

Figure 6.5. Loadings for PCs II and III of the PCA with all rivers annual data. The regional hydroclimate boundaries of Mahé and Olivry (1995, 1999) are overlaid.

All three of the output principal components showed a reasonably high degree of interannual variability. PC I shows a steadily decreasing trend throughout the series. The period from 1951 up until 1968 is characterised by relatively high values, whereas the period from 1971 to 1989 is dominated by low values. The two periods are separated by a large drop in values between 1969 and 1971. The highest values occur in 1955 and 1963 and the lowest value is found in 1983. This pattern appears very similar to that seen in the majority of river discharge series. PC II shows a slightly increasing trend throughout the series. The lowest value is seen in 1958 and the highest in 1968. Thus, this component appears to show an inverted pattern of the variability seen in the rivers of Guinea-Bissau and Guinea. PC III shows a declining trend from 1951 to 1966, with the lowest value of the series occurring in 1964. Values then rise rapidly to a peak in 1968, the highest value of the series, before

dropping off steeply again in 1969. Higher values then dominate from 1983, except during 1985 to 1988 when low values are found. A return to higher values is seen in 1989. The dominant feature of this component is the 1968 peak, which is characteristic of the majority of rivers from Sierra Leone to Benin. It is particularly noticeable in the rivers of Sierra Leone, Liberia, Côte d'Ivoire and Ghana (except for the Volta).

REGIONAL HYDROCLIMATE PCA USING ANNUAL RIVER DISCHARGE DATA

For PCA of the annual discharge data for rivers grouped according to their regional hydroclimate, only the first principal component was retained for interpretation for all groups apart from Guinée. The first two principal components were retained for this region. These components are shown in figure 6.6. The first principal component of each area explained between 61.6% (Equateur) and 92.2% (Niger) of the total variance. The second principal component for Guinée explained 12.6% of the total variance. The other components were discarded on the basis that individually they explain very little of the remaining variance.

Examination of the first principal component series for each hydroclimatic region showed each region to reflect the characteristics of its constituent rivers. A stepwise shift from high values in the 1950s and 1960s to lower values in the 1970s and 1980s was seen for all regions and a declining linear trend was also observed for all regions, except Equateur. This trend becomes less steep towards the south and east. The Fouta region showed a large drop in 1968, whereas the Guinée and Nordgolf areas showed peaks in these years. In the Adamaoua and Niger regions, this peak was seen in 1969. The Equateur region showed very low values in 1958 and 1983.

PCA USING MONTHLY RIVER DISCHARGE DATA

For PCA of monthly river discharge data, for all the rivers for which it was available, the first three principal components were retained for interpretation.

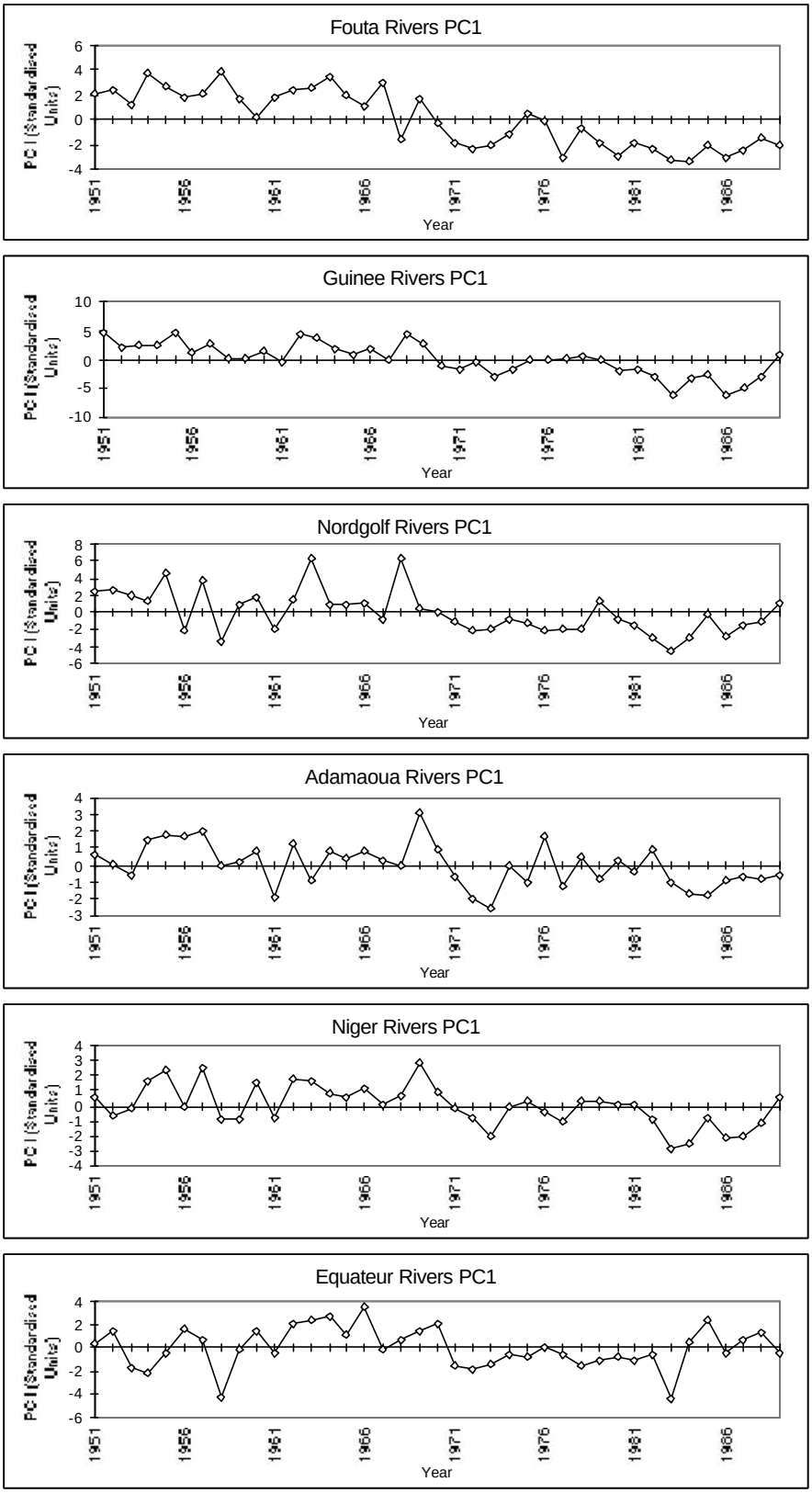

Figure 6.6. First principal component of annual river discharge for each hydroclimatic region.

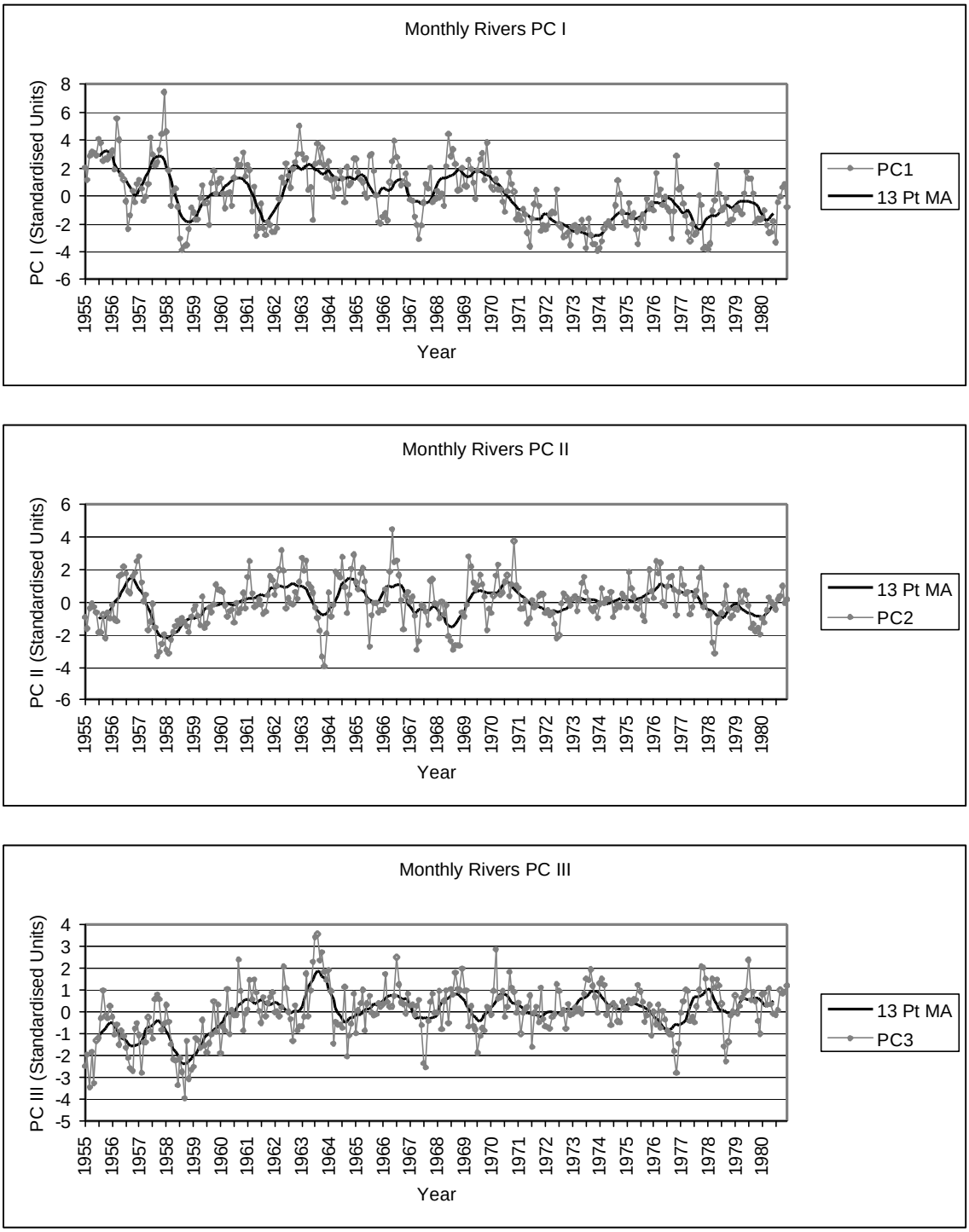

Figure 6.7. First three principal components of monthly river discharge for all rivers (grey line) and 13 point moving average (black line).

These are shown in figure 6.7 and their loadings are shown in figure 6.8. PC I loaded positively for all rivers and accounted for 33.6% of the total variance. PC II, explaining 14.1% of the total variance, loaded negatively for all rivers from the Konkoure to the Niger and positively for all rivers from the Wouri to the Nyanga. PC III explained 11.1% of the total variance and loaded negatively for the Konkoure river, positively for the Sassandra River to the Mono River, negatively for the Niger River to the Sanaga River and positively for the Nyong River to the Nyanga River. The other components were discarded on the basis that individually they explain very little of the remaining variance.

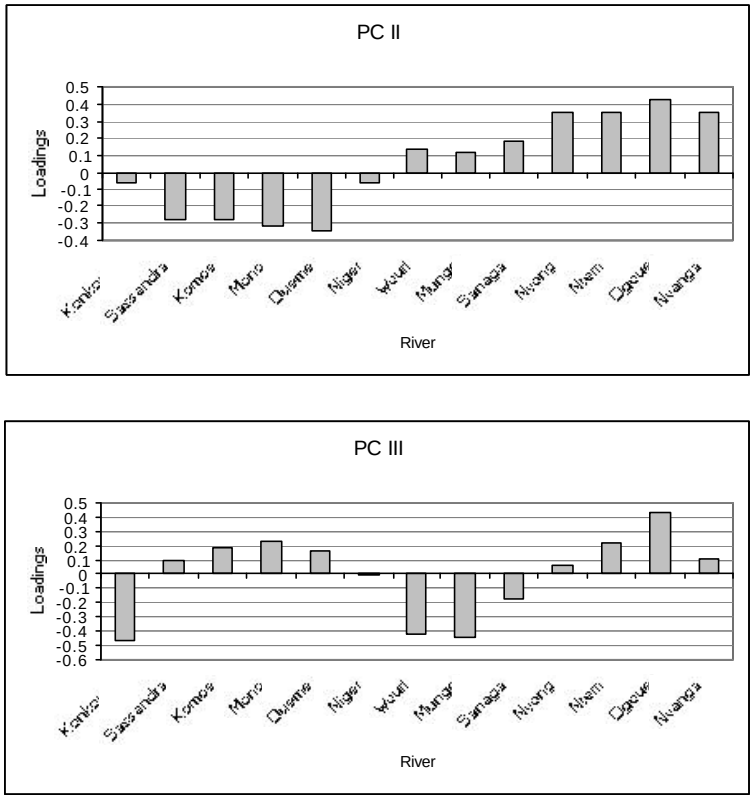

Figure 6.8. Loadings for PCs II and III of the PCA with all rivers monthly data.

The smoothed PC I series showed similar trends and long term changes to the first principal components of the previous analyses. PC II and PC III, however, do not show the same pattern as in previous analyses, although they do highlight some of the same years (1956, 1958, 1963, 1968).

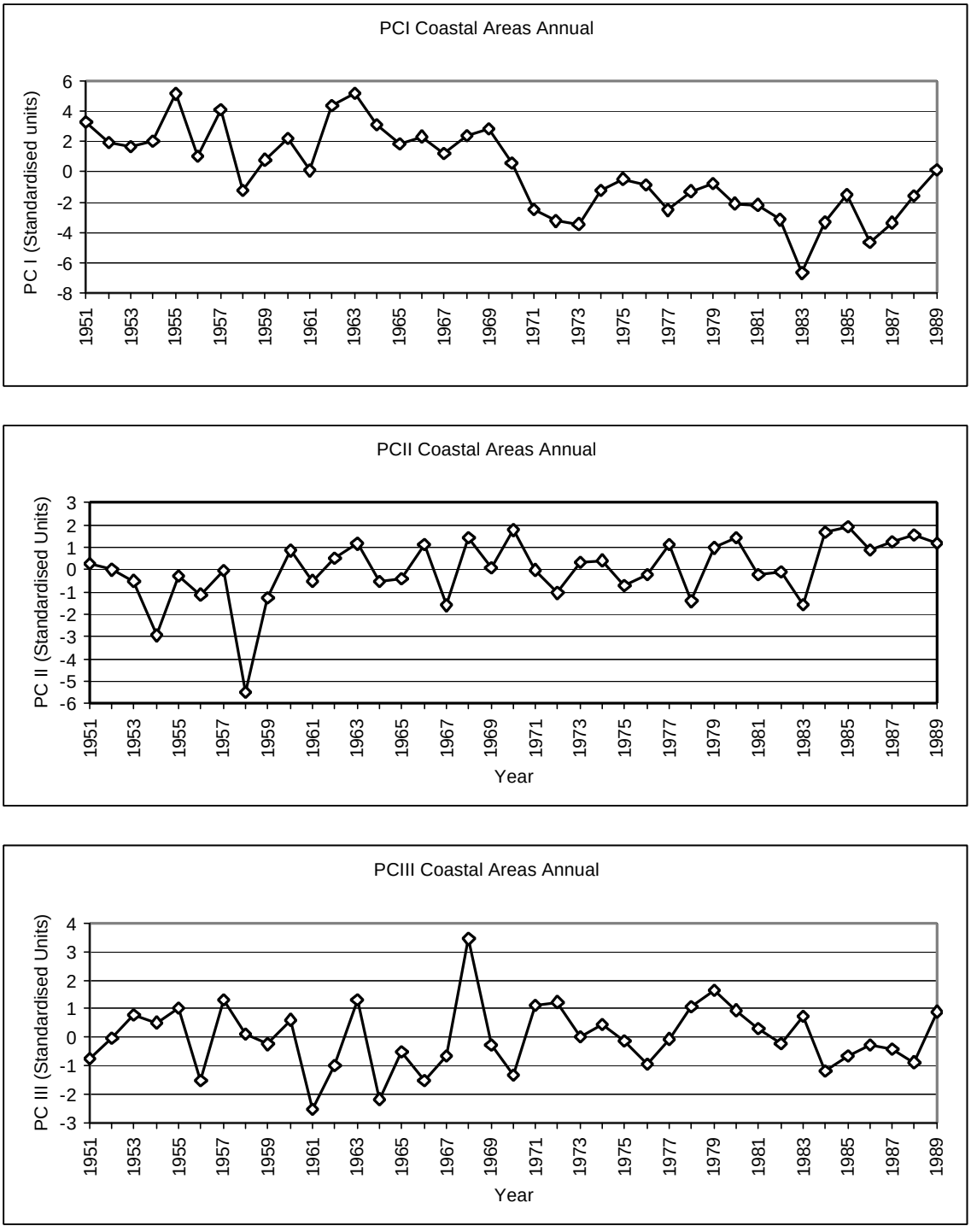

Figure 6.9. First three principal components of coastal area discharge data.

PCA USING COASTAL AREA ANNUAL DISCHARGE DATA

For PCA of the annual run-off data for coastal areas throughout the Gulf of Guinea, the first three principal components were retained for interpretation. These are shown in figure 6.9 and their loadings are shown in figure 6.10. PC I loaded positively for all areas and explained 60.0% of the total variance. PC II explained 16.5% of the total variance and loaded negatively for areas from Conakry (Guinea) to Freetown (Sierra Leone) and positively from Monrovia (Liberia) to south Equateur (Gabon). PC III, explaining 11.0% of the total variance, loaded negatively for areas from Nunez (Guinea) to Conakry, positively for areas from Freetown to Nigeria and negatively for the equatorial areas (north Equateur, Equateur, south Equateur). The other components were discarded on the basis that individually they explain very little of the remaining variance.

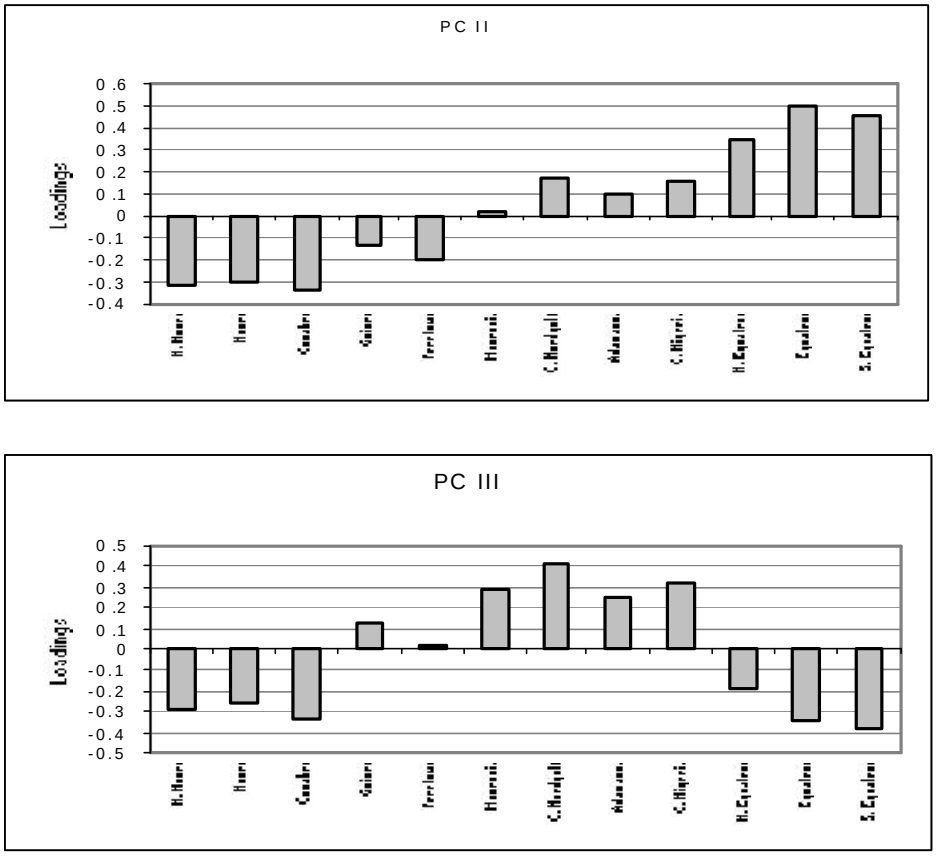

Figure 6.10. Loadings for PCs II and III of the PCA with ungauged coastal area discharge data.

The first three principal components from this analysis are very similar to those from the whole Gulf of Guinea PCA using annual river discharge data. The only notable difference is the lack of a peak in 1968 for PC II, however, this peak is still observed in PC III.

6.4 Interpretation of Results

The variations in seasonal flow show a progression in the month of peak flow from August in Guinea to September/October in northern Cameroon. The phase shift appears to be meridionally rather than zonally oriented, as peak flow occurs in September all the way from Côte d'Ivoire to Benin. The variations in month of peak river flow for the Niger and northern Cameroon rivers may be related more to the length of the rivers than longitude. Additionally, the flood of the Niger River is more related to rainfall over the Guinée and Niger hydroclimatic regions, than the Adamaoua region. The development of a second peak in the first half of the year in southern Cameroon appears to intensify southward. This has developed to such an extent in Gabon that peak flow fills the whole of the first part of the year and also the latter months of the year, leaving only the months of June to October with reduced flows. Therefore, the river flow regimes of the Gulf of Guinea can be grouped accordingly:

1. Guinea – peak flow is in August
2. Liberia to Benin – peak flow is in September
3. Nigeria to northern Cameroon – peak flow is in September or October
4. Southern Cameroon to Gabon – reduced flow through mid-late northern summer, with flow throughout the remainder of the year either showing two peaks or remaining constantly high.

These groups bear an approximate resemblance to the regional hydroclimates of Mahé and Olivry (1999) , shown in figure 6.1. Indeed, the characteristics described form part of the basis for the classification of these authors.

Interpretation of the results of PCA for the data used in this chapter is easier than for the image data used in chapter 5 because only one geophysical dimension is represented by runoff data. In this study, PC I for all the analyses showed the general pattern of interannual variability in river discharge throughout the region. This is characterised by a declining linear trend and a stepwise drop from high to low values during the late 1960s and early 1970s. PC II and III of the PCA performed on annual river discharge data for all rivers generally grouped the data according to Mahé and Olivry's (1999) regional hydroclimates. The Equateur and Adamaoua regions are clearly defined in PC II and the Fouta, Guinée and Nordgolf regions are defined in PC III. However, some boundary problems are presented by the PCA. Firstly, although the Fouta and Guinée regions are shown in PC III, loadings in PC II delineate a boundary between the rivers of Sierra Leone and Liberia. Secondly, loadings are in the opposite sense for the Niger and Benue rivers despite the two flows being almost identical and the flow of the Niger, measured at Onitsha, actually incorporating the flow of the Benue. Thirdly, the Cestos River of Liberia is separated from both the Guinée and Nordgolf regions in PC III.

The PCA on annual river discharge data for rivers grouped according to their regional hydroclimates showed only the first principal component to be significant for all regions except Guinée. This confirms the groupings of the previous PCA of this study. It also resolves two of the problems with the previous analysis. PC I is the only significant principal component for the Niger region and the high degree of variance explained by this (92.2%) justifies the grouping. Likewise, neither of the two significant principal components for the Guinée region separate the Cestos River from the rest of the grouping and between them PC I and PC II explain 90.1% of the variance.

The boundary issue between the Guinée and Fouta regions is less clearly resolved. The Fouta region is seen to be coherent, with PC I being the only significant principal component, accounting for 88.6% of the variance. However, the Guinée region is divided in two between Sierra Leone and Liberia by the loadings for PC II. Because, PC I was coherent for this

region and explained a high degree of the variance (77.6%), it was decided to keep the grouping for consistency with other studies. The boundary between the rivers of Sierra Leone and Liberia is probably due to the range of mountains between the two countries, which introduces variability into the pluviometry and, hence, river flow of the area.

Results of the PCA for ungauged coastal areas annual run-off data grouped the areas according to their regional hydroclimate. Similarly, monthly river discharge data both grouped the rivers according to their regional hydroclimate. Thus, these results confirm the groupings identified and tested in the previous analyses.

6.5 Discussion and Conclusions

The above interpretation of the results of this study confirms the grouping of river basins into hydroclimatic regions by Mahé and Olivry (1995, 1999). Seasonal cycles and interannual variability in river discharge data from this study appear to fit with these previous groupings.

The use of PCA in this study confirms the validity of these groupings because its divisions are based purely upon the variance structure of the data, rather than the mechanistic approach of interpolating from meteorological parameters. The boundaries between these areas correspond closely to those identified from the PCA of SST data and used to redefine the subsystems of the Gulf of Guinea LME in chapter 5. This suggests that oceanographic and climatic variability in the Gulf of Guinea are, to some degree, coupled. However, some differences exist between the SST and river discharge boundaries. Firstly, more boundaries exist for river discharge than for SST. The Nordgolf and Equateur regions are observed to be separate and there is also a boundary between the Fouta and Guinée regions. These results show greater spatial variability to exist in meteorological conditions in these regions than in SST for Areas 2 and 3. Secondly, there is a slight difference in position between the Adamaoua-Equateur hydroclimatic region boundary and the corresponding Area 3-Area 4 SST boundary, however, this is negligible.

7 Local Scale Environmental Variability in the Gulf of Guinea

7.1 Introduction

The Gulf of Guinea lies wholly within the equatorial humid zone and experiences generally high rainfall, much of which is carried to the ocean via the large number of rivers present throughout the region (Allersma and Tilmans 1993). This results in local climate having a marked effect on the marine environment, seen most noticeably through the permanent presence of low salinity Guinean waters in the Bight of Biafra. This influx of freshwater carries sediment and nutrients from terrestrial sources into the Gulf of Guinea, shaping benthic habitats and fuelling productivity (Binet and Marchal 1993, Longhurst 1983). Thus, local climate also influences the distribution and abundance of biological populations throughout the area (e.g. Longhurst 1958, Le Loeuff and Zabi, submitted), including both pelagic and demersal fish populations (Bard and Koranteng 1995, Koranteng 1998, Longhurst 1969).

The influence of these local climatic conditions on the marine environment has been touched upon in previous chapters. Furthermore, the spatial coherence between subsystems of the Gulf of Guinea LME defined from SST data (chapter 5) and hydroclimatic regions defined from river discharge data (chapter 6) suggests that variability in SST and local climate in the Gulf of Guinea region may be related. The aim of this chapter is, therefore, to investigate temporal coherence between oceanographic, meteorological and fluviometric parameters from the Gulf of Guinea.

7.2 Data Descriptions, Methods and Results

7.2.1 SST

CORSA-AVHRR SST AREAS

The CORSA-AVHRR data set was introduced in chapter 4. Mean SST, averaged across space, was extracted from the CORSA-AVHRR data set for each of the Areas defined by PC II in the whole Gulf of Guinea PCA of chapter 5. Preliminary investigation of these areas was also undertaken in chapter 5, giving a description of the characteristics of this data set. The results from this extraction are used in subsequent sections of this chapter. Monthly, annual and seasonal mean SST data are used for these analyses.

COADS SST AREAS

Mean SST data, averaged across space, were also extracted from the Combined Ocean-Atmosphere Data Set (COADS) for four areas, corresponding approximately to those used for the CORSA-AVHRR SST extraction, above. COADS was compiled from 'ship of opportunity' data (see Woodruff *et al.* 1987). It is used here to extend the SST record, beyond the time series available using CORSA-AVHRR data. The COADS data set provides an unbroken record of monthly mean SST over the period 1950-1990 for Areas 1 to 3 and 1970-1990 for Area 4. Therefore, data are used from 1950 for all areas but with gaps in the Area 4 record. Monthly and annual mean SST data are used for these analyses, as well as SST monthly anomalies. The monthly mean series are shown in figure 7.1a and the monthly anomaly and annual mean series are shown in figures 7.3a and 7.4a. Seasonal mean SST values were also calculated for each area, based on the seasons identified for the CORSA-AVHRR data, to be used in the analyses of future sections (see appendix 3).

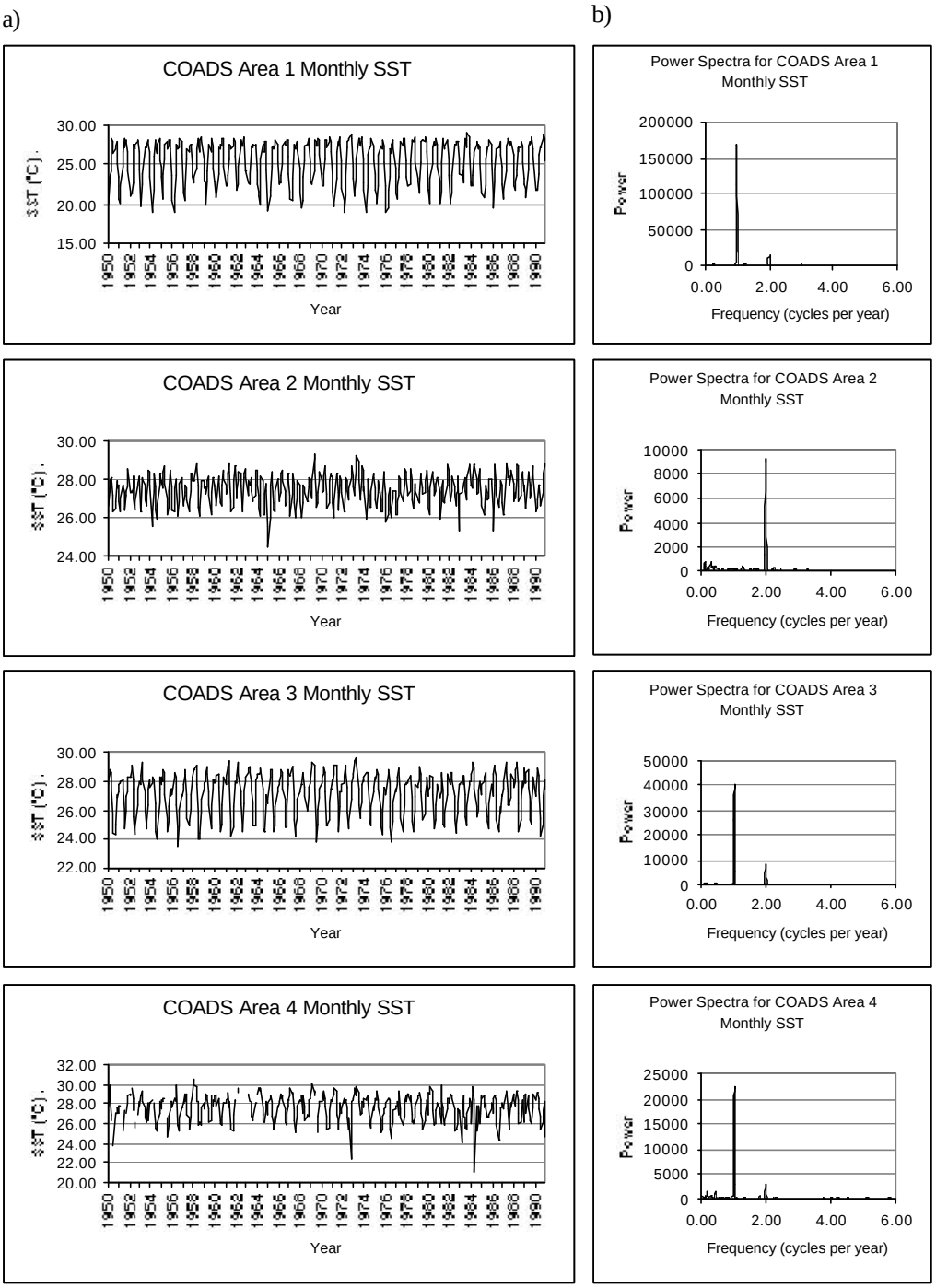

Figure 7.1. a) Monthly SST time series from the COADS data set for each of the subsystem Areas identified in chapter 5 and b) corresponding power spectra.

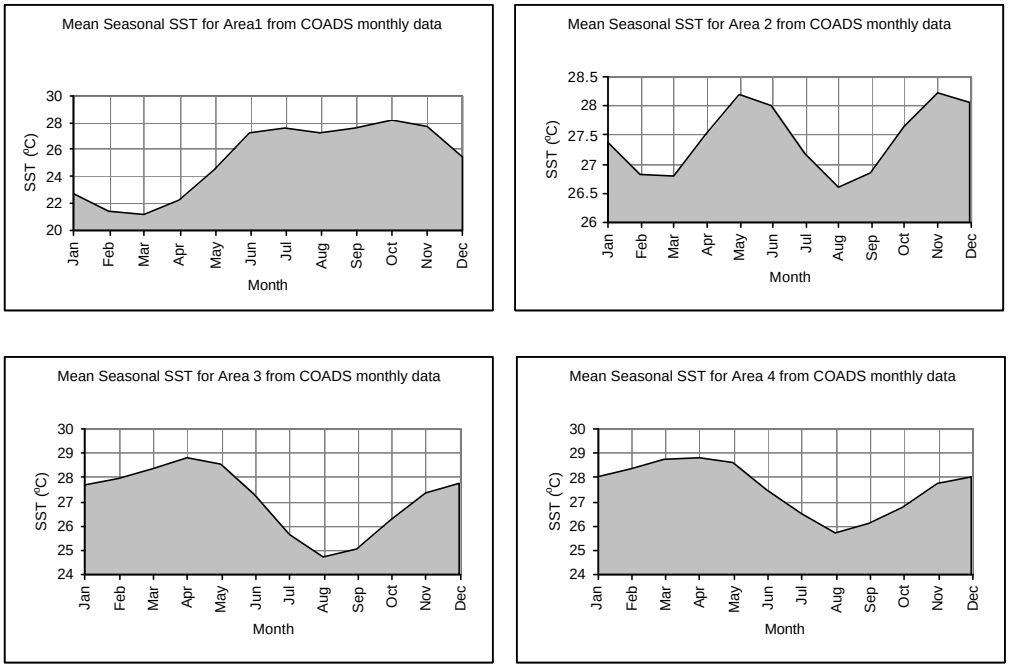

Figure 7.2. Mean seasonal SST from the COADS data set for each subsystem Area.

Correlation of the different COADS areas with each other showed Areas 3 and 4 to be most closely correlated (r=0.789). Area 2 shows only a weak correlation with Area 3 (r=0.440) and virtually no correlation with Area 4 (r=0.284). Area 1 is only weakly correlated with Area 2 (r=0.329), but shows a stronger, inverse relationship with Areas 3 and 4 (r=-0.618 and r=-0.558, respectively). The relationship in this analysis between Areas 3 and 4 is similar to that identified from the CORSA-AVHRR data, however, the relationships with Areas 1 and 2 seem very different. All results are highly significant ($P<0.01$).

Power spectra (spectral density functions) were computed for the monthly mean series (fig. 7.1b).

The spectra were filtered using a Tukey moving average window with weights 0.00, 0.25, 0.50, 0.25 and 0.00, with five degrees of freedom. This is equivalent to the Hanning window used in previous chapters. See Chatfield (1989) for a description of the use of windows and weighting options in spectral analysis. This method was used in all subsequent spectral analyses. Power spectra for the time series show all areas to be dominated by a strong

seasonal cycle. For Areas 1, 3 and 4 this cycle is annual and for Area 2 it is biannual. These seasonal cycles can also be seen in the charts of the mean seasonal SST for each area, shown in figure 7.2. Area 1 is seen to be cool from January to May and warm for the remainder of the year. The cooling during the first half of the year is due to the presence of the SUI in the area. Areas 3 and 4 are generally cool between July and October and warm from November to June. The warmest months are from March to May. The cool period is attributable to the major coastal and equatorial upwelling seasons. Area 2 is cool both during July to September and January to April. It has two warm periods; the first during May and June and the second from November to December. Thus, its seasonal cycle appears, to some degree, to be a hybrid of Area 1 and Area 3. These seasonal cycles appear similar to those derived from the CORSA-AVHRR SST data.

Because this chapter is primarily concerned with scales of variability greater than one year, the annual cycle was removed from the data by calculating monthly anomalies (fig 7.3a). Power spectra were computed for these SST monthly anomalies and for annual mean SST values. Power spectra of the SST monthly anomalies (fig. 7.3b) showed interannual peaks at periods of 3.8 years for Area 1, around 10 years and 3.6 years for Area 2, around 17 years, 5 years and at 2.2 years for Area 3 and around 42 years, 5 years and at 2.2 years for Area 4. Power spectra of the annual mean SST anomalies (fig. 7.4b) showed dominant peaks at periods around 9 and 4 years for Area 1, around 11, 4 and 3 years for Area 2, around 32 and 11 years for Area 3 and around 32 and 5 years for Area 4. The peaks at 42 years for Area 4 in the monthly data and at 32 years for Areas 3 and 4 in the annual data can be ignored because they are close to the length of the series and cannot, therefore, represent meaningful cycles in the data.

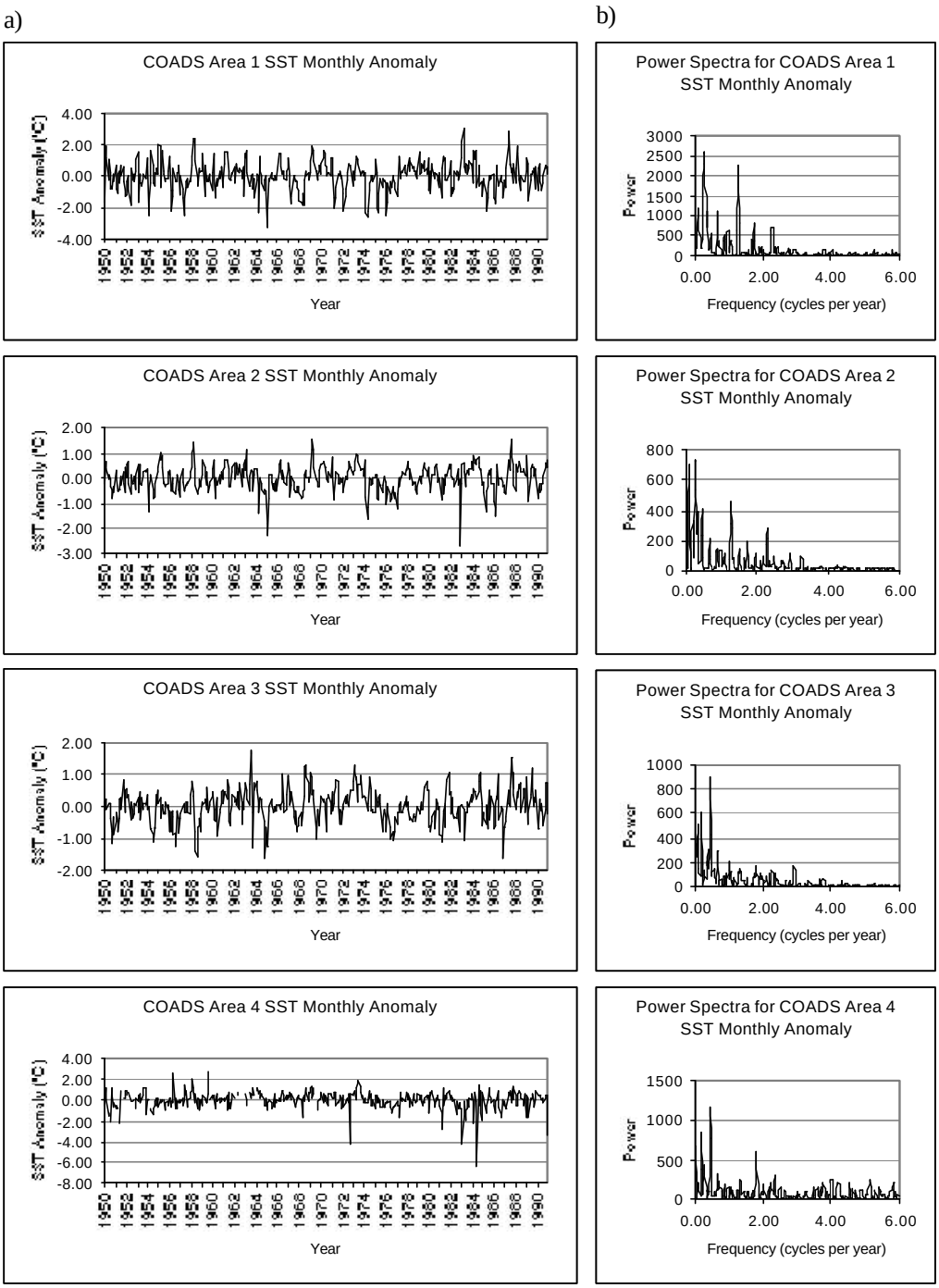

Figure 7.3. a) SST monthly anomaly time series from the COADS data set for each of the subsystem Areas and b) corresponding power spectra.

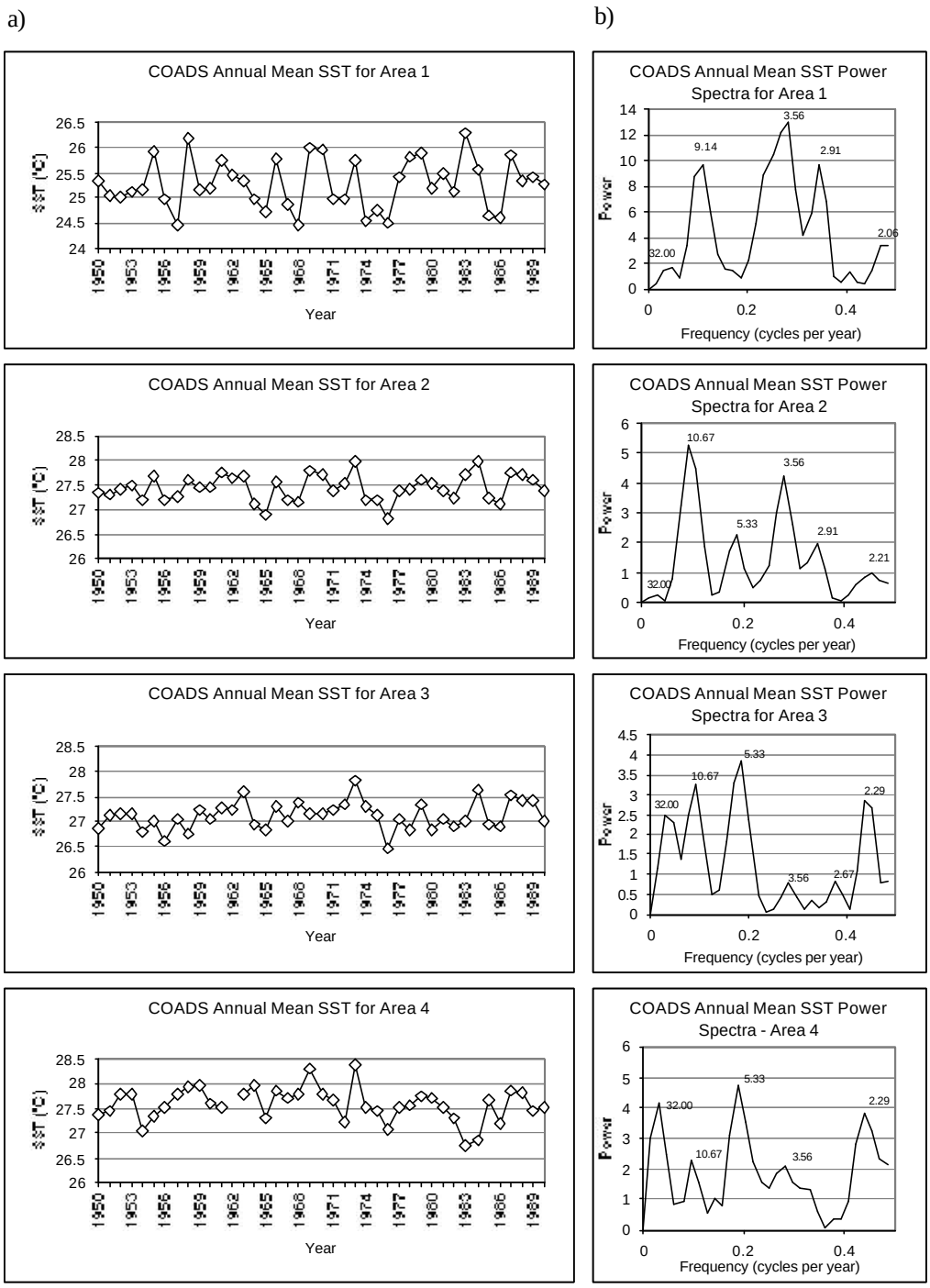

Figure 7.4. a) Annual mean SST time series from the COADS data set for each of the subsystem Areas and b) corresponding power spectra. Spectral peaks are labelled with their period.

Autocorrelation in the monthly anomaly values was calculated for each of the COADS areas at lags up to 36 months. Partial autocorrelation was also calculated to remove the effects of serial correlation. A range of two standard errors was used to show significant autocorrelation at approximately the 95% level. The partial autocorrelation standard errors assume an autoregressive order of *k*-1, where *k* is the lag. The results for Areas 1 to 3 are dominated by positive correlation at a lag of one month and this is also the most significant result for Area 4, clearly showing serial correlation to be present in the monthly SST values. Serial correlation was removed from these series by filtering the data through first order differencing. Autocorrelation was then calculated for the first-differenced series to confirm the removal of serial correlation. Significant negative autocorrelation was seen at lags 1, 2 and 3 for Area 1, at lags 1 and 2 for Area 2, at lags1 and 29 for Area 3 and at lag 1 for Area 4. Significant positive autocorrelation was seen at lag 21 for Area 1, at lag 22 for Area 2, at lag 5 for Area 3 and at lag 6 for Area 4.

Charts of annual mean SST (fig. 7.4a) show values for Areas 2 to 4 to range from around 26.5^{o}C to 28.5^{o}C, whereas Area 1 values range from around 24.5^{o}C to 26.5^{o}C. The cooler temperatures in Area 1 are caused by the presence of the SUI. Much of the interannual variability is not consistent between areas, however, from 1982 to 1990, all four areas show an early peak, a trough and then a prolonged period of warm SST. Additionally, there is a large drop in SST values for Areas 2 to 4 from 1973 to 1976, relative to the rest of the time series. A sharp drop is seen in Area 1 between 1973 and 1974 but this is not particularly large relative to the rest of the time series. The general patterns of interannual variability in Area 1 appear similar to those in Area 2, but more intense.

Autocorrelation and partial autocorrelation were calculated for the annual COADS data for each of the areas up to 10 years lag. Significant autocorrelation was only seen for Area 2 at two years lag. Partial autocorrelation supported this result and also showed a significant lag at 7 years for Area 1. Neither of these results were particularly large. None of the other areas showed any significant autocorrelation.

Correlative analysis between the areas showed Areas 1 and 2 to be most closely correlated on an interannual time scale. Additionally, Areas 2 and 3 were shown to be moderately correlated and a weaker correlation was observed between Areas 3 and 4. All other results were negligible. Correlation coefficients (r-values) for the annual mean and monthly anomaly results are shown in table 7.1. Significance appears to be inversely proportional to distance, with only nearest neighbours being significant for the annual mean SST analysis and only the correlation between Area 1 and Area 4 not being significant for the SST monthly anomaly analysis.

Table 7.1. Correlation coefficients (r-values) for different SST Areas derived from the COADS data set. Correlation analysis was undertaken for annual mean SST values and monthly SST anomaly values over the period 1950-1990. The areas correspond to those identified in PC II of the PCA from CORSA-AVHRR data for the whole Gulf of Guinea, described in chapter 5. Values in brackets are not significant.

	Correlation Coefficient (r)		Significance (P)	
Area Combination	Annual Mean SST	SST Monthly Anomaly	Annual Mean SST	SST Monthly Anomaly
Area 1 v. Area 2	*0.791*	*0.649*	*P<0.01*	*P<0.01*
Area 1 v. Area 3	*(0.236)*	*0.215*	*(P>0.05)*	*P<0.01*
Area 1 v. Area 4	*(0.146)*	*(0.075)*	*(P>0.05)*	*(P>0.05)*
Area 2 v. Area 3	*0.661*	*0.552*	*P<0.01*	*P<0.01*
Area 2 v. Area 4	*(0.275)*	*0.179*	*(P>0.05)*	*P<0.01*
Area 3 v. Area 4	*0.344*	*0.290*	*P<0.05*	*P<0.01*

These results do not agree with those from CORSA-AVHRR SST values, as described in chapter 5, which showed Areas 3 and 4 to be the most strongly correlated, Area 2 to be strongly correlated with Areas 3 and 4 and Area 1 to be only weakly correlated with all areas. The reason for the difference between these data sets is unclear.

COMPARISON OF CORSA-AVHRR AND COADS SST AREAS

To assess if both data sets area definitions are similar enough for COADS to be used to provide an extended SST time series, COADS Areas and CORSA-AVHRR Areas were compared directly.

The two data sets were compared using pairwise correlation analysis with Bonferroni corrections applied to probability values. This method was also used in all subsequent multiple correlations. The resulting Pearson correlation coefficients are shown in table 7.2, along with uncorrected and Bonferroni corrected probabilities. It can be seen that there is a high degree of correlation between both data sets for Area 1 and Area 3 and both these results are highly significant. There is also moderate correlation between the data sets for Area 2 and Area 4 and these too are highly significant. This correspondence between respective areas from the two data sets, combined with the very high significance levels of these results ($P<0.0005$), suggests that COADS SST data can be used in subsequent analyses, alongside CORSA-AVHRR data, to provide an extended SST record.

Examination of the remaining results shows that the correlation between CORSA-AVHRR and COADS SST for Area 2 is similar to that between COADS SST for Area 2 and CORSA-AVHRR Areas 1 and 4. Furthermore, COADS Area 4 shows a higher correlation with CORSA-AVHRR Area 3 than with CORSA-AVHRR Area 4 and CORSA-AVHRR Area 2 and Area 4 are most highly correlated with COADS Area 3. Generally, this suggests that neighbouring areas may heavily influence SST in each of these areas. The correlation between COADS Area 2 and CORSA-AVHRR Area 4 may be due to SST variability in both areas being related to the seasonal movement of the ITCZ, despite them being separated by an area dominated by coastal upwelling.

Table 7.2. Pearson correlation (r) and probability (P) values for corresponding areas using CORSA-AVHRR and COADS SST data. Bonferroni corrected P-values are given in brackets.

		CORSA-AVHRR Area 1	*CORSA-AVHRR Area 2*	*CORSA-AVHRR Area 3*	*CORSA-AVHRR Area 4*
COADS Area 1	r	*0.861*	*-0.119*	*-0.493*	*-0.229*
	P	*0.000 (0.000)*	*0.206 (1.000)*	*0.000 (0.000)*	*0.014 (0.227)*
COADS Area 2	r	*0.415*	*0.433*	*0.250*	*0.421*
	P	*0.000 (0.000)*	*0.000 (0.000)*	*0.007 (0.118)*	*0.000 (0.000)*
COADS Area 3	r	*-0.479*	*0.512*	*0.798*	*0.687*
	P	*0.000 (0.000)*	*0.000 (0.000)*	*0.000 (0.000)*	*0.000 (0.000)*
COADS Area 4	r	*-0.347*	*0.348*	*0.589*	*0.517*
	P	*0.000 (0.002)*	*0.000 (0.002)*	*0.000 (0.000)*	*0.000 (0.000)*

A number of oceanographic features of potential importance to fisheries recruitment were identified from CORSA-AVHRR data in chapter 4. Indices were calculated measuring the most southerly extent of the SUI (SUI index) and the spatial extent and intensity of the upwelling seasons (Combined Upwelling Index) (see figure 4.13). The patterns of variability in these indices and their similarity to patterns observed in the SST series are discussed in chapter 4. No significant autocorrelation was seen in any of these indices. The use of spectral analysis for these indices would have been inappropriate because of the small number of data points for each series (9-11).

Correlative analysis of these oceanographic indices with SST values was carried out and showed a number of significant results ($P<0.05$). Correlation with CORSA-AVHRR SST showed the SUI Index to be significantly correlated with SST in Area 1 during season 1 ($r=0.77$), in Area 2 during seasons 1 ($r=0.81$) and 2 ($r=0.74$), with Area 3 during season 1 ($r=0.68$) and with Area 4 during seasons 1 ($r=0.72$) and 2 ($r=0.67$). The Combined Upwelling Index (CUI) for the major upwelling season was significantly correlated with SST in Areas 2 to 4 during seasons 2 ($r=-0.93, -0.97, -0.93$, respectively) and 3 ($r=-0.84, -0.87, -0.88$, respectively), and this was reflected in both the spatial extent and intensity components of the upwelling index. The CUI for the minor upwelling season was significantly correlated with SST in Areas 1 and 2 during season 1 ($r=-0.77, -0.85$, respectively) and this was reflected only in the spatial extent component of the CUI. Correlation with COADS SST showed the SUI index to be significantly correlated with SST in Area 1 during season 1 ($r=0.87$) and in Areas 2 and 3 during season 2 ($r=0.79, 0.86$, respectively). The CUI for the major season was significantly correlated with SST in Area1 during season 1 ($r=-0.74$) and in Areas 2 and 3 during seasons 2 ($r=-0.75, -0.82$, respectively) and 3 ($r=-0.86, -0.79$, respectively). These correlations were generally reflected in both the spatial extent and intensity components of the CUI, although for Area 2 during season 3 only spatial extent was significant. The CUI for the minor upwelling season was not significantly correlated with SST in any Areas, although the

intensity component of this index did show significant correlation with SST in Area 1 during season 2 (r=-0.79).

Qualitative comparison of the SUI index with the CUI showed interannual variability in the spatial extent of the major upwelling season to be similar to the variability in the most southerly latitude of the SUI. However, correlative analysis between the two showed no significant correlation.

7.2.2 Local climate data

IRD ANNUAL RIVER DISCHARGE AND RAINFALL DATA

River discharge and rainfall time series were obtained from Gil Mahé of IRD (formerly ORSTOM) for each of the regional hydroclimates of Mahé and Olivry (1995, 1999). The river discharge series used are the first principal component of the PCA of mean annual discharge for rivers grouped according to their regional hydroclimate, except for the Niger River, where mean annual river discharge is used. This is because discharge is almost identical from both rivers in the Niger region, the Niger and the Benue, with the Benue flowing into the Niger ahead of the Niger gauging station at Onitsha. These data series and their derivation are described in chapter 6. Discharge for ungauged coastal areas, also used in chapter 6, could not be measured directly so was calculated from rainfall over the region, therefore, only rainfall data are used for these areas in this chapter (see below). River discharges from all regions were significantly correlated with each other, except for the Equateur region, which only showed significant correlation with the Guinée, Nordgolf and Niger regions. The significance level was $P<0.01$ for all results except for between the Equateur region and the Guinée and Niger regions and between the Niger and Nordgolf regions, where $P<0.05$.

Rainfall data are used in the form they were obtained, that is mean annual rainfall for an average station in each regional hydroclimate. The data comprise a subset of the rainfall data

collected by Mahé and Olivry (1995) from approximately 900 rainfall stations throughout central West Africa. These authors collected daily and monthly data and used them to calculate annual values. Charts of annual mean rainfall for each of the gauged hydroclimatic regions and ungauged coastal areas are shown in figure 7.5. It can be seen that, for the regional hydroclimates, rainfall is highest in the Guinée region and lowest in the Niger region. For the ungauged coastal areas, rainfall is highest in the Coastal Guinée area and lowest in the Coastal South Equateur area.

A significant declining trend in rainfall is present throughout the time series in most areas. This is steepest for the Fouta (r^2=0.56, P<0.01) and Guinée (r^2=0.62, P<0.01) regions and the Coastal Guinée area (r^2=0.60, P<0.01). A substantial, steady decline is also seen in the Nordgolf (r^2=0.33, P<0.01) and Niger (r^2=0.49, P<0.01) regions and the Coastal Nordgolf area (r^2=0.31, P<0.01). The Adamaoua region and Coastal Nigeria area show declining rainfall from the 1970s (r^2=0.16, r^2=0.12, respectively; both P<0.05). A significant decline is not seen for the Equateur region (r^2=0.04, P>0.05) and Coastal North and South Equateur areas (r^2=0.03, P>0..05 for both).

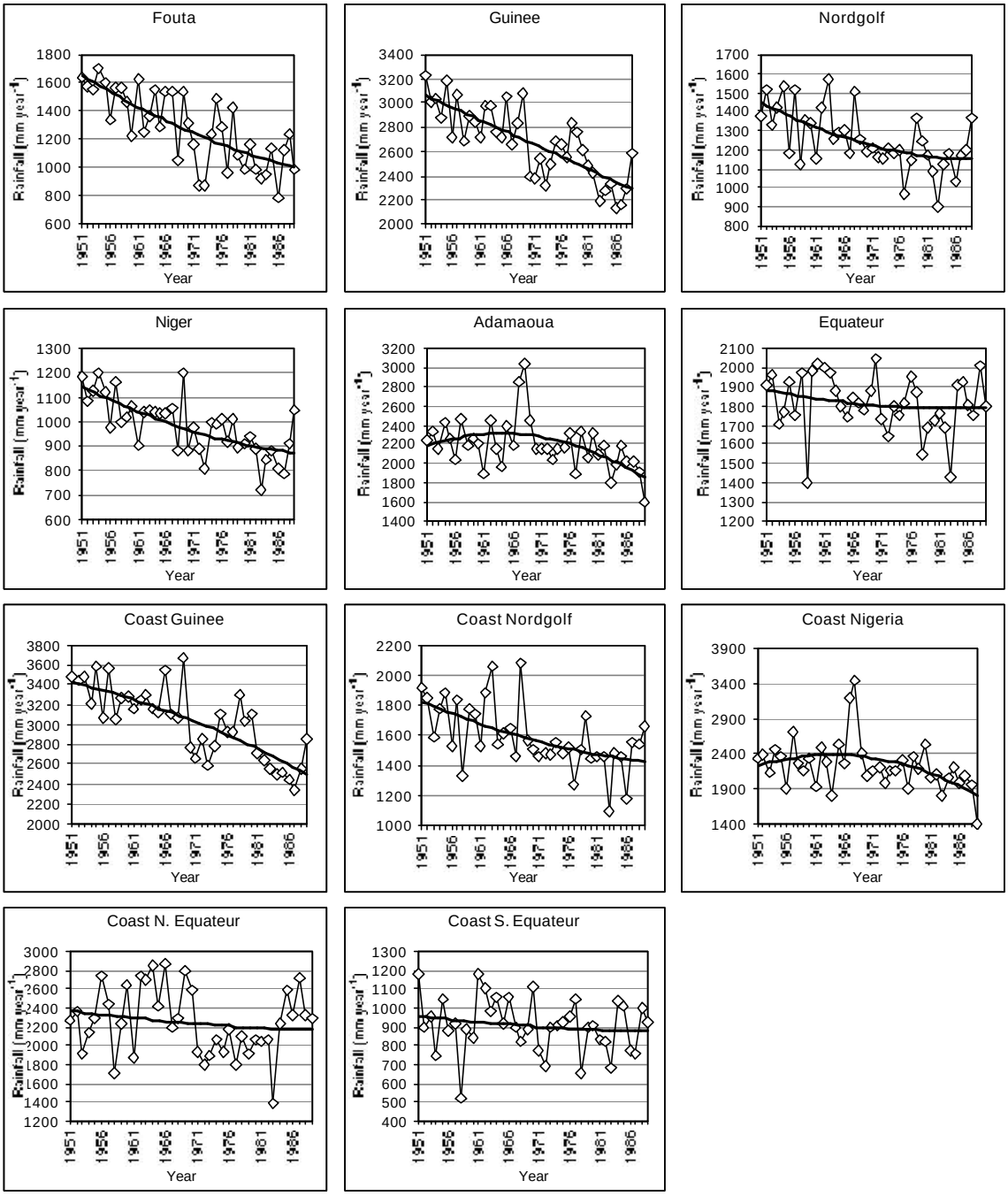

Figure 7.5. Annual rainfall time series for the regional hydroclimates and ungauged coastal areas in the Gulf of Guinea. Second order polynomial trend lines are shown for each series.

Superimposed on the declining linear trend, there appears to have been a stepwise drop from higher to lower levels of rainfall during the late 1960s in some areas. This drop is seen clearly between 1969 and 1970 for the Guinée region and Coastal Guinée area. It is also visible between 1968 and 1972 in the Fouta, Nordgolf, Niger and Adamaoua regions and Coastal Nordgolf and Coastal North Equateur areas. An additional feature of interest in the data is an unusually large peak in rainfall, seen only in the Adamaoua region and associated Coastal Nigeria area, in 1968.

Rainfall series from all regions were significantly correlated with each other, except for the Equateur region, which only showed significant correlation with the Nordgolf region. The significance level was $P<0.01$ for all results except for between the Adamaoua region and the Fouta and Niger regions, where $P<0.05$. Out of the ungauged coastal areas, the Coastal Guinée, Coastal Nordgolf and Coastal Nigeria areas were significantly correlated with each other, as were the Coastal Nordgolf, Coastal North Equateur and Coastal South Equateur area. Thus, Coastal Nordgolf was the only area showing significant correlation with all other areas. The significance level was $P<0.05$ for both the Coastal South Equateur area results and between the Coastal Guinée and Coastal Nigeria areas. For all other results $P<0.01$.

Power spectra for the annual river discharge and rainfall data (fig. 7.6) showed large peaks in the decadal range for all regions except the Nordgolf. Additionally, all areas showed peaks in the shorter scale interannual range. Comparison of these power spectra with periodogram values helped resolve the dominant peaks further.

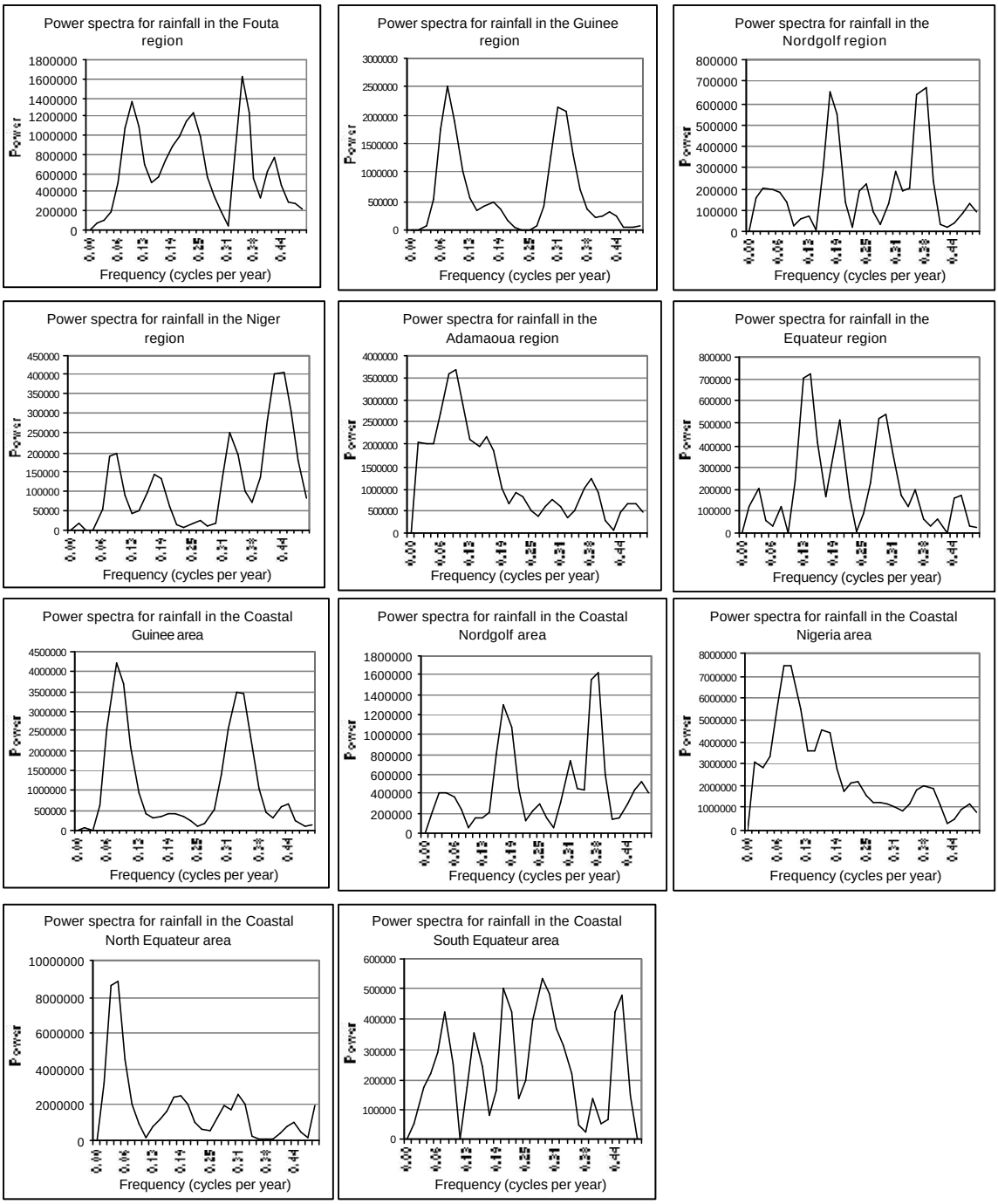

Figure 7.6. Power spectra for regional rainfall data.

The relative magnitude and dominant period of these peaks varied between regions, but 12.7 years seemed to be the predominant decadal scale peak and the short interannual scale peaks were generally in the range 2.4 to 3.2 years. Some intermediate scale peaks were seen at periods between 4.2 and 6.3 years. For two regions, multidecadal scale peaks were seen with a period of 38 years, however, this is also the length of the time series so these results cannot reflect meaningful cycles in the data. River discharge and rainfall data for the Fouta region showed peaks at periods 12.7 and 2.9 years and a peak with period of 38 years was also seen in the river discharge data. The Guinée region was dominated by a peak with period 12.7 years and also showed a minor peak at 3.2 years for both river discharge and rainfall data. The Nordgolf region was overwhelmingly dominated by a peak at 2.7 years for both river discharge and rainfall data. A 12.7 year peak was seen in both river discharge and rainfall data for the Adamaoua region, as well as peaks at periods 6.3, 2.4 and 2.0 years for river discharge data and 38 and 2.7 years for rainfall data. The Niger region showed peaks at 12.7 and 2.4 years in both the river discharge and rainfall data, as well as peaks at 6.3 and 2.9 years for river discharge and 3.2 years for rainfall. The Equateur region river discharge was dominated by a peak at 19.0 years and also showed smaller peaks at 4.8 and 3.2 years, whereas the rainfall data showed peaks at 12.7, 4.8 and 2.2 years. The 19 year peak may be the result of leakage from peaks at 38 and 12.7 years. For a discussion of leakage in power spectra see Diggle (1990). Rainfall data for the Coastal Guinée area showed peaks at 12.7 and 2.9 years, the Coastal Nordgolf area at 2.7 years and the Coastal Nigeria area at 12.7 and 2.7 years. The Coastal North Equateur area showed peaks at 19 and 3.2 years and the Coastal South Equateur area showed peaks at 12.7, 4.8 and 2.2 years.

Autocorrelation and partial autocorrelation were calculated for each of the river discharge and rainfall series for lags up to 10 years. River discharge for the Fouta, Guinée and Niger regions is dominated by the 1 year lag, showing serial correlation in the series. The other regions show no significant autocorrelation. Rainfall for the Fouta, Guinée and Niger regions and Coastal Guinée and Coastal Nordgolf areas also showed significant autocorrelation. The

Fouta and Guinée regions and Coastal Guinée area are dominated by the 1 year lag and this lag is also the most significant for the Niger region, showing serial correlation in these data series. Other significant results showed only weak autocorrelation.

Correlative analysis of river discharge with rainfall for each of the regional hydroclimates showed all results to be highly significant ($P<0.01$) and r-values were in the range 0.701 (Equateur) – 0.930 (Guinee), except for the Niger result which had an r-value of 0.447. Correlation of river discharge with coastal rainfall for each of the regional hydroclimates also showed all results to be highly significant ($P<0.01$), except for the Coastal Nigeria result, which was still significant ($P<0.05$). The range of r-values was from 0.628 (Coastal South Equateur) – 0.907 (Coastal North Equateur), except for the Coastal Nigeria result ($r=0.339$).

NCAR MONTHLY RAINFALL INDICES

Additional rainfall indices and data from individual rainfall monitoring stations for the Gulf of Guinea were obtained from Todd Mitchell of JISAO, University of Washington. The rain gauge measurements for construction of these indices were originally obtained from the NCAR World Monthly Surface Station Climatology (see NCAR 1999).

The Gulf of Guinea Rainfall Index (GGRI) was calculated by Mitchell (1996) from the standardised mean monthly rainfall values for five stations in the Gulf of Guinea region: Atakpame and Lome in Togo, Bohicon and Cotonou in Benin and Roberts Field in Liberia (see fig. 7.7). These had complete or almost complete records for 1950-1993. The method of calculation and standardisation is provided by Mitchell (1996).

This index and the original rainfall data from these five stations were obtained for this study. Although all stations lie within the Gulf of Guinea region, the Roberts Field site is remote from the other four stations and lies within a different subsystem of the LME. Inspection of the seasonal cycles and interannual variability of the stations showed the four stations in Benin and Togo to be very similar and distinct from the Roberts Field station.

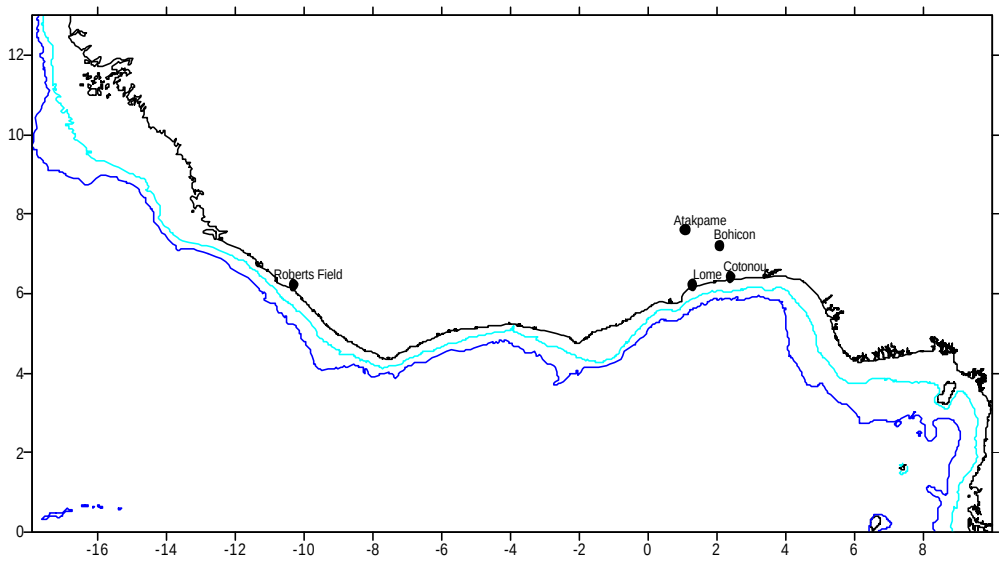

Figure 7.7. Map showing the location of rainfall stations used to compile the Gulf of Guinea Rainfall Index.

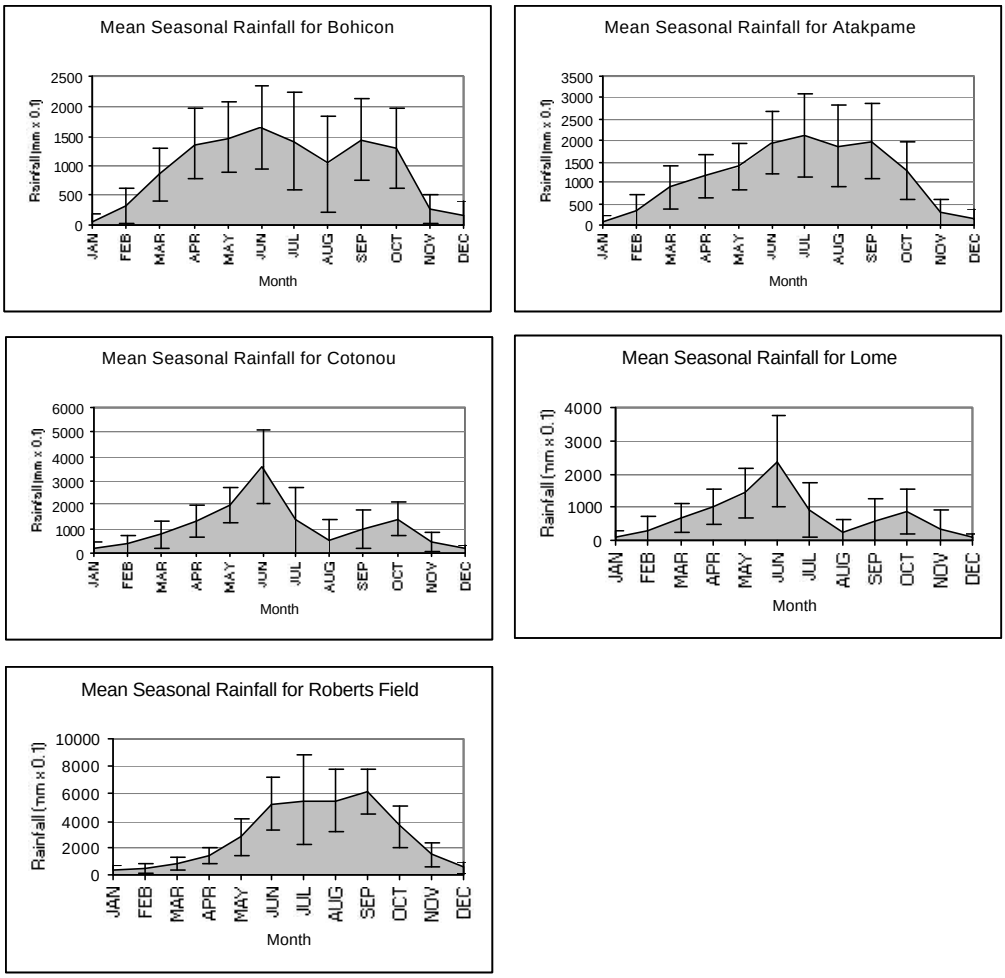

Figure 7.8. Mean seasonal rainfall for each of the Gulf of Guinea rainfall stations used. Error bars show one standard deviation from the mean.

Mean seasonal rainfall for each of the stations is shown in figure 7.8. At the Togo (Atakpame and Lome) and Benin (Bohicon and Cotonou) stations, rainfall peaks twice a year, around June-July and September-October. For the inland stations, both peaks are approximately the same size (150-220 mm). The first peak is in June for Bohicon and July for Atakpame, the second peak is in September for both areas. For the coastal stations, the first peak is in June and is much larger than the second peak. Additionally the August drop in rainfall, between the two peaks is much greater than for the inland areas. Both peaks for the coastal areas appear to dominate the annual cycle much more than in the inland areas. For Cotonou, the June peak is almost double the size of that of Bohicon, however the second peak is similar in magnitude. For Lome, the first peak is of similar size to that of Atakpame, however, the rest of the annual cycle, including the second peak, is greatly reduced compared to Atakpame. This is probably because Lome lies on the edge of the Accra dry belt, an area of reduced rainfall due to the upwelling along that part of the coast. All four stations show reduced rainfall from November to February. The Roberts Field station in Liberia shows generally much higher rainfall than the other stations. It shows the highest amount of rainfall from June to September, with peak rainfall in September. Rainfall is generally low for this station from November to March. Interannual variability in rainfall is large for all stations. A declining trend in rainfall is apparent for the Roberts Field station from about 1970 onwards. This is not seen for the other stations.

Because of the spatial distance and qualitative differences between Roberts Field and the other stations, a new rainfall index was created for the Togo and Benin stations based on mean monthly rainfall. Correlation between the mean monthly rainfall and the first principal component of the rainfall data for these stations was 99.7% ($r=0.999$) and this result was highly significant ($P<0.01$). Some of the station records, and hence the first principal component, contained gaps, so the mean rainfall record was used as the rainfall index rather than the first principal component, even though the mean record damped some of the more extreme signals in the rainfall record.

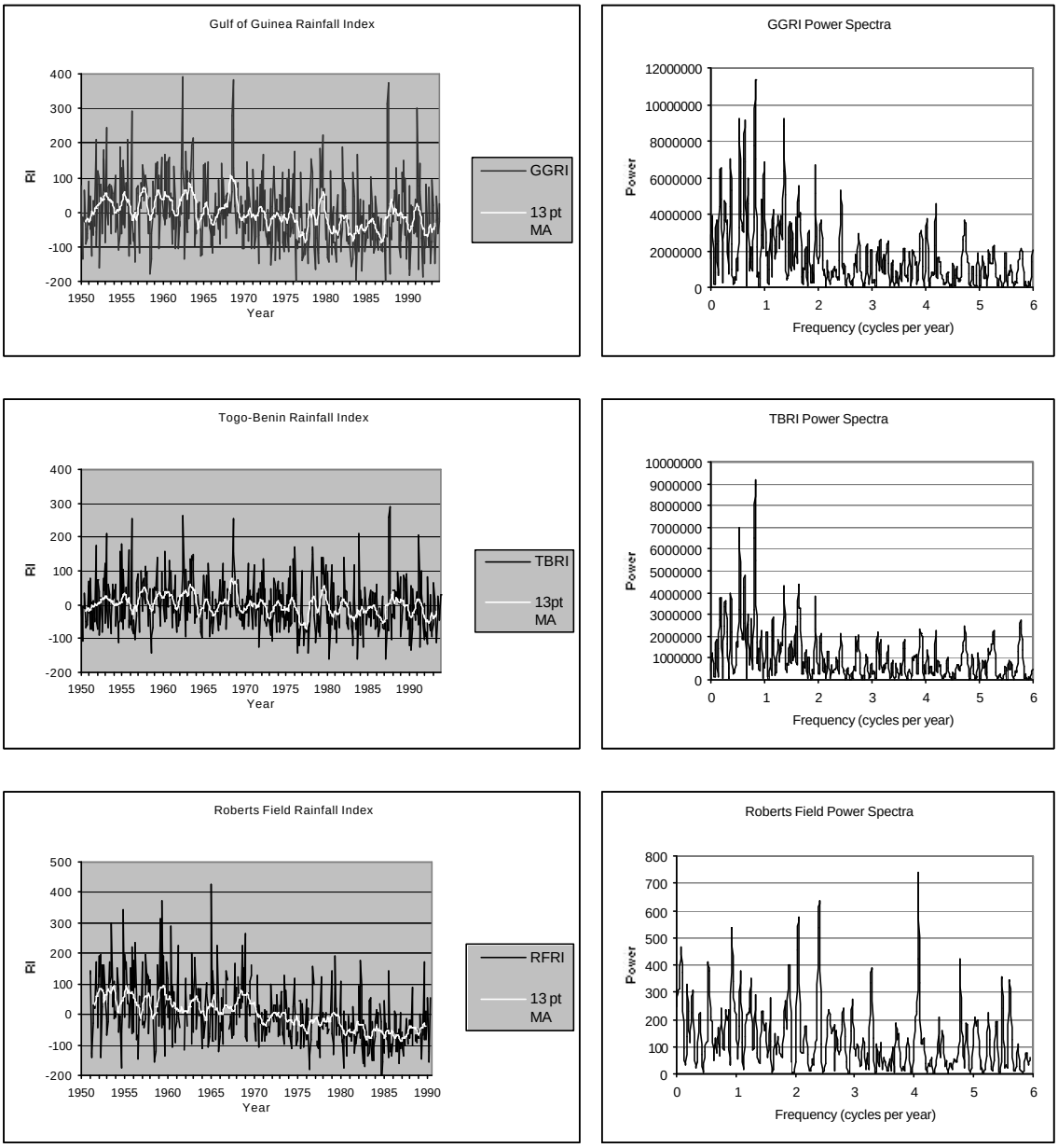

Figure 7.9. a) Monthly rainfall indices for the whole Gulf of Guinea (GGRI), the Togo and Benin rainfall stations (TBRI) and the Roberts Field rainfall station (RFRI) and b) corresponding power spectra.

Correlation between the Togo-Benin Rainfall Index (TBRI) and the Roberts Field record (RFRI) was only 5.8% (r=0.238) but this result was still highly significant (P<0.01). Correlation between the TBRI and Mitchell's GGRI was 88.0% (r=0.938) and this result was also highly significant (P<0.01). The TBRI and the RFRI are used separately to supplement the GGRI in future analyses. These three series are shown in figure 7.9a. Power spectra for the monthly GGRI, TBRI and RFRI (fig. 7.9b) appear dominated by white- and red-noise.

Autocorrelation and partial autocorrelation were calculated for each of the series up to 36 months lag. Partial autocorrelation showed positive correlation at one month lag to dominate each of the data series, demonstrating serial correlation. When this was accounted for, other significant lags only displayed weak correlation. The RFRI showed significant autocorrelation at the greatest number of lags. Serial correlation was removed from each of the series by first-order differencing. Negative autocorrelation was seen in the first-differenced series at lags 1, 2 and 27 for the GGRI, at lag 1 for the TBRI and at lags 1, 14 and 31 in the RFRI. Positive autocorrelation was seen in the first-differenced series at lags 12 and 23 for the TBRI and at lag 13 for the RFRI.

Comparison of NCAR and IRD data

The GGRI shows monthly rainfall in selected areas of the Gulf of Guinea, whereas the IRD data show annual rainfall and river discharge over the whole Gulf of Guinea. These two local climate data sets were compared to assess the level of coherence between them. This involved calculating annual mean rainfall values for the GGRI, TBRI and RFRI. Autocorrelation and partial autocorrelation was then calculated for each of these annual data series up to 10 years lag. Autocorrelation was seen in the GGRI at three years lag and the RFRI at 1 to 3 years lag. Partial autocorrelation showed positive correlation at the one year lag to dominate the RFRI, demonstrating serial correlation, although the 2 year lag was also significant. For the GGRI, the 3 years lag remained significant. No significant correlation

was seen for the TBRI series. First-order differencing was used to remove serial correlation from the RFRI. Negative autocorrelation was seen at lag 1 in the first-differenced series.

Correlative analysis was undertaken for the annual mean GGRI with annual rainfall and river discharge data for each of the regional hydroclimates and rainfall data for the ungauged coastal areas, first-differenced where appropriate. A strong correlation was seen with rainfall for the Nordgolf region ($r=0.804$, $P<0.01$) and weaker correlation with the Adamaoua ($r=0.541$, $P<0.01$) region. A strong correlation was also seen with rainfall for the Coastal Nordgolf area ($r=0.831$, $P<0.01$) and with river discharge for the Nordgolf region ($r=0.763$, $P<0.01$). The analysis was repeated for the TBRI and the RFRI. For the TBRI, the strongest correlation was seen with Nordgolf region rainfall ($r=0.736$) and river discharge ($r=0.685$) and Coastal Nordgolf area rainfall ($r=0.769$). All results are highly significant ($P<0.01$). A weaker correlation was seen with rainfall for the Adamaoua region ($r=0.477$, $P<0.05$). For the RFRI, the strongest correlation was seen with rainfall for the Guinée region ($r=0.819$) and Coastal Guinée area ($r=0.785$). This was closely followed by rainfall for the Nordgolf region ($r=0.755$) and Coastal Nordgolf area ($r=0.747$). The Nordgolf region also showed the strongest river discharge correlation ($r=0.728$) and the Fouta region river discharge also showed significant correlation ($r=0.703$). All these results were highly significant ($P<0.01$).

7.2.3 Correlation between SST and local climate data

SST data are compared here with local climate data to examine any interactions between the processes. Some of these may be direct, such as the influence of run-off on SST, however, the large areas over which SST is averaged means that any relationships are likely to be indirect, via large-scale forcing factors such as basin-wide climate cycles.

COMPARISON OF SST AND IRD DATA

Qualitative comparison of CORSA-AVHRR SST with annual river discharge and rainfall data showed some similarities for each SST Area, however these were not consistent (see

appendix 3). For Area 1 some resemblance was seen during season 1 with river discharge leading by 1 year. In season 2, no resemblance was seen. For Areas 2, 3 and 4 the strongest similarities were seen during season 2. During this season, SST appeared to lead river discharge by one year but to lag rainfall by one year, or the series seemed to vary in phase, for many of those areas where similarities were seen. The clearest resemblance was seen for rainfall leading SST in Area 4 during season 2 by one year.

Cross-correlation analysis of CORSA-AVHRR seasonal SST values and annual rainfall and river discharge values showed a number of significant relationships. This was only undertaken at up to 1 years lag because of the small number of overlapping data points in the two data sets. Significant correlation was seen between river discharge in the Guinée, Nordgolf, Niger and Equateur hydroclimatic regions and SST in various Areas during various seasons, with SST leading by one year. The strongest correlations were seen in Area 4 during season 1 with the Niger (r=0.969) and Guinée (r=0.919) regions, however, Area 2 during season 2 was seen to significantly correlate with the greatest number of regions (Guinée, Niger, Nordgolf and Equateur). Additionally, SST during season 2 for Area 4 varied in phase (lag 0) with Equateur river discharge (r=0.750).

Rainfall in the Nordgolf, Niger and Equateur regions and Coastal Nordgolf and Coastal North Equateur areas was also seen to lag SST by one year, as well as to vary in phase with SST for various Areas during various seasons. There were more significant results for SST leading rainfall than for the two varying in phase and when both lags were significant together, generally the SST lead correlation was stronger. However, there were still a large number of in phase results, especially in the coastal areas rainfall, so these should not be ignored. The strongest correlation was between Area 4 during season 1 and the Niger region, with SST leading by one year (r=0.902). The strongest in phase result was for Area 4 during season 1 with the Nordgolf region (r=0.888). Rainfall in the Coastal South Equateur area was seen to lead SST during season 1 for Area 1 by one year (r=-0.829).

Cross-correlation of COADS seasonal SST values with annual rainfall and river discharge values, at lags up to three years, was also undertaken. Significant correlation was at lags 0 (in phase), +1, +3 (river discharge and rainfall lead), -1, -2 and –3 (SST leads). The in-phase result was the most prevalent, followed by river discharge and rainfall leading by one year. These two lags were generally seen during seasons 2 and 3 for Areas 2 and 3 and season 1 for Area 4, although in phase results were also observed in Area 1 during both seasons and in Area 4 during season 2 and Coastal South Equateur rainfall was seen to lead SST in Area 1 during season 1 by one year. Occasionally, in Area 2 during season 2, both lags would be significant. The in phase result was strongest for Fouta rainfall, whereas in the Guinée region the strongest result was for SST lagging rainfall and river discharge. For the Niger region, the in phase result was strongest for rainfall but river discharge showed stronger correlation when leading. The strongest results were between river discharge in the Fouta region and SST in Area 2 during season 2, both series in phase (r=-0.645) and for rainfall in the Coastal South Equateur area leading SST in Area 2 during season 2 by one year (r=-0.617).

Other significant results showed: river discharge in the Nordgolf region lagging SST in Area 2 during seasons 1 and 2 by three years (r=-0.423, r=-0.417, respectively); river discharge in the Equateur region and Coastal Equateur areas leading SST in Areas 2 to 4 during season 1 by three years, with the strongest correlation between river discharge and SST in Area 3 (r=0.509); rainfall and river discharge in the Niger region and river discharge in the Adamaoua region lagging SST in Area 4 during season 2 by one year (r=0.483, 0.413, 0.453, respectively); Coastal Guinée and Coastal Nigeria areas rainfall lagging SST in Area 2 during season 2 by two years (r=-0.460, -0.420, respectively); river discharge in the Adamaoua region lagging SST in Area 1 during season 2 by two years (r=-0.413) and leading it by three years (r=0.487), and Adamaoua region rainfall leading SST in Area 2 during season 1 by two years (r=0.449).

SST was also compared with monthly GGRI data to see if there was any correlation with rainfall when monthly data were used. Cross correlation of CORSA-AVHRR monthly anomalies for each SST area with GGRI values showed a number of weak but significant relationships. SST leads for negative lags and GGRI leads for positive lags. Significant correlation was seen with Area 1 at lag 0 (r=-0.184), with Area 2 at lags –4 (r=0.206), +1 (r=-0.214) and +4 (r=-0.195) and with Area 4 at lags +4 (r=0.191), +9 (r=0.199) and +10 (r=0.243). No significant correlation was seen with Area 3. Cross-correlation of these SST series with TBRI values reflected a number of the lags seen with the GGRI. Significant correlation was seen with Area 1 at lag 0 (r=-0.202), with Area 2 at lags –4 (r=0.198) and +1 (r=-0.236) and with Area 4 at lags +4 (r=0.195) and + 10 (r=0.195). Again, no significant correlation was seen with Area 3. Cross-correlation with RFRI values showed significant correlation at lags not seen with the GGRI or TBRI series. Significant correlation was seen with Area 1 at lag –12 (r=0.208) and with Area 3 at lag -7 (r=0.226). No significant correlation was seen with Area 2 or Area 4.

Cross correlation of COADS monthly anomalies for each SST area with GGRI values also showed a number of weak but significant relationships. Again, SST leads for negative lags and GGRI leads for positive lags. Significant correlation was seen with Area 1 at lag -7 (r=-0.095), with Area 2 at lags –1 (r=0.147) and 0 (r=-0.092), with Area 3 at lags –8 (r=0.094), -2 (r=-0.107) and -1 (r=0.119) and with Area 4 at lags +6 (r=-0.096) and +11 (r=0.094). Cross-correlation of these SST series with TBRI values reflected a number of the lags seen with the GGRI. Significant correlation was seen with Area 1 at lag -7 (r=-0.108), with Area 2 at lags –1 (r=0.131) and 0 (r=-0.117), with Area 3 at lags –8 (r=0.099) and –1 (r=0.091) and with Area 4 at lag +6 (r=-0.134). Additionally, significant correlation was seen with Area 2 at lag +2 (r=0.096). Cross-correlation with RFRI values showed significant correlation with Area 1 at lags –9 (r=-0.135), -4 (r=-0.103), -3 (r=0.100), -2 (r=-0.105) and +2 (r=0.094), with Area 2 at lags –9 (r=-0.134) and +5 (r=0.096), with Area 3 at lags -2

(r=-0.109), -1 (r=0.111) and +5 (r=0.055) and with Area 4 at lags –4 (r=-0.102), -3 (r=0.122), +9 (r=-0.107) and +11 (r=0.102).

COMPARISON OF OCEANOGRAPHIC INDICES AND IRD DATA

Comparison of annual rainfall and river discharge values with the oceanographic indices was undertaken both qualitatively and using cross-correlation analysis. The qualitative comparison showed some similarities, mainly between the CUI during the major upwelling season and rainfall and river discharge values, however, these were not consistent (see appendix 3).

Cross-correlation analysis was undertaken at lags only up to 1 year because of the small number of overlapping data points in the two data sets. Significant negative correlation was seen between the CUI during the major upwelling season and river discharge in the Fouta (r=-0.907), Nordgolf (r=-0.784) and Niger (r=-0.793) regions at lag +1 (CUI leads). The strongest correlation was with the Fouta region and this relationship was seen in both the spatial extent (r=-0.896) and intensity (r=-0.857) components of the CUI. For the Nordgolf and Niger regions, the correlation was only seen in the spatial extent of the major upwelling (r=-0.823, -0.821, respectively). The Nordgolf and Equateur regions also showed significant negative correlation with the CUI during the major upwelling season at lag 0 (r=-0.718, -0.678, respectively). This was reflected in the intensity component of the major upwelling in the analysis with the Equateur region (r=-0.854), but was not seen in either of the upwelling components separately for the Nordgolf region analysis. Additionally, significant upwelling was seen between river discharge in the Adamaoua region and the spatial extent of the minor upwelling season at lag 0, however, this was not reflected in the CUI.

Cross-correlation between annual rainfall values and the CUI showed significant negative correlation at lag 0 with the Nordgolf (r=-0.853), Equateur (r=-0.754), Coastal Nordgolf (r=-0.854) and Coastal North Equateur (r=-0.727) regions and areas. This was also seen in both the spatial extent and intensity components of the major upwelling for the Nordgolf

region (r=-0.776, -0.712, respectively) and Coastal Nordgolf area (r=-0.770, -0.820, respectively), but only in the intensity component of the major upwelling for the Equateur region (r=-0.758) and Coastal North Equateur area (r=-0.936). Further significant correlations were seen between the CUI for the major season and rainfall in the Guinée region (r=0.741) at lag –1 (rainfall leads) and in the Niger region (r=-0.740) at lag +1 (CUI leads). Both of these were reflected in the spatial extent component of the CUI (Guinée r=0.744, Niger r=-0.829). Additionally, the spatial extent of upwelling during the major season was significantly correlated with rainfall in the Nordgolf region at lag +1 (r=-0.738), but this was not reflected in the CUI.

Cross-correlation between the SUI index and annual rainfall data showed significant correlation at lag +1 (SUI index leads) with the Fouta region (r=0.847) and at lag 0 with the Adamaoua region (r=-0.790). No significant correlation was seen with river discharge.

7.3 Discussion

7.3.1 SST variability

Direct correlation of the two SST data sets showed them similar enough for the COADS data to be used to extend the SST record back to the 1950s. However, some quite large differences were observed between the data sets, particularly regarding the relationship between different Areas on interannual scales. Some of these differences may be explained by the way the COADS data is collected. The data are obtained from ‘ships of opportunity’, thus their sampling distribution is largely clumped in shipping lanes. Additionally, filtering of the data as quality control for COADS has been reported to remove many of the more extreme values, classifying realistic observations as erroneous for poorly sampled regions, when they may actually represent extremes of natural variability (Wolter 1997).

Comparison of the interannual trend in the data sets over the 1980s showed the same pattern in CORSA-AVHRR and COADS data. This trend was also seen in the indices of

oceanographic features. The COADS data also showed a drop in the 1970s. Power spectra for both data sets showed peaks in the biennial, interannual and decadal period ranges. For the CORSA-AVHRR data set, decadal scale peaks had to be treated as suspect because the time series was only 10.5 years long, however, the presence of peaks in this period range in the COADS data show cyclic variability on this time scale can be considered a real feature of the data. Seasonal cycles were also seen to be similar in both data sets. Koranteng (1998) also showed a large shift in the SST trend in the mid 1970s and a smaller increase from 1987 to 1989.

7.3.2 Local climate variability

River discharge is probably the primary mechanism by which terrestrial rainfall influences the marine environment. Correlation between different hydroclimatic regions was seen to be greatest for the river discharge data, with all areas being significantly correlated. Only two regions were significantly correlated for rainfall data. This may be explained by the more persistent nature of river levels (Briquet *et al.* 1997) compared to the transience of rainfall. These results show, for the main part, the close relationship between rainfall and river discharge values throughout the Gulf of Guinea region. Other authors have also shown this relationship (Mahé and Olivry 1995). This is unsurprising, not least because some of the river discharge values used here were reconstructed from rainfall data (Mahé and Olivry 1995, 1999). However, this analysis does show spatial coherence in these relationships at the regional level.

The general trend in many regions was a persistent decline in rainfall and river discharge throughout the series. This shows the link between rainfall in the Gulf of Guinea and the long drought suffered in the Sahel to the north over this period (Lamb 1982). A stepwise drop in rainfall levels is also observed during the late 1960s and early 1970s. Mahé and Olivry (1999) also identified individual years over this period in which large drops in rainfall and run-off occurred, terming them ‘rupture years’.

The Nordgolf region is seen to be more closely related than other regions to the TBRI and the Guinée region to be more closely related than other regions to the Roberts Field data, as expected from their geographical similarity. Surprisingly, the Nordgolf relationship with the TBRI was weaker than that with the GGRI. This is explained by another surprising result, the relatively strong relationship between the Nordgolf region and the Roberts Field data. These results are, however, understandable in terms of local climate dynamics. The Roberts Field station lies directly in the path of the West African monsoon so should be correlated with all areas under it's influence. The Togo and Benin stations, on the other hand, are in the vicinity of the Atakora Mountains which considerably alter rainfall patterns in the area (G. Mahé, IRD, Ouagadougou, Burkina Faso, pers. comm.). This is seen particularly in the presence of a declining long term trend in the Roberts Field data, similar to that observed in the IRD data, which is absent from the TBRI. Nonetheless, rainfall for the two data sets do appear sufficiently correlated for both to be used as representations of the same parameter, with different temporal sample intervals.

The power spectra for each series showed short period cycles to dominate the interannual variability, however, decadal scale variability was also seen in most areas. The short term cycles generally have periods of between two and three years and the decadal scale variability has a period of around 13 years. Interannual variability in some series was also seen in the intermediate period range. River discharge data for the Adamaoua and Niger regions showed cycles with periods around 6.3 years and the Equateur region and Coastal South Equateur area rainfall showed cycles with periods around 4.8 years. Cycles with similar frequencies to some of those identified here have been noted in other meteorological data sets. Most obvious is the similarity between the 4.8 year cycle and the frequency of ENSO events, however, cycles with approximate two years periods have also been noted in many series (e.g. European air temperatures and rainfall, equatorial stratospheric winds), termed the quasi-biennial oscillation (QBO) (Burroughs 1992). Decadal scale variability has been noted in a number of global climate records, as described in chapter 1. In the Equateur region's river

discharge and the Coastal North Equateur area's rainfall, a 19-year period cycle was observed. Whether this was produced by leakage from cycles around 38 and 13 years or has a meteorological interpretation is unsure.

7.3.3 Comparison of SST and local climate data

In the cross-correlation of regional rainfall and river discharge with CORSA-AVHRR SST, the strongest correlations were seen between SST in Area 4 during season 1 and rainfall and river discharge in the Guinée and Niger regions, with SST leading by 1 year. The link between the Guinée and Niger regions is easily explained because the Niger river has its source in the Guinée region. Also, Area 4 SST preceding rainfall is understandable in terms of the meteorological dynamics of the region, because the ITCZ is situated above Area 4 during season 1, before it migrates north over the source areas for the Guinée and Niger regions. However, why SST during the beginning of the year in Area 4 should lead rainfall and river discharge in the following year is less apparent, especially because this SST relates to rainfall in the Nordgolf region in the same year. The dominant result from the cross-correlation analysis presents similar difficulties in its interpretation. SST in Area 2 during season 2 was seen to lead river discharge along the whole coast from Sierra Leone (Guinée region) to Gabon (Equateur region) by one year. Certainly, during season 2 the ITCZ is positioned overhead of Area 2, leading to rain over the source areas of many of the rivers which are found in these regions, however, the one year lag again presents problems. Perhaps, delays between rainfall and discharge to the ocean are responsible in the case of the larger rivers (e.g. Niger), but the rivers of the Guinée region discharge into the sea a few months after the first rains. Alternatively, residual flow in the rivers may be influenced by the previous years rainfall, showing a "memory' effect in discharges, however, serial correlation was removed from these series. Indeed, perhaps the one year lag is an artefact of processing, due to the removal of serial correlation from the Guinée and Niger series, but not from the

Nordgolf. Another difficulty in explaining this relationship is the lack of significant correlation between SST in Area 2 and rainfall.

For the cross-correlation of COADS SST with regional rainfall and river discharge, most significant correlations occurred with both series in phase, however, a number of results with rainfall and river discharge leading SST by one year were also seen. The strongest result, of SST in Area 2 during season 2 varying in phase with Fouta region river discharge, is explainable in terms of the position of the ITCZ during season 2 producing rainfall over the Fouta region. The in phase correlation between these two series makes this the most probable interpretation. It is unlikely that the correlation is due to river discharge influencing SST because peak river discharge does not occur until the end of season 2. Additionally, the SST images in chapter 4 showed river discharge to influence SST over the shelf areas in this region, but Area 2 has a large offshore extent which is not seen to be influenced by run-off waters and would make the run-off component of the signal negligible. The correlation between Coastal South Equateur rainfall and SST in Area 2 during season 2, with rainfall leading by one year is also interpretable in terms of ITCZ dynamics. The ITCZ is far south in December and January, so rainfall in the Coastal South Equateur area during this period is representative of the presence of the ITCZ. The ITCZ then migrates north until it is over Area 2 during season 2. This is the following year to when it first produced rain over the Coastal South Equateur area. Thus, this correlation appears to be an indirect representation of the migration of the ITCZ.

Correlations between SST and rainfall indices were too weak to be interpretable.

7.3.4 Indices of oceanographic features

Comparison of the indices of oceanographic features, identified in chapter 4, with SST showed a high degree of correlation at appropriate times of the year. This was expected as the indices were derived from SST data. The indices were also compared with each other, but

showed no significant correlation, suggesting they are not forced by the same processes. Comparisons of the oceanographic indices with regional rainfall and river discharge data showed two main results. Firstly, the major upwelling was seen to lead river discharge and rainfall in the Fouta, Nordgolf and Niger regions by one year, seen mainly in the spatial extent of the upwelling. This is similar to the relationship seen between river discharge and rainfall and SST in Area 2 during this season and, therefore, suggests a link between ITCZ dynamics and the spatial extent of the major upwelling season. Secondly, rainfall and river discharge in the Nordgolf region, Coastal Nordgolf area, Equateur region and Coastal North Equateur area were seen to vary in phase with the major upwelling season. It is already known that coastal upwelling along the coast of Ghana influences local rainfall, resulting in the 'Accra dry-belt', so the relationship between the major upwelling season and Nordgolf climate appears clear. The link between coastal upwelling intensity and rainfall and river discharge in the Equateur region and Coastal North Equateur area is less obvious, but is probably due to the influence of the equatorial upwelling both in the Equateur region and on coastal upwelling. The correlation between the SUI index and rainfall in the Fouta region, is consistent with their geographic similarity. Why the SUI should lead Fouta rainfall by one year is unclear, but this lag is consistent with relationships seen between SST and rainfall in this area. The in phase correlation between the SUI index and rainfall in the Adamaoua region has no clear explanation and may well be erroneous.

7.4 Conclusions

SST was seen in chapter 4 to vary over scales from the seasonal to the decadal. The use of COADS here extends this data set and confirms the existence of decadal scale signals in SST in the Gulf of Guinea. Local climate data are also seen to vary over these time scales and long term trends, such as the Sahelian drought, are clearly observable. Comparison of SST and local climate data show some similarities between the two, however, these are not consistent enough to pinpoint one mode of variability forcing all processes to any noticeable

degree. The ITCZ and equatorial dynamics may well play important roles in explaining the relationships observed. The lag times seen in the correlations are open to speculation.

Both the combined upwelling index and river run-off are putative nutrient enrichment mechanisms. Run-off may also concentrate these nutrients in river plumes. Some similarities were seen between these two parameters over interannual time scales, however, they do not generally appear coupled. Nonetheless, both these factors may well influence productivity and similarities in patterns' variability between these factors may add to such an effect.

8 Ocean-Atmosphere Interactions on Global and Local Scales

8.1 Introduction

In chapter 1, some recent developments in understanding of ocean-atmosphere interactions were described. Subsequent chapters of this thesis have investigated spatial and temporal variability of local environmental parameters in the Gulf of Guinea and relationships between them. SST, river discharge, rainfall and the oceanographic indices used all show variability on time scales relevant to known global climate features, although this is not dominated by one clear mode. The purpose of this chapter is to assess the extent, if any, to which large scale climate features may be forcing local environmental parameters, or vice versa, in the Gulf of Guinea.

8.2 Global/Basin Scale Climate Data

8.2.1 Southern Oscillation Index

The Southern Oscillation is calculated as the sea level pressure (SLP) difference between Tahiti and Darwin, Australia. The Southern Oscillation Index (SOI) used in this study is the same as was used by Taylor *et al.* (1998) and is calculated as the Southern Oscillation anomaly over the period 1951 to 1996. The SOI is a measure of the atmospheric component of El Niño–Southern Oscillation (ENSO) activity in the Pacific Ocean. Low (negative) values of the SOI correspond to El Niños, or warm events and high (positive) values correspond to La Niñas, or cold events.

The SOI is calculated for all months of the year, as shown in figure 8.1a. Figure 8.1b was calculated from SOI values standardised (zero mean, unit standard deviation) with respect to the month over the period 1951 to 1996, to emphasise interannual variability. The formula for this calculation is essentially the same as that in equation 4.2a, using monthly data rather than weekly. There is no seasonal cycle in the SOI.

a)

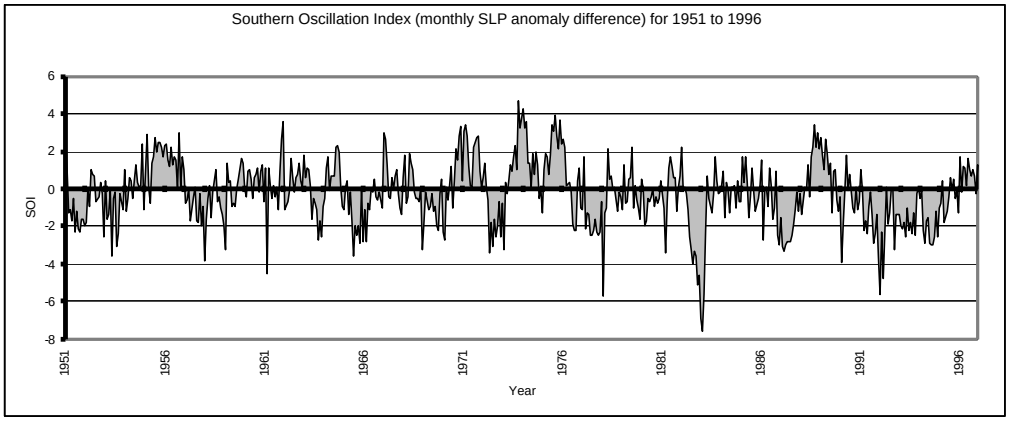

b)

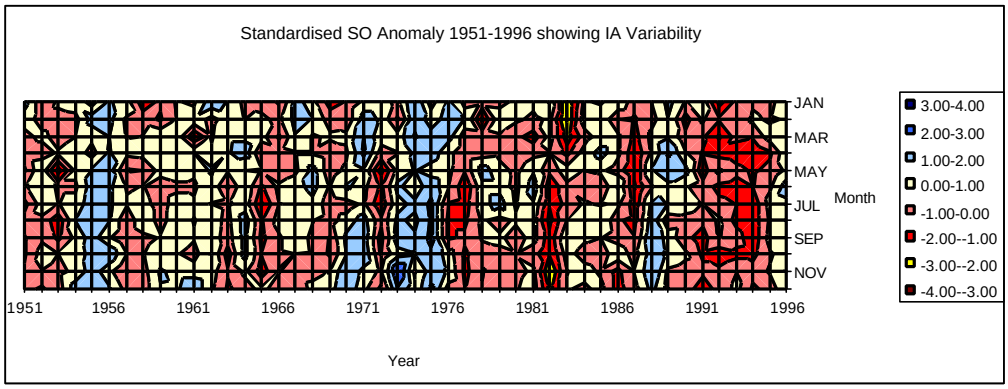

c)

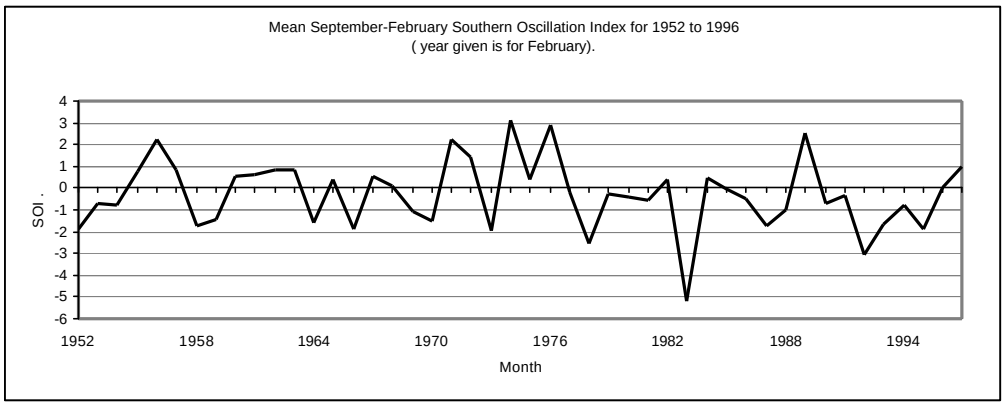

d)

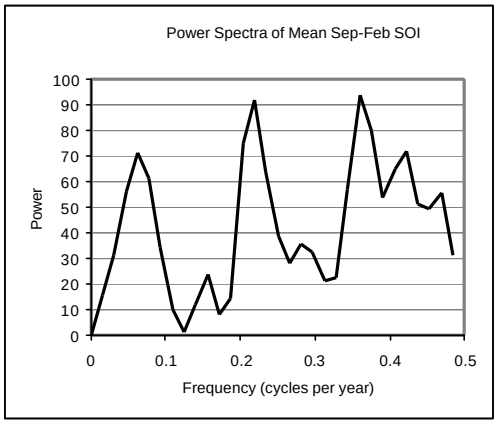

Figure 8.1. Southern Oscillation Index (SOI). a) Monthly SOI for 1951 to 1996, b) monthly standardised SOI showing interannual variability, c) mean September-February SOI over the same period and d) power spectra of the mean September-February SOI.

It can also be seen from figure 8.1b that warm El Niño events and cool La Niña events are strongest during the boreal autumn and winter. Therefore, the mean September-February SOI series was calculated from unstandardised data. The monthly record of unstandardised SOI values clearly shows El Niño events in 1951/52, 1953, 1957-59, 1963/64, 1965/66, 1968-70, 1972/73, 1977/78, 1982/83, 1986-88 and 1991-95 and La Niña events in 1955/56, 1970/71, 1973-76 and 1988/89. Most of these events are also reflected in the mean September to February series (fig. 8.1c). Thus, the period between El Niño events appears to vary from 2 to 5 years. La Niña events appear to occur much less frequently, with 15 years between the larger events. No long-term linear trend is seen in the SOI, however, it appears that from 1976 onwards the series enters a period of generally lower index values.

Autocorrelation and partial autocorrelation in the SOI were calculated for lags up to 36 months. Positive autocorrelation at a lag of one month dominates the results, demonstrating serial correlation in the series. The two-month lag result is also highly significant. Serial correlation was removed from the series by first-order differencing. Negative autocorrelation was seen in the first-differenced series at lags of 1, 10 and 24 months.

Spectral analysis of the September-February SOI showed three major peaks, with periods of 16.1 years, 4.6 years and 2.8 years. The power spectra for the September to February SOI are shown in figure 8.1d.

8.2.2 Hurrell's North Atlantic Oscillation (NAO) Index

The NAO has generally been measured as the sea level pressure (SLP) difference between Stykkisholmur in Iceland and Ponta Delgada in the Azores. However, Hurrell (1995) found the SLP record at Lisbon, Portugal to be a better proxy of changes in the Azores high pressure centre so recalculated the NAO from 1864 using SLP data from Stykkisholmur and Lisbon. This is the version of the NAO used in this study (fig. 8.2a). It was calculated from COADS SLP anomalies for these sites and normalised by dividing each seasonal pressure by the long-

term mean (1864-1994) (Hurrell 1995). The mean winter (December to March) value is used as the annual NAO Index value (Hurrell 1995).

The chart of winter NAO values for the period 1951 to 1991 (fig. 8.2b) shows a great deal of interannual variability. This period was selected because it coincides with the SST, river discharge and rainfall data examined in chapter 7. High values exist in 1952, 1957, 1961, 1967, 1973, 1981, 1983 and 1989 and low values in 1955, 1963, 1969, 1977, 1979. Additionally, there appears to be a longer-term change, with lower values dominating until 1970 and higher values from 1971 onwards. No linear trend is observed consistently throughout the time series.

Autocorrelation in the NAO was calculated for lags up to 10 years. The only significant result was at a lag of one year. Partial autocorrelation also showed positive correlation at a lag of one month to be significant. Serial correlation was removed from the series by first-order differencing. No autocorrelation was seen in the first-differenced series.

Spectral analysis of the NAO over the period 1951 to 1991 showed three major peaks, with periods of 16.1 years, 8.1 years and 2.8 years. Power spectra for the NAO over this period are shown in figure 8.2c. The first and last of these peaks are identical in period, if not magnitude, to those identified in the SOI, however, the second peak has a much longer period than the El Niño events identified in the SOI. Spectral analysis of the full NAO series (1864-1992) helped resolve some of these peaks more finely, as well as showing longer-term variability (fig. 8.2d). Initially, there is a peak with period 85.3 years. After this, there are two smaller peaks at 23.3 and 12.8 years. The 16-year cycle observed in the shorter time series is probably produced by leakage from these two cycles. There are additional large peaks at 7.7 and 5.82 years. The first of these corresponds to the peak at 8.1 years seen in the shorter series; the latter does not appear in the shorter series.

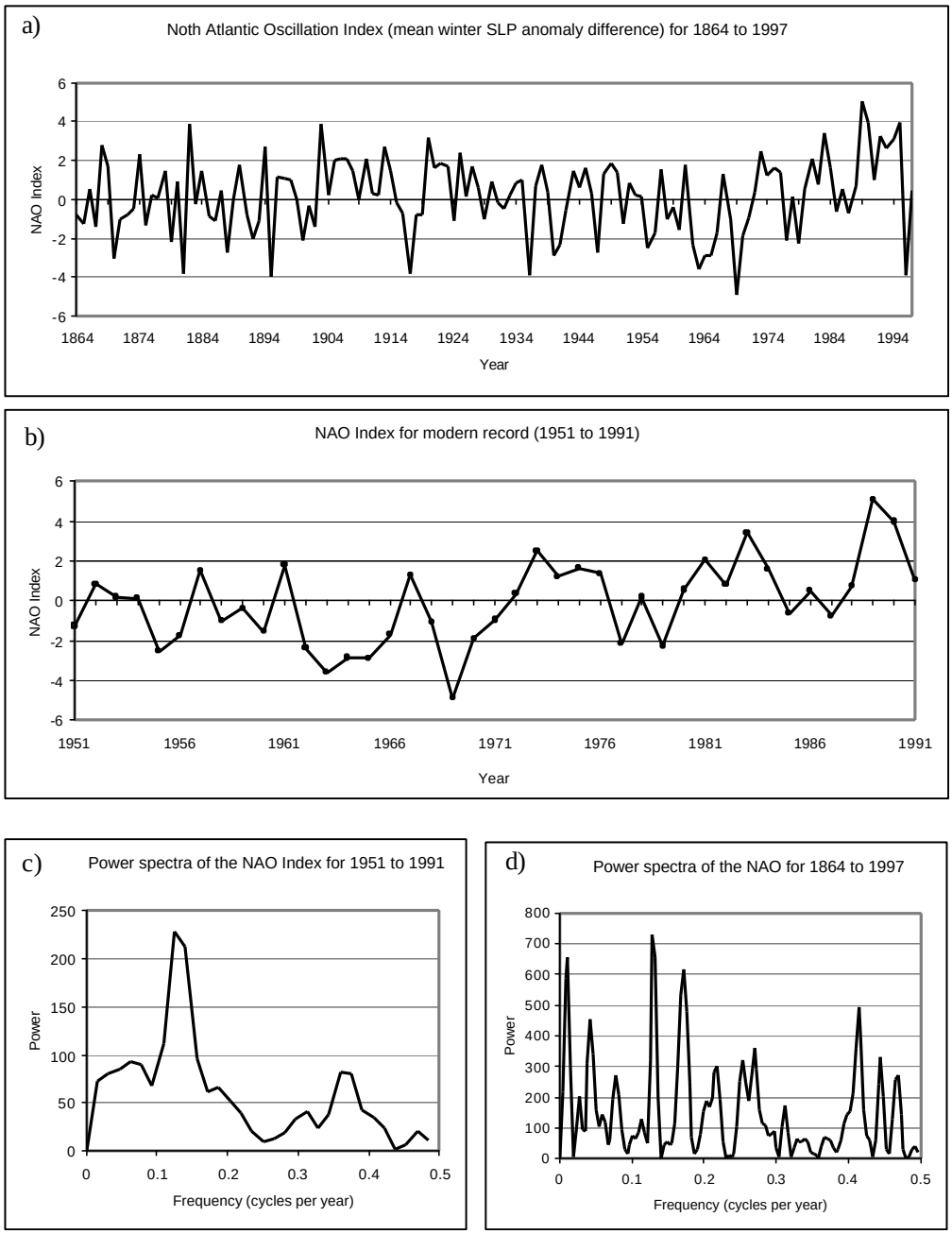

Figure 8.2. North Atlantic Oscillation (NAO) index. a) NAO index for the period 1864 to 1997, b) NAO Index for the modern record (1951 to 1991), c) power spectra for the modern NAO record and d) power spectra for the full NAO record.

8.2.3 Lisbon Sea Level Pressure (SLP) data

The NAO is generally only acknowledged as a winter phenomenon. For a measure of year-round variability in North Atlantic atmospheric conditions, monthly SLP data from Lisbon were used. This represents fluctuations in the Azores high pressure centre, the closest NAO pressure centre to the Gulf of Guinea. This was available from COADS as a continuous record from 1964 to 1993. SLP anomalies were calculated by subtraction of the long term (1964-1993) mean from the data.

Seasonal variability in SLP (fig. 8.3a) is greatest during the northern winter months (October to March) and pressures are usually highest during this period. Lisbon SLP values over the December to March period closely resemble winter NAO values (r^2=0.77). Over the summer months, SLP values are generally lower than the seasonal average and more constant. The least variable period is from May to September. SLP monthly anomaly values were calculated to remove any seasonal cycle from the data. The series is shown in figure 8.3b. Even with the seasonal cycle removed a large amount of within year variability remains. The 13-point moving average shows the mean pattern of interannual variability.

Power spectra of the Lisbon SLP anomaly values show a dominant annual cycle (fig. 8.3c). Power spectra of the SLP monthly anomaly values (fig. 8.3d) show no major cycles and appear to be dominated by white noise processes.

Autocorrelation and partial autocorrelation were calculated for the Lisbon SLP data at lags up to 36 months. Positive autocorrelation at a lag of one month was the only significant outcome and this result is marginal.

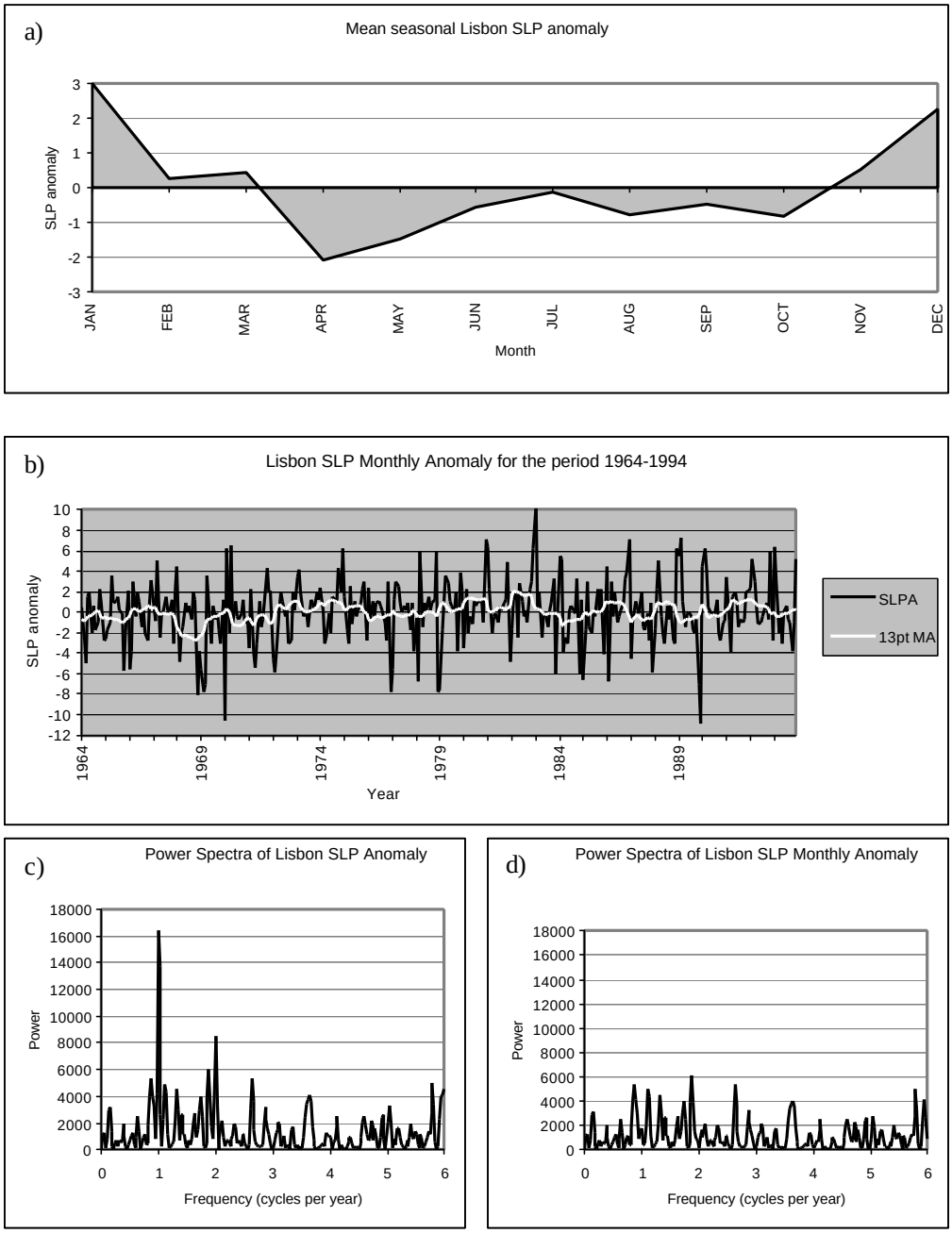

Figure 8.3. Lisbon Sea Level Pressure (SLP) anomaly. a) Mean seasonal Lisbon SLP anomaly for the period 1964 to 1994, b) Lisbon SLP monthly anomaly (black line) with 13 point moving average (white line) to show interannual variability, c) power spectra of the Lisbon monthly SLP anomaly and d) power spectra of the Lisbon SLP monthly anomaly.

8.2.4 Subtropical North Atlantic Zonal Index (SNAZI)

In the Pacific Ocean, the Southern Oscillation is a well known mode of zonal climate variability and links with the Aleutian low pressure centre are leading to a better understanding of meridional modes in that ocean (Kerr 1999). In the Atlantic, however, only a meridional mode, the NAO, has been documented to any degree. The Subtropical North Atlantic Zonal Index (SNAZI) is proposed by this study[1] as a measure of zonal SLP variability in the North Atlantic. It measures the SLP difference between Bermuda and Lisbon. The choice of these areas is supported by the first Empirical Orthogonal Function (EOF) of SST in the North Atlantic, as calculated by Venzke *et al.* (1999), which showed a tripole effect. Two of the tripole areas correspond to the Icelandic low and Azores high pressure centres, used in calculation of the NAO; the third is situated around Bermuda. SLP data for the index are taken from COADS and Lisbon SLP data have been used as a proxy for the Azores pressure centre for consistency with the NAO Index.

The index has been calculated as the mean difference in SLP over the boreal winter (Dec-Mar), autumn-winter (Oct-Mar) and summer (Jun-Sep) months. The winter index corresponds to those months used to calculate the NAO. Similarly, the autumn-winter index is calculated for nearly the same months as the winter SOI. The summer index was calculated as a contrast to the other two indices. To calculate the index, first the seasonal mean SLP was calculated and normalised with respect to the standard deviation. The Lisbon normalised seasonal mean was then subtracted from the Bermuda normalised seasonal mean. Finally, the normalised seasonal mean difference anomaly, that is the seasonal index, was calculated by subtraction of the long-term seasonal index mean. The winter and autumn-winter indices are highly correlated ($r=0.893$, $P<0.01$) due to the overlap between them. The summer index shows a strong, significant correlation with the autumn-winter index ($r=0.512$, $P<0.01$),

[1] The original idea for measuring the SLP difference between Bermuda and Lisbon came out of discussions between Michael Jordan and Arnold Taylor of CCMS, UK, and both are involved in studying this index in a different context to the current study. The title of Subtropical North Atlantic Zonal Index is original to this thesis and its author.

probably due to the closeness of the seasons, however, it is also significantly correlated with the winter index ($r=0.380$, $P<0.05$).

Monthly SNAZI values are shown in figure 8.4a. This series is highly variable. Charts of seasonal SNAZI values for the period 1964 to 1993 are shown in figure 8.4b-d. These series also show a high degree of interannual variability. In the winter mean SNAZI, high values are observed in 1965, 1972, 1976, 1979 and 1991. Low values are present in 1968, 1981, 1983, 1987 and 1992. The autumn-winter mean SNAZI also shows high and low values in these years, with the exception of 1979. Additionally, high values are seen in 1969 and 1986. The summer mean SNAZI displays a different pattern of interannual variability, with high values in 1964, 1966, 1986, 1988-89 and 1991 and low values in 1968, 1977-81 and 1984. A longer-term change appears to exist in all seasons, with higher values dominating until 1979 and lower values from 1980 onwards, with the exception of a period of high values from 1988 to 1991. No linear trend was observed consistently throughout the series.

An annual peak dominated power spectra for the monthly mean SNAZI (fig. 8.4e). Power spectra for the seasonal mean SNAZI are shown in figure 8.4f-h. Both the winter and autumn-winter spectra show large peaks with periods around 16 years. Additionally, the winter mean SNAZI spectra showed a large peak at 2.67 years. The summer mean SNAZI spectra shows a large peak at periods around 32 (series length) to 16 years.

Autocorrelation and partial autocorrelation were calculated for the monthly and seasonal SNAZI series. The monthly SNAZI only showed lags at eight and ten months to be significant and these were weakly correlated. None of the seasonal SNAZI series showed any significant autocorrelation.

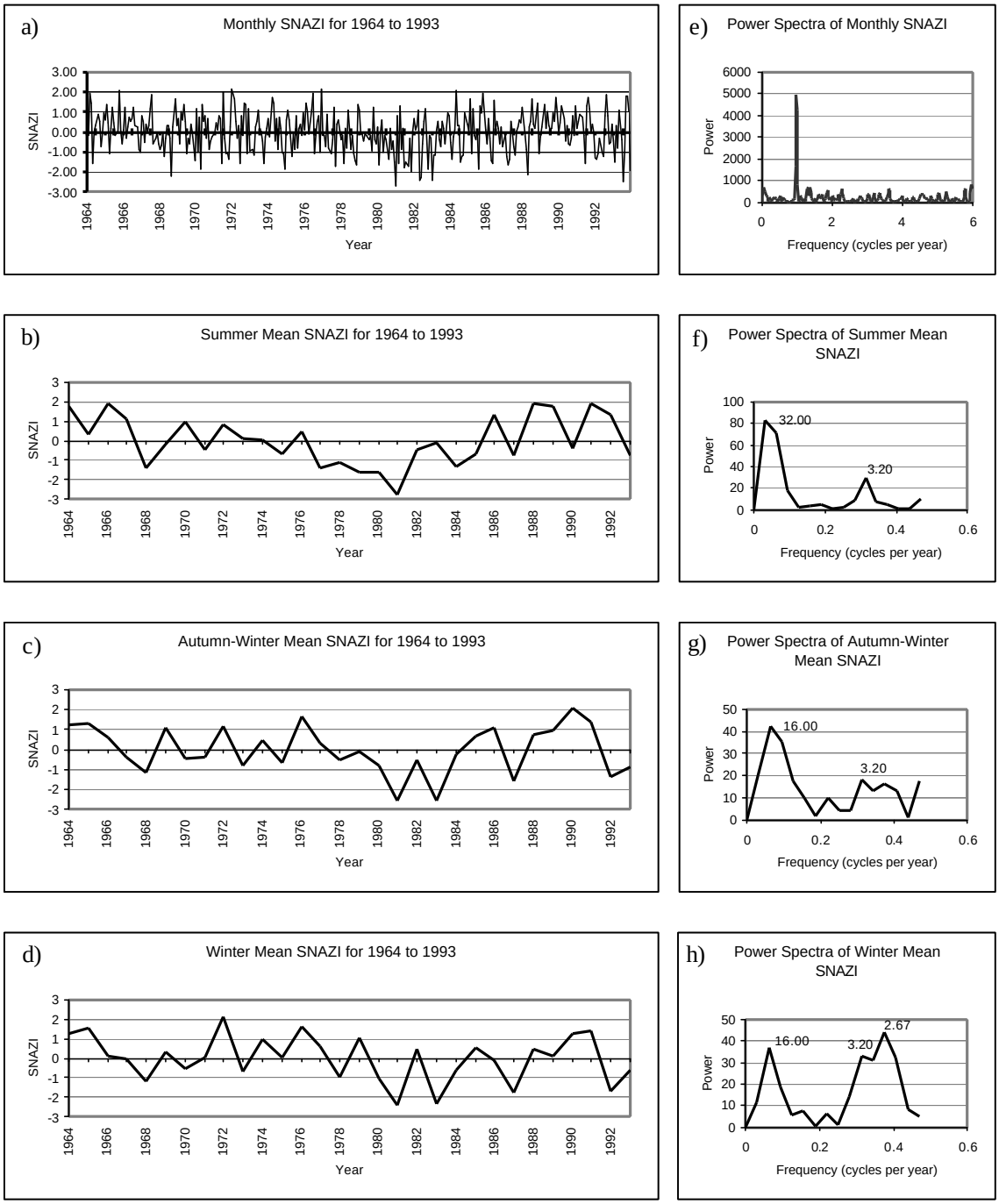

Figure 8.4. Subtropical North Atlantic Zonal Index (SNAZI). a) Monthly SNAZI series for the period 1964 to 1993; b) summer mean SNAZI, c) autumn-winter mean SNAZI and d) winter mean SNAZI over the same period; e-f) corresponding power spectra. The periods of individual spectral peaks are labelled on the power spectra of the seasonal series.

8.2.5 Comparison of climate indices

Correlation analysis of September-February SOI values, winter mean NAO values and seasonal SNAZI values with each other showed a strong correlation between the winter SNAZI and the SOI ($r=0.563$, $P<0.01$) and a weaker correlation between the autumn-winter SNAZI and the SOI ($r=0.461$, $P=0.01$). Cross-correlation analysis at lags up to three years confirmed these results and showed no other significant correlations.

8.3 Southern Oscillation Index Relationships

8.3.1 SST Areas

To assess if any relationship exists between the SOI and SST in the Gulf of Guinea, SST values for each subsystem Area were compared with SOI values. Firstly, qualitative comparison of CORSA-AVHRR annual and seasonal mean SST values with SOI winter values showed no relationship between SOI and SST for any Areas (see appendix 4). Then cross-correlation analysis was undertaken for CORSA-AVHRR seasonal mean SST with SOI winter values at lags up to three years. This showed no significant correlation for any Areas. Cross-correlation was also carried out for first-differenced CORSA-AVHRR SST monthly anomalies with first-differenced SOI monthly values at lags up to 36 months. This showed weak significant correlation at lags -11 ($r=0.192$) and -12 ($r=-0.204$) for Area 2, -1 ($r=0.192$) for Area 3 and +13 ($r=0.200$) for Area 4. There was no significant correlation with Area 1.

The cross-correlation analyses were then repeated using COADS SST values. Cross-correlation of COADS seasonal mean SST with SOI winter values at lags up to three years showed a number of significant results. For Area 1, lag +1 was significant in both seasons, with the strongest correlation in season 1 ($r=-0.709$; season 2: $r=-0.457$). It also showed a weakly significant correlation at lag -1 for season 2 ($r=0.400$). Area 2 showed significant correlation at lag +1 in season 1 ($r=-0.445$). Area 3 showed no significant correlation for any seasons and Area 4 showed a weakly significant correlation at lag 0 for season 2 ($r=0.391$).

Cross-correlation of first-differenced COADS SST monthly anomalies with first-differenced SOI values was undertaken at lags up to 36 months. Significant correlation was seen for Area 1 at lags -24 (r=-0.135), -23 (r=0.117) and +35 (r=0.108), for Area 2 at lags -2 (r=0.106), +12 (r=-0.102) and +14 (r=0.116), for Area 3 at lags -16 (r=-0.117), -2 (r=0.110), +1 (r=-0.102), +12 (r=-0.101), +13 (r=0.097) and +31 (r=0.112) and for Area 4 at lags -27 (r=0.119), -19 (r=-0.095), -16 (r=0.097), -8 (r=0.126), -4 (r=0.126), -3 (r=-0.100), +31 (r=-0.106) and +32 (r=0.134). All these monthly results were only weakly significant.

8.3.2 Local climate data

The following analyses were undertaken to assess if any relationship exists between the SOI and rainfall in the Gulf of Guinea. Firstly, annual rainfall and river discharge data were compared with SOI winter values. Qualitative comparison of SOI winter values with annual river discharge and rainfall for each of the regional hydroclimates, over the period 1951 to 1989, showed no resemblance between the data sets, however, rainfall for the Equateur region does reflect the strong 1982/1983 ENSO signal at one year lag (fig. 8.5).

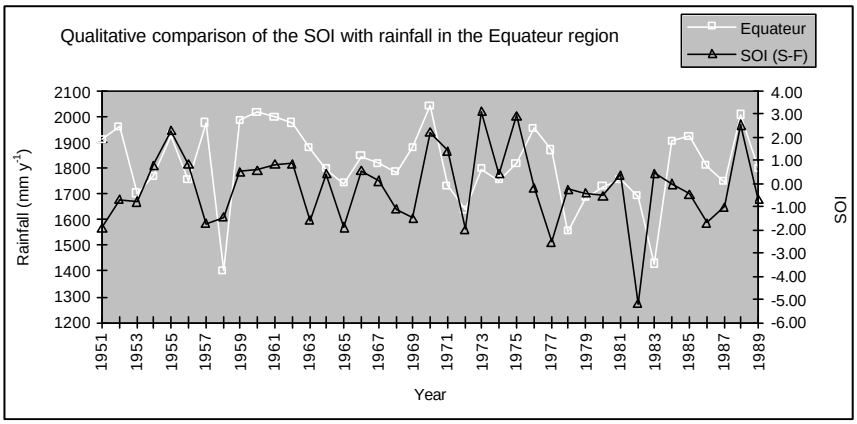

Figure 8.5. Chart comparing the September-February SOI with rainfall in the Equateur region. The year given for the SOI is that of September, because it is during the boreal autumn that peak rainfall occurs in the Equateur region.

Cross-correlation analysis of SOI winter values with annual rainfall and river discharge values for each hydroclimatic region at lags up to three years was undertaken. Series that showed significant positive autocorrelation at lag 1 were filtered using first-order differencing prior to cross-correlation analysis. Significant correlation was seen for river discharge in the Guinée region at lag +1 (r=0.354) and in the Niger region at lag -3 (r=-0.350) but no significant correlation was observed for rainfall data.

To see if any relationship could be detected in monthly rainfall data, cross-correlation analysis of first-differenced GGRI monthly values with first-differenced SOI monthly values was undertaken at lags up to 36 months. Significant correlation was seen at lags -21 (r=0.118), +22 (r=-0.094), +26 (r=-0.121), +27 (r=0.158) and +34 (r=-0.097). These were all only weakly significant. Cross-correlation of the first differenced TBRI monthly values and first differenced Roberts Field monthly data with first differenced SOI monthly values at lags up to 36 months showed the TBRI to most closely resemble the GGRI, having significant lags at -21 (r=0.124), +26 (r=-0.139), +27 (r=0.162) and +34 (r=-0.108). The Roberts Field data, however, showed no resemblance to the GGRI, having significant correlation at lags -26 (r=0.119), -25 (r=-0.125), -24 (r=0.095), -19 (r=0.104), -16 (r=-0.099) and +6 (r=0.095).

8.3.3 Indices of oceanographic features

To see if any relationship exists between the SOI and particular oceanographic features, the SOI was compared with the SUI index and CUI. Qualitatively, no consistent resemblance was seen throughout both series, however, the reduced spatial extent of the major upwelling in 1984 appears to match the strong, negative SOI signal in 1983 (see appendix 4). Cross-correlation of these series with SOI winter values at lags up to three years showed no significant correlation.

8.4 North Atlantic Oscillation/Lisbon SLP Relationships

8.4.1 SST Areas

To assess if the NAO has any relationship with Gulf of Guinea SST, it was compared with the CORSA-AVHRR and COADS SST records for each SST area. Firstly, qualitative comparison between CORSA-AVHRR annual mean SST values and NAO values showed that Area 1 SST appears to lag behind the NAO by 2-3 years and Area 2 appears to lag 2 years behind the NAO. Areas 3 and 4 did not appear to resemble the NAO (sse appendix 4). However, cross-correlation analysis of CORSA-AVHRR seasonal mean SST with NAO winter values at lags up to three years showed no significant correlation. Repeating the analysis for COADS seasonal mean SST with first-differenced NAO winter values at lags up to three years showed significant correlation for Area 3 in season 2 at lag +1 (r=0.433). First-differenced NAO values were only used with COADS SST values because autocorrelation showed significant serial correlation was only present in the longer NAO series.

Cross-correlation analysis of first-differenced SST monthly anomalies and Lisbon SLP monthly anomalies was then undertaken at lags up to 36 months for both the CORSA-AVHRR and COADS data sets. Significant correlation was seen in the CORSA-AVHRR series for Area 1 at lags +1 (r=0.243) and +12 (r=0.208), for Area 2 at lag +29 (r=0.225), for Area 3 at lag +3 (r=0.259) and for Area 4 at lags -19 (r=0.207) and -9 (r=0.203).

The COADS series showed significant correlation for Area 1 at lags -9 (r=-0.167), 0 (r=0.115) and +3 (r=-0.120), for Area 2 at lags -33 (r=0.147) and -9 (r=-0.117), for Area 3 at lags +3 (r=-0.174) and +27 (r=-0.134) and for Area 4 at lags -19 (r=-0.125), -18 (r=0.116), +4 (r=-0.126) and +22 (r=-0.133).

8.4.2 Local climate data

To assess if any relationship exists between the NAO and rainfall in the Gulf of Guinea, the following comparisons and analyses were undertaken. Qualitative comparison of NAO

values with river discharge and rainfall during the 1980s showed that the rainfall signal for the Coastal Nigeria and Coastal North Equateur areas resembled that of the NAO (fig. 8.6).

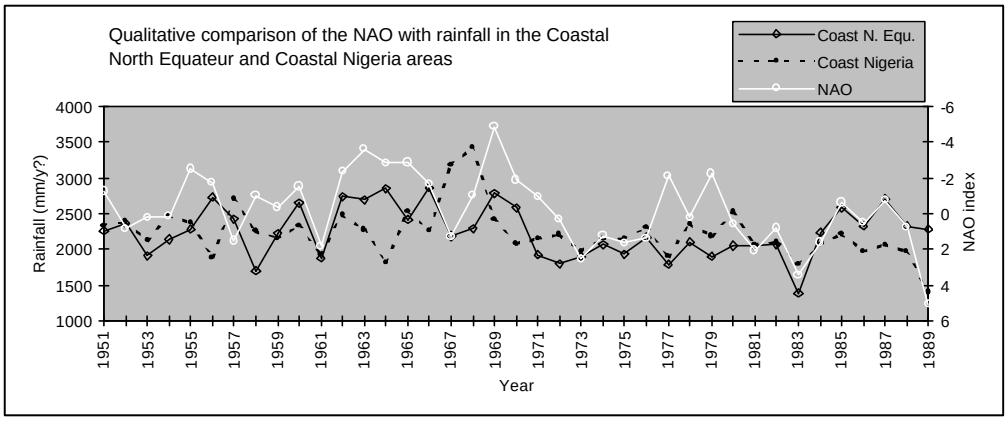

Figure 8.6. Chart comparing the winter mean NAO index with rainfall in the Coastal North Equateur and Coastal Nigeria areas.

Correlative analysis of NAO values with annual river discharge values for each regional hydroclimate over the period 1951 to 1989 showed r-values in the range -0.4 to -0.5. The Fouta region showed the lowest value and the Equateur region the highest. All these results were highly significant ($P<0.01$) except for the result for the Fouta region, which was still significant ($P<0.05$).

Correlative analysis of NAO values with annual rainfall data for each regional hydroclimate was undertaken. Only the Guinée and Niger areas showed significant r-values ($r=-0.439$, $P<0.01$; $r=-0.322$, $P<0.05$, respectively). Additionally, for correlative analysis of NAO values with rainfall from coastal areas only the results for the Coastal Guinée, Coastal Nordgolf and Coastal North Equateur areas were significant ($r=-0.418$, $P< 0.01$; $r=-0.342$, $P<0.05$; $r=-0.534$, $P<0.01$, respectively).

Cross-correlation analysis of rainfall and river discharge data for each regional hydroclimate and coastal area with first-differenced NAO values at lags up to three years only showed significant correlation at lags 0 ($r=-0.325$) and +1 ($r=0.430$) for Guinée region river discharge and lag -3 for Guinée region ($r=-0.424$) and Coastal Nordgolf area ($r=-0.325$) rainfall.

To see if any relationship could be detected in monthly data, cross-correlation analysis for the GGRI with Lisbon SLP monthly anomalies was carried out at lags up to 36 months. This showed no significant correlation. Repeating the analysis for the first differenced TBRI and first differenced Roberts Field data also showed no significant correlation.

8.4.3 Indices of oceanographic features

Comparison of the NAO with indices of oceanographic features was undertaken to investigate any relationship between the series. Qualitative comparison of NAO values with the SUI index showed the two series to be very similar for most years, with the NAO from 1981 to 1988 leading the SUI from 1983 to 1990, a lead-time of two years (fig. 8.7).

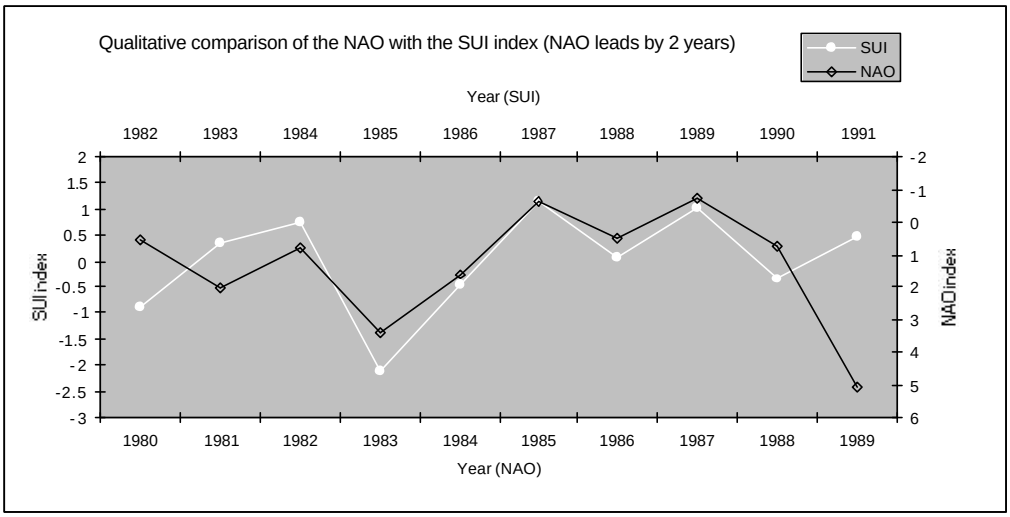

Figure 8.7. Chart comparing the winter mean NAO index with the SUI index. The NAO leads the SUI by two years.

Correlative analysis of NAO values with the SUI index over this period showed the two series to be very highly correlated ($r=-0.853$, $P<0.01$). However, cross-correlation analysis for the SUI index with the NAO, at lags up to three years, did not pick up this relationship as significant because of the divergence of SUI values in 1982 and 1991 from those of the NAO two years previously.

Qualitative comparison of the NAO with the CUI and its constituents showed some similarity with spatial extemt of upwelling during the major season, lagging the NAO by two years (see appendix 4). Cross-correlation analysis of the CUI and its constituents with the NAO at lags up to three years showed no significant correlation

8.5 Subtropical North Atlantic Zonal Index Relationships

8.5.1 SST Areas

SST areas were compared with the SNAZI to assess if any relationships existed between them. SNAZI seasonal values were compared qualitatively with CORSA-AVHRR derived annual and seasonal mean SST values for 1981 to 1991 (see appendix 4). The strongest similarities were seen in Areas 2 to 4 during season 3, with SST leading SNAZI winter values by one year (fig. 8.8).

Cross-correlation analysis was undertaken for CORSA-AVHRR seasonal mean SST with SNAZI seasonal values at lags up to three years. SNAZI winter values showed significant, strong correlation at lag -1 with Areas 2 and 3 during season 2 (r=0.658, 0.651, respectively) and season 3 (r=0.723, 0.714, respectively) and with Area 4 during season 3 (r=0.697). SNAZI autumn-winter values showed significant correlation at lag +1 with Area 1 during season 2 (r=0.656) and also at lag -1 with Area 2 during season 3 (r=0.703), Area 3 during season 2 (r=0.652) and season 3 (r=0.673) and Area 4 during season 3 (r=0.669). SNAZI summer values showed significant correlation at lag +1 with Area 1 during season 2 (r=0.706), Area 2 during season 2 (r=0.724) and season 3 (r=0.842), Area 3 during season 3 (r=0.752) and Area 4 during season 3 (r=0.753).

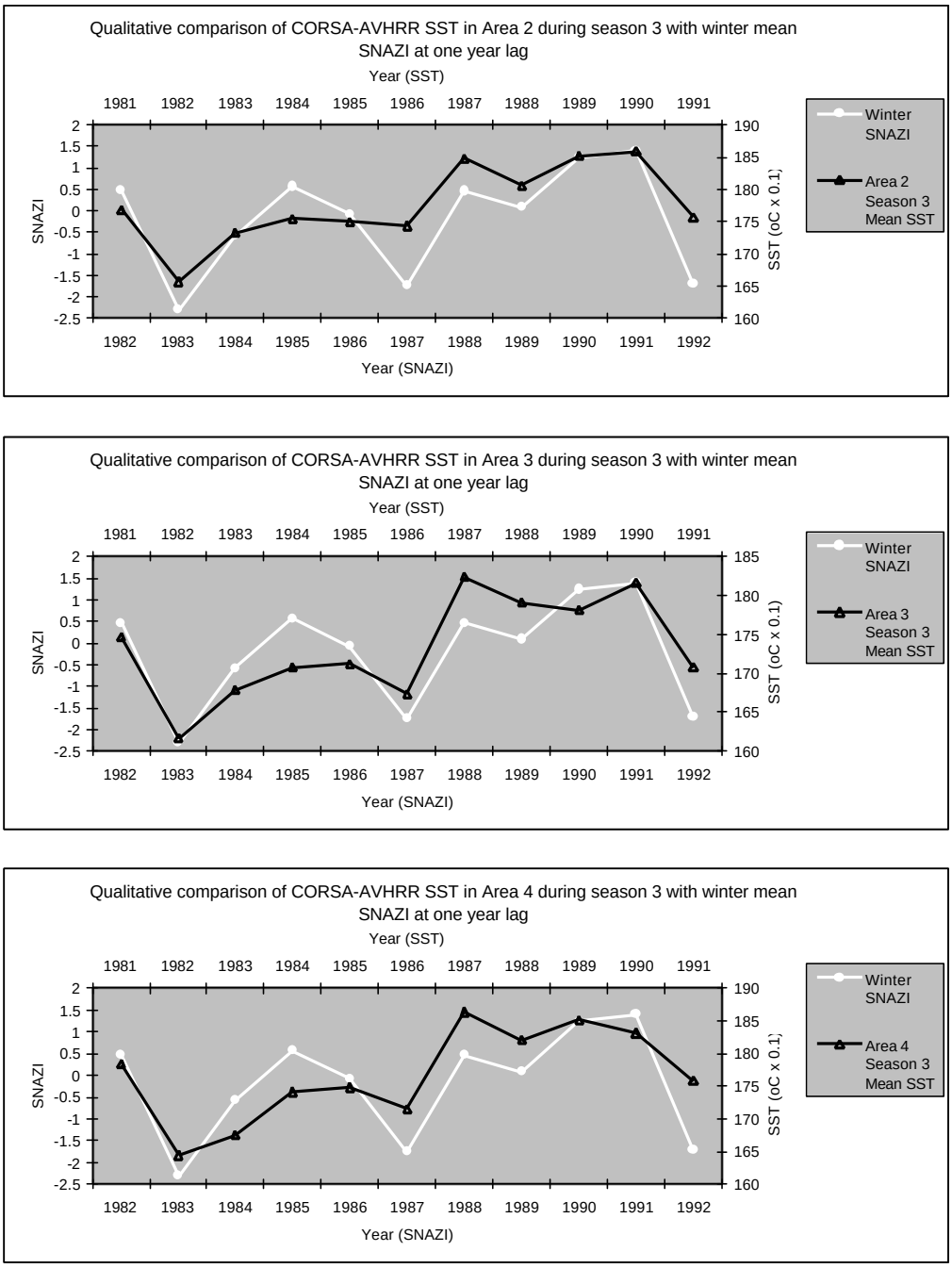

Figure 8.8. Charts comparing winter mean SNAZI values with CORSA-AVHRR mean SST in Areas 2 to 4 during season 3. SNAZI values lag SST by one year.

Cross-correlation analysis was also undertaken for first-differenced CORSA-AVHRR SST monthly anomalies with SNAZI monthly values at lags up to 36 months. Significant correlation was seen at lags +6 (r=0.233) and +17 (r=-0.194) for Area 2 and +3 (r=-0.223) and +17 (r=-0.195) for Area 3.

To further resolve the pattern of correlation seen in the seasonal analysis, correlative analysis was undertaken between SNAZI monthly values and CORSA-AVHRR SST monthly anomalies for individual months at lags up to 12 months. SNAZI values from May and June showed significant relationships with June-October SST values from the same year, SNAZI values from October showed significant relationships with SST values from November and December of the same year and SNAZI values from October and November showed significant relationships with SST values from February to May of the following year. Additionally, SNAZI values from January to March showed significant relationships with July-December SST values from the previous year and January SST values of the same year. The highest correlation was for SST in October with SNAZI values in the following January ($r=0.933$, $P<0.01$).

To see if this relationship would hold for a longer time series, cross-correlation was undertaken between COADS seasonal mean SST and SNAZI seasonal values. SNAZI winter values showed significant correlation at lag 0 for Area 1 during season 1 (r=-0.493). SNAZI autumn-winter values showed significant correlation at lag +2 for Area 4 during season 1 (r=0.405) and at lag +3 for Area 4 during season 3 (r=0.544). SNAZI summer values showed significant correlation at lag 0 (r=0.416) for Area 3 during season 1.

Cross-correlation analysis was undertaken for COADS SST monthly anomalies with SNAZI monthly values at lags up to 36 months. Significant correlation was seen for Area 1 at lags -3 (r=0.140), 0 (r=-0.173) and +8 (r=-0.121), for Area 2 at lags -32 (r=0.121), -3 (r=0.136), 0 (r=-0.238) and +34 (r=0.120), for Area 3 at lags +3 (r=0.122) and +15 (r=-0.116) and for Area 4 at lags +4 (r=0.134), +5 (r=-0.119) and +30 (r=0.124).

8.5.2 Local climate data

The following analyses were undertaken to assess if any relationship exists between local climate in the Gulf of Guinea and the SNAZI. Cross-correlation analysis for annual river discharge and rainfall data with SNAZI seasonal values was carried out at lags up to three years. SNAZI winter values showed no significant correlation with river discharge, however, weakly significant correlation was seen for rainfall in the Adamaoua region at lags +2 (r=0.409) and +3 (r=0.419) and in the Coastal Nigeria area at lags +2 (r=0.409) and +3 (r=0.428). SNAZI autumn-winter values showed significant correlation for river discharge in the Nordgolf region at lag +3 (r=0.417) and in the Equateur region at lag 0 (r=0.463) and for rainfall at lag +2 in the Adamaoua region (r=0.457) and Coastal Nigeria area (r=0.466) and at lag 0 for the Coastal North Equateur area (r=0.417). SNAZI summer values showed significant correlation for river discharge in the Guinée (r=0.460), Nordgolf (r=0.418) and Equateur (r=0.412) regions at lag +2 and in the Equateur region at lag -1 (r=0.473). SNAZI summer values also showed significant correlation with rainfall in the Guinée (r=0.525), Nordgolf (r=0.417) and Adamaoua (r=0.508) regions and Coastal Guinée (r=0.474), Coastal Nordgolf (r=0.477) and Coastal Nigeria (r=0.491) areas at lag +2 and in the Coastal North Equateur area at lags -2 (r=0.410), -1 (r=0.517) and 0 (r=0.394).

Cross-correlation analysis for the first-differenced GGRI with SNAZI monthly values was undertaken at lags up to 36 months. Significant correlation was seen at lags -14 (r=0.117), -9 (r=-0.127), +6 (r=-0.112) and +24 (r=-0.137). Repeating the analysis for the first-differenced TBRI also showed significant correlation at lags -14 (r=0.139), -9 (r=-0.125) and +24 (r=-0.141). Cross-correlation for the first-differenced Roberts Field data with SNAZI monthly values at lags up to 36 months showed significant correlation at lag -12 (r=0.119).

8.5.3 Indices of oceanographic features

Qualitatively, a strong resemblance was seen between upwelling spatial extent during the major season and SNAZI winter and autumn-winter values, both series in phase (fig. 8.9). A

weaker resemblance was also seen between upwelling intensity during the major season and SNAZI winter and autumn-winter values from 1984 onwards, both series in phase. These similarities were reflected in the CUI for the major season. Some similarity was also seen between upwelling intensity during the major season and SNAZI summer values, both series in phase. For the minor upwelling season, no general resemblance was seen between either spatial extent or intensity, however, both parameters showed a decline between 1986 and 1987, coinciding with a steep drop in the SNAZI seasonal values between these years. No resemblance was seen between the SUI index and SNAZI seasonal values (see appendix 4).

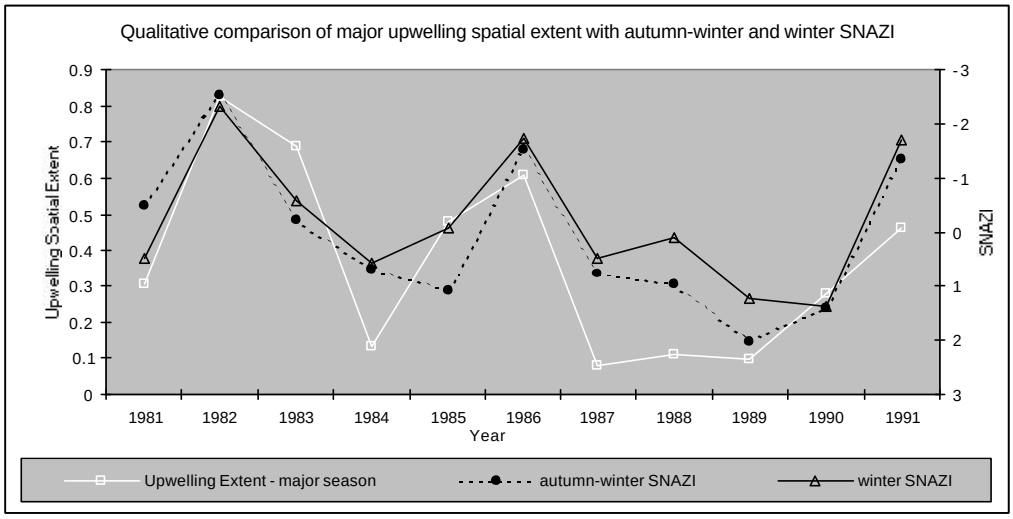

Figure 8.9. Chart comparing the spatial extent of the major upwelling season with the autumn-winter and winter mean SNAZI values.

Cross-correlation analysis for SUI index values with SNAZI seasonal values at lags up to three years showed no significant correlation for any of the seasons. Cross-correlation analysis for CUI values and its constituents with SNAZI seasonal values at lags up to three years showed significant correlation between SNAZI winter values and the CUI during the major season at lag -1 (r=-0.663). This relationship was due to the high correlation between SNAZI winter values and the spatial extent of upwelling seen at the same lag (r=-0.706). Significant correlation is also seen between SNAZI autumn-winter values and spatial extent of upwelling during the major season (r=-0.668), however, this relationship is not reflected in

the CUI at a significant level. For the SNAZI summer values, significant correlation is seen at lag +1 with the spatial extent of upwelling during the major season (r=-0.661), however, this relationship is not reflected in the CUI at a significant level.

8.6 Discussion

8.6.1 Global/basin scale climate variability

Power spectra showed cycles at periods around 16 and 3 years in the SOI, NAO and SNAZI series. Therefore these cycles appear to have a global influence. The longer scale NAO showed that the 16 year cycle may well be produced by leakage from cycles at periods around 23 and 13 years. These have a similar period to cycles of variability in the output of the sun, seen as the sunspot and double sunspot cycles at periods of 11 and 22 years, respectively (Burroughs 1992). The cycle with an approximate 3-year period may correspond to a quasi-biennial oscillation identified in a number of environmental time series from around the world (Burroughs 1992). Differences are seen between the SOI, NAO and SNAZI in the period of their intermediate scale interannual variability. The SOI varies on a scale of around 4.5 years and the NAO shows approximate 8 year and 6 year cycles. No intermediate scale variability is seen in the SNAZI.

Examination of the winter mean SOI series showed years with particularly low values, corresponding to El Niño years, to occur every two to five years. However, particularly high values, corresponding to major La Niña events, only appear to occur approximately every 15 years. Thus, the 4.5 year cycle seen in the power spectra probably represents the El Niño cycle and the 16 year cycle may represent the La Niña cycle. The strongest El Niño event is seen in 1983 and the strongest La Niña events in 1974 and 1976. High NAO values occur every two to eight years. Pre-1973, high values are generally seen every five to six years, however, after this their occurrence is more sporadic. This post 1973 pattern could be interpreted as repeating every eight years with an abnormal interruption in 1983. Low values

appear to repeat every six to eight years up until 1977, there is then only a two year gap before the next low value. After 1979, there are no low values for the rest of the series. The lowest value occurs in 1969 and the highest in 1989. The SNAZI shows no quasi-regular pattern of repeating high and low values. Its highest values occur in 1972 and 1990 and its lowest values are seen in 1981 and 1983. All three series show shifts from periods of generally high values to periods of generally low values, however, these occur at different times in each index. This jump occurs between 1976 and 1977 in the SOI, between 1969 and 1973 for the NAO and between 1976 and 1981 for the SNAZI, although only in the winter SNAZI do the lower values continue beyond 1985.

8.6.2 Southern Oscillation Index

SST

Qualitatively, CORSA-AVHRR seasonal mean SST values do not resemble SOI winter values. The lack of correlation between the series is also seen quantitatively through cross-correlation. On the finer, monthly scale, cross-correlation did appear to show an approximate annual pattern, however, no annual cycle is observed in the SOI and all seasonality was removed from the SST data prior to the analysis. The one month lag seen between SST in Area 3 and the SOI may be explained by negative autocorrelation at one month lag, a possible artefact of removing serial correlation by first-order differencing. From these results, no significant relationship can be concluded to exist between the SOI and CORSA-AVHRR SST data in the Gulf of Guinea.

Examination of SST over a longer time scale, using COADS SST, showed a greater number of significant relationships. However, when seasonal means were compared, the only strongly significant result showed the SOI to lead SST by one year during season 1 in Area 1. This Area is dominated by the SUI and its influence is strongest during season 1. Thus, it appears that the SOI may have an influence over SST variability in the SUI. This conclusion

also explains the weaker correlation seen for Area 1 during season 2 and Area 2 during season 1, as these series are neighbours in time and space, respectively. No conclusions can be drawn from the in-phase correlation between the SOI and Area 4 during season 2.

Cross-correlation analysis of COADS SST monthly anomalies with SOI monthly values showed a number of weakly significant correlations, however, none of these supported the seasonal results, above. The strongest correlation for Area 1 showed SST leading the SOI by 24 months. This could be caused by the quasi-biennial oscillations identified from power spectra within both these series, however, in that case a corresponding correlation with the SOI leading SST by around 24 months would be expected and this is not seen. For Area 2, the 12-month correlation appears to support the seasonal result, above, of the SOI leading SST by one year in Area 2 during season 1. However, this result is also reflected in Area 3 and not in Area 1, suggesting it is not associated with the seasonal influence of the SUI. For Area 4, eight weakly significant results were seen, the strongest of which showed SST to lead the SOI by four months. Initially, this appears to support the seasonal result, above, of SST in Area 4 during season 2 varying in phase with the SOI, however, this is not the case. If SST were to lead the SOI by 4 months from season 2, then they would correspond to SOI values in the late autumn, which would contribute to the following years September-February SOI value. Therefore, the two seasonal series would not vary in phase.

Local climate

Qualitatively, the SOI does not resemble river discharge and rainfall patterns in any of the regional hydroclimates, however, a strong signal was seen in rainfall and river discharge in 1983, most prominently in the Equateur region, corresponding to the large ENSO event occurring at this time. Cross-correlation showed the SOI to lead river discharge in the Guinée region by one year and river discharge in the Niger region was observed to lead the SOI by three years. The Guinée region is geographically close to Area 1 so this may be a reflection in the river discharge data of the relationship seen between SST and the SOI in this location.

This explanation is plausible because the cold SUI was seen in chapter 4 to have an influence on rainfall. No meaningful conclusions can be drawn from the observed correlation between Niger region river discharge and the SOI.

OCEANOGRAPHIC INDICES

No relationship was seen either qualitatively or quantitatively between the SOI and oceanographic indices. Therefore, it appears that the SOI has no influence either on the spatial extent of the SUI or on coastal upwelling.

8.6.3 North Atlantic Oscillation and Lisbon SLP

SST

A qualitative resemblance was seen between the NAO and CORSA-AVHRR annual mean SST for Areas 1 and 2, with SST appearing to lag the NAO by two to three years in Area 1 and by two years in Area 2. However, no evidence for any significant relationship between CORSA-AVHRR SST and the NAO was found on a seasonal basis from cross-correlation. On the other hand, the weakly significant correlation between the NAO and COADS seasonal SST, with the NAO leading SST by one year for Area 3 during season 2, suggests a relationship between the strength of the NAO and SST in the equatorial Atlantic during the major upwelling period. Although also only weak, the three-month correlation between SST in Area 3 and Lisbon SLP on a monthly basis, seen in both the CORSA-AVHRR and COADS data sets, lends some support to this suggestion, in spite of the difference in time scale. The three-month time lag suggests a possible relationship between the strength of the Azores high pressure centre and the major upwelling season. Certainly, the strength of the Azores pressure centre determines the strength of the trade winds in the North Atlantic and several studies have shown a relationship between the intensification of the trade winds in the western tropical Atlantic and the equatorial and coastal upwellings to the east (Houghton and Colin 1986, Servain *et al.* 1982). More difficult to interpret is the one year time lag between

the NAO and SST. The weak 19-month lag between Lisbon SLP and SST, with SST leading SLP, was also seen in both the CORSA-AVHRR and COADS cross-correlations. The time scale of this result is of the same order as the one-year lag between the NAO and the major upwelling season, however, the Area is wrong. Nevertheless, the upwelling season is seen to have an effect on the seasonal cycle of Area 4 in both data sets (see chapters 6 and 7).

Local climate

The correlation seen between the NAO and river discharge in all hydroclimatic regions, as well as rainfall in several hydroclimatic regions and coastal areas, suggests the NAO to have a strong influence on meteorological conditions in the Gulf of Guinea. The qualitative resemblance seen between the NAO and rainfall in certain coastal areas supports this theory. However, these results are not shown when first differenced series are used.

The lack of a significant relationship between monthly rainfall and Lisbon SLP data means no further light can be shed on the relationship from the results of this study.

Oceanographic indices

Qualitatively, the SUI Index between 1983 and 1990 was almost identical to the NAO, with the NAO leading the SUI by 2 years. Thus, latitude of the SUI appears to be forced by the NAO, however, this relationship was not picked up by cross-correlation because of the deviation from this pattern seen in 1982 and 1991. The two-year lag is the same as that observed between the NAO and the north wall of the Gulf Stream (Taylor and Stephens 1998), again a measure of latitude. Both the Gulf Stream and the Canary Current, from which the SUI derives, form limbs of the North Atlantic's subtropical ocean gyre so it appears that the NAO may be instrumental in driving this circulation.

8.6.4 Subtropical North Atlantic Zonal Index

SST

The results from comparisons of the SNAZI with SST show the strongest evidence of large scale climate forcing on SST in the Gulf of Guinea. Qualitative comparison of CORSA-AVHRR seasonal SST values with SNAZI seasonal values showed a strong resemblance with SNAZI winter values for Areas 2 to 4 during seasons 2 and 3. These similarities were supported by cross-correlations which showed strong relationships between the SNAZI and SST during seasons 2 and 3 from throughout the Gulf of Guinea (Areas 2 to 4). Furthermore, cross-correlation showed both SST to lead the SNAZI by one year (winter and autumn-winter values) and the SNAZI to lead SST by one year (summer values). Because of seasonal differences, these relationships actually show SST to lead the SNAZI by zero to six months and SNAZI to lead SST by 12 to 18 months. This suggests that not only is SST in the Gulf of Guinea being forced by atmospheric variability, it is also forcing it. The SNAZI (summer and autumn-winter values) was also seen to lead SST during season 2 in Area 1 by one year. During this season, the SUI is greatly reduced in extent and conditions in Area 1 are dominated by the warmer waters seen more generally in Area 2.

The significant correlations seen on a monthly basis showed SNAZI to lead SST by 6 and 17 months for Area 2 and by 3 and 17 months for Area 3. The 17-month results support the SNAZI summer results. Within year relationships were further pinpointed on a month-to-month basis and showed SNAZI values to lead SST by zero to seven months, supporting the three and six month results from cross-correlation. Additionally, SST values were seen to lead the SNAZI by zero to eight months. The strongest relationship was for October SST values in Area 2 forcing SNAZI values in the following January. SST values are warmest in Area 2 from October to December and in May. During the autumn months the ITCZ is situated south of the Gulf of Guinea and the warm SST helps drive the North Atlantic Hadley cell. In May, however, the ITCZ is further north so any effect would feed into the West

African monsoon and South Atlantic Hadley cell. Therefore, no correlation is seen with the SNAZI. Sutton *et al.* (2000) also showed that SST in the tropical Atlantic during these months forces atmospheric variability.

Repeating the analysis with COADS SST data did not support the strong results seen with CORSA-AVHRR SST data. However, the significant relationship seen between COADS SST values for Area 1 during season 1 and SNAZI winter values, both series in phase (lag 0), suggests that over the longer time series, the SNAZI has an effect on SST in the SUI. Some support is also found for this relationship from the monthly cross-correlation results, however, these correlations are only weak. No obvious interpretation exists for the other significant relationships seen between COADS SST values and the SNAZI.

Local climate

SNAZI summer values appear to lead river discharge in the Guinée, Nordgolf and Equateur regions and rainfall in the Guinée, Nordgolf and Adamaoua regions and their associated coastal areas by two years. The wide distribution of this relationship suggests that the SNAZI influences local climate in the Gulf of Guinea through a large scale meteorological feature, such as the ITCZ or the West African monsoon. The relationship between SNAZI summer values and rainfall in the Coastal North Equateur area is strongest when SNAZI lags rainfall by one year and this lag is also seen between SNAZI summer values and equateur river discharge. However, this relationship was seen less strongly for SNAZI autumn-winter values which varied in phase with Equateur river discharge and Coastal North Equateur area rainfall. Nonetheless, it appears that a relationship exists between equatorial climate dynamics and the SNAZI. SNAZI autumn-winter values also lead river discharge in the Nordgolf region by three years and rainfall in the Adamaoua region and its associated coastal area by two years. This relationship was seen less strongly for SNAZI winter values leading by two to three years. All of these results are supported by cross-correlation of the monthly series.

The spatial extent of upwelling is significantly correlated to SNAZI winter and autumn-winter values and leads the SNAZI by one year. This is similar to the relationship with SST so it is surprising that the relationship is not seen in upwelling intensity. This suggests a connection between warm SST in October to November and the spatial extent of the major upwelling. Indeed, direct comparison of SST and the CUI in chapter 7 showed such a relationship to exist. It has been postulated that the end of the major upwelling season and the onset of warm temperatures are caused by a downwelling, equatorially trapped Kelvin wave becoming entrained along the coast (Verstraete 1992). It is also thought that the upwelling season itself is caused by equatorial wave dynamics, with the width of upwelling being determined by the Rossby radius of the wave. Thus, there is a physical explanation of this link between spatial extent of the major upwelling and the warm SST seen during October and November. The SNAZI summer values are also significantly correlated with the spatial extent of the major upwelling but this time the SNAZI leads upwelling by one year. This is also similar to the relationship between SST and SNAZI summer values.

8.7 Conclusions

The SNAZI appears to be the dominant large scale climatic factor forcing SST and local climate in the Gulf of Guinea. Additionally, SST may be forcing the SNAZI. The NAO is also seen to have some influence and the possibility of ENSO having an effect cannot be ruled out, especially in the SUI/Guinée region. The 1983 El Niño event appears to have had a particularly strong impact on environmental variability in the Gulf of Guinea. The SNAZI is the dominant factor forcing upwelling, however, the NAO is also seen to be influential and the effect of the 1983 El Niño is prominent. The position of the SUI appears to be forced by the NAO. The SOI and NAO appear independent of each other, however, some degree of coupling may exist between the winter SNAZI and the SOI. Coupling between the SNAZI

and upwelling shows how large scale climate variability can be reflected in oceanic structures of potentially direct relevance to productivity and fisheries recruitment.

9 Overall Discussion and Conclusions

9.1 Introduction

This thesis has focused on oceanographic and meteorological variability in the Gulf of Guinea over seasonal and interannual time scales with the aims of identifying and describing relevant spatio-temporal scales over which environmental forcing can be detected and investigating the relationships between these environmental forcing factors and interannual variability in ecosystem behaviour.

9.2 Physical Environmental Variability in the Gulf of Guinea

To investigate variability of the physical marine environment in the Gulf of Guinea, remotely sensed SST was studied. Because fresh water input plays an important role in this system, river discharge data were used to supplement the investigation. Both these parameters were used to investigate variability of features that are potentially important for forcing the Gulf of Guinea ecosystem.

9.2.1 Seasonal variability

The results of chapter 4 clearly demonstrate the usefulness of remote sensing for showing seasonal variability in SST, even in the humid, equatorial Gulf of Guinea. The discussion in chapter 4 attempted to interpret the observed features in the context of physical processes known to exist in the region.

Of particular interest are observations associated with the coastal upwellings. Chapter 3 reviewed much of the previous research on these phenomena. The observed westward propagation of the upwelling corroborates other studies (e.g. Picaut 1983) which used this as evidence of a coastally trapped internal wave propagating along the coast. Additionally, the observed one month lag between the equatorial and coastal upwelling events is in line with other studies (Houghton 1983, Servain *et al.* 1982) and supports the theory of remote forcing

from the western tropical Atlantic via an equatorially trapped internal wave (Moore *et al.* 1978), as does the rapid onset of the upwellings. The observation of the main upwelling centres being situated to the east of the two main capes supports the theory of Marchal and Picaut (1977), that interaction of the Guinea current with these headlands enhances the upwelling downstream. The timing of the coastal upwelling seasons and position of the major upwelling observed in this study are in agreement with previous observations (Aman and Fofana 1995, 1998, Roy 1995), however, the position of the minor upwelling contradicts the results seen in the Ghana and Côte d'Ivoire coastal station SST time series, which recorded its presence only along the Ivorian coast (Arfi *et al.* 1991).

The cooling observed along the coasts of Liberia and Sierra Leone, coincident with the minor upwelling, has not been described previously in the literature (as far as the author is aware). Shelf-break cooling is a common feature in remotely sensed SST images and can be caused by a number of mechanisms, the most obvious being differential heat absorption and mixing between oceanic and coastal areas. In this case, however, the feature appears to propagate poleward along the shelf break suggesting a hydrodynamical process. Two possible such mechanisms were proposed for this feature in chapter 4: cooling produced by mixing in a poleward slope current and extension of the minor upwelling through the action of coastally trapped waves propagating beyond Cape Palmas. Certainly, the upwelling propagates in a poleward direction along the coasts of Ghana and Côte d'Ivoire just prior to the establishment of cooling along the coast west of Cape Palmas and the cooling appears to advance at a rate consistent with the speed of a coastally trapped Kelvin wave. Alternatively, the meridional trend of the Sierra Leone and Liberia coast makes it amenable to a poleward slope current and the pool of cool water at Sherbro Island is redolent of the overshoot observed by Pingree *et al.* (1999) at Goban Spur on the European shelf edge. Additionally, for the slope current to advect cool water along the Liberia and Sierra Leone coast, it would have to be travelling from the coastal upwelling area to the south and a poleward undercurrent (the Guinea undercurrent) is already known to exist in this area. These proposals are purely conjectural

and unfortunately, Merle's (1978) *Hydrological Atlas of the Intertropical Atlantic* does not resolve this feature sufficiently for further speculation. Therefore, additional *in situ* data are required to solve this problem.

Investigation of this cooling is further complicated by the intrusion of the SUI into the Gulf of Guinea at this time of year and its connection with the cold pool off Sherbro Island. Because these two cool areas appear to move in different directions it seems unlikely that they are related. This view is supported by Longhurst's (1983) paper which shows muddy deposits to dominate along the southern coast of Sierra Leone in the shelf edge region and to turn offshore at Sherbro Island, again following the shelf edge. The area of these muddy deposits is the same as that observed for the cooling along this coast, however, the shelf edge muddy deposits do not continue into the area of the SUI. Muddy deposits along the shelf edge are typical of areas with high productivity so their presence under the coastal cooling area and their absence in the SUI region suggests that these two features have different water mass characteristics. The coastal cooling area appears to be characterised by productive waters, whereas the SUI water, although originally of upwelling origin, appears to have become oligotrophic by the time it has been advected to the Gulf of Guinea region.

Surface fronts were observed at the edge of the coastal upwelling and between waters over the continental shelf of the Sierra Leone and Guinea Plateau and offshore, oceanic water. Particularly strong is the front between the SUI and coastal waters around the Bijagos Islands. Warm areas seen around the larger river mouths were attributed to river run-off, however, these were not sufficiently resolvable to give an accurate indication of variability through time. Therefore, in Chapter 6, monthly river discharge data for several rivers in the region were used to show the seasonal cycle of run-off. A progression in the month of peak river discharge was observed from Guinea to Cameroon, consistent with the migration of the ITCZ over this area. In southern Cameroon two peaks in river discharge were observed and the length of these periods expands southward so that in Gabon, peak flow dominates for most of the year. These results are consistent with those of Mahé and Olivry (1995, 1999).

9.2.2 Interannual variability

In chapter 4, quasi-cyclic behaviour of SST was observed in the Gulf of Guinea on interannual time scales. From 1982 to 1986 this occurred with a period of around 3 years, but from 1987 to 1990 an extended warm period was seen. This pattern was also observed in the spatial component of the combined upwelling index, however, the initial approximate three year oscillation continued throughout the series for the intensity component of upwelling. This analysis of the upwellings also confirmed the results of Pezennec and Bard (1992) showing an intensification of the minor upwelling season, relative to the major upwelling system, but provided no evidence that any change had taken place in the spatial distribution of the major upwelling season (Binet and Marchal 1993, Arfi *et al.* 1991). Further analysis of remotely sensed SST data, extracted from each of the subsystems identified in chapter 5 also showed this pattern throughout the Gulf of Guinea, as did *in situ* SST data from the COADS data set, used in chapter 7. The between-year index of the most southerly latitude reached by the SUI, calculated in chapter 4, and SST in the SUI region, extracted in chapter 5, showed different patterns to those in the Gulf of Guinea system and to each other. The longer time series available from COADS also showed the existence of decadal scale variability in the SST record and a large drop in SST values during the mid-1970s. River discharge data for each hydroclimatic region from chapter 6 and corresponding rainfall data, analysed in chapter 7, showed interannual and decadal scale cycles to be present throughout the series. Additionally, large drops in rainfall and river discharge values were seen during the late 1960s to early 1970s and this declining trend continued throughout the 1970s and 1980s, corresponding to the Sahelian drought (Lamb 1982). These changes were also noted by Mahé and Olivry (1995, 1999). Some similarity was seen between SST and river discharge and rainfall patterns, often with one parameter lagging the other by a year, however, this similarity was not consistent enough to authenticate a link between them.

The period of variability identified during the 1970s in these series has also been detected by other studies of the tropical Atlantic. Koranteng (1998) showed large changes in coastal sea

temperatures off Ghana throughout the 1970s, with a reversal in the long-term trend occurring in 1976/77, and a smaller scale increase in SST from 1987 to 1990, on top of the steadily increasing long-term trend. Furthermore, the opposite pattern was seen in coastal salinity measurements. McLain *et al.* (1985) examined monthly mean SST anomalies in 3^{o} blocks of latitude and longitude along the whole of the eastern Atlantic from Cherbourg to Cape Town over the period 1970 to 1984. This analysis shows some notable results not commented on by the authors. From 1970 to 1974, cool anomalies are prevalent north of Senegal and warm anomalies dominate the southern hemisphere and perhaps the northern hemisphere tropics. From 1975 to 1979, the cool anomalies appear to move southwards, in turn pushing the southern hemisphere warm anomalies further south, and warm anomalies push in from the north. By 1976 the cold anomalies are present in the Gulf of Guinea area and during 1977 to 1978 they cross the equator. From 1979 onwards, cool anomalies dominate the southern hemisphere and warm anomalies prevail in the northern hemisphere. However, warm anomalies appear to dominate both the north and south Atlantic in 1984, coinciding with the Atlantic Niño of that year. This reversal between the two hemispheres coincides with the reversal of trend seen in Koranteng (1998).

9.3 Definition of Natural Boundaries Within and Between Systems

The use of principal components analyses at different spatial scales to investigate the variance structure of SST data in chapter 5 identified patterns of SST that gave structure to the observed variability of the system, based on the 'windows of correlation' concept of Keeling *et al.* (1997). Firstly, the Gulf of Guinea was classified within its tropical context, that is in the equatorial region between the two subtropical gyres of the North and South Atlantic Oceans. This result suggests that latitude, corresponding to solar irradiance, is the primary factor governing SST horizontal structure in the ocean.

Secondly, boundaries to the Gulf of Guinea system were determined. The northern boundary of the Gulf of Guinea was defined as the interface between the SUI and warmer tropical

Atlantic waters to the south, with the SUI lying outside the Gulf of Guinea. Additionally, the Gulf of Guinea can be divided into three subsystems, which correspond closely to the coastal subsystems defined by Tilot and King (1993). These subsystems were validated through investigation of their SST signals, on both seasonal and interannual time scales and the names SLGP, CWAU and EGOG could now be applied to the new subsystem areas. The importance of these boundaries is that they are delineated by the variance structure of physical data, rather than being arbitrarily determined as has previously been the case. The southern boundary of the LME could not be determined from this study.

Thirdly, individual features of the system, such as upwelling, are shown within the context of the whole system and its constituent subsystems, but cannot be resolved as separate entities.

Chapter 6 also used PCA to group rivers from throughout the Gulf of Guinea region according to their discharge patterns. The results from this analysis are almost identical to those from a classification based on isohyetal lines, general climatic conditions and variability in rainfall and river flow on seasonal and interannual time scales, carried out by Mahé and Olivry (1999). Thus, as with the SST data, structures identified from the natural variance structure of the data have a meaningful physical interpretation. The boundaries between these hydroclimatic regions, as interpolated by PCA, correspond closely to the subsystem boundaries identified from the PCA of SST data. This suggests a relationship between meterological and oceanographic variability in the Gulf of Guinea. Showing coherence between these hydroclimatic regions and marine subsystems is an important part of defining the Gulf of Guinea LME, as the trophic functioning of coastal marine ecosystems is, any many ways, intimately coupled with variability in their freshwater catchment basins.

Although these results show the temperature structure of the Gulf of Guinea system, no biological data have been analysed to assess if these boundaries can truly be used to define the ecosystem. However, previous work on the biota of the Gulf of Guinea does lend some support to these results. Le Loeuff and Zabi (in press) showed benthic fauna throughout the

Gulf of Guinea to be spatially distributed according to hydrological regimes, corresponding to the subsystems defined by this thesis.

9.4 Ocean-Atmosphere Interactions and Global Climate Forcing

Ocean-atmosphere interactions in the Gulf of Guinea have previously been noted in this thesis in the similarity between mean SST patterns and cloud cover, described in chapter 4. Also, the presence of an El Niño scale (3-5 year) cycle in SST and the presence of warmer than average temperatures throughout the region in 1984, coinciding with an Atlantic Niño event, suggested that global scale climate interactions may be forcing SST in the Gulf of Guinea. Further evidence of ocean atmosphere interactions in the Gulf of Guinea was provided in chapter 5 by the SST dipole shown through PCA. The boundary between these regions appeared to match the climatological position of the ITCZ and the loadings of this component showed a strong seasonal cycle generally corresponding to the seasonal migration of the ITCZ.

The predominance of these signals in oceanographic and meteorological data from throughout the Gulf of Guinea region suggests that large-scale processes may be forcing variability in this region on interannual time scales. Chapter 7 investigated local scale ocean-atmosphere interactions in the Gulf of Guinea by comparing SST with local climate variability and these analyses showed some relationships between the two parameters, however, they were not consistent enough for one mode of variability to be forcing all the processes. This is consistent with the assertion of Sutton *et al.* (2000): that "the tropical Atlantic, unlike the tropical Pacific, is not dominated by any single mode of climate variability such as [ENSO]. Rather, this region is subject to multiple competing influences of comparable importance." On the other hand, all the parameters looked at showed large, in some cases stepwise, shifts during the 1970s.

In chapter 8, therefore, three different indices of large-scale climate variability were used to investigate these relationships. Firstly, the presence of an El Niño scale cycle in SST coupled with the 1984 warm 'Atlantic Niño' event, pointed to ENSO as an important mode of interannual variability in this region. Therefore, the SOI was used as a measure of ENSO activity. Secondly, the NAO was considered as it is the major mode of climate variability known in higher latitudes of the North Atlantic. Thirdly, to give an Atlantic based zonal index of atmospheric variability, the SLP pressure difference between Lisbon and Bermuda was calculated, termed the SNAZI. The three pressure centres used in this study for calculating the NAO and SNAZI correspond to the SST tripole identified by Venzke *et al.* (1999) as areas of high ocean-atmosphere correlation. Cycles with quasi-biennial and decadal scale variability appeared in all three of the climate indices, suggesting a global scale influence on climate, however, the period of intermediate scale variability differed between the NAO and SOI and no cycle was seen in the SNAZI data in this range. All three indices showed large changes during the 1970s. These were during the early 1970s for the NAO, the mid-1970s for the SOI and the mid to late 1970s for the SNAZI.

Although only weak relationships were seen between the SOI and local environmental parameters in the Gulf of Guinea, ENSO may be forcing rainfall in the Guinée region and SST in the SUI to some degree, but appears to have no influence on the spatial extent of the SUI. A much stronger relationship is seen between the NAO and the most southerly extent of the SUI, with the NAO leading by two years, but only for a limited number of years. This is the same lead time as observed between the NAO and the north wall position of the Gulf Stream by Taylor and Stephens (1998). The Gulf Stream and the Canary Current form the western and eastern limbs of the central subtropical ocean gyre in the North Atlantic. The SUI is an extension of cold water from just south of the Canary Current region which appears to be under its seasonal influence. Thus, for the NAO to force both limbs of this circulation makes sense. The mechanism by which such forcing takes place must be focused over the whole gyre and not just one part of it because the lead time is the same for both limbs. If the

atmospheric connection were only to one part of the gyre, a delay would be expected in transmission of the signal around the gyre. A number of relationships were seen between the NAO and local meteorological conditions, however, some of these broke down when autocorrelation was removed.

The strongest control over SST and local climate in the Gulf of Guinea appears to be from the SNAZI. Relationships are seen between the SNAZI and meteorological variability at a range of lag and lead times, up to three years, however, generally the summer SNAZI leads rainfall and river discharge by two years. The relationship between SST and the SNAZI is particularly strong with summer SNAZI values leading SST by three to eighteen months. The same relationship was seen between the SNAZI and SST in the SUI, but not with spatial extent of the SUI. This time scale is shorter than for the NAO forcing the SUI. Additionally, it appears that SST may actually force SNAZI values during winter months. The strongest relationship was for October SST values in the Gulf of Guinea forcing SNAZI values in the following January. SST values are warmest in the Gulf of Guinea from October to December and in May. During the boreal autumn months the ITCZ is situated south of the Gulf of Guinea and the warm SST helps drive the North Atlantic Hadley cell. In May, however, the ITCZ is further north so any effect would feed into the West African monsoon and South Atlantic Hadley cell. Therefore, no correlation is seen with the SNAZI.

This relationship did not hold for the longer COADS time series. It appears that this may be partly related to a change in the position of the ITCZ over this period. During the mid to late 1970s and early 1980s, the ITCZ migrated less far south than normal (Citeau *et al.* 1988). The timing of this change is also consistent with the environmental time blocks identified for the Gulf of Guinea by Koranteng (1998). This analysis, based on a number of oceanographic physico-chemical parameters, divided the period from 1963 to 1992 into three blocks based on consistent patterns of interannual variability, namely the pre-1972 block, the 1972 to 1982 block and the post-1982 block. In this thesis, the relationship observed between the SNAZI and CORSA-AVHRR SST corresponds to the post-1982 time block, whereas the lack of

relationship seen with the COADS SST corresponds to a much longer time series spanning periods with differing patterns of environmental variability.

Following on from the study of Venzke *et al.* (1999), Sutton *et al.* (2000) investigated the dominant modes of climate variability in the tropical Atlantic. They characterised three different SST forced signals: a) a remote response to ENSO, b) a response to the Atlantic dipole SST pattern and c) a response to equatorial Atlantic SST anomalies. They also identified equatorward extensions of the NAO as the dominant mode of internal atmospheric variability in this region. The Atlantic SST dipole pattern exerts maximum influence between March and August, whereas the equatorial Atlantic SST anomalies exert maximum influence between July and November. The results of Sutton *et al.* are consistent with the findings of this study, that SST in the Gulf of Guinea is forcing atmospheric variability as part of a coupled ocean-atmosphere mode of variability. These authors also support the view that the SST dipole is related to the climatological position of the ITCZ.

Underlying the oscillations identified in this thesis is an increasing trend in SST and a decreasing trend in rainfall, identified with the Sahelian drought. Whether these signals relate in any way to global warming and anthropogenically induced climate change is impossible to determine from these studies.

9.5 Fisheries Recruitment and Generation of Testable Hypotheses Regarding Ecosystem Forcing

It was shown in chapter 4 how satellite derived SST time series can be used to resolve oceanographic features of relevance to fisheries, and therefore ecosystem functioning. For some of these features, measures of seasonal and interannual variability were obtained, but for others this was not possible. In chapter 6, river discharge data were used to supplement the remotely sensed SST images and provide a more accurate measure of run-off to the marine environment. A comparison of SST based features and river run-off was made in chapter 7,

giving a better idea of how features from these two important parameters might work in tandem. Finally, in chapter 8, the role of large scale climate features in forcing physical parameters important for successful recruitment in fisheries was considered. To review the findings related to seasonal variability, a summary of putative triad factors in the Gulf of Guinea is given for each quarter of the year in table 9.1.

Table 9.1. Coincidence of environmental factors relevant to fisheries recruitment during different seasons in each subsystem of the Gulf of Guinea.

Months	**Subsystem**	**Enrichment mechanisms**	**Concentration mechanisms**	**Transport/retention mechanisms**
Jan-Mar	*SLGP*	*Sierra Leone/Liberia coastal cooling*	*SUI/Bijagos front* *SLGP shelf-edge front*	*Sierra Leone/Liberia coastal cooling* *SUI/Bijagos front* *SLGP shelf-edge front*
	CWAU	*Minor upwelling* *Cape effect*	*Upwelling front*	*Upwelling front* *Cape effect*
	EGOG	*Run-off, especially in Gabon*	*River plumes*	
Apr-Jun	*SLGP*	*Minor run-off*	*SUI/Bijagos front* *River plumes*	*SUI/Bijagos front*
	CWAU	*Minor run-off* *Beginnings of upwelling*		
	EGOG	*Run-off, peak in Gabon*	*River plumes*	
Jul-Sep	*SLGP*	*Peak run-off*	*River plumes*	
	CWAU	*Major upwelling* *Cape effect* *Peak run-off*	*Upwelling front*	*Upwelling front* *Cape effect*
	EGOG	*Peak run-off* *Equatorial upwelling*	*River plumes*	
Oct-Dec	*SLGP*	*Run-off*	*Small shelf-edge front* *SUI/Bijagos front*	*small shelf-edge front* *SUI/Bijagos front*
	CWAU	*Run-off*		
	EGOG	*Peak run-off*	*River plumes*	

It can be seen from this table the areas and times when coincidence between factors is most likely to occur. The strongest coincidence is seen in the CWAU subsystem during the major and minor upwelling seasons and in the SLGP subsystem during the first half and last quarter of the year. During these periods, examples of all triad elements were observed in these regions. The absence of triad elements at other times and in other areas does not mean that they do not exist, just that they were not observed in the data used for this thesis. For example, Binet and Marchal (1993) described the retention of zooplankton by interaction of

the surface Guinea current and Guinea undercurrent during the major upwelling season, however, the flow of these two currents is not observable in the remotely sensed SST data used here. On an interannual basis, much variability has been observed in these environmental factors. Whether these correlate with changes observed in the ecosystem is an area for further work.

Other studies have attempted to relate environmental variability to ecosystem changes in the Gulf of Guinea. On a seasonal basis, Binet and Marchal (1993) described the relationship between enrichment from upwellings and river flows and plankton biomass in the coastal upwelling area. Primary production throughout the boreal summer is first stimulated by nutrient input from the run-off of the first rains over the land in June, then by the major upwelling season, and finally by the flood of the larger rivers in September and October. The number of phytoplankton cells is, therefore, at a peak from June to September. Zooplankton (copepod) biomass follows the same seasonal pattern but with a two week lag time (Binet 1976). The taxonomic composition of phytoplankton and zooplankton is also highly related to the different hydrological seasons (Binet and Marchal 1993). Mendelssohn and Cury (1987) correlated catch per unit effort (CPUE) of *Sardinella aurita* to the upwelling intensity of the preceding fortnight and Binet and Marchal (1993) mention empirical results that suggest recruitment strength in the Ghanaian population of this species may depend solely on food supply, which is in turn dependant on the upwelling intensity. Whether such clear relationships are available for populations in other parts of the Gulf of Guinea, such as the Bijagos Islands, is an area for further work.

On an interannual basis, clear relationships between environmental parameters, global/basin scale climate features and biological populations are harder to establish. Koranteng (1998) points out a remarkable similarity between his environmental time blocks, changes in the *S. aurita* fishery and the proliferation of *Balistes capriscus*. He also showed changes in the diversity of demersal fish assemblages during the 1970s (the middle environmental time block). The shift to warmer SST in 1987, identified in this thesis and by Koranteng (1998),

coincides with biological changes seen in other areas. For example, Reid *et al.* (2000) showed a substantial increase in phytoplankton colour from the Continuous Plankton Recorder survey in the North Sea, coinciding with large increases in catches of horse mackerel *Trachurus trachurus* in the northern North Sea, after 1987. These similarities suggest that, despite the obvious dependence on small scale features already discussed, control of interannual variability in marine biota is via large (basin) scale forcing. The strongest candidate for this forcing, identified from this thesis, is the SNAZI. Coupling between this feature and the NAO may explain the links to variability in biological populations from higher latitudes in the North Atlantic.

This leads to the final aim of this thesis: to generate testable hypotheses regarding mechanisms by which the ecosystem may be forced on seasonal and interannual time scales. Based upon the modes of ecosystem forcing on seasonal to interannual time scales identified in this thesis, two hypotheses are now proposed:

1. Variability in pelagic fish populations throughout the Gulf of Guinea can be directly related to interannual variability in the strength of large scale climate indices, of which the SNAZI will account for the largest part.
2. Variability in small to mesoscale oceanographic features (e.g. upwelling filaments, eddies) on short (daily to weekly) time scales is determined by large scale climate forcing.

9.6 Recommendations for Future Research

Apart from the hypotheses given above for testing, a number of other areas for future research have become apparent from this study:

1. Investigation of the relationship between environmental features identified in this thesis, spawning and recruitment success around the Bijagos Islands of Guinea-Bissau.

2. Investigation of the dynamics of the coastal cooling seen along the coast of Liberia and Sierra-Leone during the minor upwelling season.
3. Update the remotely sensed SST time series used in these analyses to include the 1990s and compare the use of SST data in this thesis with other remote sensing data, such as SeaWiFS chlorophyll and TOPEX/Poseidon sea level anomalies.

References

Adamec, D. and J.J. O' Brien (1978). The Seasonal Upwelling in the Gulf of Guinea due to Remote Forcing. *Journal of Physical Oceanography* **8**: 1050-1060.

Aiken, J., N. Rees, S. Hooker, *et al.* (2000). The Atlantic Meridional Transect: Overview and synthesis of data. *Progress in Oceanography* **45**(3-4): 257-312.

Ajayi, T.O. and A.O. Anyanwu (1997). *Marine Fisheries of Nigeria: Recent investigations, resource evaluation, state of exploitaion and management strategies*. Prepared for the CECAF (Commitee for Eastern Central Atlantic Fisheries) Working Party on Resources Evaluation, Accra, Ghana, 24-26 September 1997.

Aleem, A.A. (1979). Marine Microplankton from Sierra Leone (West Africa). *Indian Journal of Marine Science* **8**(4): 291-295.

Allen, J.S. and R.D. Romea (1980). On coastal waves trapped at low latitudes. *Journal of Fluid Mechanics* **98**: 555-585.

Allersma, E. and W.M.K. Tilmans (1993). Coastal Conditions in West Africa - A Review. *Ocean and Coastal Management* **19**: 199-240.

Aman, A. and S. Fofana (1995). Coastal Sea Surface Temperature as Detected by Meteosat Satellite and Received at the University of Abidjan. In: *Dynamics and Use of Sardinella Resources from Upwelling off Ghana and Ivory Coast*. F.X. Bard and K. Koranteng, Eds. ORSTOM Editions, Paris. pp. 52-59.

Aman, A. and S. Fofana (1998). Spatial dynamics of the upwelling off Côte d'Ivoire. In: *Global versus local changes in upwelling systems*. M.H. Durand, P. Cury, R. Mendelssohn, C. Roy, A. Bakun and D. Pauly, Eds. ORSTOM Editions, Paris. pp. 139-147.

Anang, E.R. (1979). The seasonal cycle of the phytoplankton in the coastal waters of Ghana. *Hydrobiologia* **2**(1): 33-45.

Arfi, R., O. Pezennec, S. Cissoko and M. Mensah (1991). Variations spatiales et temporelles de la résurgence ivoiro-ghanéenne. In: *Variabilité, instabilité et changement dans les pêcheries ouest africaines*. P. Cury and C. Roy, Eds. ORSTOM Editions, Paris.

ATSR (2000). The ATSR Project. http://www.atsr.rl.ac.uk/.

Bah, A. (1981). Upwelling in the Gulf of Guinea. Results of a mathematical model. In: *Ecohydrodynamics. Proceedings of the 12th International Liège Colloquium on Ocean Hydrodynamics*. Elsevier Oceanography Series Vol. 32. J.C.J. Nihoul, Ed. Elsevier Scientific Publishing Company, Amsterdam. pp. 99-140.

Baird, D., J.M. McGlade and R.E. Ulanowicz (1991). The Comparative Ecology of 6 Marine Ecosystems. *Philosophical Transactions of the Royal Society of London Series B* **333**(1266): 15-29.

Bakun, A. (1978). Guinea Current Upwelling. *Nature* **271**: 147-150.

Bakun, A. (1993). The California Current, Benguela Current and Southwestern Atlantic Shelf Ecosystems: A Comparative Approach to Identifying Factors Regulating Biomass Yields. In: *Large Marine Ecosystems - Stress Mitigation and Sustainability.* K.

Sherman, L.M. Alexander and B. Gold, Eds. American Association for the Advancement of Science, Washington.

Bakun, A. (1996). *Patterns in the Ocean: Ocean Processes and Marine Population Dynamics* . California Sea Grant College System, NOAA, La Jolla, California.

Bakun, A., D.R. McClain and F.V. Mayo (1973). *Upwelling studies based on surface observations*. Coastal Upwelling Experiment Workshop Abstracts, Florida State University, Tallahassee. (Number). .

Banse, K. and D.C. English (1993). Revision of satellite based phytoplankton pigment data from the Arabian Sea during the northeast monsoon. *Marine Research* **2**: 83-103.

Barber, R.T. (1988). Ocean basin ecosystems. In: *Concepts of Ecosystem Ecology*. L.R. Pomeroy and J.J. Alberts, Eds. Springer-Verlag, Berlin. pp. 171-193.

Bard, F.X. and K. Koranteng, Eds. (1995). *Dynamics and Use of Sardinella Resources from Upwelling off Ghana and Ivory Coast*. Proceedings of Scientific Meeting, Accra, Ghana. ORSTOM Editions, Paris. .

Bartlett, M.S. (1950). Tests of significance in factor analysis. *British Journal of Psychology (Statistical Section)* **3**: 77-85.

Binet, D. (1976). Biovolumes et poids sec zooplanctoniques en relation avec le milieu pélagique au-dessus du plateau ivoirien. *Cahiers ORSTOM Série Océanographie* **14**: 301-326.

Binet, D. and E. Marchal (1993). The Large Marine Ecosystem of Shelf Areas in the Gulf of Guinea: Long-Term Variability Induced by Climatic Changes. In: *Large Marine Ecosystems - Stress Mitigation and Sustainability*. K. Sherman, L.M. Alexander and B. Gold, Eds. American Association for the Advancement of Science, Washington. pp. 104-118.

Blaxter, J.H.S. and J.R. Hunter (1982). The biology of clupeoid fishes. *Advances in Marine Biology* **20**: 1-223.

BODC (1997). General Bathymetric Chart of the Oceans (GEBCO) '97 Digital Atlas, British Oceanographic Data Centre/International Oceanographic Commission/International Hydrographic Organisation/Natural Environment Research Council, UK.

Bowman, M.J. (1978). Introduction and Historical Perspective. In: *Oceanic Fronts in Coastal Processes: Proceedings of a workshop held at the Marine Sciences Research Center, State University of New York, May 25-27, 1977*. M.J. Bowman and W.E. Esaias, Eds. Springer-Verlag, Berlin. pp. 2-5.

Bowman, M.J. and W.E. Esaias, Eds. (1978). *Oceanic Fronts in Coastal Processes: Proceedings of a workshop held at the Marine Sciences Research Center, State University of New York, May 25-27, 1977*. Springer-Verlag, Berlin. 114 p.

Bowman, M.J. and R.L. Iverson (1978). Estuarine and Plume Fronts. In: *Oceanic Fronts in Coastal Processes: Proceedings of a workshop held at the Marine Sciences Research Center, State University of New York, May 25-27, 1977*. M.J. Bowman and W.E. Esaias, Eds. Springer-Verlag, Berlin. pp. 87-104.

Bricquet, J.P., F. Bamba, G. Mahé, M. Toure and J.C. Olivry (1997). Water resource variations of the Atlantic river basins of Africa: the long term effects of rain shortage. *Revue des Sciences de l'Eau* **3**: 321-337.

Brink, K.H. and T.J. Cowles (1991). The Coastal Transition Zone Program. *Journal of Geophysical Research* **96**(C8): 14,637-14,647.

Burroughs, W.J. (1992). *Weather Cycles: Real or Imaginary?* . Cambridge University Press, Cambridge, UK. 207 p.

Busalacchi, A.J. and J. Picaut (1983). Seasonal Variability From a Model of the Tropical Atlantic-Ocean. *Journal of Physical Oceanography* **13**(9): 1564-1588.

Cane, M.A. (1979). The response of an equatorial ocean to simple wind stress patterns: II. Numerical results. *Journal of Marine Research* **37**(2): 253-299.

Cane, M.A. and E.S. Sarachik (1979). Forced baroclinic ocean motions, III: The linear equatorial basin case. *Journal of Marine Research* **37**(2): 355-398.

Chatfield, C. (1989). *The Analysis of Time Series: An Introduction* . Chapman & Hall, London. 241 p.

Christensen, V. and D. Pauly, Eds. (1993). *Trophic Models of Aquatic Ecosystems*. Conference Proceedings. ICLARM, Manila, Philippines. 390 p.

Citeau, J., J.C. Bergés, H. Demarcq and G. Mahé (1988). The watch of ITCZ migrations over the tropical Atlantic Ocean as an indicator in drought forecast over the Sahelian area. *Tropical Ocean-Atmosphere Newsletter* **45**: 1-3.

Clarke, A.J. (1977). Observational and numerical evidence for wind-forced coastal trapped long waves. *Journal of Physical Oceanography* **7**: 231-247.

Clarke, A.J. (1979). On the generation of the seasonal coastal upwelling in the Gulf of Guinea. *Journal of Geophysical Research* **84**(C7): 3743-3751.

Cole, J. and J. McGlade (1998). Clupeoid population variability, the environment and satellite imagery in coastal upwelling systems. *Reviews in Fish Biology and Fisheries* **8**(4): 445-471.

Cole, J.F.T. (1997). *The Surface Dynamics of the Northern Benguela Upwelling System and its Relationship to Patterns of Clupeoid Production*. PhD Thesis. University of Warwick, Coventry, UK. 208 p.

Cole, J.F.T. and J. McGlade (1998). Temporal and spatial patterning of sea surface temperature in the northern Benguela upwelling system; possible environmental indicators of clupeoid production. *South African Journal of Marine Science* **19**: 143-157.

Coombs, S.H., J.A. Lindley and C.A. Fosh (1983). *Vertical Distribution of Larvae of Mackerel (Scomber scombrus) and microplankton, with some conclusions on feeding conditions and survey methods*. IOC Report No. 33. UNESCO.

Corti, S., F. Molteni and T.N. Palmer (1999). Signature of recent climate change in frequencies of natural atmospheric circulation regimes. *Nature* **398**(6730): 799-802.

Cromwell, T. (1953). Circulation in a meridional plane in the central equatorial Pacific. *Journal of Marine Research* **12**: 196-213.

Cury, P. and C. Roy (1989). Optimal Environmental Window and Pelagic Fish Recruitment Success in Upwelling Areas. *Canadian Journal of Fisheries and Aquatic Sciences* **46**(4): 670-680.

Cushing, D.H. (1975). *Marine Ecology and Fisheries* . Cambridge University Press.

Cushing, D.H. (1989). A difference in structure between ecosystems in strongly stratified waters and those that are rarely stratified. *Journal of Plankton Research* **11**: 1-13.

Cushing, D.H. (1996). *Towards a science of recruitment in fish populations.* Excellence in Ecology 7. Ecology Institute, Nordbunte, Germany.

Delecluse, P. and S.G.H. Philander (1983). Variability of coastal zones in low latitudes (with application to the Somali Current, the Gulf of Guinea and the El Nino Current). In: *Hydrodynamics of the Equatorial Ocean.* Elsevier Oceanography Series Vol. 36. J.C.J. Nihoul, Ed. Elsevier, Amsterdam, Netherlands. pp. 219-235.

Demarcq, H. and A. Aman (in press). A multi-data approach to assess the spatio-temporal variability of the Ivoro-Ghanaian coastal upwelling: interest for understanding pelagic fish stock dynamics. In: *The Gulf of Guinea Large Marine Ecosystem: Environmental forcing and sustainable development of marine resources*. J. McGlade, P. Cury, K.A. Koranteng and N.J. Hardman-Mountford, Eds.

Demarcq, H. and J. Citeau (1995). Sea surface temperature retrieval in tropical area with Meteosat: the case of the Senegalese coastal upwelling. *International Journal of Remote Sensing* **16**(8): 1371-1395.

Diggle, P.J. (1990). *Time Series: A Biostatistical Introduction.* Oxford Statistical Science Series 5. Oxford University Press. 257 p.

Dyke, P. (1996). *Modelling Marine Processes* . Prentice Hall, London. 152 p.

Eastman, J.R. (1992). *Time Series Map Analysis using Standardized Principle Components*. Conference on Global Change and Education, Washington, 3-8 August 1992. ASPRS ACSM RT Technical Papers 1. ASPRS/ACSM/RT. pp. 195-204.

Eastman, J.R. and M. Fulk (1993). Long sequence time series evaluation using standardized principal components. *Photogrammetric Engineering and Remote Sensing* **59**(8): 1307-1312.

Emery, W.J. and J. Meincke (1986). Global water masses: Summary and review. *Oceanologica Acta* **9**: 383-391.

EOS (1999). *EOS: Transactions of the American Geophysical Union* **80**(3).

ESA (1997). ENVISAT-1. http://www.envisat.estec.esa.nl/.

Fanning, K.A. (1991). Nutrient provinces in the sea: Concentration ratios, reaction rate ratios and ideal covariation. *Journal of Geophysical Research* **97**: 5693-5712.

Fedorov, K.N. (1986). *The Physical Nature and Stucture of Oceanic Fronts.* Lecture Notes on Coastal and Estuarine Studies 19. Springer-Verlag, Berlin. 333 p.

Frankignoul, C. (1985). Sea-Surface Temperature Anomalies, Planetary-Waves, and Air-Sea Feedback in the Middle Latitudes. *Reviews of Geophysics* **23**(4): 357-390.

Frankignoul, C. and K. Hasselmann (1977). Stochastic climate models, Part II: Application to sea-surface temperature anomalies and thermocline variability. *Tellus* **29**: 289-305.

FRU (1970). *The NCOR report on the mechanism of the upwelling of Ghana's coastal waters.* Marine Fisheries Report No. 3. Fisheries Research Unit, Tema, Ghana.

Fung, T. and E. LeDrew (1987). Application of Principle Components Analysis to Change Detection. *Photogrammetric Engineering and Remote Sensing* **53**(12): 1649-1658.

Gallaudet, T.C. and J.J. Simpson (1994). An Empirical Orthogonal Function Analysis of Remotely Sensed Sea Surface Temperature Variability and its Relation to Interior Oceanic Processes off Baja California. *Remote Sensing of the Environment* **47**: 375-389.

Gershunov, A. and T.P. Barnett (1998). Interdecadal modulation of ENSO teleconnections. *Bulletin of the American Meteorological Society* **79**(12): 2715-2725.

Gill, A.E. (1982). *Atmosphere-Ocean Dynamics*. International Geophysics Series 30. Academic Press, New York. 662 p.

Gill, A.E. and A.J. Clarke (1974). Wind induced upwelling, coastal currents and sea-level changes. *Deep Sea Research* **21**: 325-345.

GOG-LME (1996). *Gulf of Guinea Large Marine Ecosystem Project*. Brochure. The Regional Coordination Centre, Abidjan, Côte d'Ivoire.

Goodberlet, M.A., C.T. Swift, K.P. Kiley, J.L. Miller and J.B. Zaitzeff (1997). Microwave remote sensing of coastal zone salinity. *Journal of Coastal Research* **13**(2): 363-372.

Gregg, W.W. (1999). Initial analysis of ocean color data from the ocean color and temperature scanner. *Applied Optics* **38**(3): 476-485.

Greze, V.N., K.T. Gordejeva and A.A. Shmeleva (1969). *Distribution of zooplankton and biological structure in the Tropical Atlantic.* Proceedings of the Symposium on the Oceanography and Fisheries Resources of the Tropical Atlantic, Abidjan, Ivory Coast, 20-28 October 1966. Results of ICITA and GTS (Number). UNESCO Publications, Paris. pp. 85-90.

Haidvogel, D.B., A. Beckmann and K.S. Hedstrom (1991). Dynamical simulations of filament formation and evolution in the coastal transition zone. *Journal of Geophysical Research* **96**: 15,017-15,040.

Hardman-Mountford, N.J., K.A. Koranteng and A.R.G. Price (2000). The Gulf of Guinea Large Marine Ecosystem. In: *Seas at the Millenium: An Environmental Evaluation*. C. Sheppard, Ed. Elsevier, Amsterdam. pp. 129-152 (in press).

Herbland, A. and E. Marchal (1991). Variations locale de l'upwelling, répartition et abondance des sardinelles en Côte d'Ivoire. In: *Variabilité, instabilité et changement dans les pêcheries ouest africaines*. P. Cury and C. Roy, Eds. ORSTOM Editions, Paris.

Hernàndez-Guerra, A. and L. Nykjaer (1997). Sea surface temperature variability off north-west Africa: 1981-1989. *International Journal of Remote Sensing* **18**(12): 2539-2558.

Hisard, P., C. Hénin, R. Houghton, B. Piton and P. Rual (1986). Oceanic conditions in the tropical Atlantic during 1983 and 1984. *Nature* **322**: 243-245.

Hjort, J. (1914). Fluctuations in the great fisheries of northern Europe viewed in the light of biological research. *Rapports et Proces-verbaux des Reunions. Conseil International pour l'Exploration de la Mer* **20**: 1-228.

Horel, J.D., V.E. Kousky and M.T. Kagano (1986). Atmospheric Conditions in the Atlantic Sector During 1983 and 1984. *Nature* **322**(6076): 248-251.

Houghton, J.J., L.G. Meiro Filho, B.A. Callander, N. Harris, A. Kattenberg and A. Maskell (1996). *Climate Change 1995 - The Science of Climate Change: Contribution of Working Group I to the Second Assessment Report of the Intergovernmental Panel on Climate Change* . Cambridge University Press.

Houghton, R.W. (1973). Evaporation during upwelling in Ghanaian coastal waters. *Journal of Physical Oceanography* **3**: 487-489.

Houghton, R.W. (1976). Circulation and hydrographic structure over the Ghana continental shelf durinng the 1974 upwelling. *Journal of Physical Oceanography* **6**: 909-924.

Houghton, R.W. (1983). Seasonal variations of the subsurface thermal structure in the Gulf of Guinea. *Journal of Physical Oceanography* **13**: 2070-2081.

Houghton, R.W. and C. Colin (1986). Thermal structure along 4^{o}W in the Gulf of Guinea during 1983-1984. *Journal of Geophysical Research* **91**(C10): 11727-11739.

Houghton, R.W. and M.A. Mensah (1978). Physical Aspects and Biological Consequences of Ghanaian Coastal Upwelling. In: *Upwelling Ecosystems*. R. Boje and M. Taniczak, Eds. pp. 167-180.

Hulburt, H.E., J.C. Kindle and J.J. O'Brien (1976). A numerical simulation of the onset of El Niño. *Journal of Physical Oceanography* **6**(5): 621-631.

Hurrell, J.W. (1995). Decadal trends in the North Atlantic Oscillation: regional temperatures and precipitation. *Science* **269**: 676-679.

Huthnance, J.M. (1984). Slope currents and 'JEBAR'. *Journal of Physical Oceanography* **14**: 195-810.

Iles, T.D. and M. Sinclair (1982). Atlantic herring: Stock discreteness and abundance. *Science* **215**: 627-633.

Ingham, M.C. (1970). Coastal upwelling in the Northwestern Gulf of Guinea. *Bulletin of Marine Science* **20**: 1-34.

Katz, E.J. and Collaborators (1977). Zonal pressure gradient along the equatorial Atlantic. *Journal of Marine Research* **35**(2): 293-307.

Katz, E.J. and S. Garzoli (1982). Response of the western Equatorial Atlantic Ocean to an annual wind cycle. *Journal of Marine Research* **40**(Supplement): 307-327.

Katz, E.J., P. Hisard, J.M. Verstraete and S.L. Garzoli (1986). Annual Change of Sea-Surface Slope Along the Equator of the Atlantic- Ocean in 1983 and 1984. *Nature* **322**(6076): 245-247.

Kawasaki, T. (1983). Why do some pelagic fishes have wide fluctuations in their numbers? Biological basis of fluctuation from the viewpoint of evolutionary ecology. *FAO Fisheries Reports* **291**(3): 1065-1080.

Keeling, M.J., I. Mezic, R.J. Hendry, J. McGlade and D.A. Rand (1997). Characteristic length scales of spatial models in ecology via fluctuation analysis. *Philosophical Transactions of the Royal Society of London Series B* **352**(1361): 1589-1601.

Kerr, R.A. (1999). Atmospheric science - Does a globe-girdling disturbance jigger El Nino? *Science* **285**(5426): 322-323.

Koranteng, K., J.M. McGlade and B. Samb (1996). *Review of the Canary Current and Guinea Current Large Marine Ecosystems*. ACP-EU Fisheries Research Initiative Second Dialogue Meeting.

Koranteng, K.A. (1995). *Fish and Fisheries of Three Coastal Lagoons in Ghana*. Report No. GW/A.285/SF2/31. Global Environment Facility/Ghana Coastal Wetlands Management Programme.

Koranteng, K.A. (1998). *The impacts of environmental forcing on the dynamics of demersal fishery reources of Ghana*. PhD Thesis. University of Warwick, Coventry, UK. 377 p.

Kushnir, Y., V.J. Cardone, J.G. Greenwood and M.A. Cane (1997). The recent increase in North Atlantic wave heights. *Journal of Climate* **10**(8): 2107-2113.

Kwok, R. and D.A. Rothrock (1999). Variability of Fram Strait ice flux and North Atlantic Oscillation. *Journal of Geophysical Research* **104**(C3): 5177-5189.

Lamb, P.J. (1982). Persistence of sub-Saharan drought. *Nature* **299**: 46-48.

Lasker, R. (1975). Field criteria for survival of anchovy larvae: the relation between inshore chlorophyll maximum layers and succesful first feeding. *US National Marine Fisheries Service Fisheries Bulletin* **73**: 453-462.

Laurence, G.C. (1992). Growth, survival and recruitment in large marine ecosystems. In: *Large Marine Ecosystems - Patterns, Processes and Yields*. K. Sherman, L.M. Alexander and B.D. Gold, Eds. American Association for the Advancement of Science, Washington. pp. 132-150.

Lavender, S.J. (in prep.). Optical Remote Sensing of the Oceans. In: *Optical Techniques in Oceanography*. D. Pilgrim, J. Aiken and D. Robins, Eds. Gordon and Breach Publishing Group.

Le Borgne, R. (1983). Note on swarms of Thaliacea in the Gulf of Guinea. *Océanographie Tropicale* **18**(1): 49-54.

Le Loeuf, P. and G.S.F. Zabi (in press). Spatial and temporal variations in benthic fauna and communities of the tropical Atlantic coast of Africa. In: *The Gulf of Guinea Large Marine Ecosystem: Environmental forcing and sustainable development of marine resources*. J.M. McGlade, P. Cury, K.A. Koranteng and N.J. Hardman-Mountford, Eds.

LeGrand, P. and J.F. Minster (1999). Impact of the GOCE gravity mission on ocean circulation estimates. *Geophysical Research Letters* **26**(13): 1881-1884.

Lemasson, L. and J.-P. Rébert (1973a). Circulation dans le Golfe de Guinée. Etude de la région d'origine du sous-courant ivoirien. *Cahiers ORSTOM, Série Océanographie* **11**(3): 303-316.

Lemasson, L. and J.-P. Rébert (1973b). Les courants marins dans le Golfe Ivoirien. *Cahiers ORSTOM, Série Océanographie* **11**(1): 67-95.

Lighthill, M.J. (1969). Dynamic response of the Indian Ocean to the onset of the southwest monsoon. *Philosophical Transactions of the Royal Society of London, Series A* **265**: 45-92.

Lillesand, T.M. and R.W. Kiefer (1987). *Remote Sensing and Image Interpretation* . John Wiley and Sons, New York. 721 p.

Linthicum, K.J., A. Anyamba, C.J. Tucker, P.W. Kelley, M.F. Myers and C.J. Peters (1999). Climate and satellite indicators to forecast Rift Valley fever epidemics in Kenya. *Science* **285**(5426): 397-400.

Lluch-Belda, D., R. Schwartzlose, R. Serra, *et al.* (1992). Sardine and anchovy regime fluctuations of abundance in four regions of the worlds oceans: A workshop report. *Fisheries Oceanography* **1**: 339-347.

Longhurst, A. (1983). Benthic-Pelagic Coupling and Export of Organic-Carbon from a Tropical Atlantic Continental-Shelf - Sierra-Leone. *Estuarine Coastal and Shelf Science* **17**(3): 261-285.

Longhurst, A. (1998). Cod: Perhaps if we all stood back a bit? *Fisheries Research* **38**(2): 101-108.

Longhurst, A. (1998). *Ecological Geography of the Sea* . Academic Press, San Diego and London. 398 p.

Longhurst, A., S. Sathyendranath, T. Platt and C. Caverhill (1995). An Estimate of Global Primary Production in the Ocean From Satellite Radiometer Data. *Journal of Plankton Research* **17**(6): 1245-1271.

Longhurst, A.R. (1958). *An ecological survey of the West African marine benthos* 11. Colonial Office Fishery Publication. 102 p.

Longhurst, A.R. (1962). A review of the oceanography of the Gulf of Guinea. *Bulletin IFAN* **24**(A3): 633-663.

Longhurst, A.R. (1964). The coastal oceanography of Western Nigeria. *Bulletin IFAN* **26**(A2): 337-402.

Longhurst, A.R. (1969). *Species assemblages in tropical demersal fisheries.* Proceedings of the Symposium on the Oceanography and Fisheries Resources of the Tropical Atlantic, Abidjan, Ivory Coast, 20-28 October 1966. Results of ICITA and GTS (Number). UNESCO Publications, Paris. pp. 147-168.

Longhurst, A.R. and W.G. Harrison (1989). The biological pump: Profiles of plankton production and consumption in the open ocean. *Progress in Oceanography* **22**: 47-123.

Longhurst, A.R. and D. Pauly (1987). *Ecology of Tropical Oceans* . Academic Press, Inc., San Diego, CA. 407 p.

Lukas, R. (1981). *The termination of the equatorial undercurrent in the eastern Pacific.* PhD Thesis. University of Hawaii.

Lutjeharms, J.R.E. and P.L. Stockton (1987). Kinematics of the upwelling front off southern Africa. *South African Journal of Marine Science* **5**: 35-49.

Mahé, G. (1991). La variabilité des apports fluviaux au Golfe de Guinée utilisée comme indice climatiques. In: *Pêcheries Ouest-africaines: variabilité, instabilité et changement.* P. Cury and C. Roy, Eds. ORSTOM Editions, Paris. pp. 147-161.

Mahé, G. (1993). *Les écoulements fluviaux sur la façade atlantique de l'Afrique. Étude des éléments du bilan hydrique et variabilité interannuelle, analyse de situations hydroclimatiques moyennes et extrêmes.* PhD Thesis. l'université Paris XI Orsay, Paris. 438 p.

Mahé, G. and J.-C. Olivry (1995). Variations des précipitations et des écoulements en Afrique de l'Ouest et centrale de 1951 à 1989. *Sécheresse* **6**(1): 109-117.

Mahé, G. and J.-C. Olivry (1999). Assessment of freshwater yields to the ocean along the intertropical Atlantic coast of Africa (1951-1989). *C. R. Acad. Sci. Paris, Earth and Planetary Sciences* **328**: 621-626.

Malmgren, B.A., A. Winter and D.L. Chen (1998). El Nino southern oscillation and North Atlantic oscillation control of climate in Puerto Rico. *Journal of Climate* **11**(10): 2713-2717.

Mann, K.H. and J.R.N. Lazier (1996). *Dynamics of Marine Ecosystems* . Blackwell Science, Inc., Cambridge, MA. 394 p.

Mantua, N.J., S.J. Hare, Y. Zhang, J.M. Wallace and R.C. Francis (1997). A Pacific interdecadal climate oscillation with impacts on salmon production. *Bulletin of the American Meteorological Society* **78**(6): 1069-1079.

Marchal, E. (1991). Nanisme et sedentarité chez certaines espèces de poissons pélagique: deux aspects d'un même réponse à des conditions défavorables. In: *Pêcheries Ouest-africaines: variabilité, instabilité et changement.* P. Cury and C. Roy, Eds. Orstom Editions, Paris. pp. 192-200.

Marchal, E. and J. Picaut (1977). Répartition et abondonce évaluées par échointégration des poissons du plateau continental ivoiro-ghanéen en relation avec les upwellings locaux. *J. Res. Océanogr.* **2**: 39-57.

Maus, J. (1997). *Sustainable Fisheries Management in Mauritania.* PhD Thesis. University of Warwick, Coventry, UK. 269 p.

Mayr, E. (1982). *The Growth of Biological Thought* . Harvard University Press, Cambridge, MA. 974 p.

McClain, C.R., M.L. Cleave, G.C. Feldman, W.W. Gregg, S.B. Hooker and N. Kuring (1998). Science quality SeaWiFS data for global biosphere research. *Sea Technology*: 10-15.

McCreary, J. (1976). Eastern tropical ocean response to changing wind systems: with application to El Niño. *Journal of Physical Oceanography* **6**: 632-645.

McCreary, J.P. (1981). A Linear Stratified Ocean Model of the Equatorial Undercurrent. *Philosophical Transactions of the Royal Society of London Series a- Mathematical Physical and Engineering Sciences* **298**(1444): 603-635.

McCreary, J.P. (1984). Equatorial Beams. *Journal of Marine Research* **42**(2): 395-430.

McCreary, J.P., J. Picaut and D.W. Moore (1984). Effects of Remote Annual Forcing in the Eastern Tropical Atlantic Ocean. *Journal of Marine Research* **42**(1): 45-81.

McGlade, J.M. (1999). Ecosystem analysis and the governance of natural resources. In: *Advanced Ecological Theory*. J. McGlade, Ed. Blackwell Science Ltd., Oxford. p. 353.

McLain, D.R., R.E. Brainard and J.G. Norton (1985). Anomalous warm events in eastern boundary current systems. *CalCOFI Reports* **26**: 51-64.

Mee, L.D. (1992). The Black-Sea in Crisis - a Need For Concerted International Action. *Ambio* **21**(4): 278-286.

Meehl, G.A., J.M. Arblaster and W.G. Strand (1998). Global scale decadal climate variability. *Geophysical Research Letters* **25**(21): 3983-3986.

Mendelssohn, R. and P. Cury (1987). Fluctuations of a Fortnightly Abundance Index of the Ivorian Coastal Pelagic Species and Associated Environmental Conditions. *Canadian Journal of Fisheries and Aquatic Sciences* **44**(2): 408-421.

Mendelssohn, R. and C. Roy (1994). *Changes in mean level, seasonal cycle and spectrum in long term coastal time series from various Eastern Ocean Systems*. 26th Liège International Colloquium Ocean Hydrodynamics, May 2-6 1994. (Number). .

Mensah, M.A. (1995). The occurrence of zooplankton off Tema during the period 1969-1992. In: *Dynamics and Use of Sardinella Resources from Upwelling off Ghana and Ivory Coast*. F.X. Bard and K.A. Koranteng, Eds. ORSTOM Editions, Paris. pp. 290-304.

Mensah, M.A. and K.A. Koranteng (1988). *A review of the oceanography and fisheries resources in the coastal waters of Ghana*. Marine Fisheries Research Report No. 8. Fisheries Research and Utilization Branch, Tema, Ghana.

Merle, J. (1978). *Atlas Hydrologique saisonnier de l'océan Atlantique intertropicale*. Travaux et Documents de l'ORSTOM 82. ORSTOM, Paris.

Merle, J. (1980). Seasonal heat budget in the equatorial Atlantic ocean. *Journal of Physical Oceanography* **10**: 464-469.

Merle, J., M. Fieux and P. Hisard (1980). Annual signal and interannual anomalies of sea surface temperature in the eastern equatorial Atlantic ocean. *Deep Sea Research* **26**(Suppl. 2): 77-101.

Mitchell, T.P. (1996). Gulf of Guinea standardized rainfall index (8-4N, 20W-10E). http://tao.atmos.washington.edu/data_sets/guinea.

Mooers, C.N.K., C.N. Flagg and W.C. Boicourt (1978). Prograde and Retrograde Fronts. In: *Oceanic Fronts in Coastal Processes: Proceedings of a workshop held at the Marine Sciences Research Center, State University of New York, May 25-27, 1977*. M.J. Bowman and W.E. Esaias, Eds. Springer-Verlag, Berlin. pp. 43-58.

Moore, D.W. (1968). *Planetary gravity waves in an equatorial ocean*. PhD Thesis. Harvard University, Cambridge, MA.

Moore, D.W., J.P. McCreary, P. Hisard, *et al.* (1978). Equatorial adjustment in the eastern Atlantic Ocean. *Geophysical Research Letters* **5**: 637-640.

Moore, D.W. and S.G.H. Philander (1977). Modelling of the tropical oceanic circulation. In: *The Sea* Vol. VI. Wiley-Interscience, New York. pp. 319-361.

Moore, G.F., J. Aiken and S.J. Lavender (1999). The atmospheric correction of water colour and the quantitative retrieval of suspended particulate matter in Case II waters: application to MERIS. *International Journal of Remote Sensing* **20**(9): 1713-1733.

Morlière, A. (1970). Les saisons marines devant Abidjan. *Documents Scientifique Centre de Recherche Océanographique Abidjan* **1**: 1-15.

Morlière, A. and J.-P. Rébert (1972). Etude hydrologique du plateau continental ivoirien. *Documents Scientifique Centre de Recherche Océanographique Abidjan* **1**: 1-15.

Morton, O. (1998). The storm in the machine. *New Scientist* **157**(2119): 22-27.

NAG (1997). *NAG Fortran Library*. The Numerical Algorithms Group (NAG) Ltd., Oxford, UK.

NASA (2000). Background of the SeaWiFS Project. http://seawifs.gsfc.nasa.gov/SEAWIFS.html.

NCAR (1999). NCAR's Data Support Section. http://www.scd.ucar.edu/dss/.

O' Brien, C.M., C.J. Fox, B. Planque and J. Casey (2000). Climate variability and North Sea cod. *Nature* **404**: 142.

O' Brien, J.J., D. Adamec and D.W. Moore (1978). A simple model of upwelling in the Gulf of Guinea. *Geophysical Research Letters* **5**(8): 641-644.

Olivry, J.-C. (1986). *Fleuves et rivieres du Cameroun*. These d'Etat . ORSTOM, Paris. 733 p.

Open University (1989). *Ocean Circulation*. Oceanography Series 3. Open University/Pergamon Press, Oxford. 238 p.

Parrish, R.H., A. Bakun, D.M. Husby and C.S. Nelson (1983). *Comparative climatology of selected environmental processes in relation to eastern boundary current pelagic fish reproduction*. Proceedings of the Expert Consultation to Examine Changes in Abundance and Species Composition of Neritic Fish Resources, San José, Costa Rica. FAO Fisheries Reports 293(Number). . pp. 731-777.

Pauly, D. and V. Christensen (1995). Primary production required to sustain global fisheries. *Nature* **374**: 255-257.

Pauly, D., V. Christensen, J. Dalsgaard, R. Froese and F. Torres (1998). Fishing down marine food webs. *Science* **279**(5352): 860-863.

Pezennec, O. and F.X. Bard (1992). Importance écologique de la petite saison d'upwelling ivoiro-ghanéenne et changements dans la pêcherie de Sardinella aurita. *Aquatic Living Resources* **5**: 249-259.

Philander, S.G.H. (1979). Upwelling in the Gulf of Guinea. *Journal of Marine Research* **37**: 23-33.

Philander, S.G.H. (1981). The Response of Equatorial Oceans to a Relaxation of the Trade Winds. *Journal of Physical Oceanography* **11**(2): 176-189.

Philander, S.G.H. (1986). Unusual Conditions in the Tropical Atlantic-Ocean in 1984. *Nature* **322**(6076): 236-238.

Philander, S.G.H. (1990). *El Niño, La Niña and the Southern Oscillation*. International Geophysics Series . Academic Press, Inc. 293 p.

Philander, S.G.H. and R.C. Pacanowski (1980). The generation of equatorial currents. *Journal of Geophysical Research* **85**(C2): 1123-1136.

Philander, S.G.H. and R.C. Pacanowski (1981a). The Oceanic Response to Cross-Equatorial Winds (With Application to Coastal Upwelling in Low Latitudes). *Tellus* **33**(2): 201-210.

Philander, S.G.H. and R.C. Pacanowski (1981b). Response of Equatorial Oceans to Periodic Forcing. *Journal of Geophysical Research* **86**(C3): 1903-1916.

Philander, S.G.H. and R.C. Pacanowski (1986). A Model of the Seasonal Cycle in the Tropical Atlantic-Ocean. *Journal of Geophysical Research* **91**(C12): 14192-14206.

Picaut, J. (1983). Propagation of the seasonal upwelling in the eastern equatorial Atlantic. *Journal of Physical Oceanography* **13**(1): 18-37.

Pingree, R.D. (1978). Mixing and stabilization of phytoplankton distributions on the northwest European continental shelf. In: *Spatial Pattern in Plankton Communities*. NATO Conference Series. Series IV: Marine Sciences Vol. 3. J.H. Steele, Ed. Plenum Press, New York. pp. 181-220.

Pingree, R.D. (1984). Some Applications of Remote-Sensing to Studies in the Bay of Biscay, Celtic Sea and English-Channel. In: *Remote Sensing of Shelf Sea Hydrodynamics*. Elsevier Oceanography Series Vol. 38. J.C.J. Nihoul, Ed. Elsevier, Amsterdam. pp. 287-315.

Pingree, R.D. (1995). The Droguing of Meddy Pinball and Seeding With Alace Floats. *Journal of the Marine Biological Association of the United Kingdom* **75**(1): 235-252.

Pingree, R.D. and D.K. Griffiths (1980). Currents driven by a steady uniform wind stress on the shelf seas around the British Isles. *Oceanologica Acta* **3**: 227-236.

Pingree, R.D. and B. LeCann (1992). 3 Anticyclonic Slope Water Oceanic Eddies (Swoddies) in the Southern Bay of Biscay in 1990. *Deep-Sea Research* **39**(7-8A): 1147-1175.

Pingree, R.D., B. Sinha and C.R. Griffiths (1999). Seasonality of the European slope current (Goban Spur) and ocean margin exchange. *Continental Shelf Research* **19**(7): 929-975.

Platt, T. and A.W. Herman (1983). Remote-Sensing of Phytoplankton in the Sea - Surface-Layer Chlorophyll As an Estimate of Water-Column Chlorophyll and Primary Production. *International Journal of Remote Sensing* **4**(2): 343-351.

Pople, W. and M.A. Mensah (1971). Evaporation as the Upwelling Mechanism in Ghanaian Coastal Waters. *Nature Physical Science* **234**(44): 18-20.

Potter, I.C., D.J. Bird, P.N. Claridge, K.R. Clarke, G.A. Hyndes and L.C. Newton (submitted). The fish fauna of the Severn estuary: Are there medium term changes in abundance and species composition and are the recruitment pattens of the main marine species correlated? . *Marine Ecology Progress Series*.

Rast, M., J.L. Bézy and S. Bruzzi (1999). The ESA Medium Resolution Imaging Spectrometer MERIS - a review of the instrument and its mission. *International Journal of Remote Sensing* **20**(9): 1681-1702.

Reid, P.C., M.d.F. Borges and E. Svendsen (2000). A regime shift in the North Sea circa 1988 linked to changes in the North Sea fishery. *Fisheries Research*(in press).

Reynolds, R.W. and T.M. Smith (1995). A High Resolution Global Sea Surface Temperature Climatology. *Journal of Climate* **8**(6): 1571-83.

Robertson, J., J. McGlade and I. Leaver (1996). *Ecological effects of the North Sea industrial fishing industry on the availability of human consumption species: a review*. Univation at The Robert Gordon University. 76 p.

Robins, D.B. and J. Aiken (1996). The Atlantic Meridional Transect: An oceanographic research programme to investigate physical, chemical, biological & optical variables of the Atlantic Ocean. *Underwater Technology* **21**: 8-14.

Rodwell, M.J., D.P. Rowell and C.K. Folland (1999). Oceanic forcing of the wintertime North Atlantic Oscillation and European climate. *Nature* **398**(6725): 320-323.

Rogers, J.C. (1984). The association between the North Atlantic Oscillation and the Southern Oscillation in the Northern Hemisphere. *Monthly Weather Review* **112**: 1999-2015.

Rothschild, B.J., T.R. Osborn, T.D. Dickey and D.M. Farmer (1989). The physical basis for recruitment variability in fish populations. *Journal du Conseil Permanent International pour l'Exploration de la Mer* **45**: 136-145.

Roy, C. (1995). The Côte d'Ivoire and Ghana Coastal Upwellings: Dynamics and Changes. In: *Dynamics and Use of Sardinella Resources from Upwelling off Ghana and Ivory Coast*. F.X. Bard and K.A. Koranteng, Eds. ORSTOM Editions, Paris.

Schiller, H. and R. Doerffer (1999). Neural network for emulation of an inverse model - operational derivation of Case II properties from MERIS data. *International Journal of Remote Sensing* **20**(9): 1735-1746.

Schwartzlose, R.A., J. Alheit, A. Bakun, *et al.* (1999). Worldwide large-scale fluctuations of sardine and anchovy populations. *South African Journal of Marine Science* **21**: 289-347.

Scowcroft, C.P. (1995). *Africa: Background Paper*. ICLARM Research Planning Workshop, Cairo, Egypt, 23-27 September 1995. (Number). Agriculture Australia, Consultants. p. 60.

Servain, J., J. Picaut and A.J. Busalacchi (1985). Interannual and seasonal variability of the tropical Atlantic Ocean depicted by sixteen years of sea-surface temperature and wind stress. In: *Coupled Ocean-Atmosphere Models.* J.C.J. Nihoul, Ed. Elsevier, New York.

Servain, J., J. Picaut and J. Merle (1982). Evidence of remote forcing in the equatorial Atlantic ocean. *Journal of Physical Oceanography* **12**: 457-463.

Shannon, L.V., N.M. Walters and S.A. Mostert (1985). Satellite observations of surface temperature and near surface chlorophyll in the southern Benguela region. In: *South African Ocean Colour and Upwelling Experiment*. L.V. Shannon, Ed. Sea Fisheries Research Institute, Cape Town.

Shatz, Y. (1998). Fishstat Plus, Food and Agriculture Organization of the United Nations.

Sherman, J.W., III (1985). Introduction to 'Satellite Oceanic Remote Sensing'. *Advances in Geophysics* **27**: 1-9.

Sherman, K., L.M. Alexander and B.D. Gold, Eds. (1992). *Large Marine Ecosystems: Patterns, Processes and Yields*. American Association for the Advancement of Science, Washington, D.C. xiv+242 p.

Sherman, K., E.N. Okemwa and M.J. Ntiba (1998). Background and Focus. In: *Large Marine Ecosystems of the Indian Ocean: Assessment, Sustainability and Management*. K. Sherman, E.N. Okemwa and M.J. Ntiba, Eds. Blackwell Science, Malden, MA, USA. pp. ix-xvi.

Smith, R.L. (1995). The Physical Processes of Coastal Ocean Upwelling Systems. In: *Report of the Dahlem Workshop on Upwelling in the Ocean: Modern Processes and Ancient Records, Berlin 1994, September 25-30.* Environmental Sciences Research Report Vol. ES 18. C.P. Summerhayes, K.-C. Emeis, M.V. Angel, J.M. Smith and B. Zeitzschel, Eds. John Wiley and Sons, Chichester, West Sussex, UK. pp. 39-64.

Ssentongo, G.W., E.T. Ukpe and T.O. Ajayi (1986). *Marine Fishery Resources of Nigeria: A review of exploited fish stocks.* 86/40 (En). FAO, Rome.

Stockton, P.L. and J.R.E. Lutjeharms (1988). Observations of vortex dipoles on the Benguela upwelling front. *South African Geographer* **15**(1/2): 27-35.

Stoffelen, A. and D. Anderson (1995). *The ECMWF contribution to the characterisation, interpretation, calibration and validation of ERS-1 scatterometer backscatter measurements and winds, and their use in numerical weather prediction models.* ESA Contract Report.

Stommel, H. (1963). Varieties of oceanographic experience. *Science* **139**: 572-576.

Summerhayes, C.P., K.-C. Emeis, M.V. Angel, R.L. Smith and B. Zeitzschel, Eds. (1995). *Report of the Dahlem Workshop on Upwelling in the Ocean: Modern Processes and Ancient Records, Berlin 1994, September 25-30*. Environmental Sciences Research Report. John Wiley and Sons, Chichester, West Sussex, UK. 422 p.

Summerhayes, C.P., K.-C. Emeis, M.V. Angel, R.L. Smith and B. Zeitzschel (1995). Upwelling in the Ocean: Modern Processes and Ancient Records. In: *Report of the Dahlem Workshop on Upwelling in the Ocean: Modern Processes and Ancient Records, Berlin 1994, September 25-30*. Environmental Sciences Research Report Vol. ES 18. C.P. Summerhayes, K.-C. Emeis, M.V. Angel, R.L. Smith and B. Zeitzschel, Eds. John Wiley and Sons, Chichester, West Sussex, UK. pp. 1-38.

Sutton, R.T. and M.R. Allen (1997). Decadal predictability of North Atlantic sea surface temperature and climate. *Nature* **388**(6642): 563-567.

Sutton, R.T., S.P. Jewson and D.P. Rowell (2000). The elements of climate variability in the tropical Atlantic region. *Journal of Climate* **in press**.

Taylor, A.H., M.B. Jordan and J.A. Stephens (1998). Gulf Stream shifts following ENSO events. *Nature* **393**(6686): 638.

Taylor, A.H. and J.A. Stephens (1998). The North Atlantic Oscillation and the latitude of the Gulf Stream. *Tellus* **50**(A): 134-142.

Tilot, V. (1993). *Description of the Different Large Marine Ecosystems of West Africa*.

Tilot, V. and A. King (1993). *A Review of the Subsystems of the Canary Current and Gulf of Guinea Large Marine Ecosystems*. IUCN Marine Programme.

UNEP/IUCN (1988). *Coral Reefs of the World Volume 1: Atlantic and Eastern Pacific* . IUCN, Gland, Switzerland and Cambridge, UK/UNEP, Nairobi, Kenya.

Uppenbrink, J. (1999). Climate variability - The North Atlantic Oscillation. *Science* **283**(5404): 948-949.

Valdes, E.S., P.A. Shelton, M.J. Armstrong and J.G. Field (1987). Cannabalism in South African anchovy: egg mortality and egg consumption rates. *South African Journal of Marine Science* **5**: 613-622.

Valdes Szeinfeld, E.S. and K. Cochrane (1992). The potential effects of cannabilism and intraguild predation on anchovy recruitment and clupeoid fluctuations. *South African Journal of Marine Science* **12**: 695-702.

Vandenhouten, R., G. Goebbels, M. Rasche and H. Tegtmeier (1996). *SANTIS - a tool for Signal ANalysis and TIme Series processing. Version 1.1: User Manual.*

Venzke, S., M.R. Allen, R.T. Sutton and D.P. Rowell (1999). The Atmospheric Response over the North Atlantic to Decadal Changes in Sea Surface Temperature. *Journal of Climate* **12**: 2562-2584.

Verstraete, J.-M. (1970). Etude quantitative de l'upwelling sur le plateau continental ivoirien. *Documents Scientifique Centre de Recherche Océanographique Abidjan* **1**(3): 1-17.

Verstraete, J.-M. (1985). Equatorial Counter-Currents and Seasonal-Variations of Heat-Content and Mean Sea-Level in the Eastern Tropical Atlantic. *Oceanologica Acta* **8**(3): 249-261.

Verstraete, J.-M. (1987). *Seasonal heat content of the eastern tropical Atlantic.* Proceedings of the International Symposium on equatorial vertical motions, Paris, 6-10 May 1985. (Number). Oceanologica Acta. pp. 85-90.

Verstraete, J.-M. (1992). The Seasonal Upwellings in the Gulf of Guinea. *Progress in Oceanography* **29**(1): 1-60.

Verstraete, J.-M., J. Picaut and A. Morlière (1980). Atmosphere and tidal observations along the shelf of the Guinea Gulf. *Deep Sea Research* **26**(Suppl. 2): 343-356.

Verstraete, J.-M. and J. Vassie (1990). The Vertical Structure of the Zonal and Meridional Pressure-Gradients in the Equatorial Atlantic During 1983 and 1984. *Deep-Sea Research* **37**(1A): 1-26.

Visser, P. (1999). Gravity field determination with GOCE and GRACE. *Advances in Space Research* **23**(4): 771-776.

Ware, D.M. and G.A. McFarlane (1989). Fisheries production biomes in the northeast Pacific Ocean. *Can. Spec. Publ. Fish. Aquat. Sci.* **108**: 359-379.

Webster, P.J. and T.N. Palmer (1997). The past and the future of El Nino. *Nature* **390**(6660): 562-564.

Weeks, S.J. and F.A. Shillington (1994). Interannual scales of variation of pigment concentrations from coastal zone colour scanner data in the Benguela Upwelling system and the Subtropical Convergence zone south of Africa. *Journal of Geophysical Research* **99**(C4): 7385-7399.

Weisberg, R.H. and C. Colin (1986). Equatorial Atlantic-Ocean Temperature and Current Variations During 1983 and 1984. *Nature* **322**(6076): 240-243.

Weisberg, R.H., A. Horigan and C. Colin (1979). Equatorially trapped Rossby-gravity wave propagation in the Gulf of Guinea. *Journal of Marine Research* **37**(1): 67-86.

Weisberg, R.H. and T.J. Weingartner (1986). On the Baroclinic Response of the Zonal Pressure-Gradient in the Equatorial Atlantic-Ocean. *Journal of Geophysical Research* **91**(C10): 1717-1725.

Williams, F. (1968). *Report on the Guinean Trawling Survey* 99. Organisation of African Unity Scientific and Technical Research Commission.

Wolter, K. (1997). Trimming problems and remedies in COADS. *Journal of Climate* **10**(8): 1980-1997.

Woodruff, S.D., R.J. Slutz, R.L. Jenne and P.M. Steurer (1987). A Comprehensive Ocean-Atmosphere Data Set. *Bulletin of the American Meteorological Society* **68**(10): 1239-1249.

Yasudo, I., H. Sugisaki, Y. Watanabe, S. Minobe and Y. Oozeki (1999). Interdecadal variations in Japanese sardine and ocean/climate. *Fisheries Oceanography* **8**(1): 18-24.

Zimmermann, G. (1997). German program for ocean remote sensing. In: *Space Remote Sensing of Sub-tropical Oceans*. L. Cho-Teng, Ed. Elsevier Science Ltd., Oxford. pp. 45-54.

Zimmermann, G. and A. Neumann (1997). MOS a spaceborne imaging spectrometer for ocean remote sensing. *Backscatter,* May 1997, 9-13.

Appendix 1 – Principal Components Analysis

PCA Theory

Although PCA is a commonly applied technique, its wide range of uses means there is no standardised methodology and the interpretation of results from analyses is, by definition, subjective. Therefore, it is useful to review briefly the theory and mathematics behind PCA as an aid to understanding the results of the analysis.

What is PCA?

According to Kendall and Stuart (1966), a major problem in the practical application of multivariate analyses is the difficulty in disentangling a complicated inter-relationship among the variables and of interpreting the results of the analysis. PCA is a statistical technique, related to factor analysis (Eastman 1992, Systat 1996), which attempts to deal with this problem by describing the variance with a reduced set of components and transforming them to independence (Kendall and Stuart 1966). In this way, it can estimate the underlying dimensions of the data (Fung and LeDrew 1987). It works upon the variance structure of the data to determine its dimensions upon linearly uncorrelated, or orthogonal, axes, hence it is sometimes called Empirical Orthogonal Function (EOF) analysis. PCA has the characteristics of preserving the total variance in the transformation and minimising the mean square approximate errors (Fung and LeDrew 1987). The technique is especially useful for large, multi-dimensional data sets, where many of the dimensions are highly correlated, as described above for multi-channel remotely sensed data.

Standardised and unstandardised PCA

Depending on the purpose of PCA, it can be performed using standardised or unstandardised data. Standardisation gives zero mean and unit standard deviation to each of the vectors in the input matrix. This can be calculated directly if a variance-covariance matrix is to be used

for the PCA, however, if a correlation matrix is used then standardisation prior to PCA is not required as results are standardised regardless of the state of the original data. If unstandardised results are required, a variance-covariance matrix must be used with unstandardised data. Standardisation can be calculated spatially or temporally, depending on the type of data used and the output requirements.

Unstandardised PCA results in input vectors with a higher degree of variance contributing more to the total variance than those with less variance. Thus, it is useful in remote sensing studies for data-compression of multi-spectral images. However, with time series information, it is better to give equal weight to each input vector, regardless of the variance within each. This gives each vector an equal contribution to the total variance and prevents dominant features masking changes in the data. Both Fung and LeDrew (1987) and Eastman (1992) indicate that spatially standardised PCA appears more effective than unstandardised PCA in detecting change in remotely sensed time series data sets.

Outputs of PCA

For remotely sensed image data, each principal component is composed of a spatial output, the principal component (PC) images and an associated temporal output, termed the loadings. An eigenvalue is also associated with each component. Eigenvalues represent the proportion of the total variance in the input data that each principal component accounts for, with the largest eigenvalues accounting for the greatest proportion of the total variance. By convention, these are ordered according to decreasing magnitude. Thus, the first principal component accounts for the proportion of the total variance given by the largest eigenvalue, the second principal component accounts for the proportion of the total variance given by the second largest eigenvalue, and so on for successive components. Principal components are linearly uncorrelated. Both the PC images and their associated loadings are numbered according to the relative magnitude of their eigenvalues. The PC images show a spatial pattern that explains a pattern of variance in the input data, equivalent to the proportion of the

total variance given by its eigenvalue. The loadings show the strength of the pattern in the associate PC image for each time step of the original data series, relative to previous and subsequent time steps.

Mathematical Basis of PCA

The following mathematical explanation of PCA, for use with spatially oriented time series data, is taken from Cole (1997) and Cole and McGlade (1998a), but is modified using Gallaudet and Simpson (1994), Fung and LeDrew (1987) and Kendall and Stuart (1966). The technique is described here in three stages: calculation of the correlation or variance-covariance matrix, calculation of the eigenvectors (eigenmatrix) and eigenvalues and calculation of the principal component images.

Calculation of the correlation or variance-covariance matrix

The variance-covariance matrix $\mathbf{C}_x$ is a $t \times t$ matrix derived from the $t \times n$ input matrix $\mathbf{X}$ and its transpose $\mathbf{X}^T$, where t is the number of time steps, or layers, and n is the number of pixel sites within each layer. The number of time steps is the number of monthly composites used. The number of pixel sites is the number of pixel rows in the image multiplied by the number of pixel columns in the image. This only forms one dimension of the input matrix because it is, in effect, a concatenation of all the pixel rows of the image.

$$\mathbf{C}_x = [1/(tn-1)]\mathbf{X}\mathbf{X}^T \qquad \text{(A1.1)}$$

Standardisation is equivalent to calculation of the correlation coefficients, therefore, calculating a correlation matrix from unstandardised input data actually produces the same matrix $\mathbf{C}_x$.

Calculation of the eigenvectors (eigenmatrix) and eigenvalues

For each principal component, an eigenvalue and an eigenvector are calculated. Eigenvalues represent the proportion of the total variance in $\mathbf{X}$ that each principal component accounts for. The eigenmatrix is a series of column vectors, termed eigenvectors, which describe the direction each principal component takes in the *t*-dimensional space. Both the eigenvalues and the eigenmatrix are found by solving

$$\mathbf{E}\mathbf{C}_X\mathbf{E}^T = \mathbf{V} \qquad \text{(A1.2)}$$

where $\mathbf{E}$ is the $t \times t$ eigenmatrix, $\mathbf{V}$ is the $t \times t$ matrix of eigenvalues (in which all the non-diagonal elements are zero) and $\mathbf{E}^T$ is the transpose of $\mathbf{E}$.

The eigenvectors give the temporal output of the PCA and are equivalent to the loadings. Each element of the eigenvector represents one time step and they are ordered according to the temporal sequence, i.e. the order of rows, in the input matrix $\mathbf{X}$.

Calculation of the Principal Component Images

Principal component images are the spatial output from the PCA. Calculation of the component images is achieved by linearly recombining the input matrix $\mathbf{X}$ with the transform of the eigenmatrix $\mathbf{E}$

$$\mathbf{Y} = \mathbf{E}^T\mathbf{X} \qquad \text{(A1.3)}$$

Where $\mathbf{Y}$ is the $t \times n$ output matrix of principal component images, in which the pixel values of the i^{th} principal component are found along row i. The units for the output images (i.e. in $\mathbf{Y}$) are the same as for the input images, namely standardised units.

Differences for PCA with non-spatial data

Data with no spatial component, can be temporally standardised. This results in a few changes in the implementation of PCA. Firstly the input matrix is an n x t matrix, where n is the number of samples (e.g. rivers or coastal areas) and t is the number of time steps (e.g. years or months). This leads to the variance-covariance matrix $\mathbf{C}_x$ being an n x n matrix, rather than a t x t matrix. The eigenvectors, or loadings, in the eigenmatrix **E**, then give the relative correlation of different samples to each other while the output principal component matrix gives the temporal output in the n x t matrix **Y**, where n is the number of the principal components and t is the number of time steps. The eigenvalues, in the matrix **V**, represent the variance explained by each principal component, as before.

Appendix 2 – Monthly SST Composites

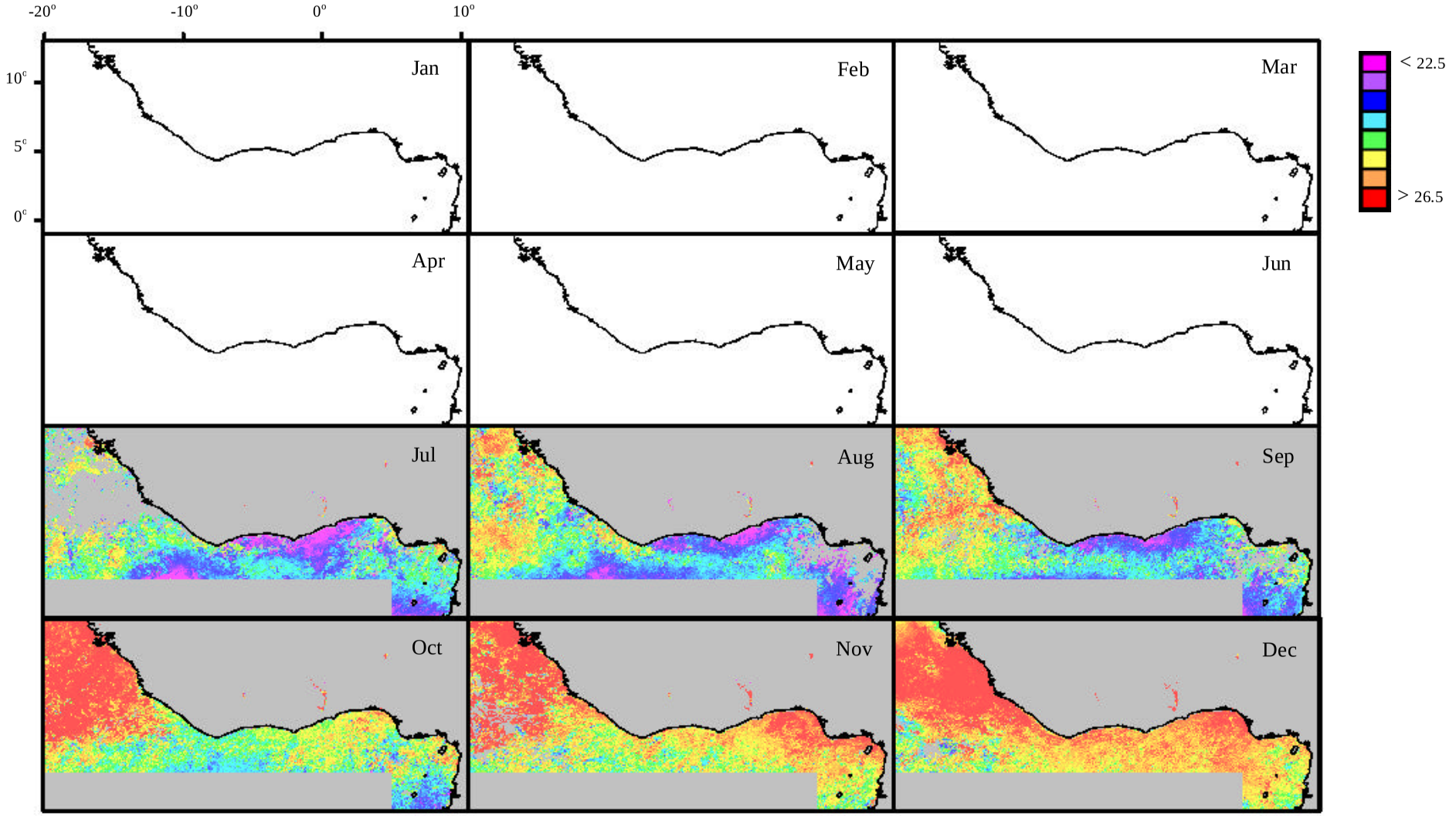

CORSA-AVHRR monthly SST composites for 1981.

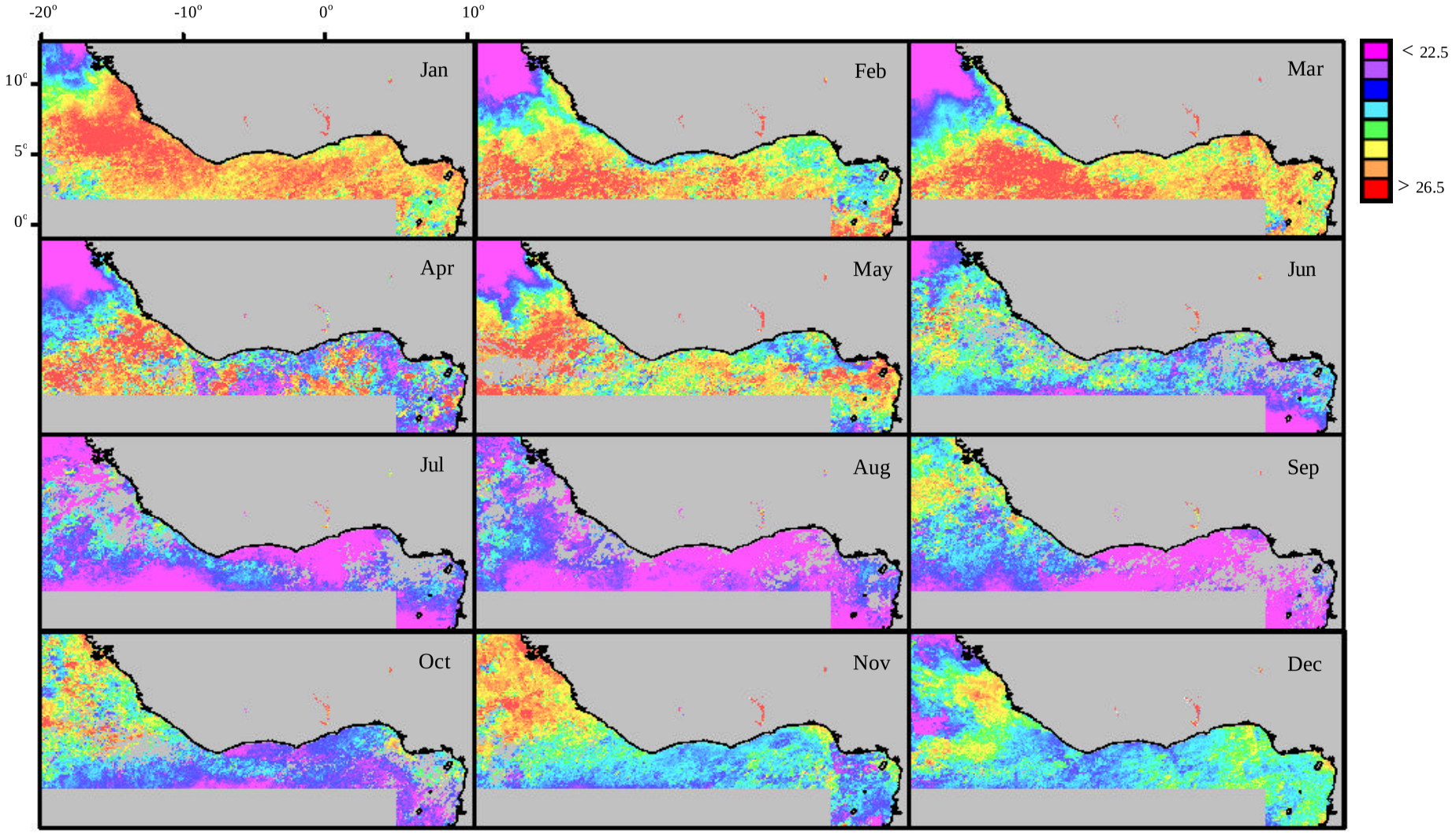

CORSA-AVHRR monthly SST composites for 1982.

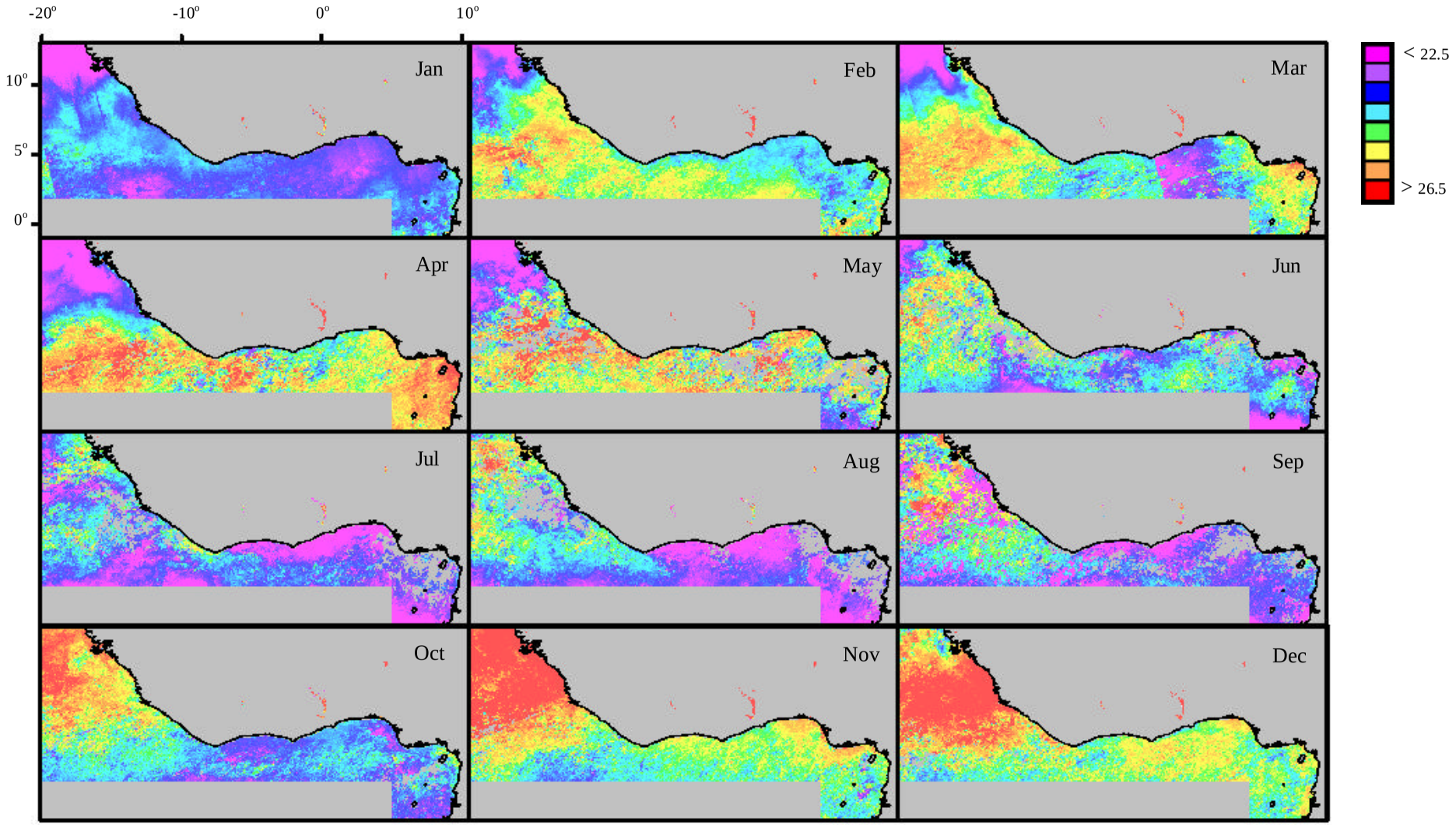

CORSA-AVHRR monthly SST composites for 1983

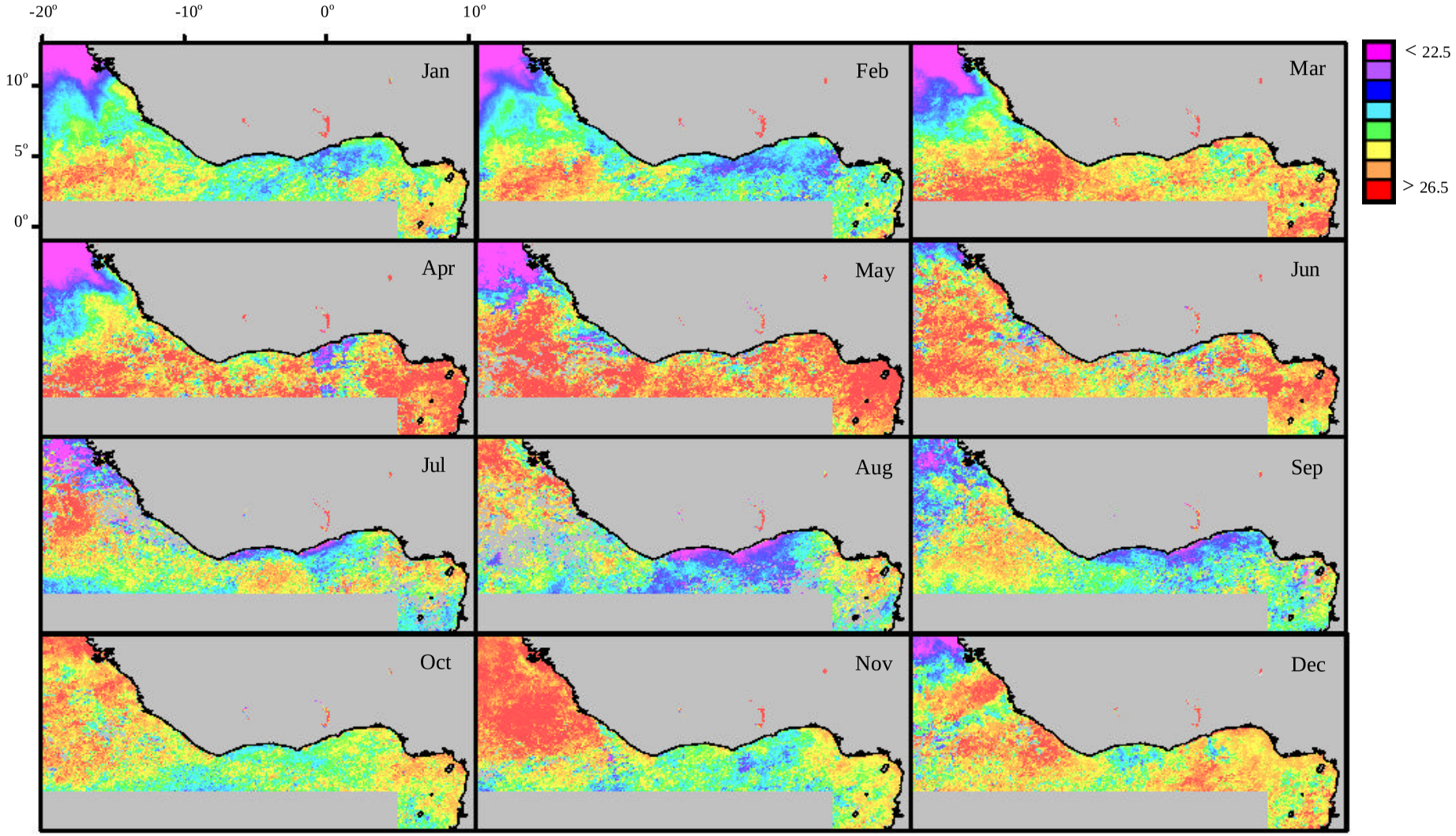

CORSA-AVHRR monthly SST composites for 1984.

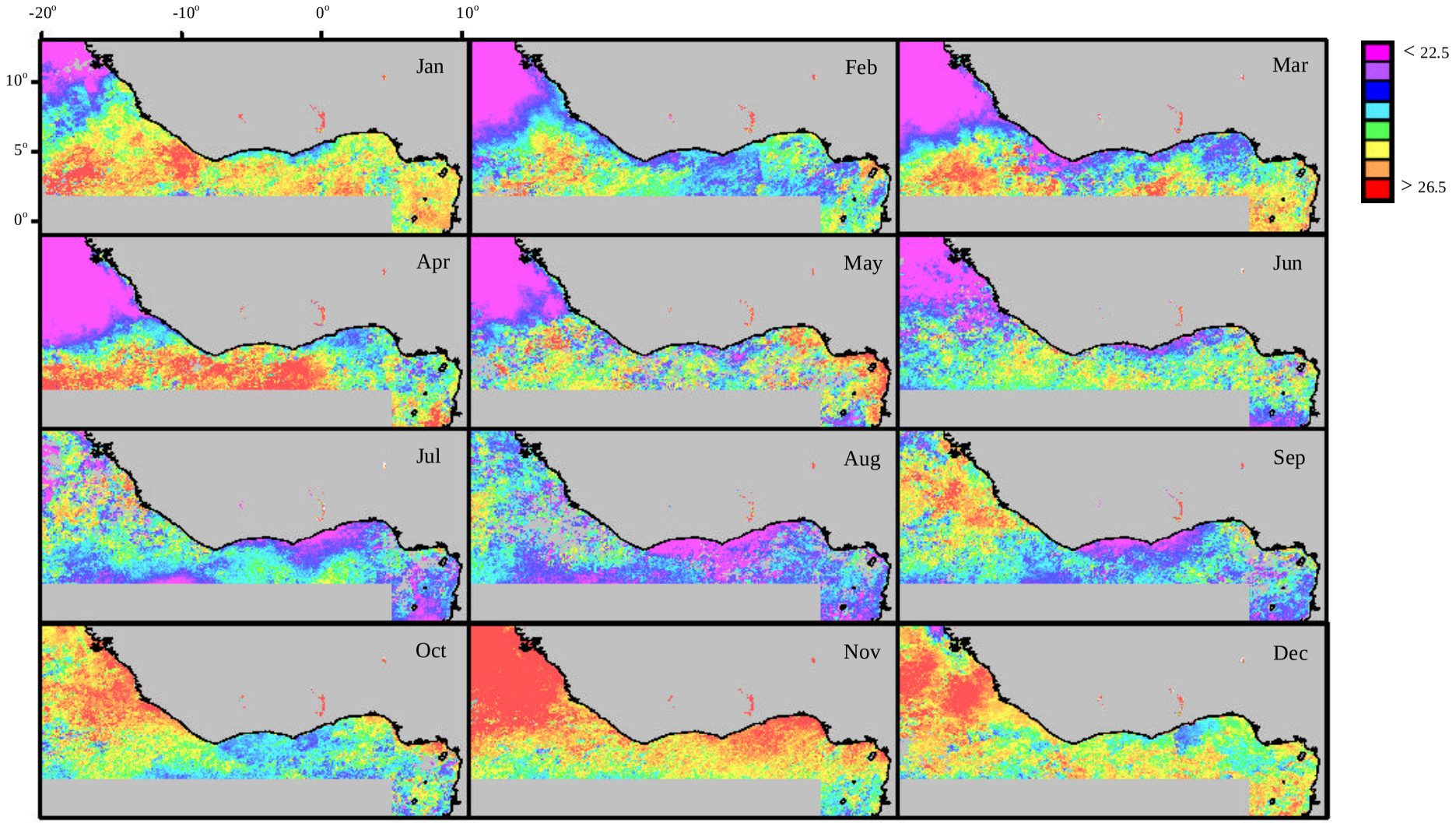

CORSA-AVHRR monthly SST composites for 1985.

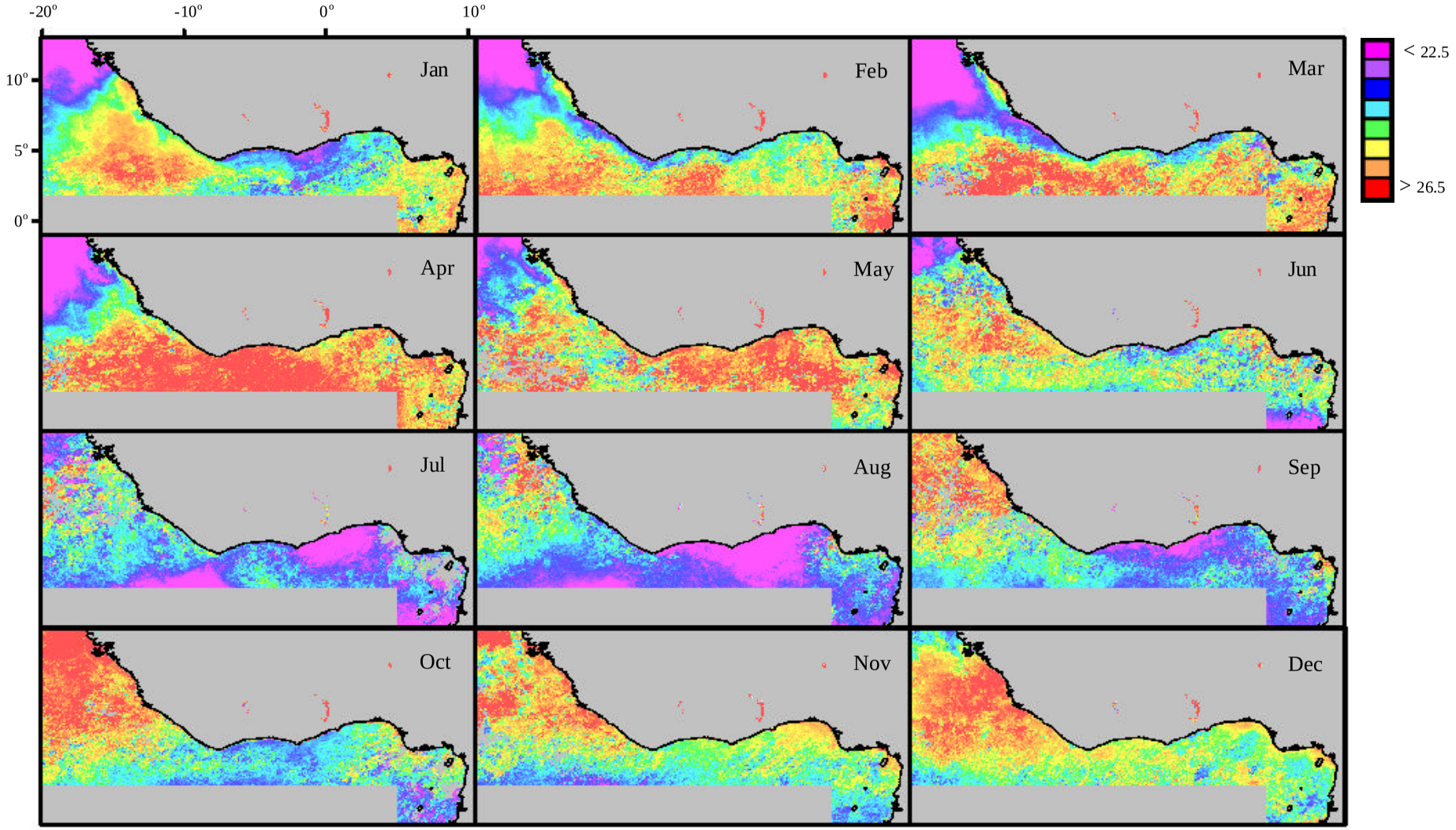

CORSA-AVHRR monthly SST composites for 1986.

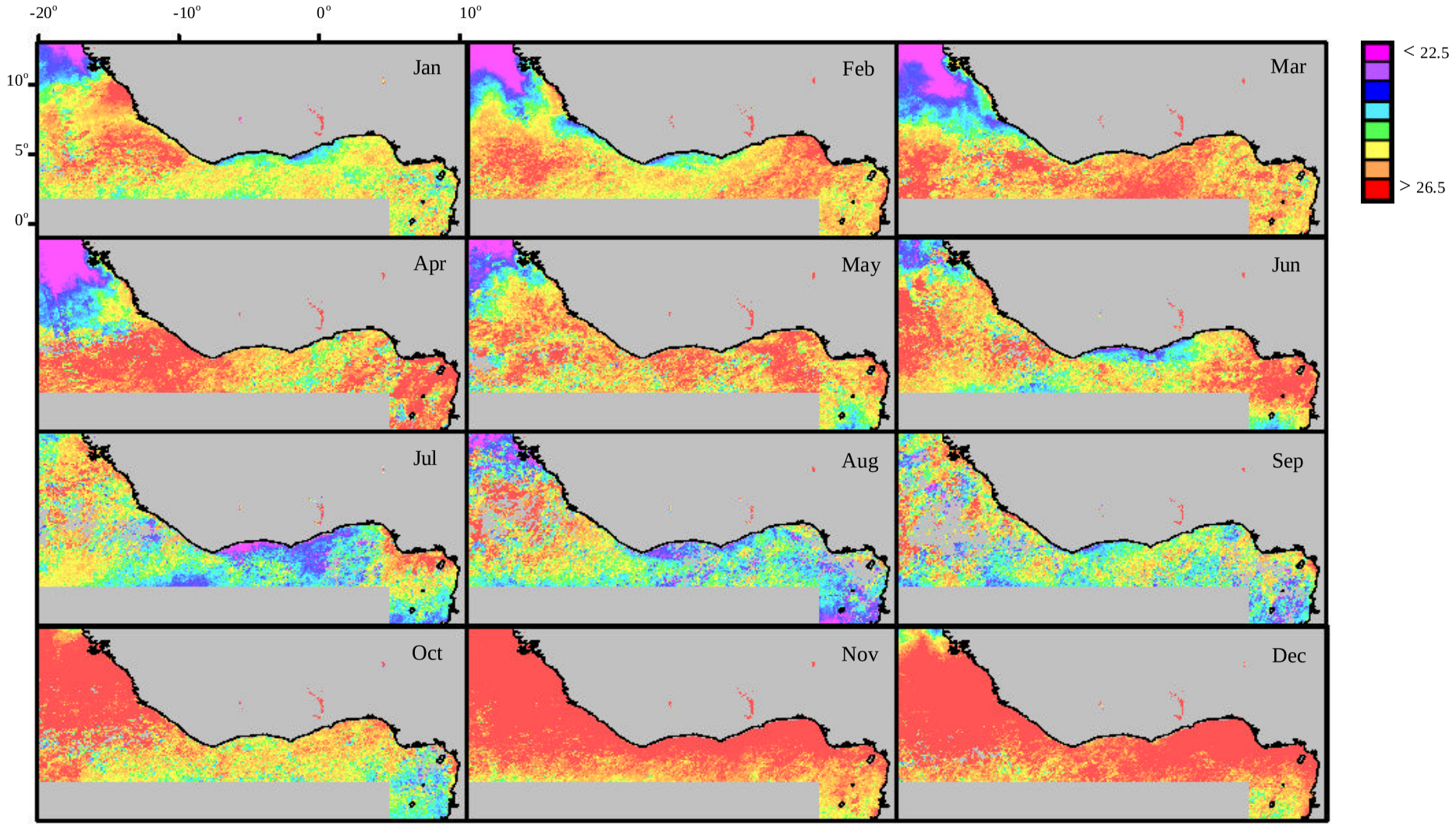

CORSA-AVHRR monthly SST composites for 1987.

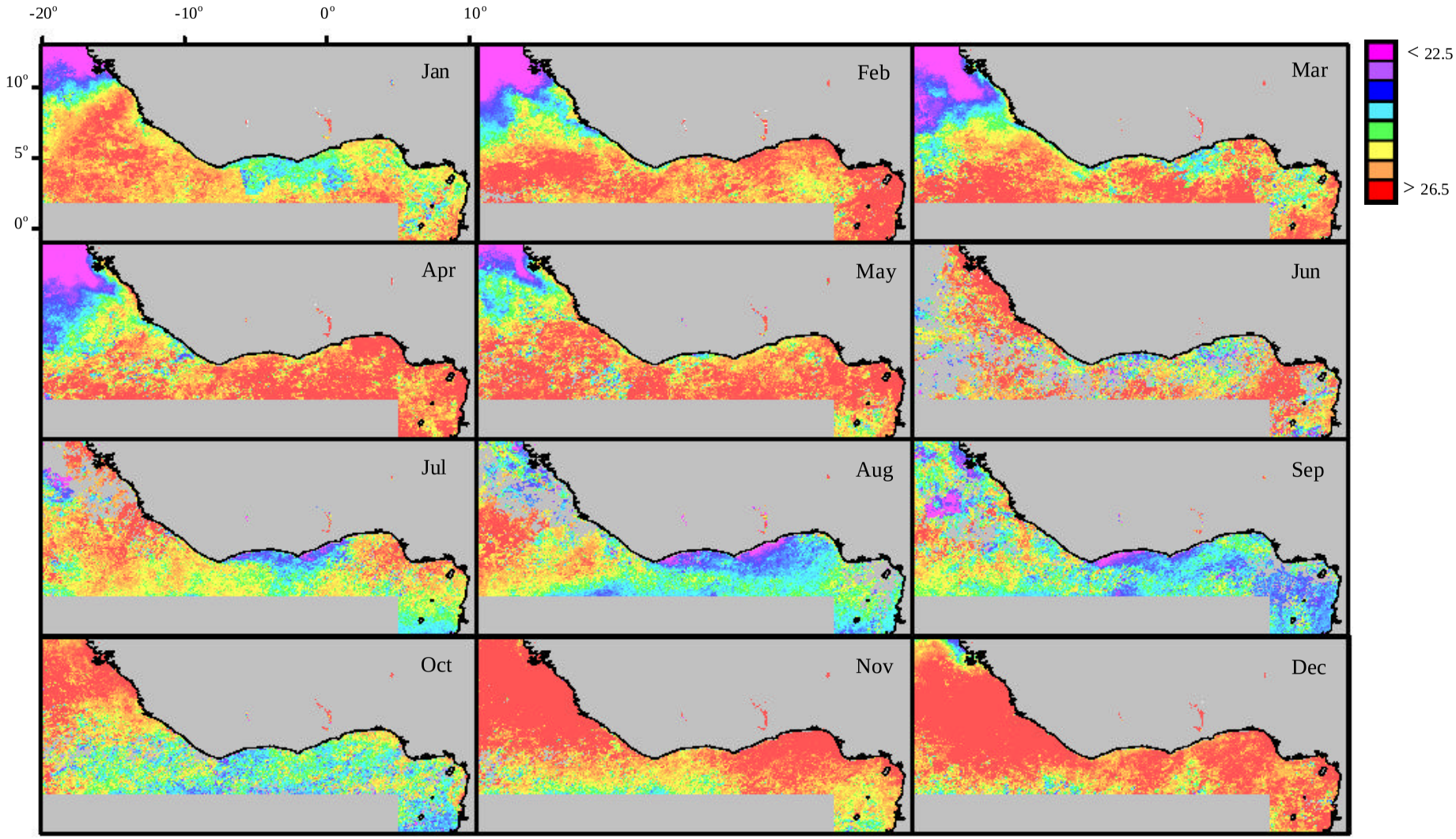

CORSA-AVHRR monthly SST composites for 1988.

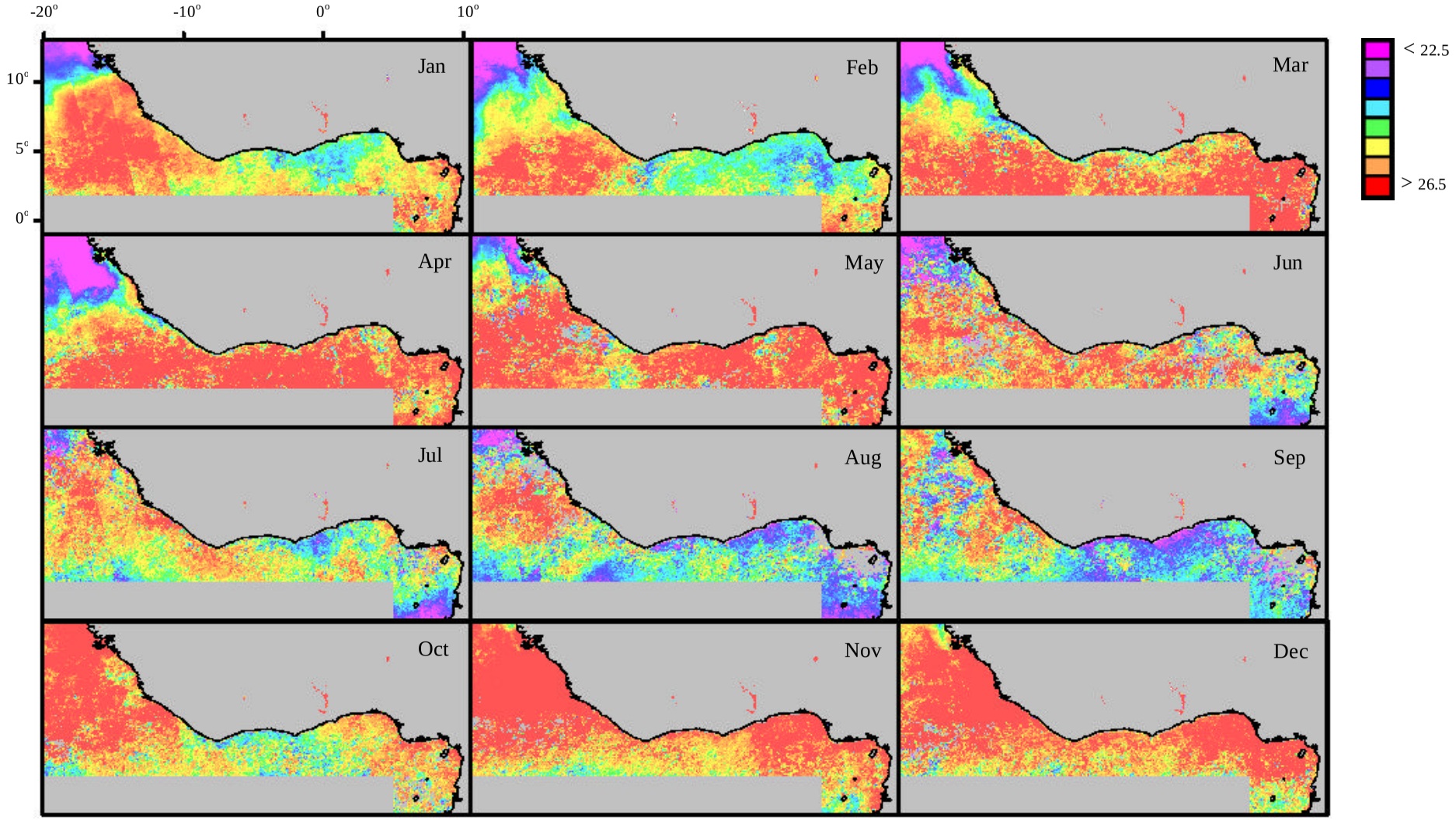

CORSA-AVHRR monthly SST composites for 1989.

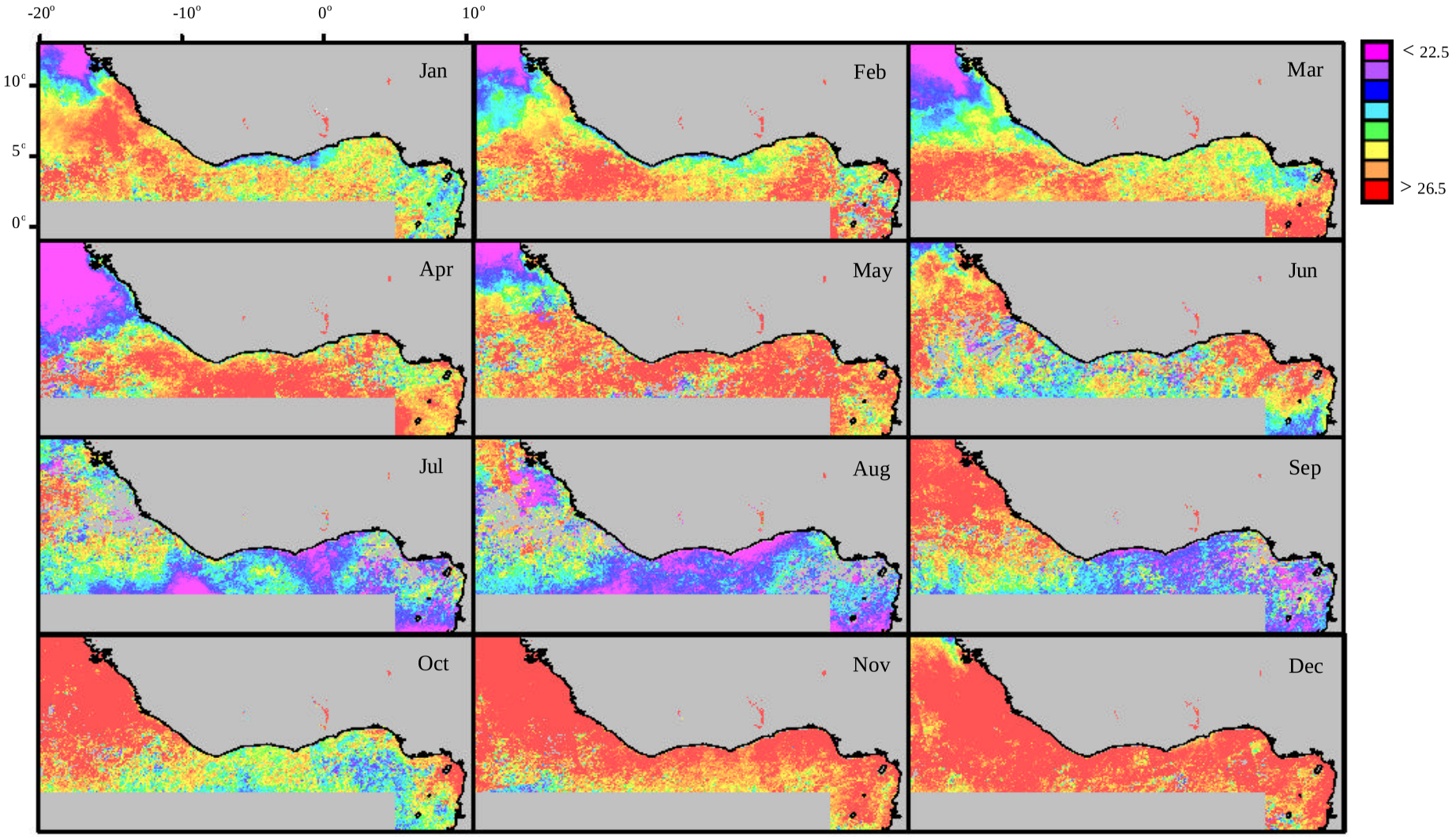

CORSA-AVHRR monthly SST composites for 1990.

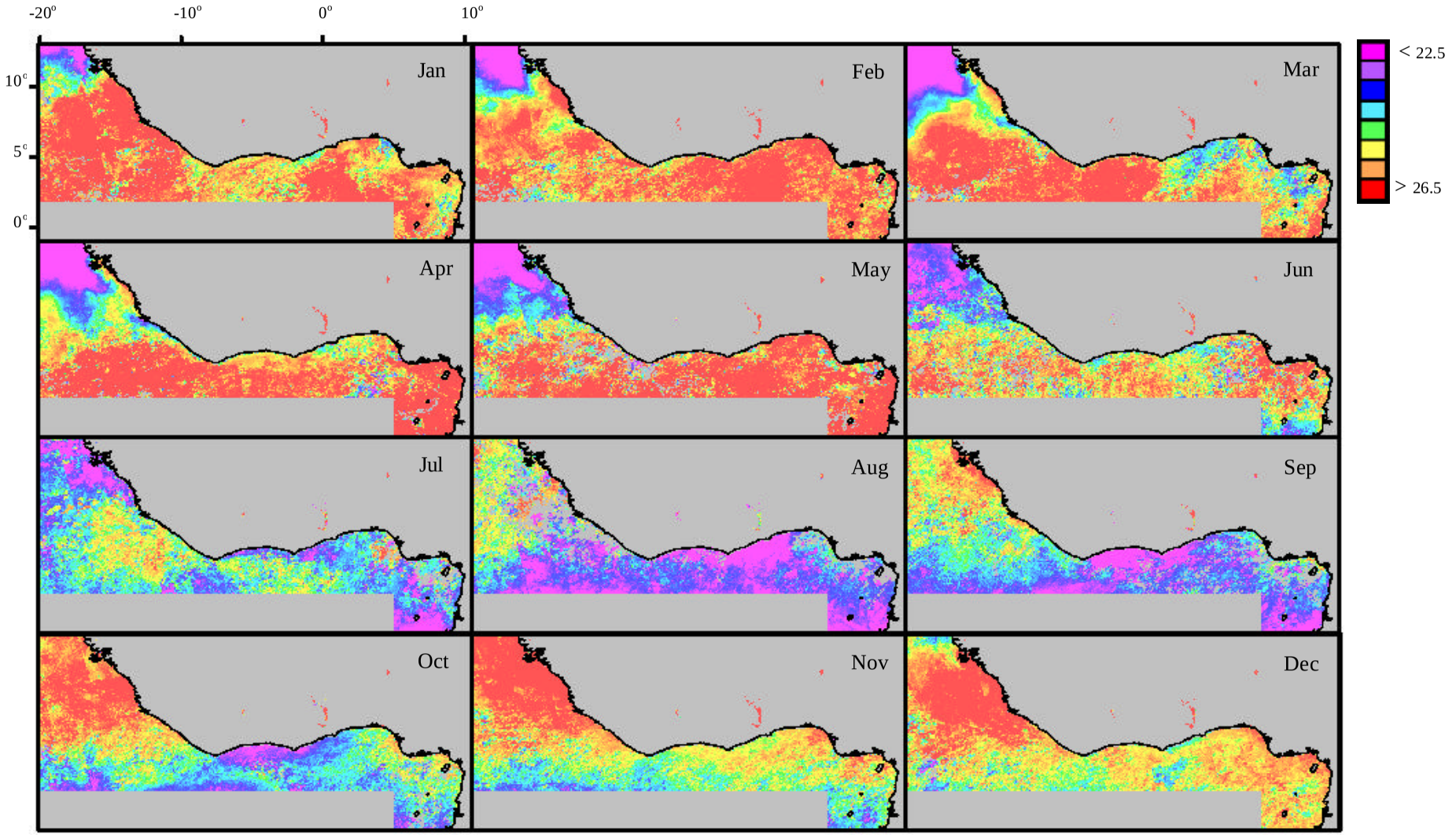

CORSA-AVHRR monthly SST composites for 1991.

Appendix 3 – Qualitative Comparisons from Chapter 7

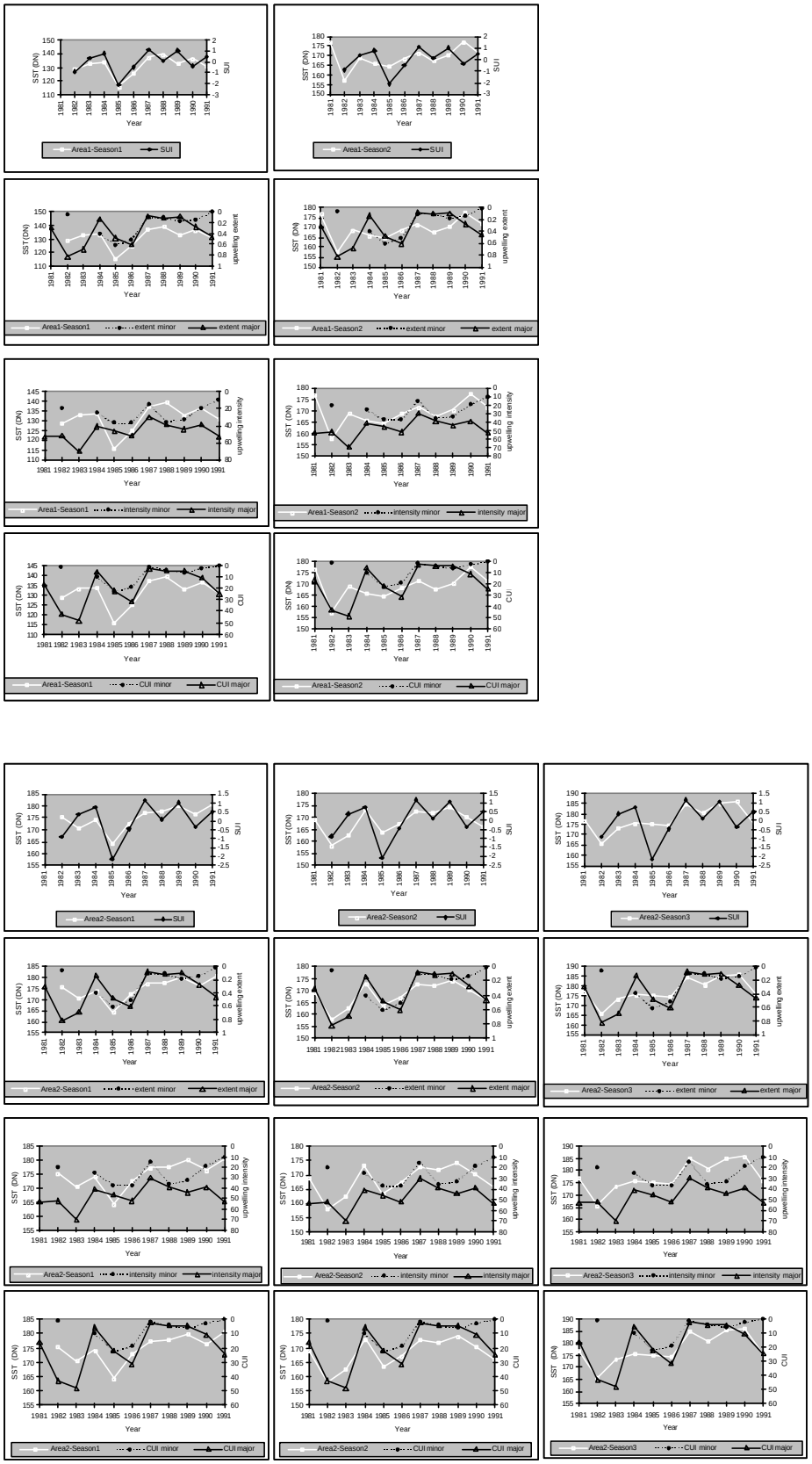

Qualitative comparison of seasonal CORSA-AVHRR SST in Areas 1 and 2 and the oceanographic indices.

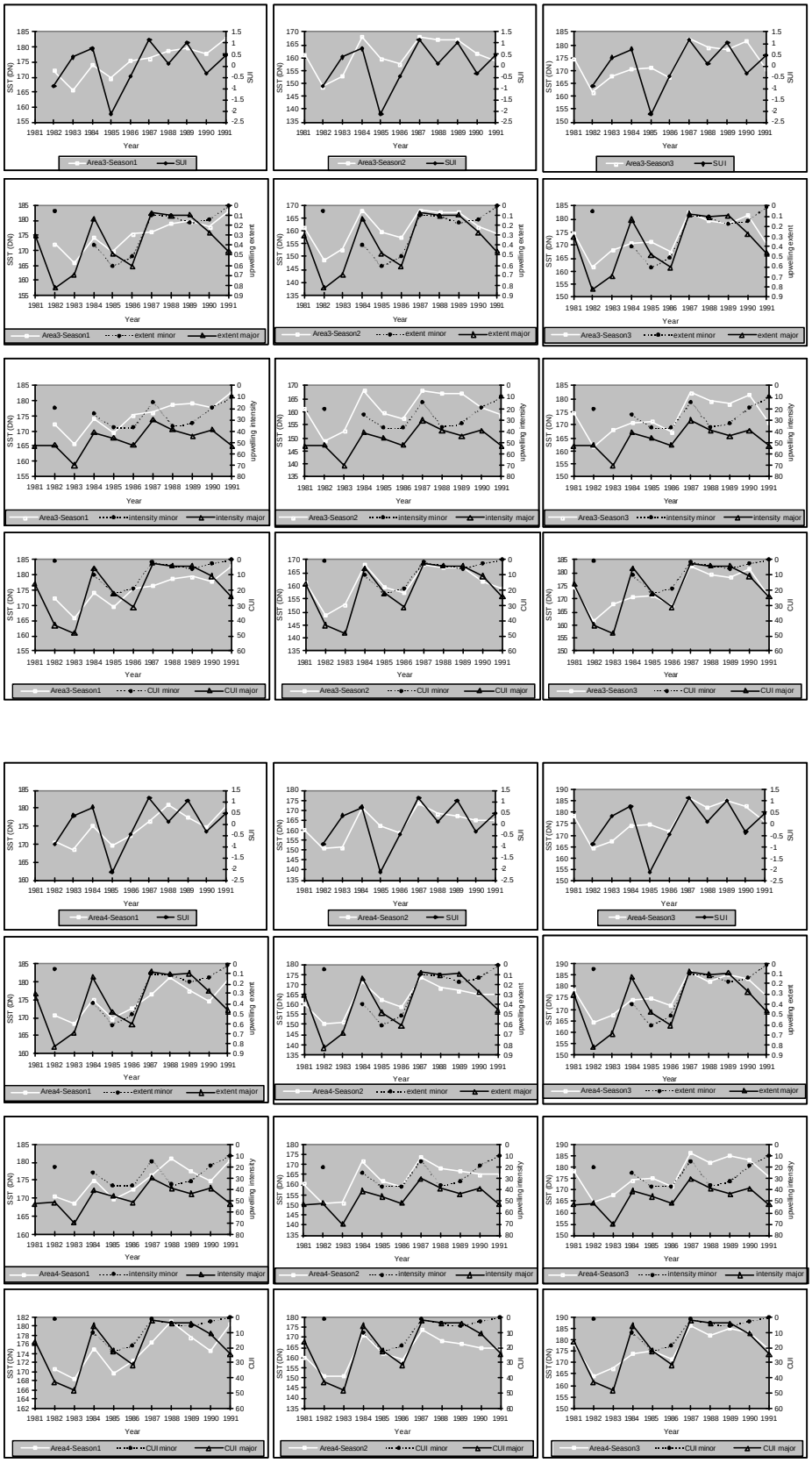

Qualitative comparison of seasonal CORSA-AVHRR SST in Areas 3 and 4 and the oceanographic indices.

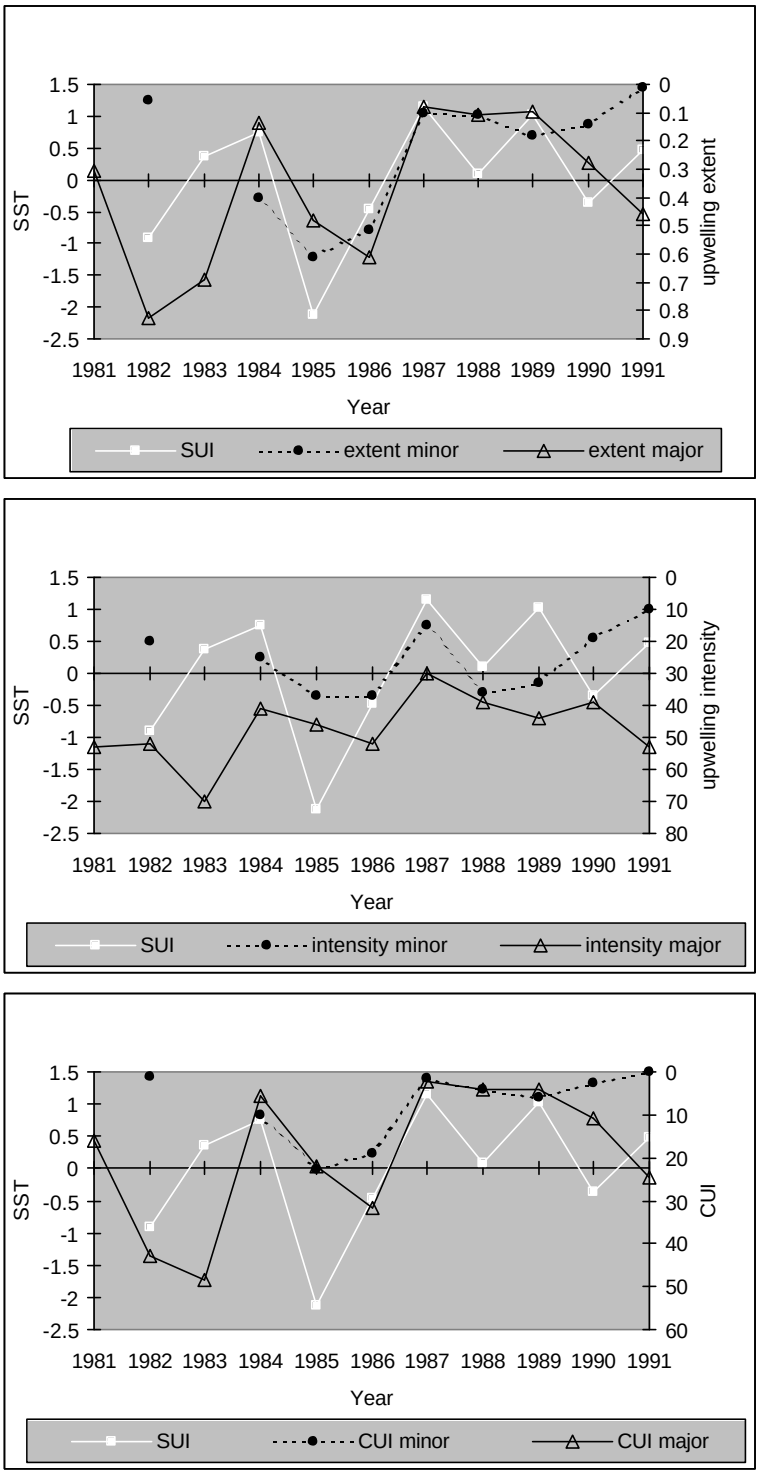

Qualitative comparison of the SUI index with the CUI and upwelling components.

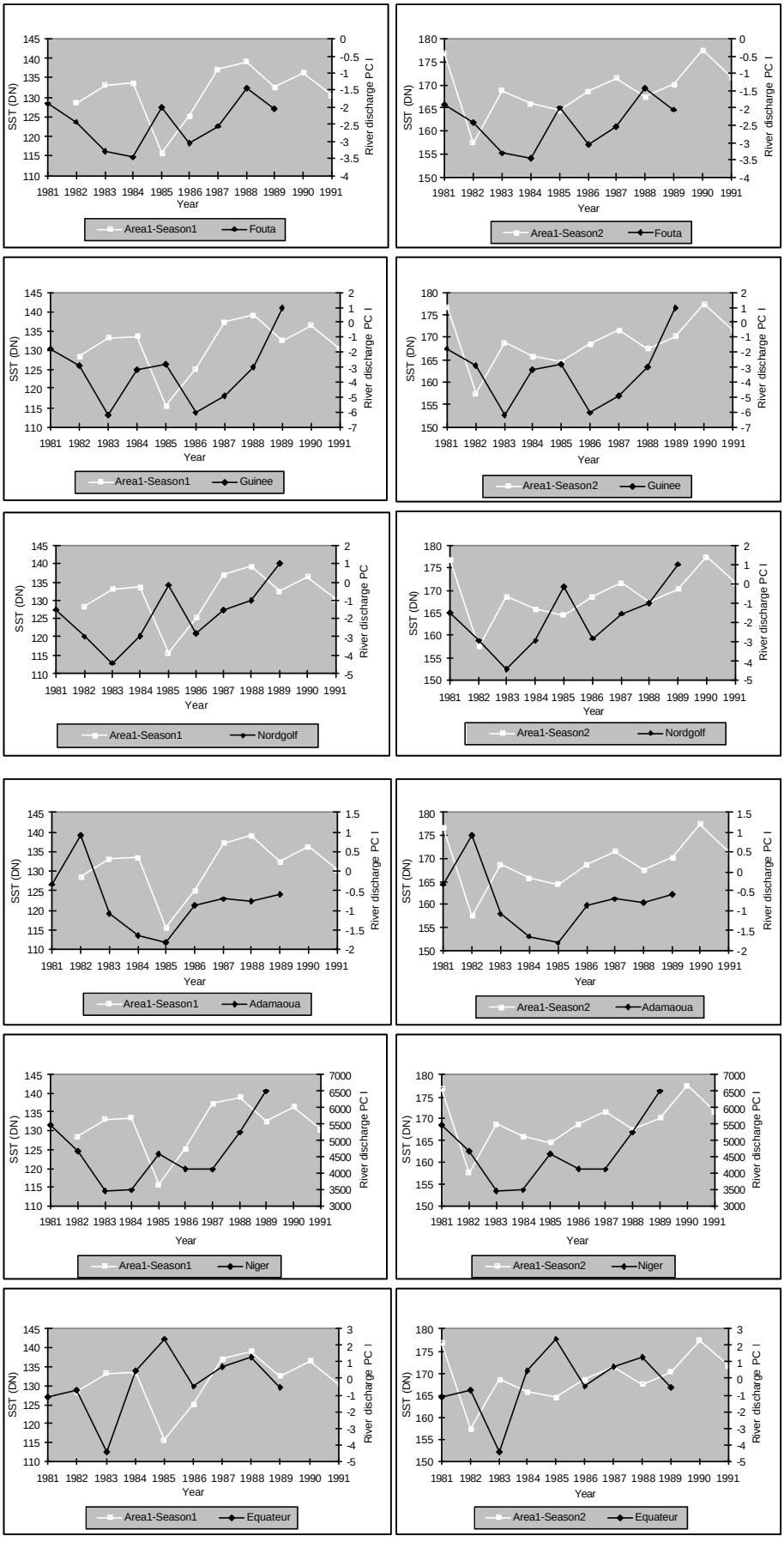

Qualitative comparison of CORSA-AVHRR SST for Area 1 with PC I of regional river discharge.

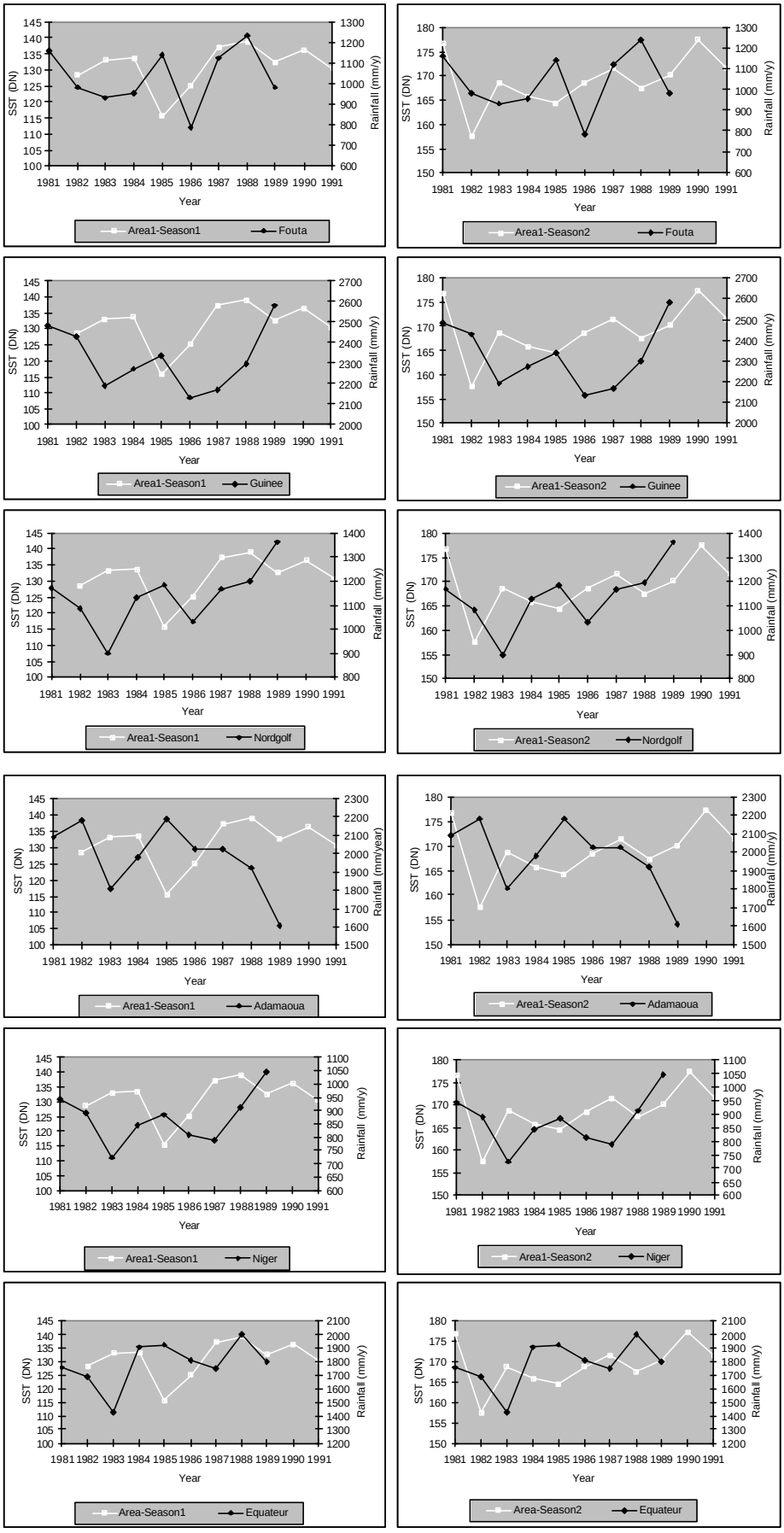

Qualitative comparison of CORSA-AVHRR SST for Area 1 with regional rainfall.

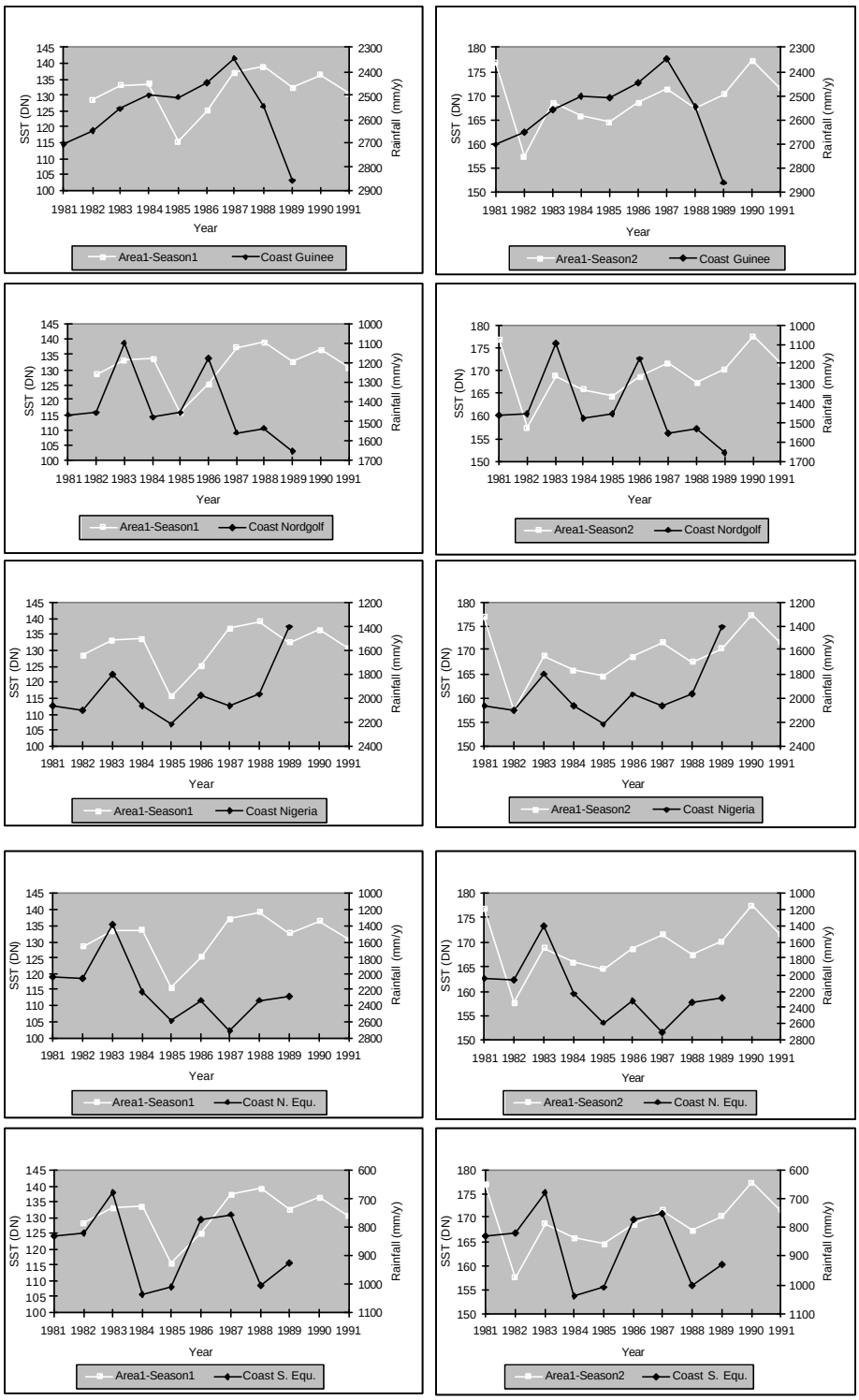

Qualitative comparison of CORSA-AVHRR SST for Area 1 with coastal area rainfall.

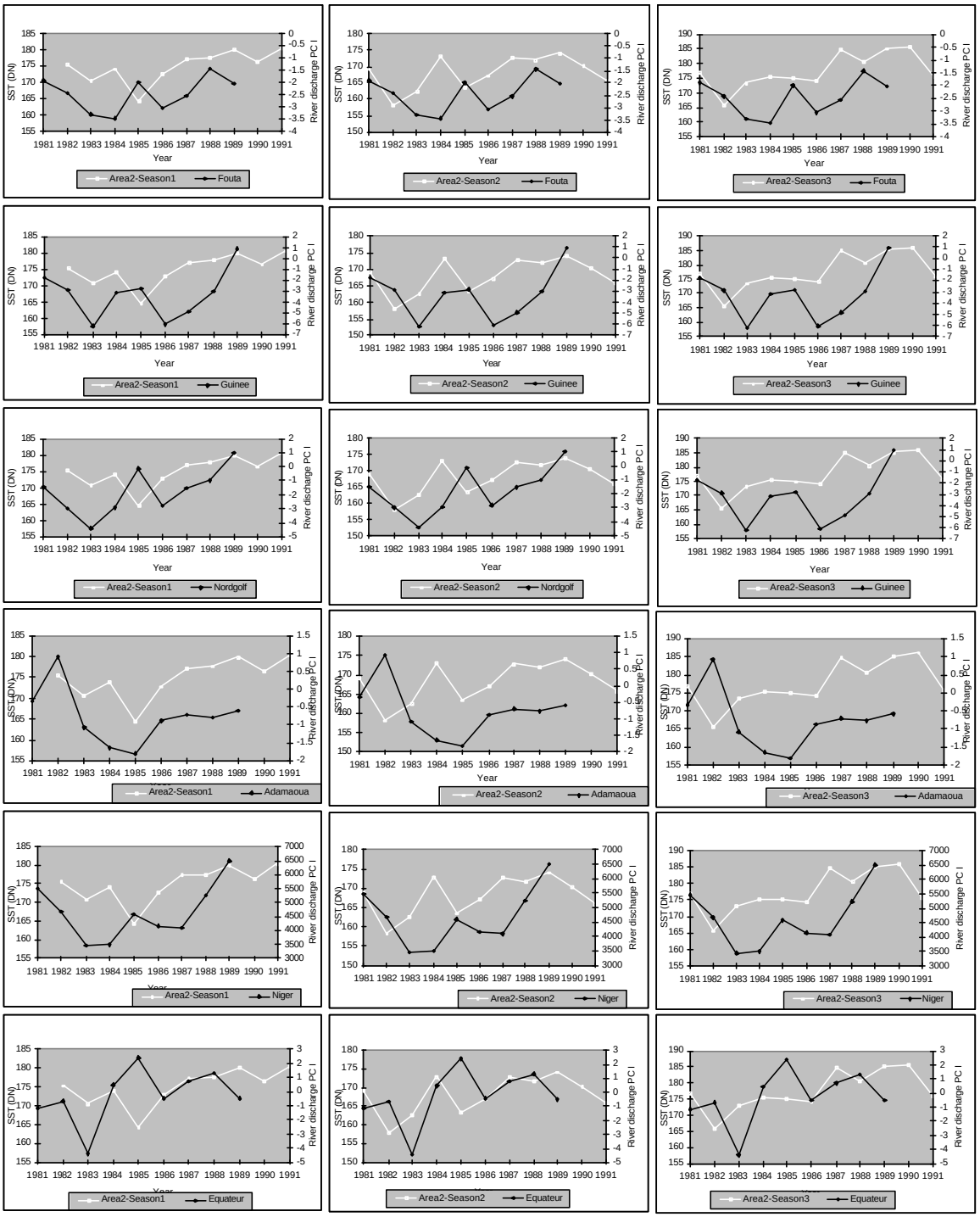

Qualitative comparison of CORSA-AVHRR SST for Area 2 with PC I of regional river discharge.

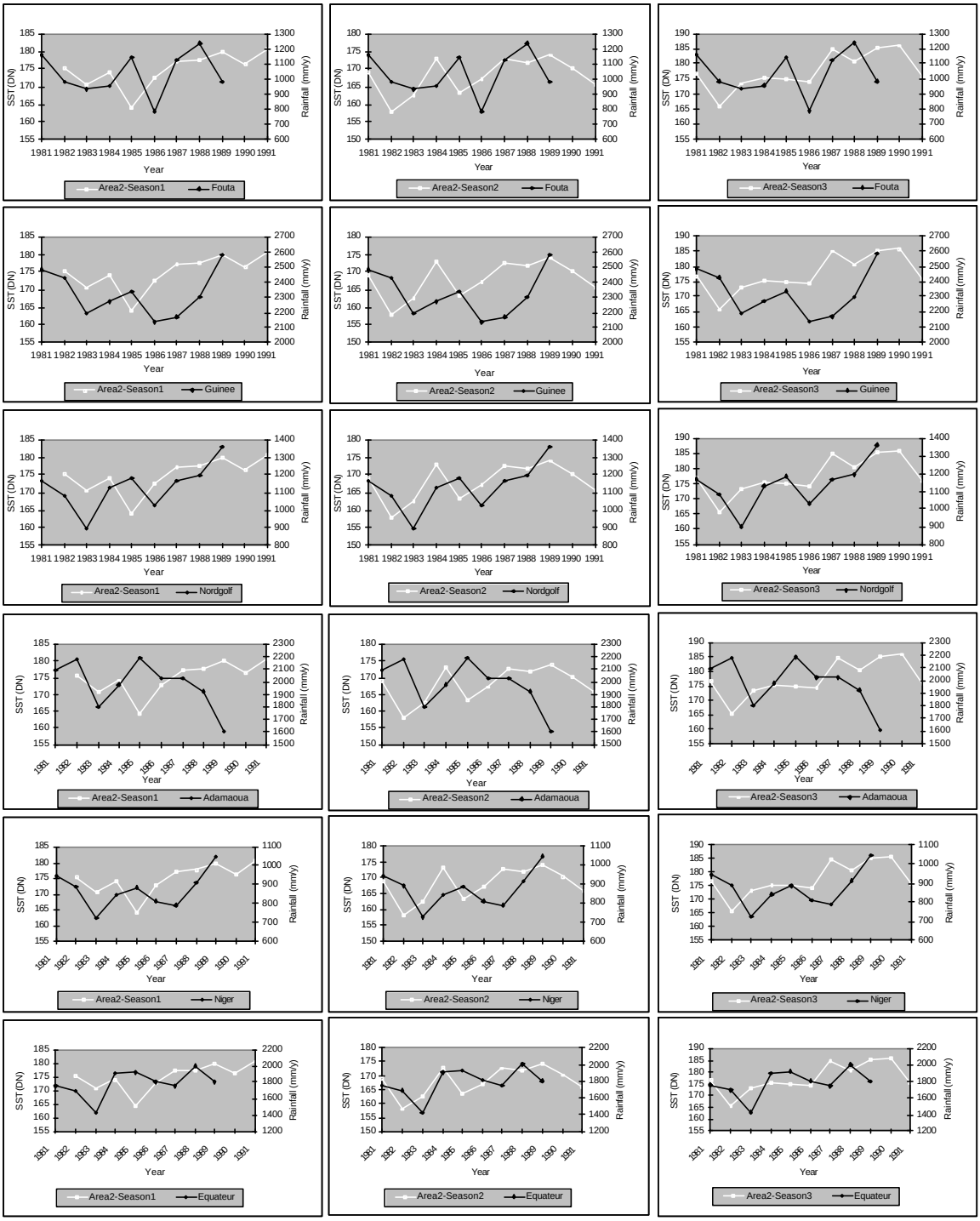

Qualitative comparison of CORSA-AVHRR SST for Area 2 with regional rainfall.

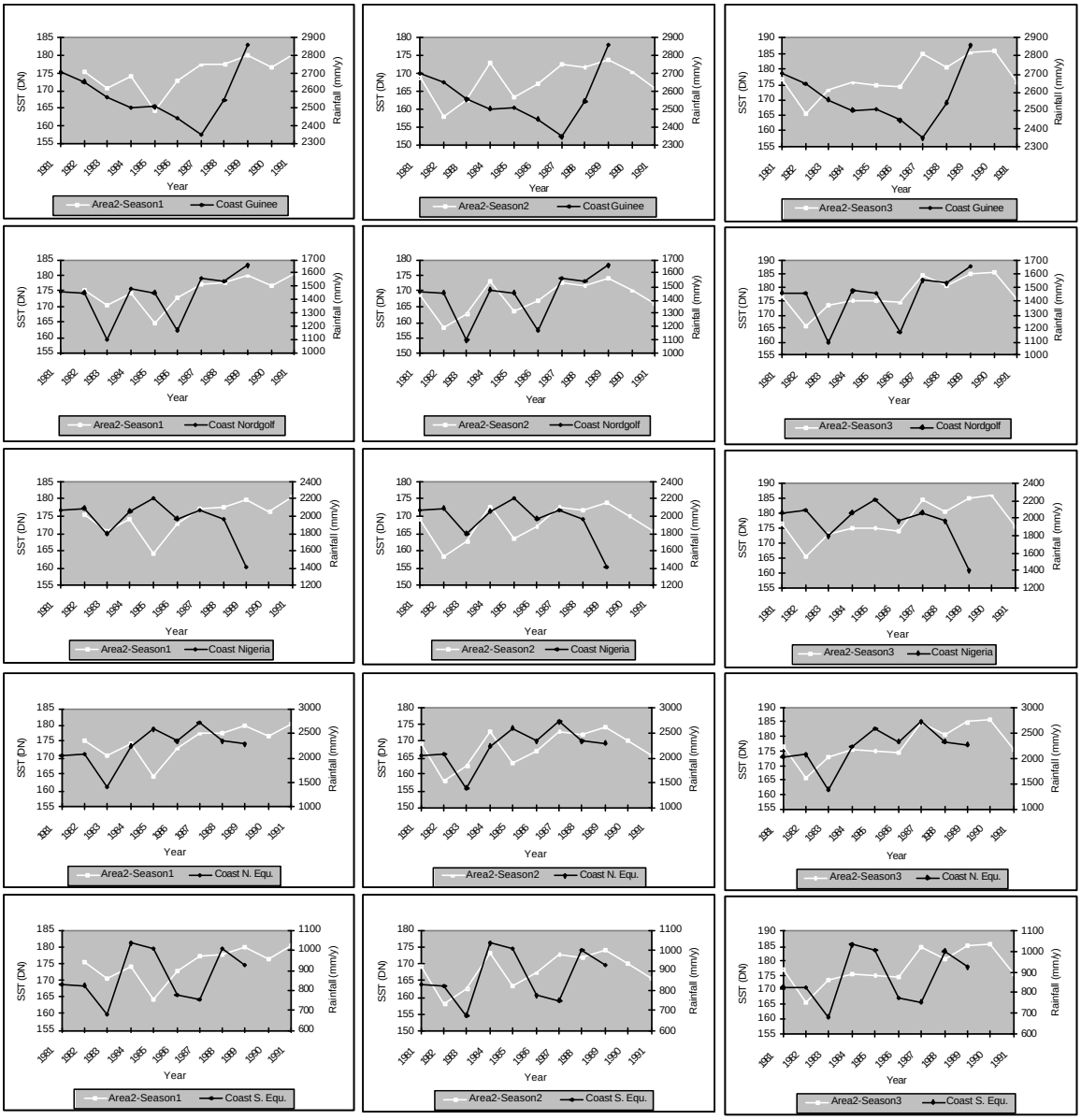

Qualitative comparison of CORSA-AVHRR SST for Area 2 with coastal area rainfall.

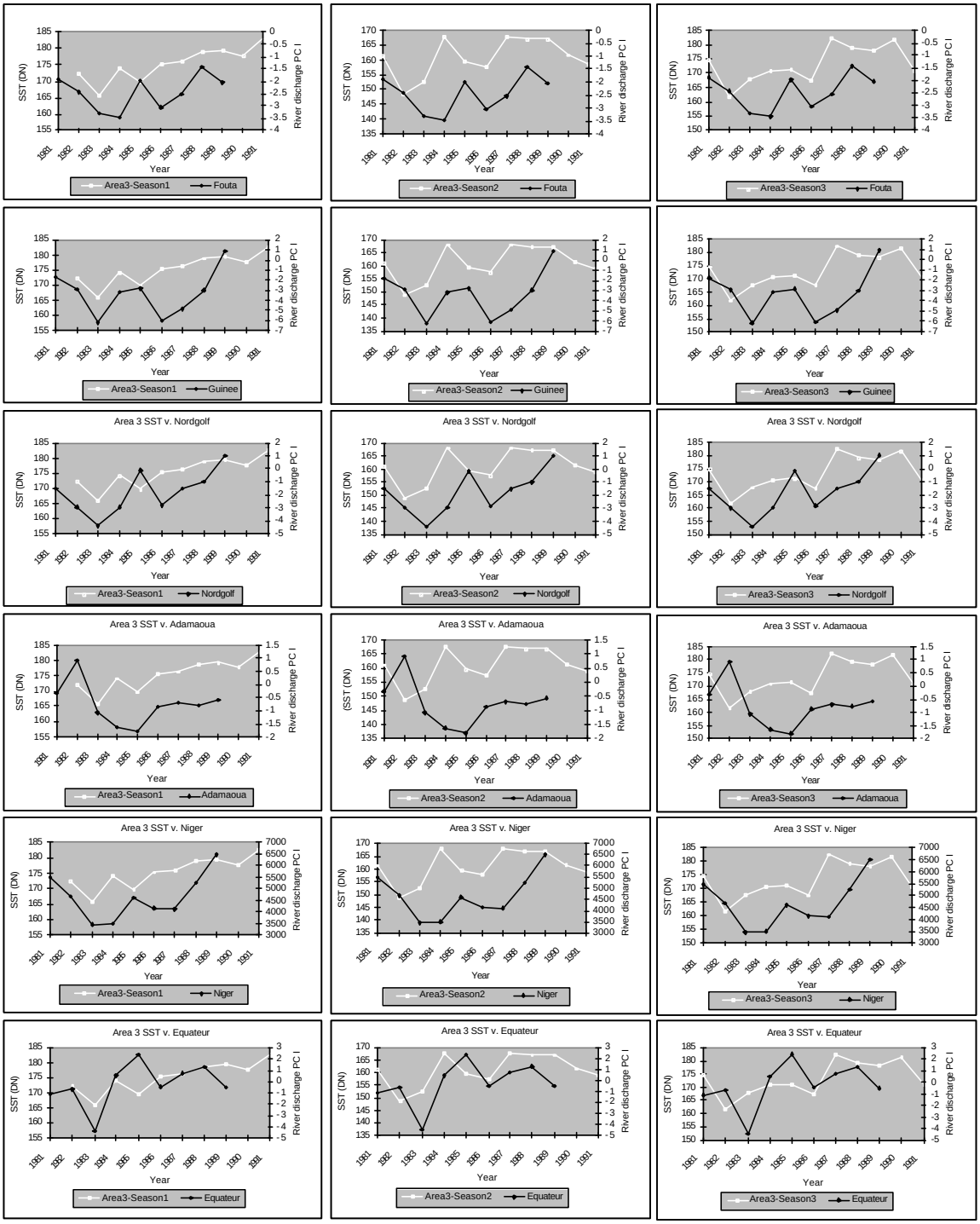

Qualitative comparison of CORSA-AVHRR SST for Area 3 with PC I of regional river discharge.

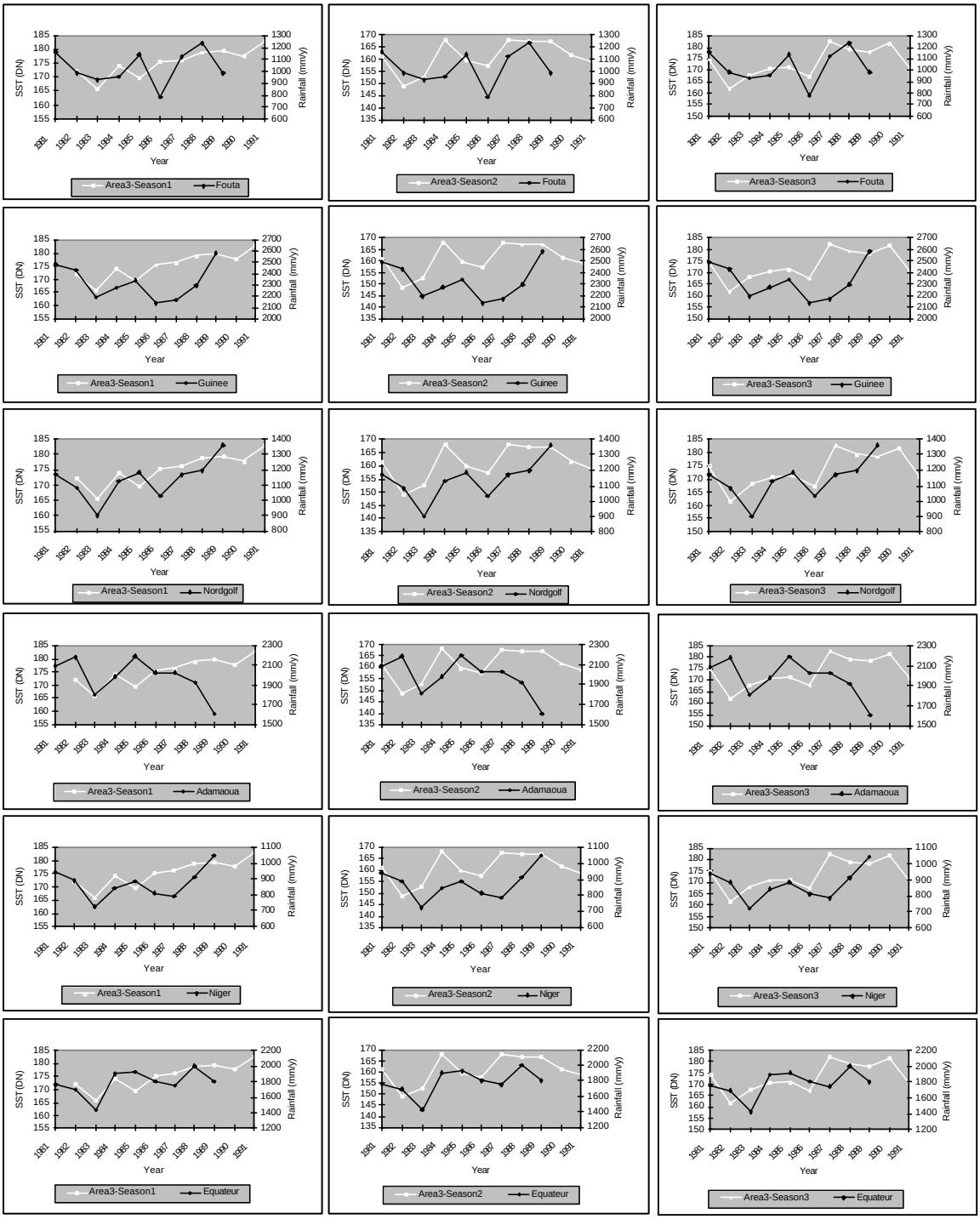

Qualitative comparison of CORSA-AVHRR SST for Area 3 with regional rainfall.

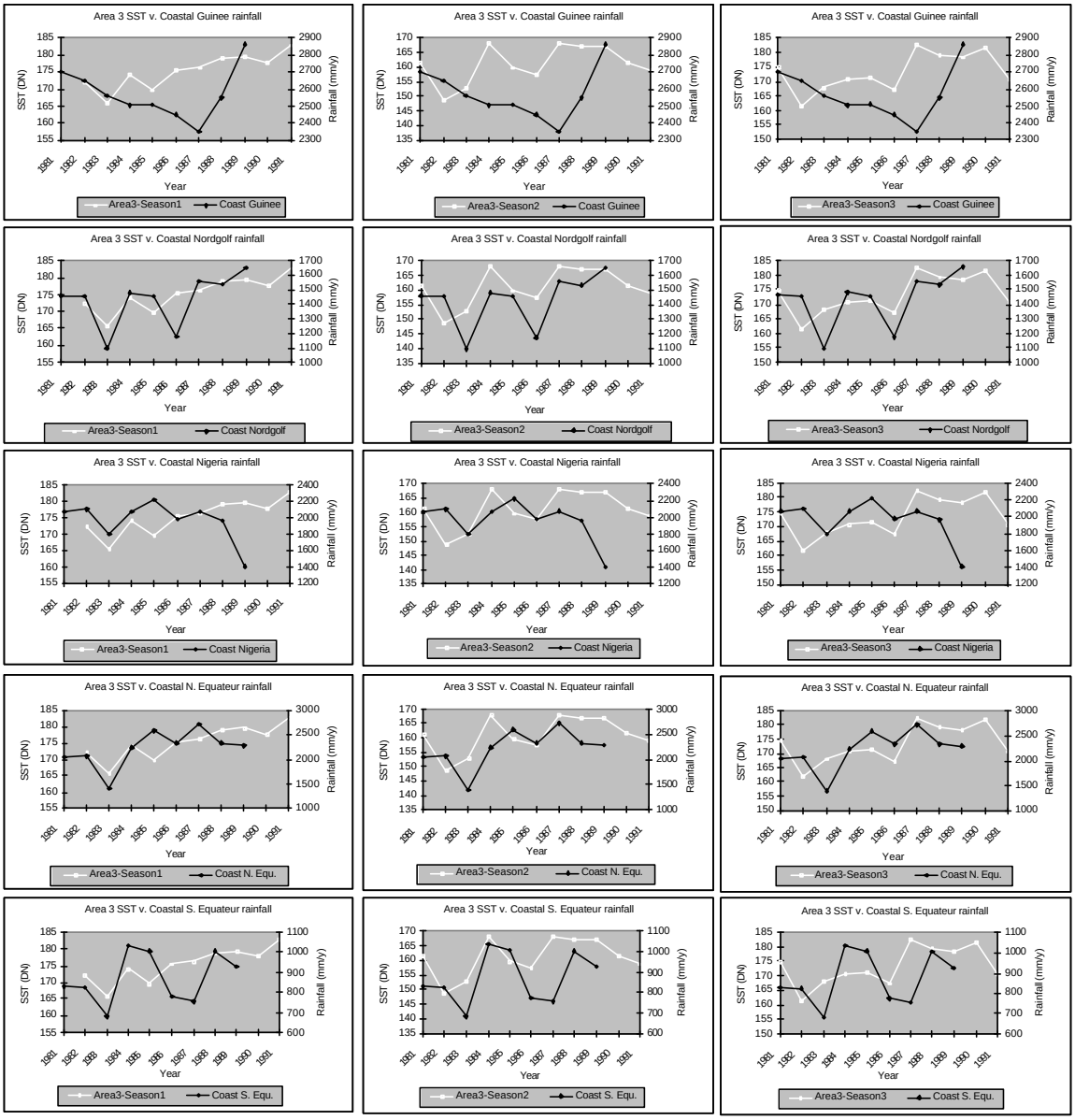

Qualitative comparison of CORSA-AVHRR SST for Area 3 with coastal area rainfall.

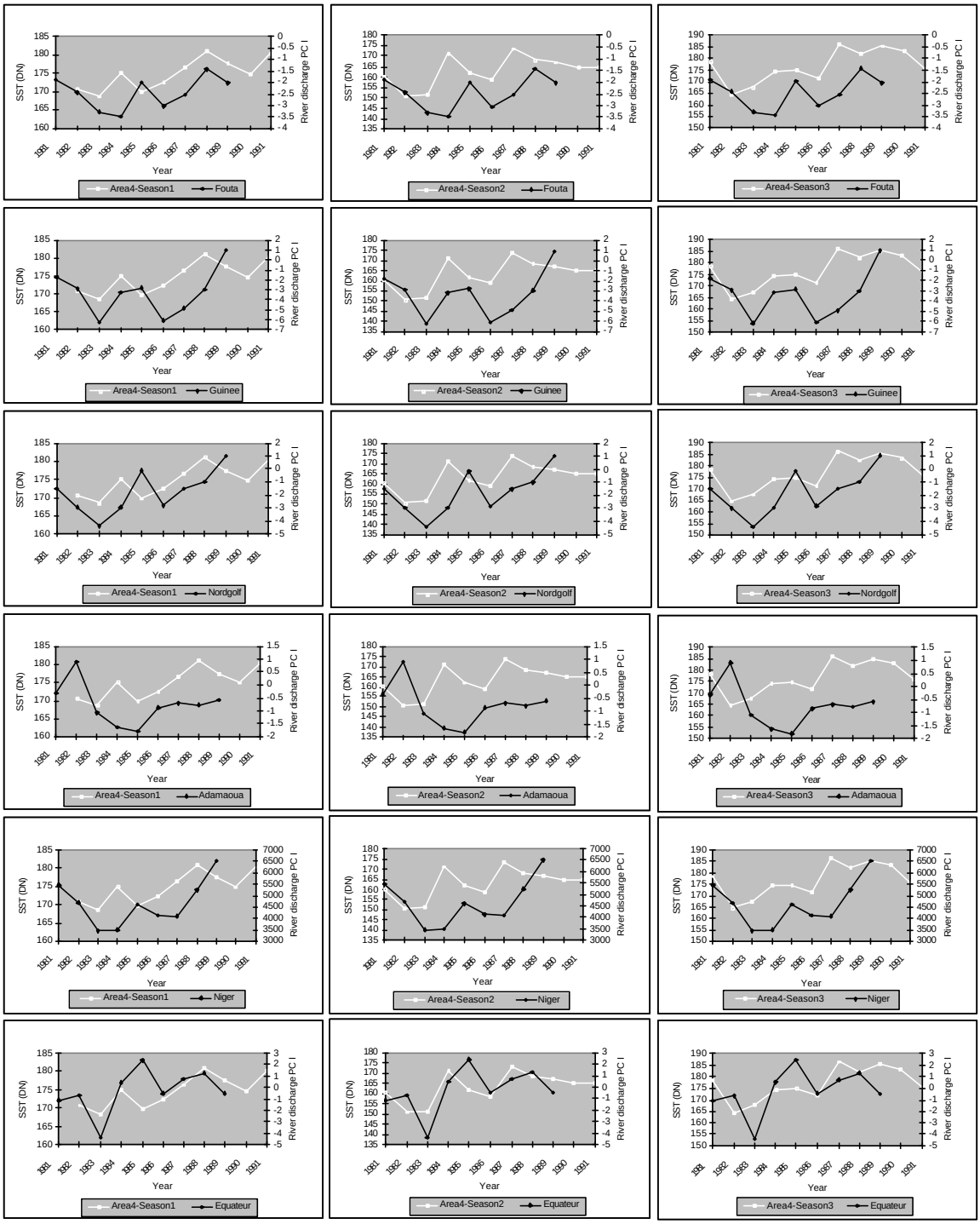

Qualitative comparison of CORSA-AVHRR SST for Area 4 with PC I of regional river discharge.

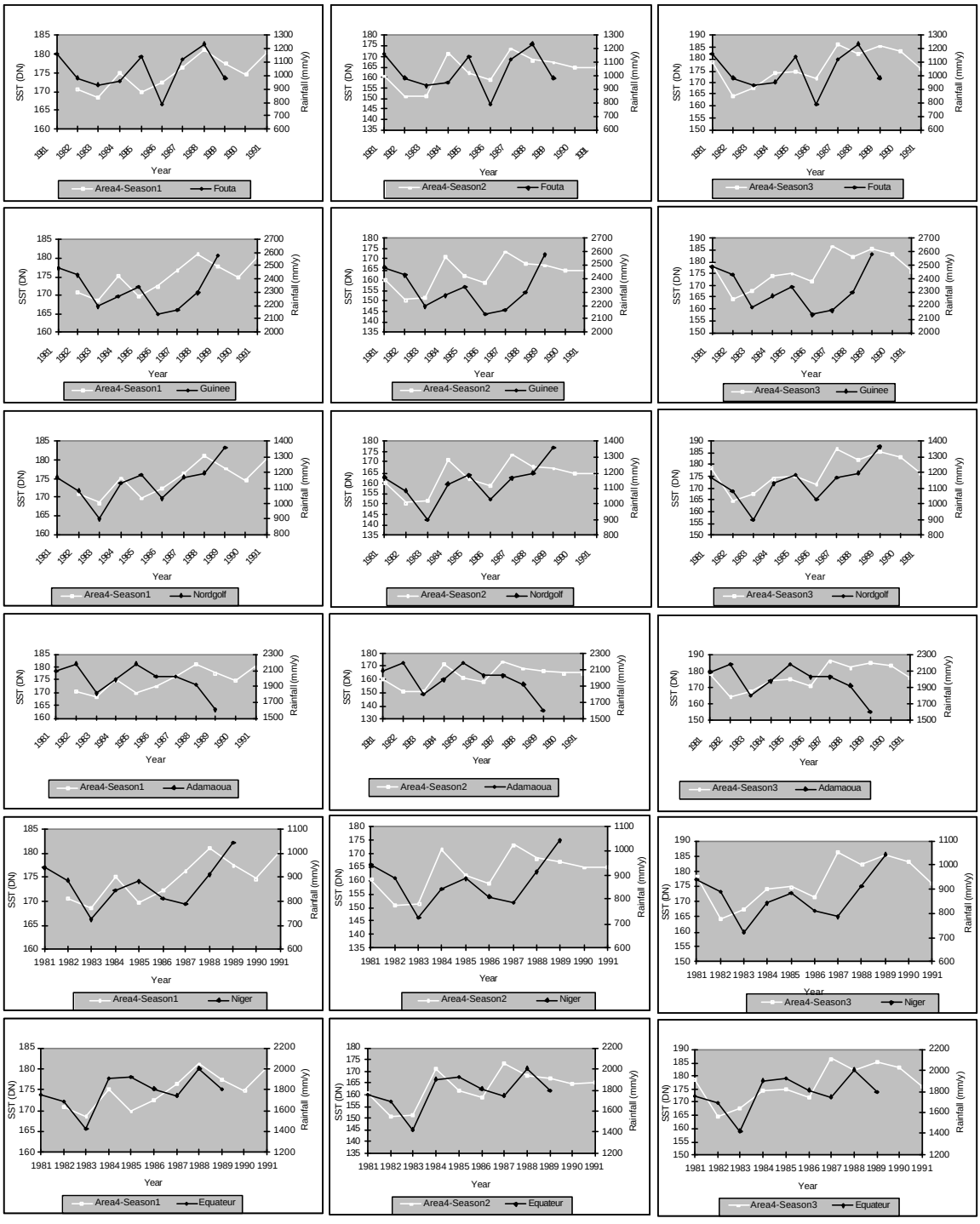

Qualitative comparison of CORSA-AVHRR SST for Area 4 with regional rainfall.

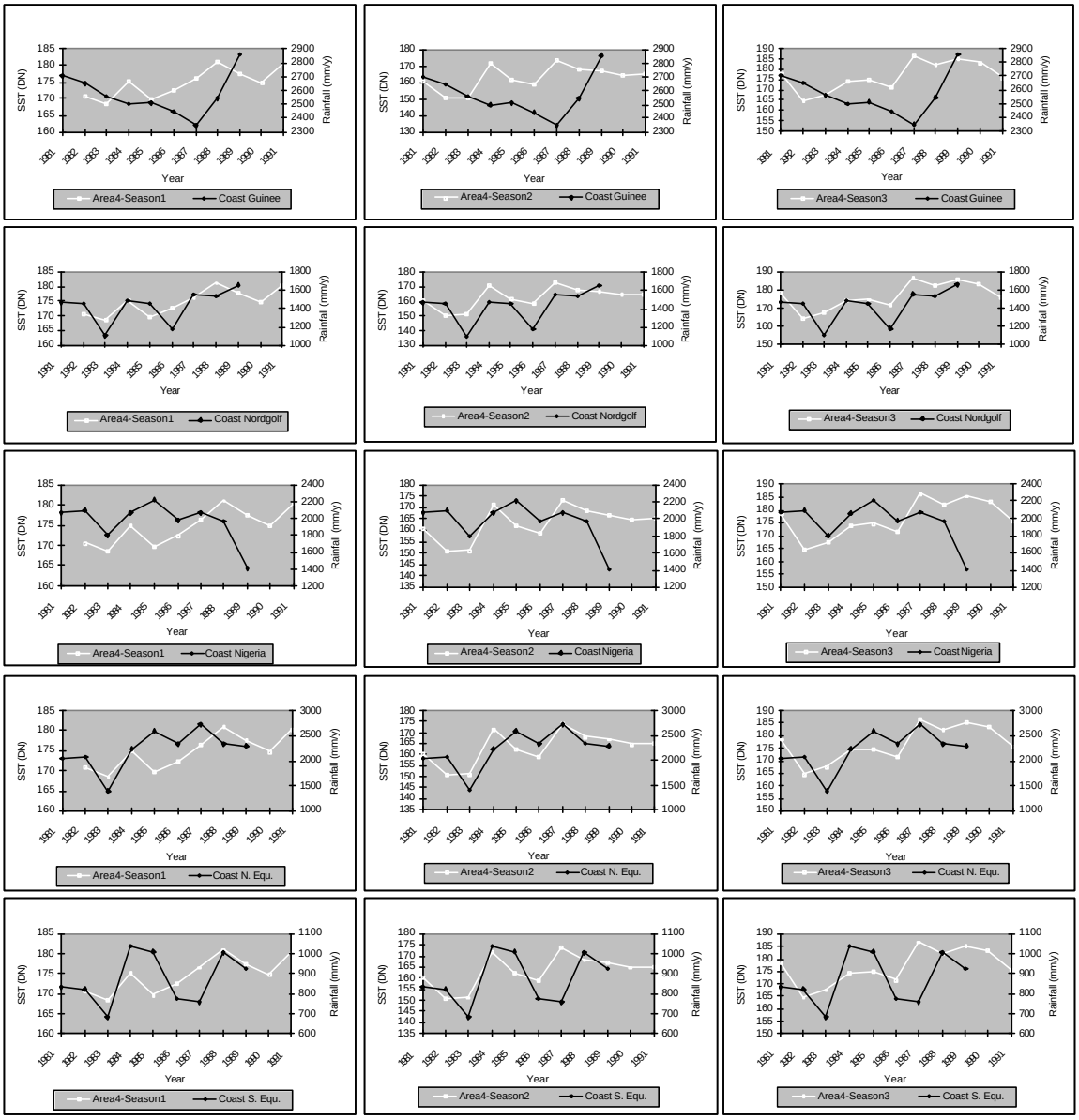

Qualitative comparison of CORSA-AVHRR SST for Area 4 with coastal area rainfall.

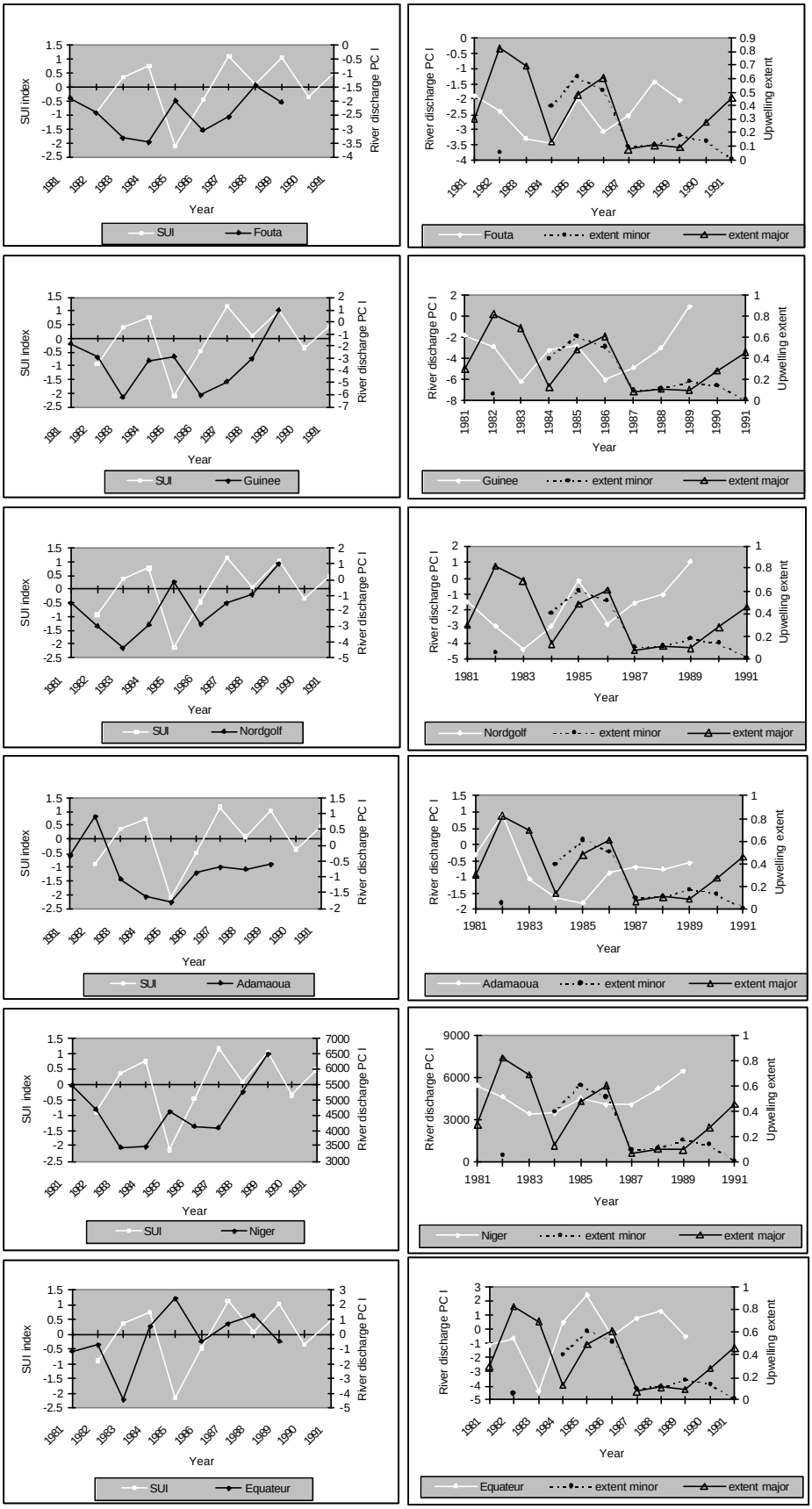

Qualitative comparison of the SUI index and upwelling extent with PC I of regional river discharge.

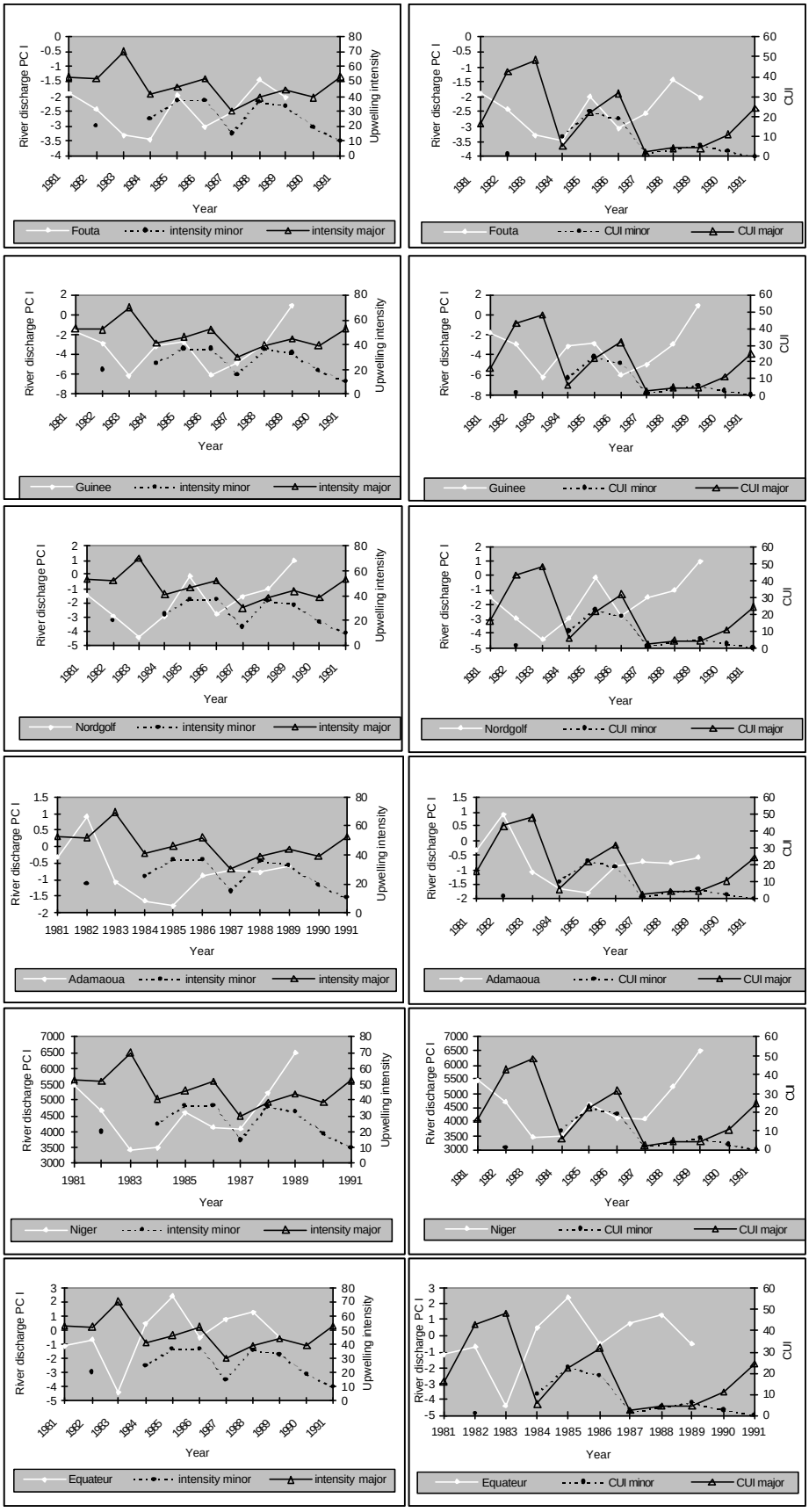

Qualitative comparison of upwelling intensity and the CUI with PC I of regional river discharge.

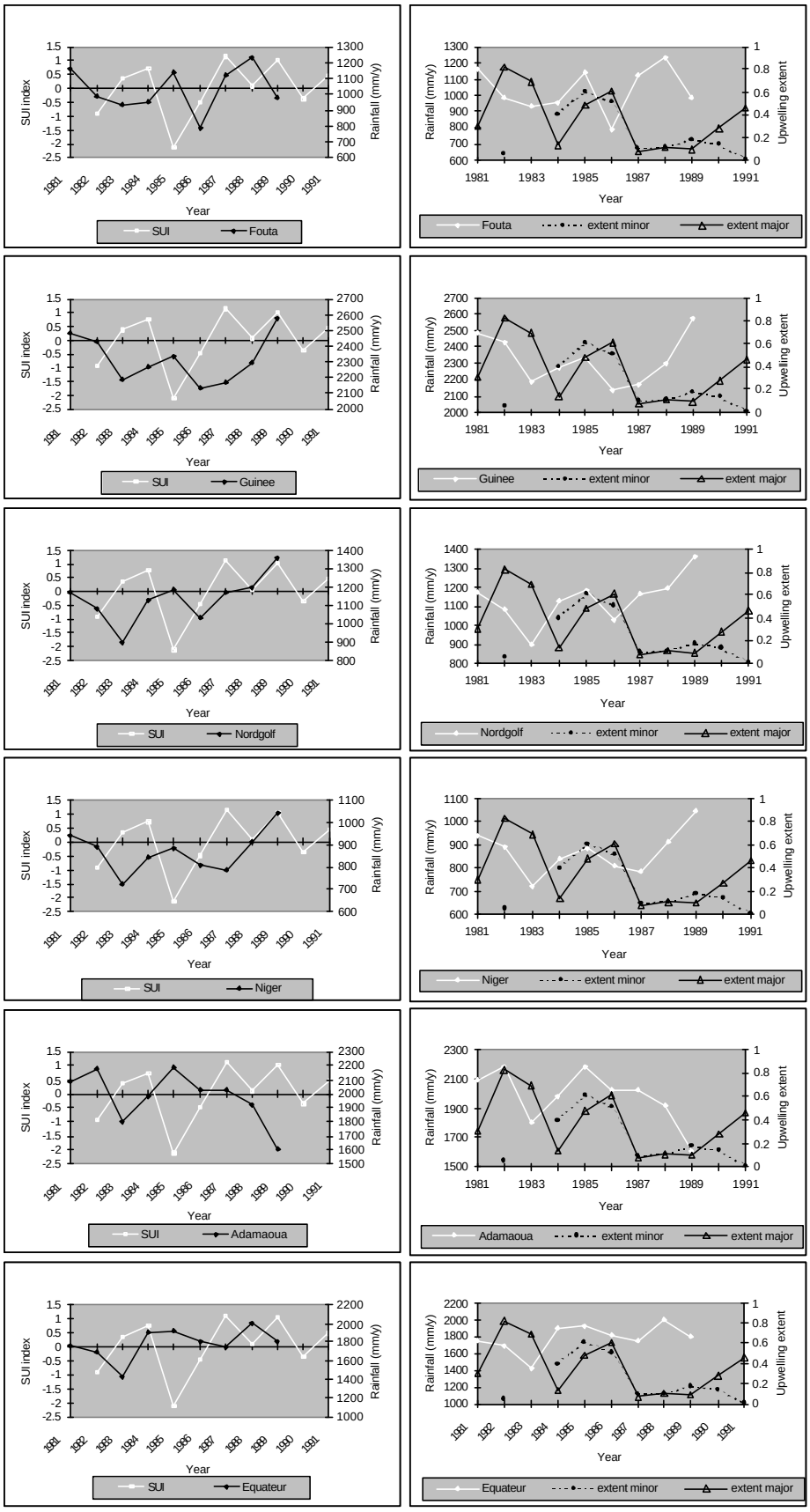

Qualitative comparison of the SUI index and upwelling extent with regional rainfall.

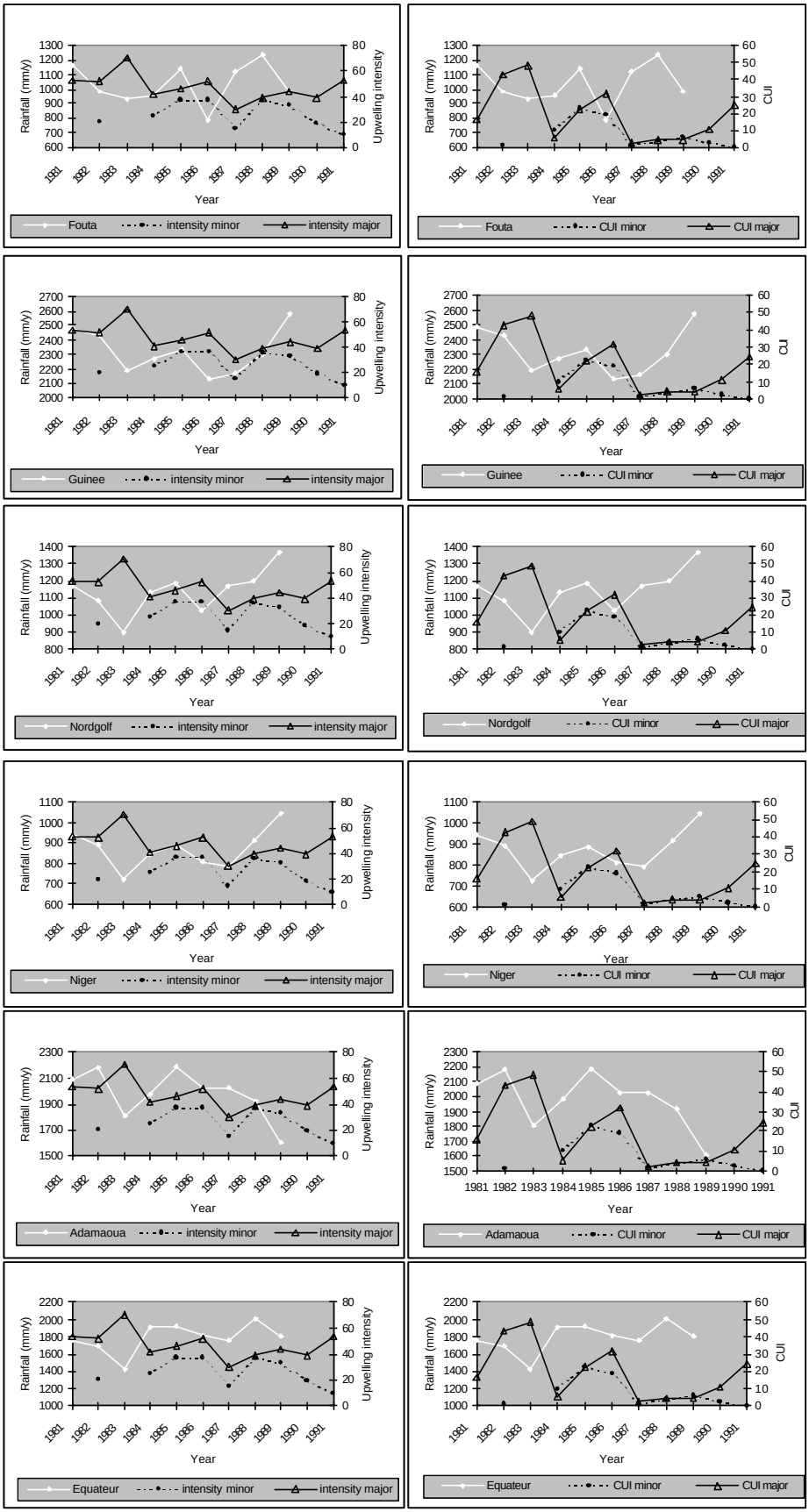

Qualitative comparison of upwelling intensity and the CUI with regional rainfall.

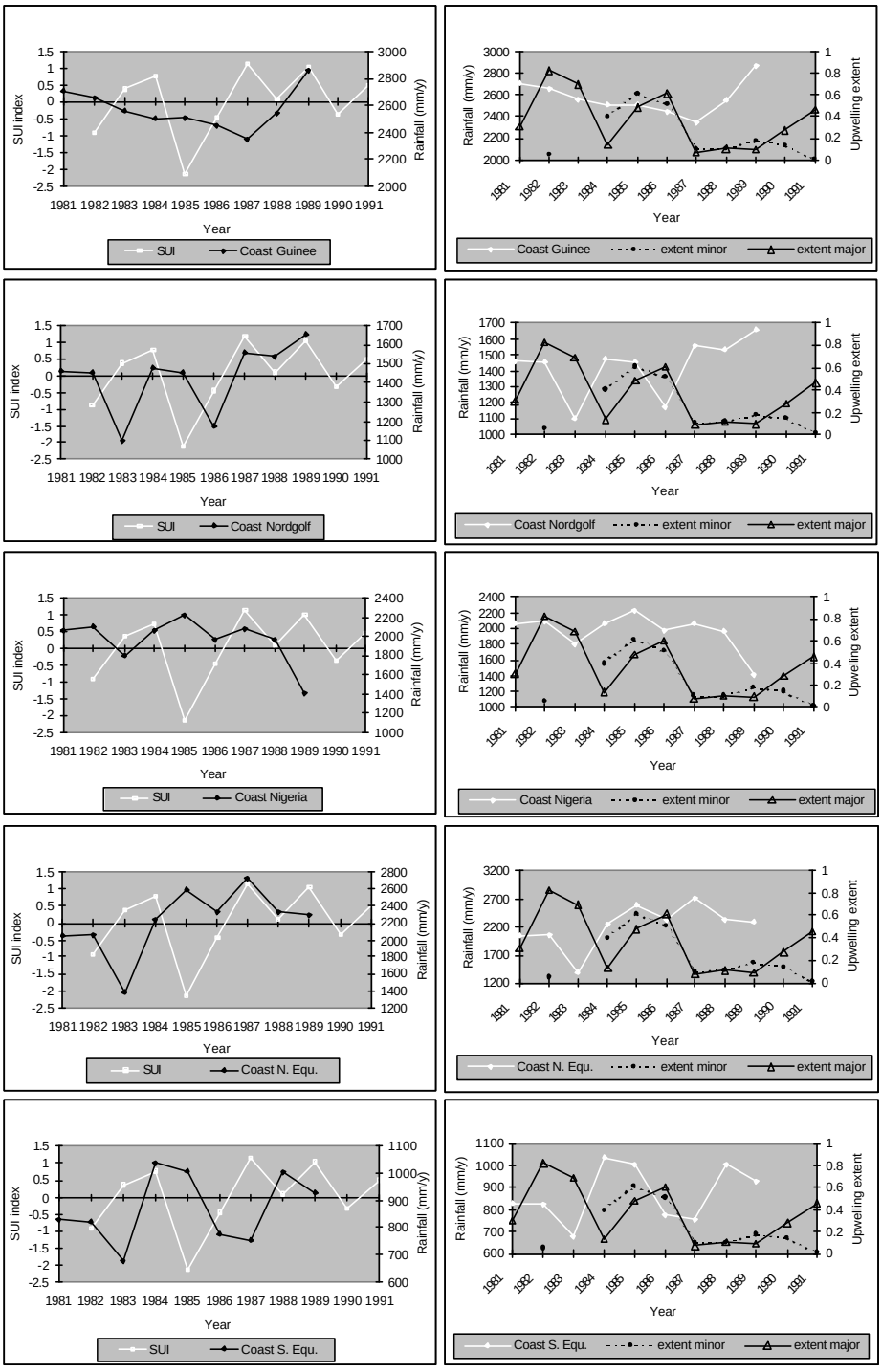

Qualitative comparison of the SUI index and upwelling extent with coastal rainfall.

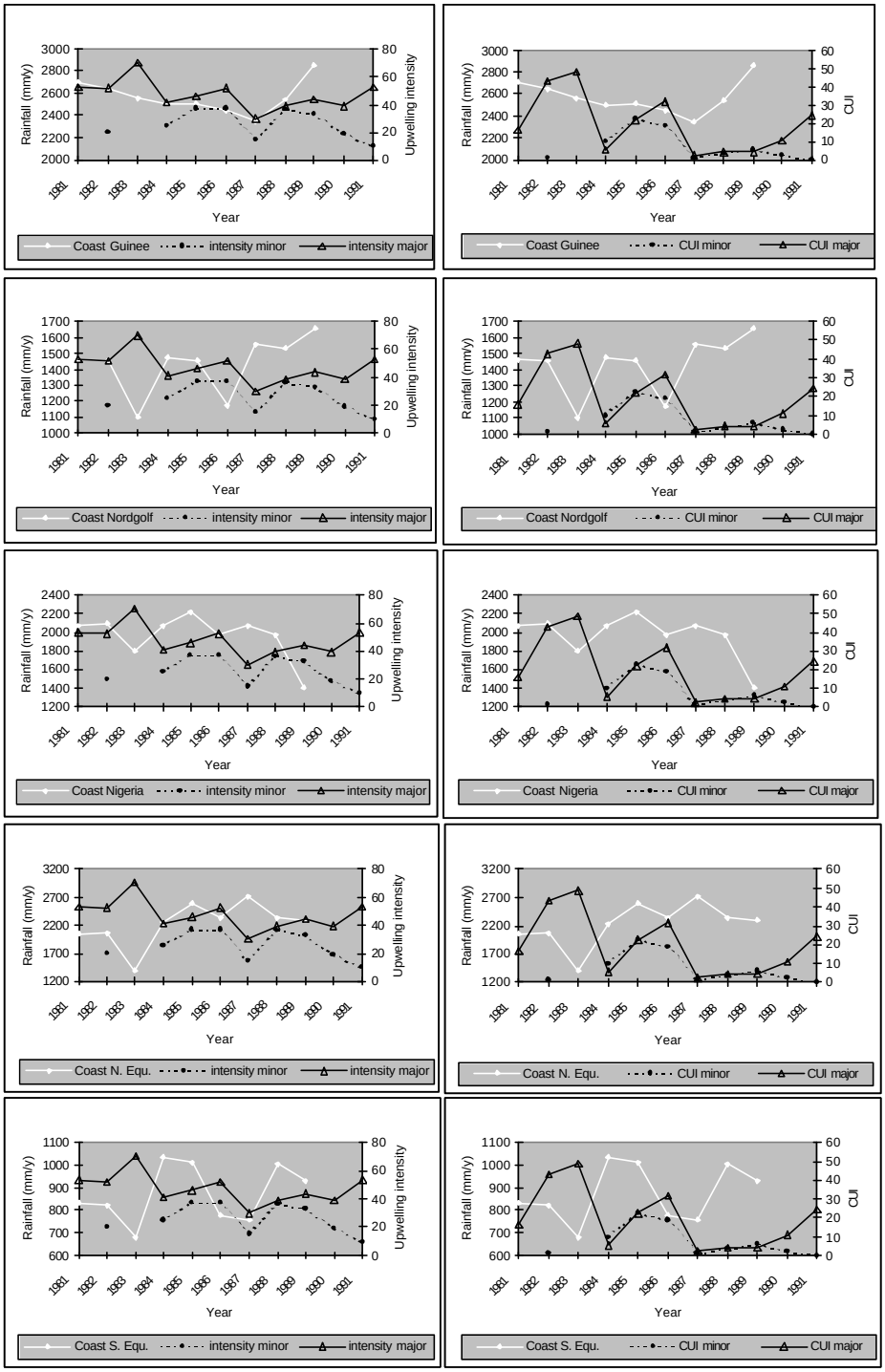

Qualitative comparison of upwelling intensity and the CUI with coastal rainfall.

Appendix 4 – Qualitative Comparisons from Chapter 8

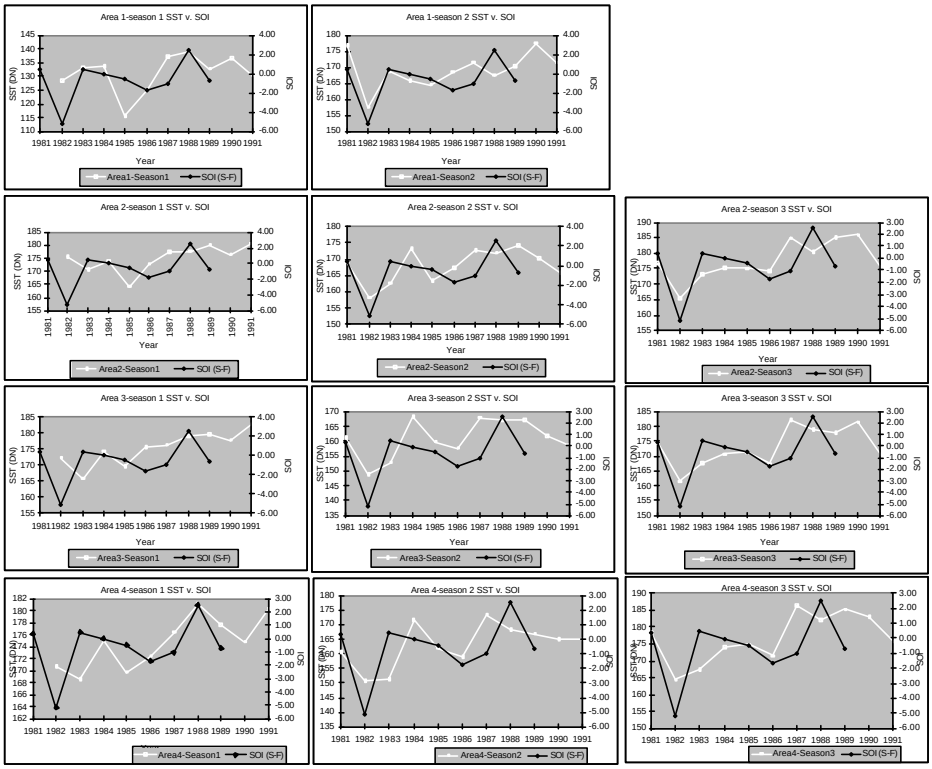

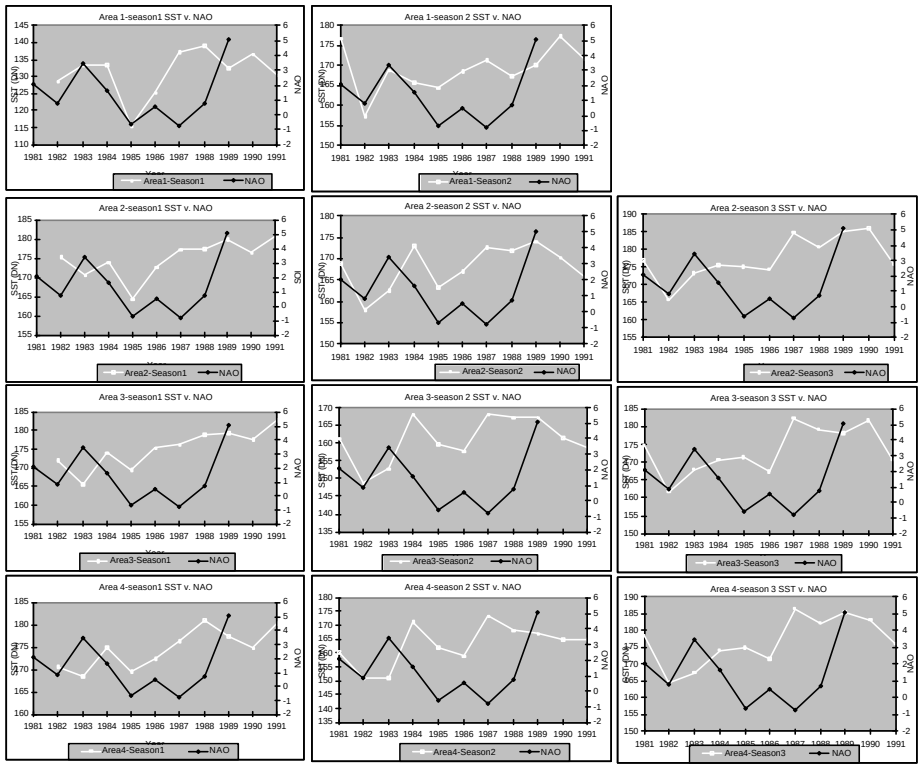

Qualitative comparison of seasonal SST with the SOI and NAO.

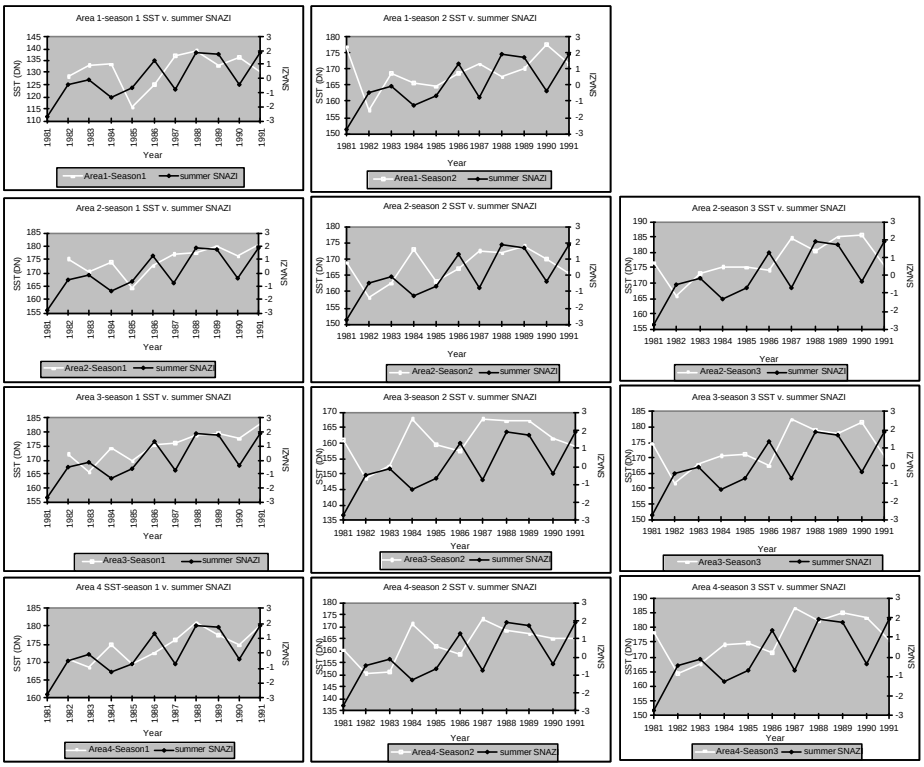

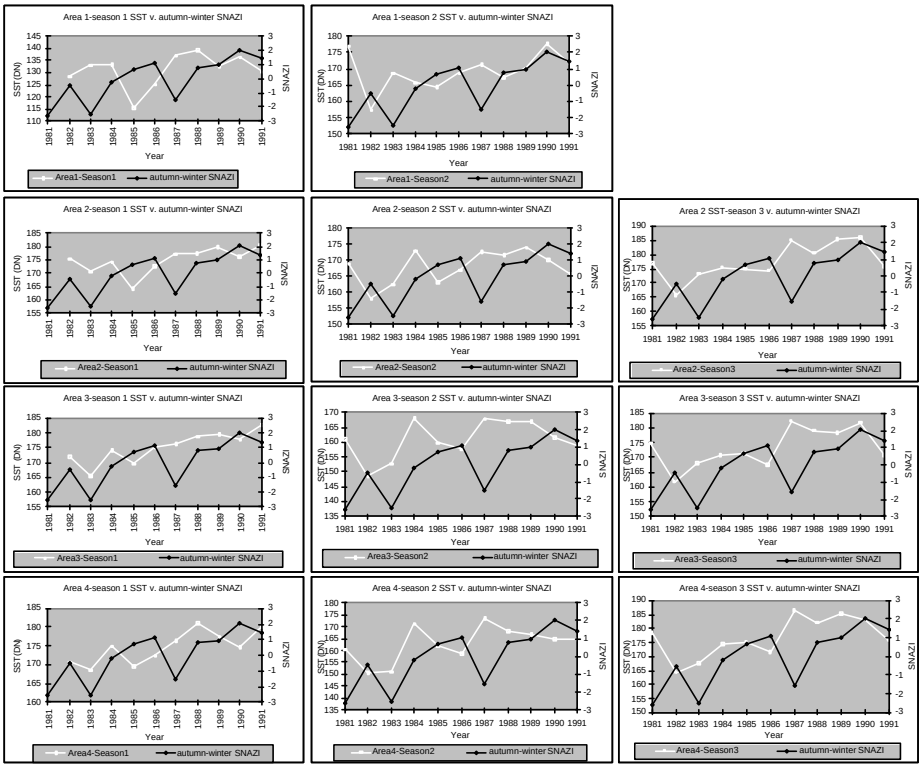

Qualitative comparison of seasonal SST with the summer and autumn-winter SNAZI.

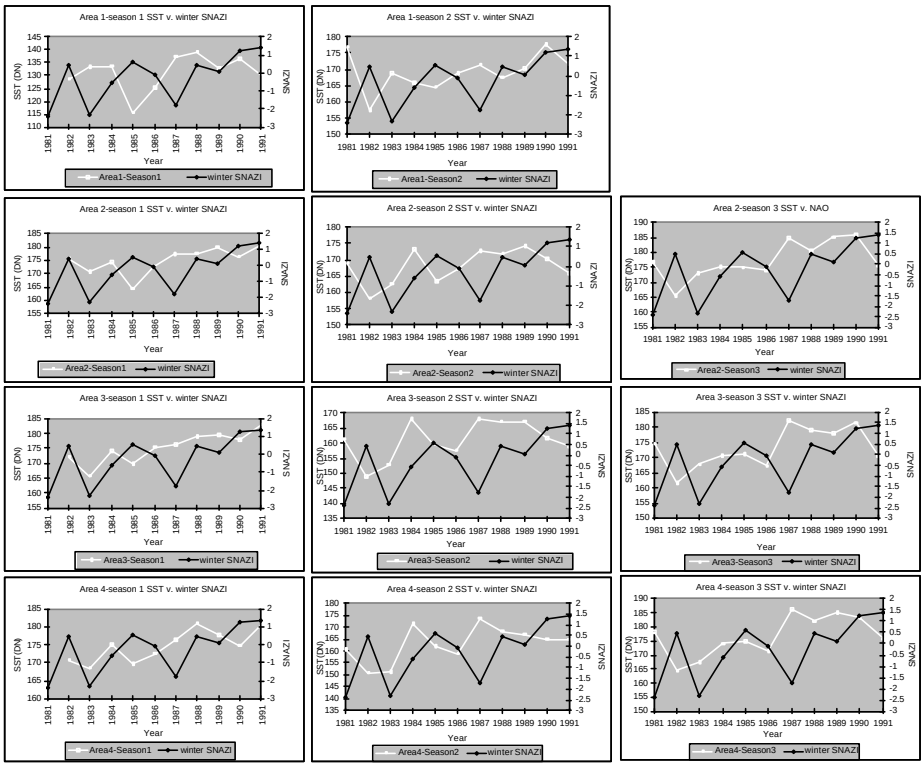

Qualitative comparison of seasonal SST with the winter SNAZI.

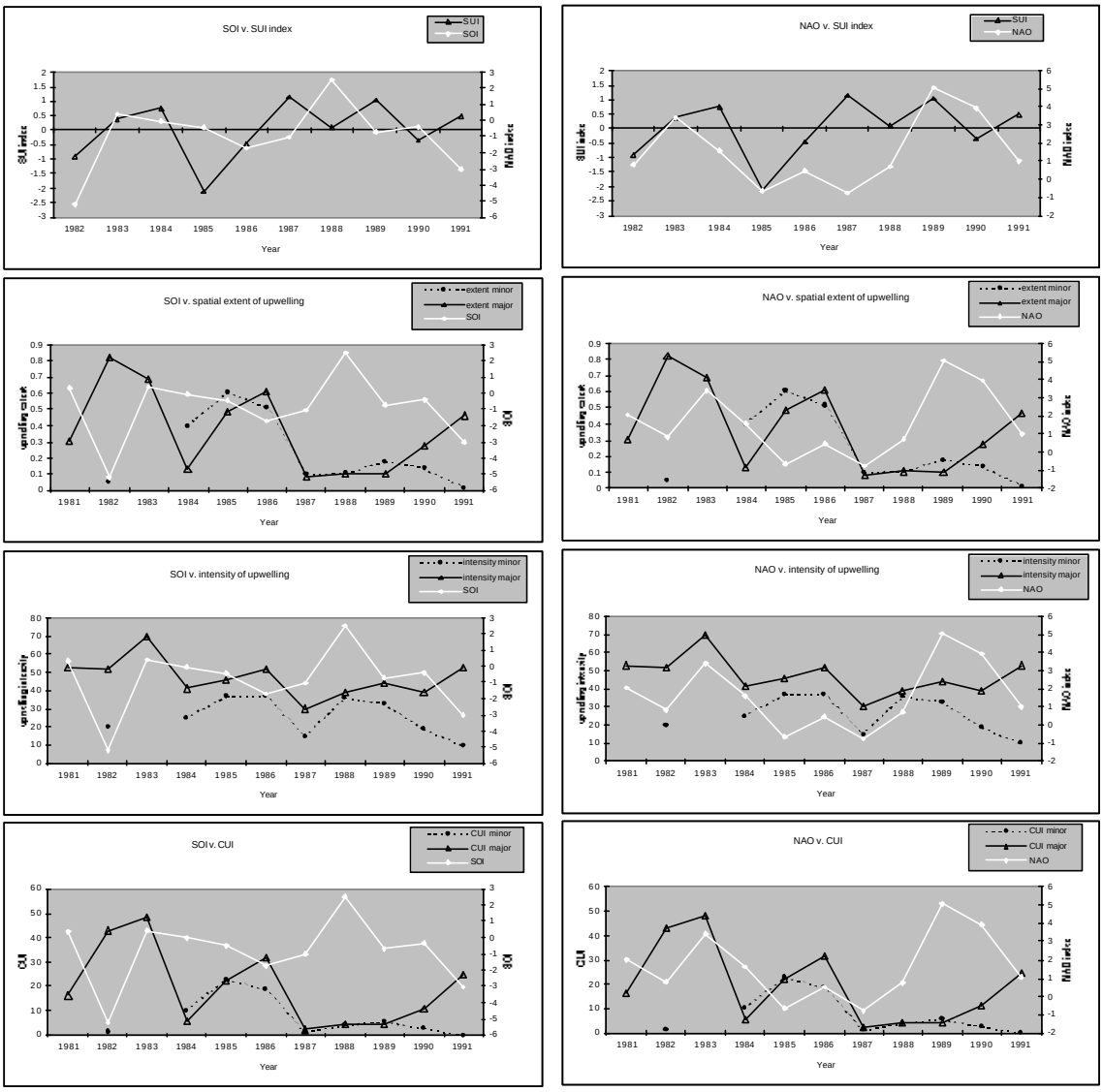

Qualitative comparison of the SOI and NAO with the oceanographic indices.

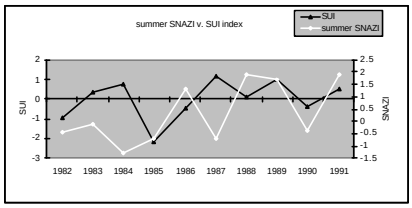

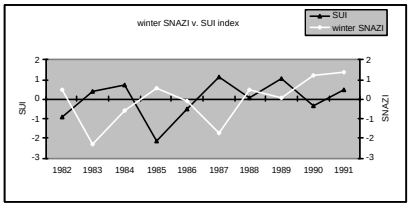

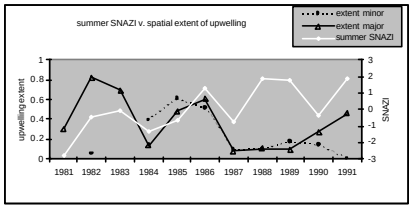

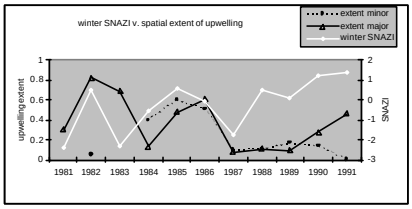

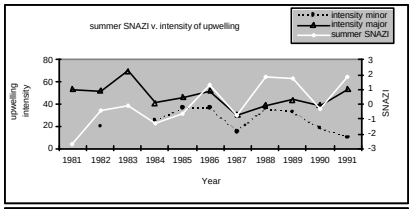

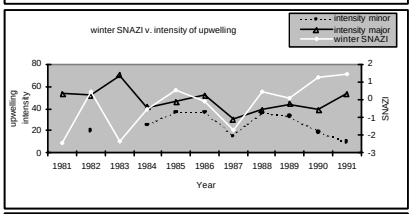

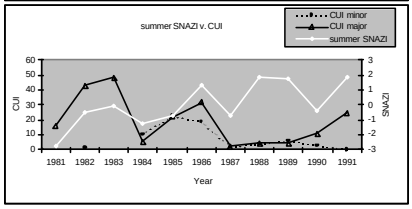

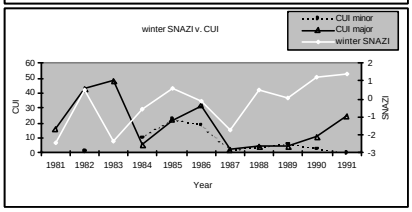

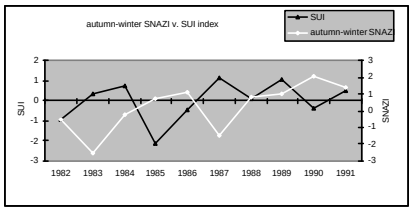

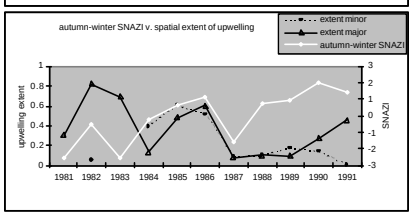

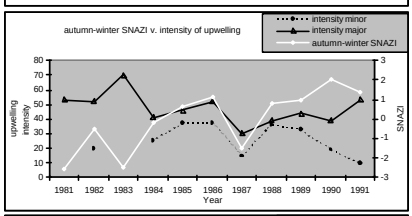

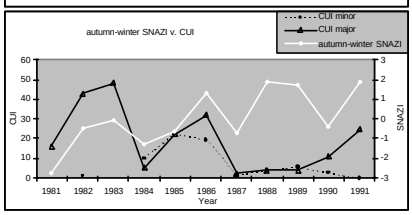

Qualitative comparison of the SNAZI with the oceanographic indices.

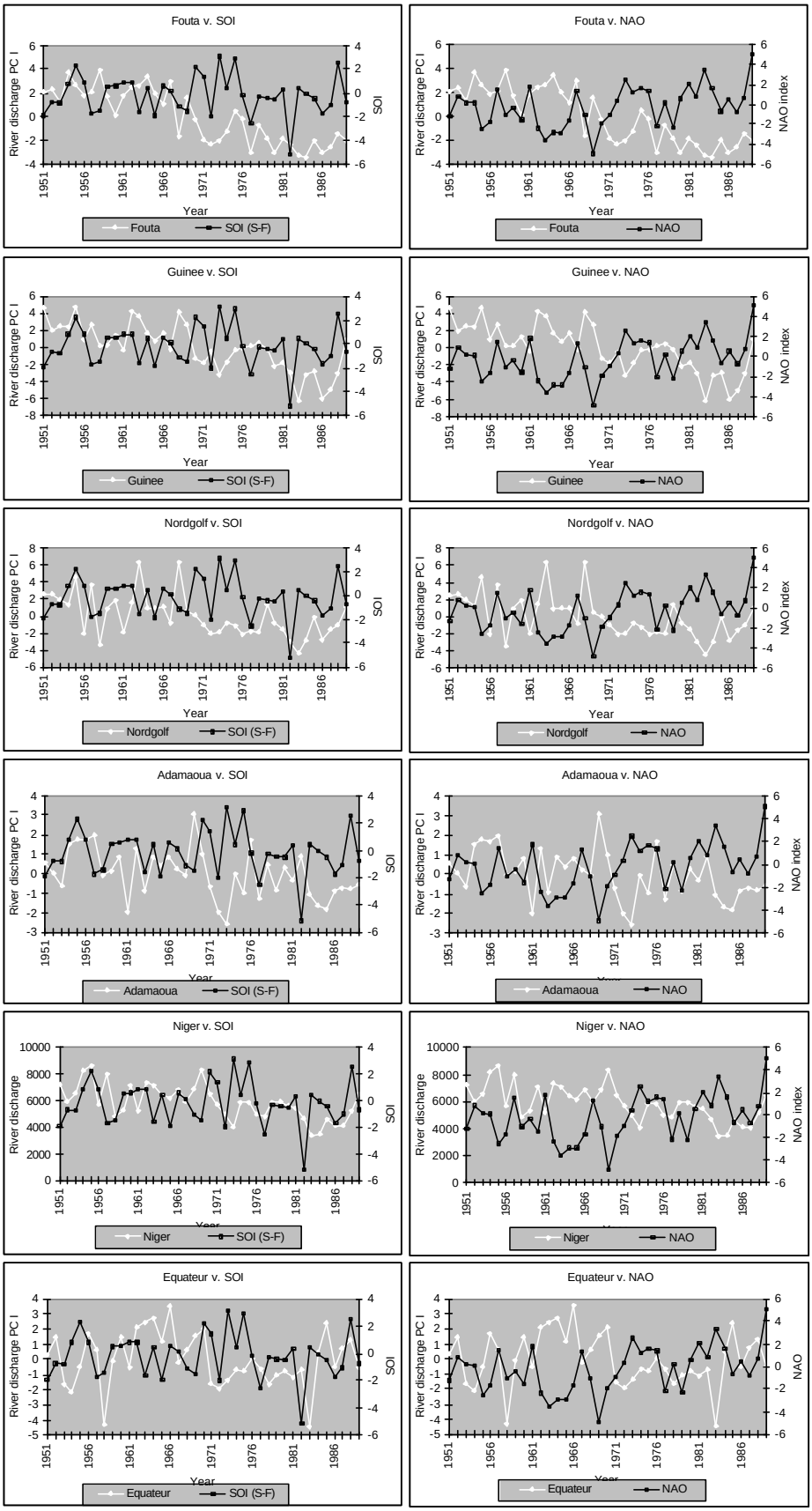

Qualitative comparison of regional river discharge PC I with the SOI and NAO.

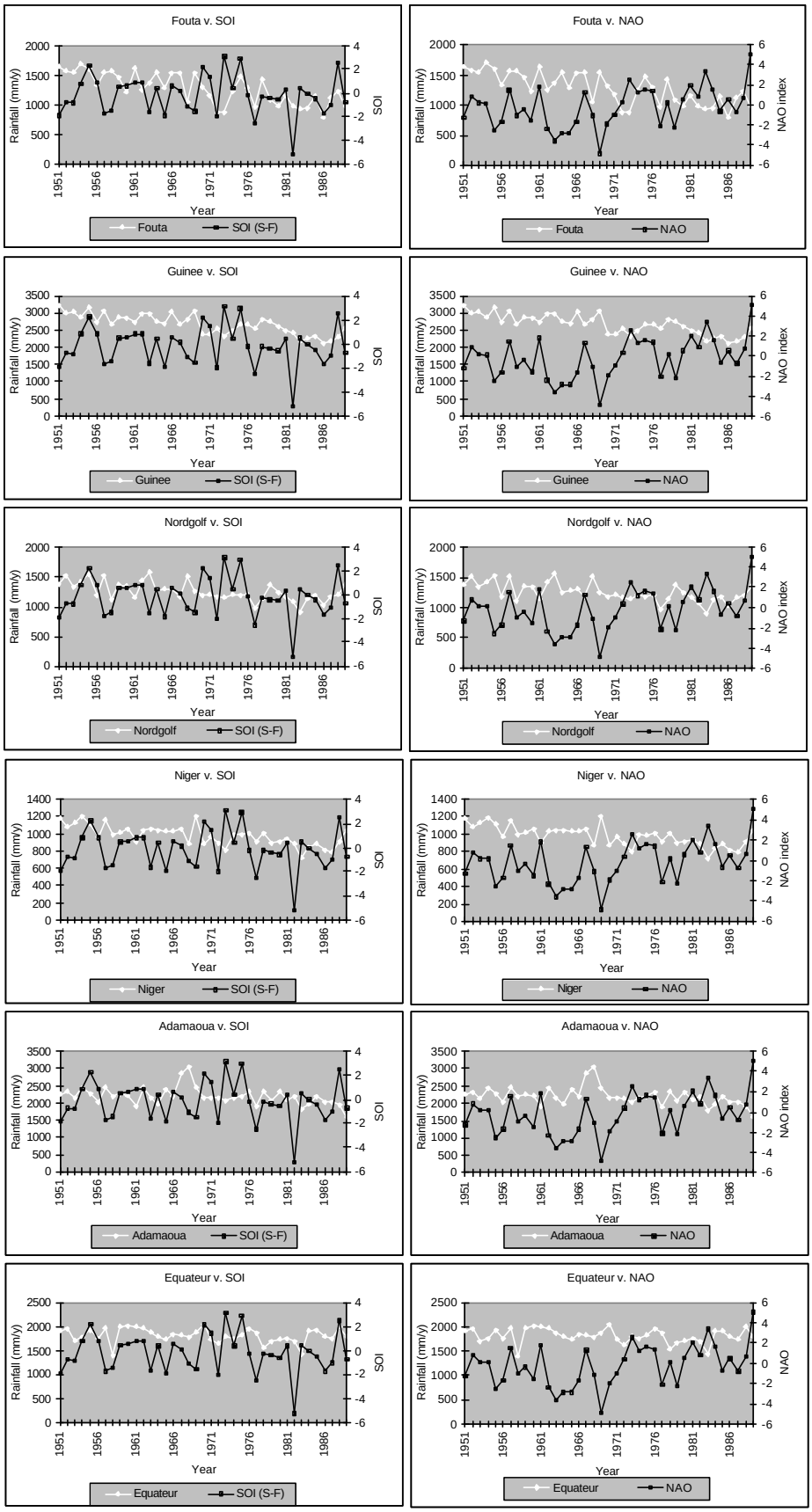

Qualitative comparison of regional rainfall with the SOI and NAO.

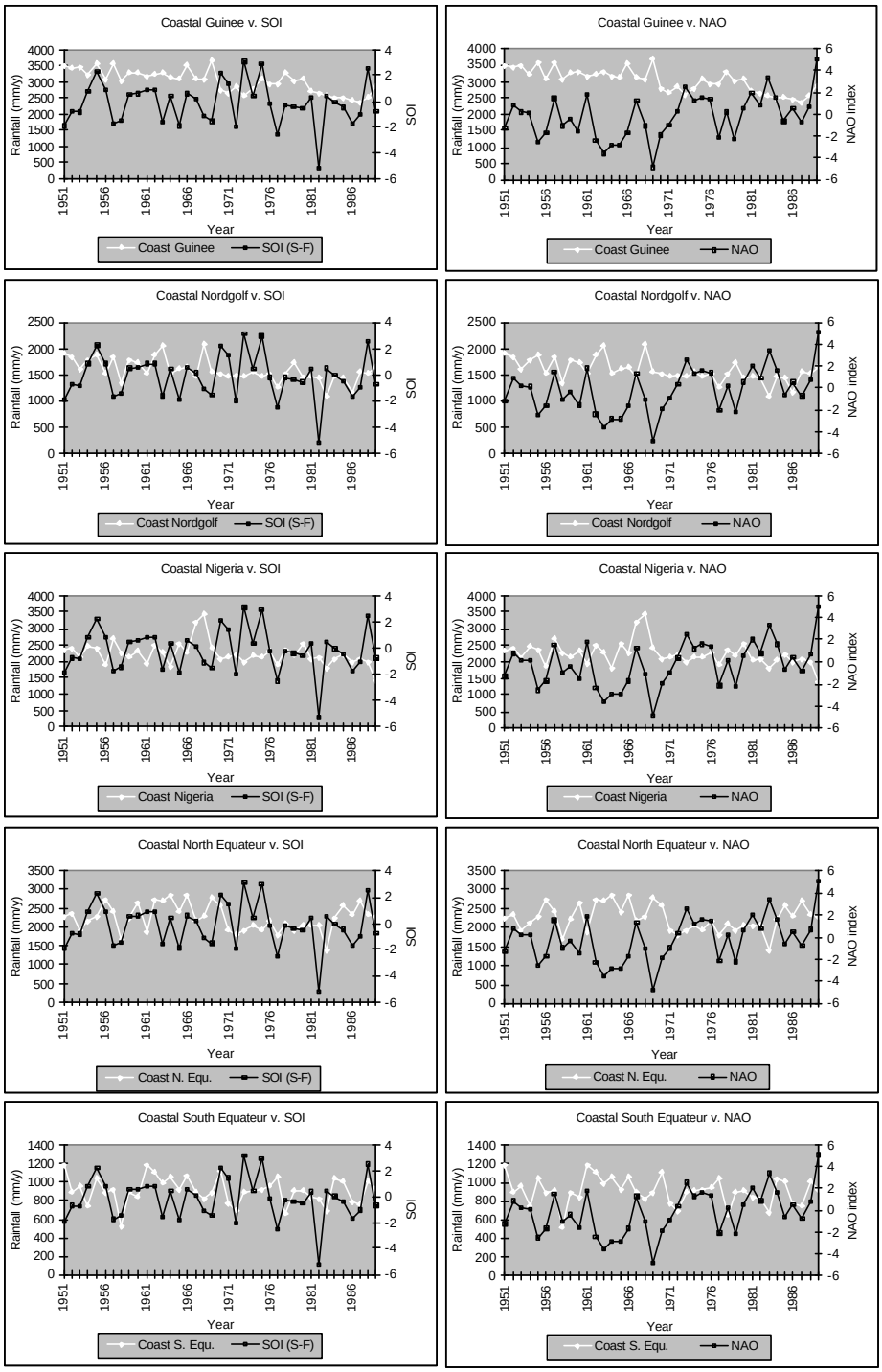

Qualitative comparison of coastal area rainfall with the SOI and NAO

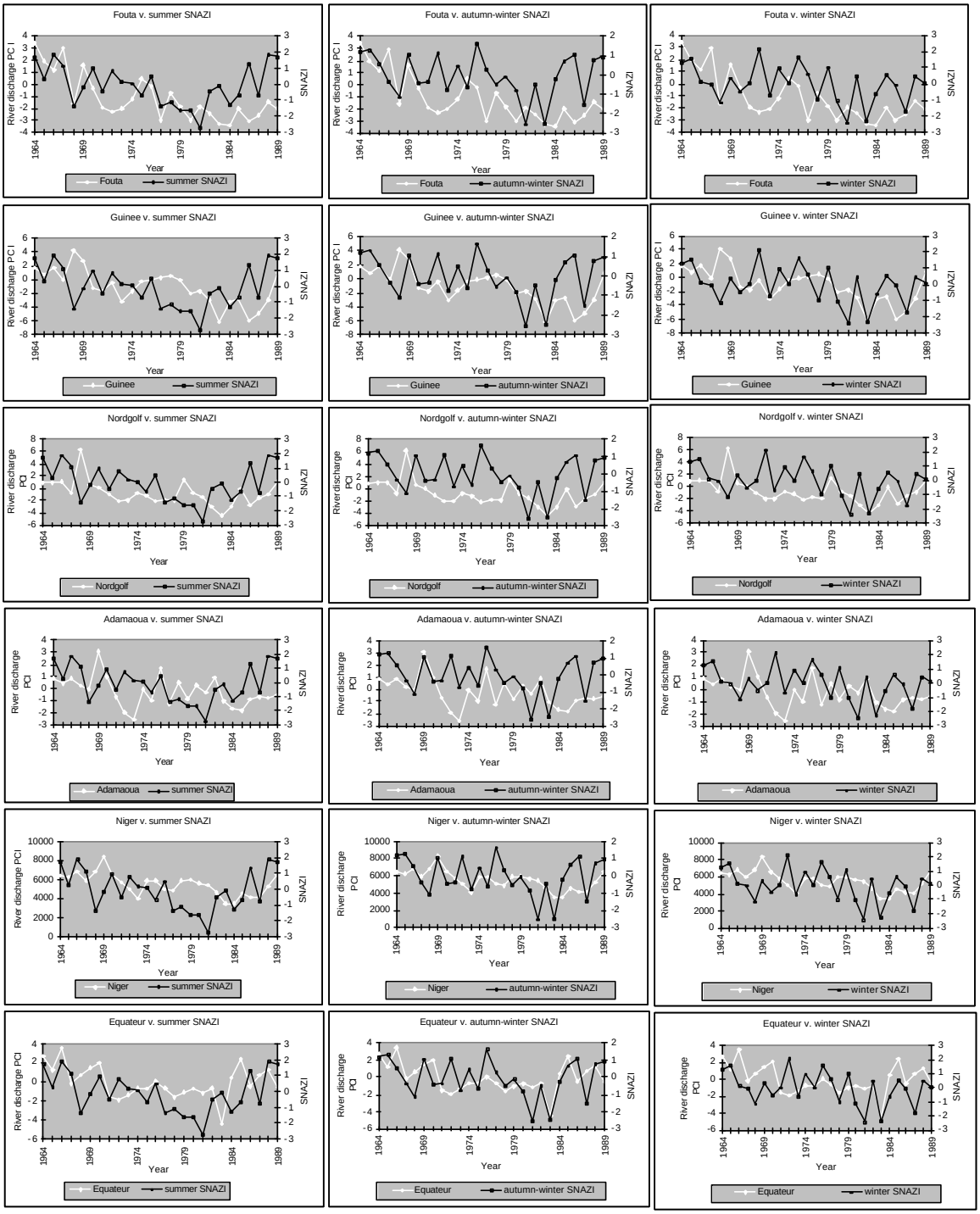

Qualitative comparison of regional river discharge PC I with the SNAZI.

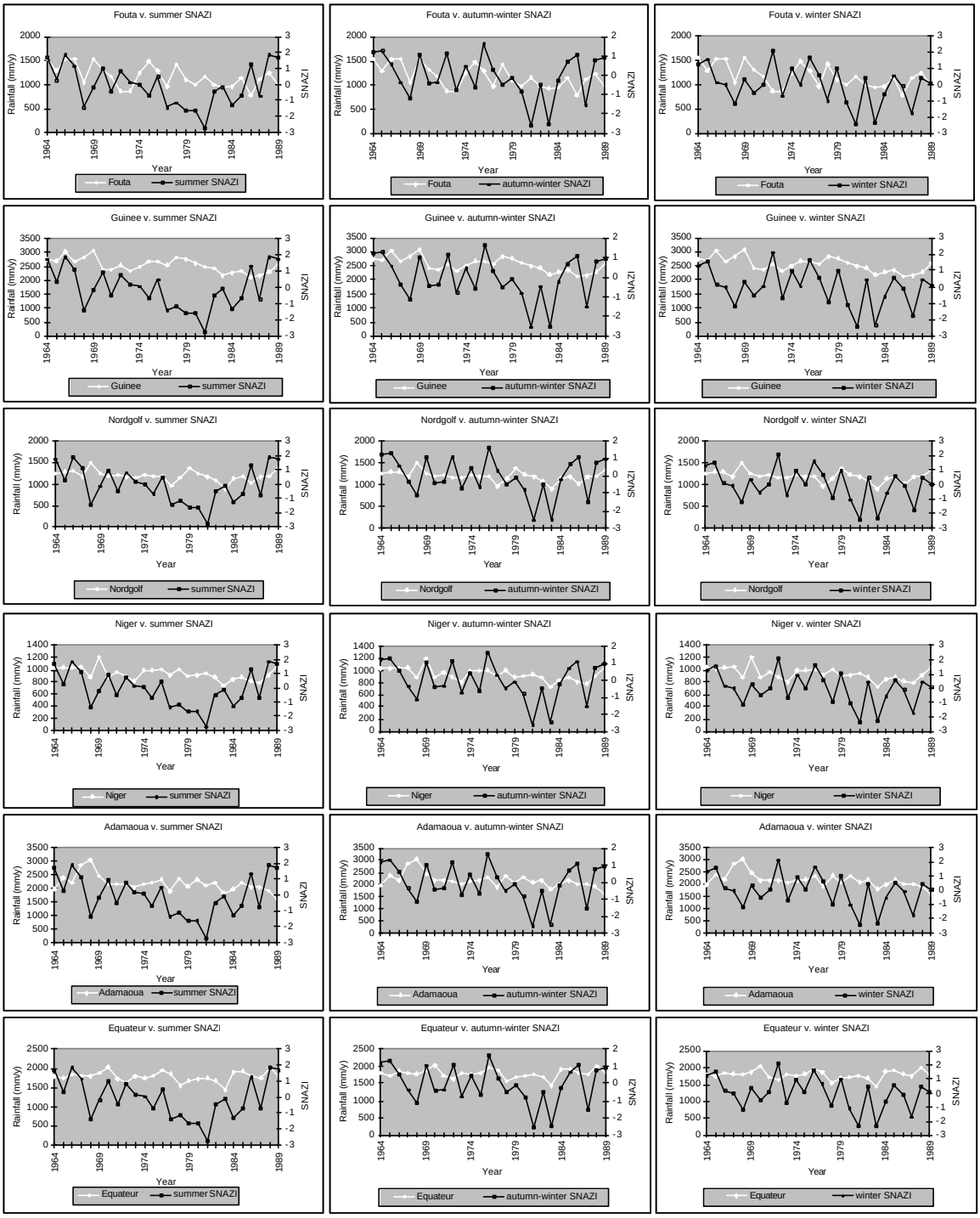

Qualitative comparison of regional rainfall with the SNAZI

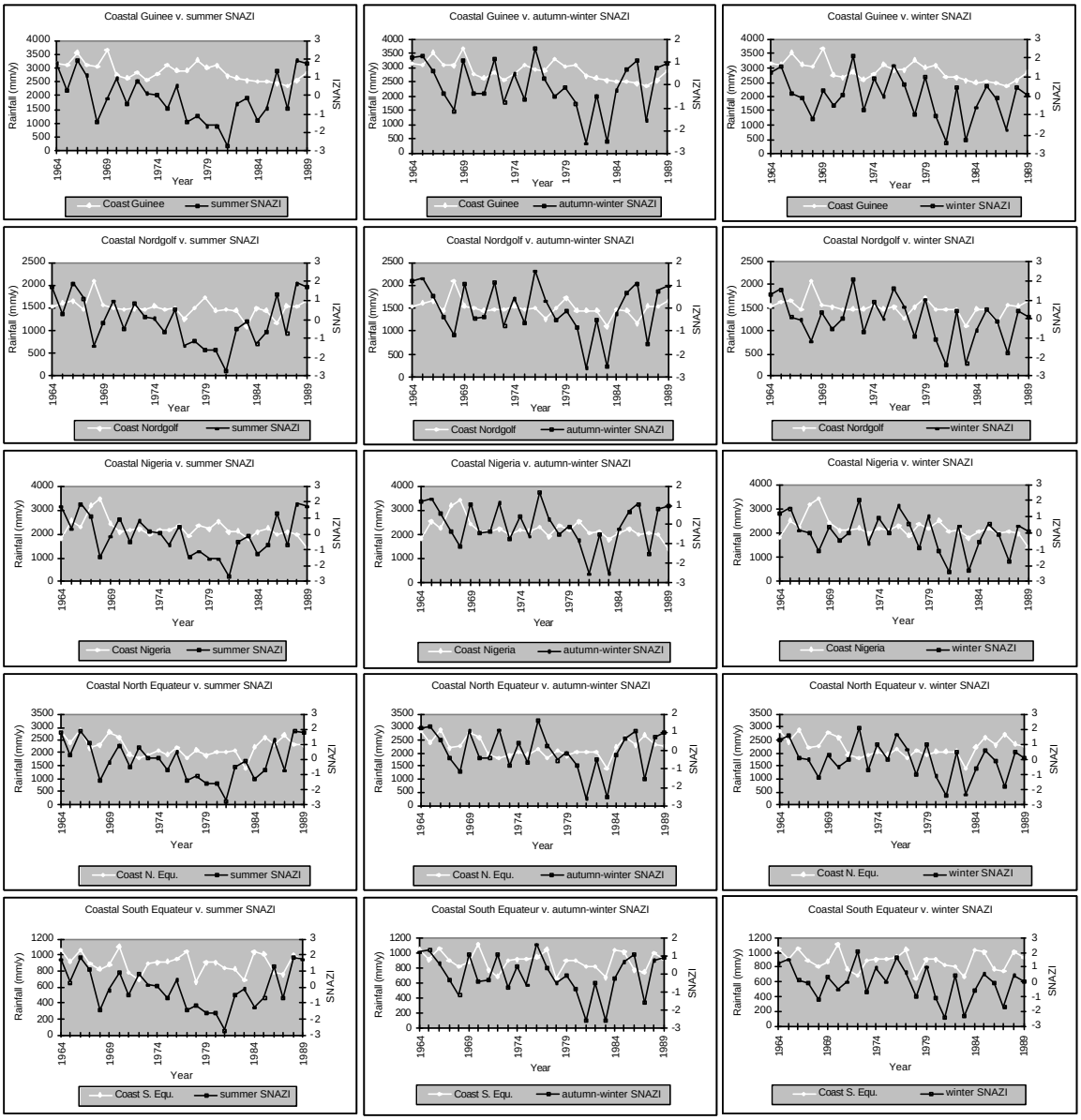

Qualitative comparison of coastal area rainfall with the SNAZI.